POLARIZABLE FORCE FIELDS

by

DENNY ELKING

(Under the Direction of Robert J. Woods)

ABSTRACT

Force fields have recently begun to model electrostatic interactions with explicit charge densities composed of Gaussian functions. A Gaussian multipole formalism is presented which is based on previous work done on Hermite Gaussian functions. The treatment for Gaussian multipoles parallels standard derivations of Cartesian point multipoles. The results obtained for Gaussian multipoles are used to develop a new polarization model based on induced Gaussian dipoles. In contrast to the original induced point dipole model, the induced Gaussian dipole model is capable of finite interactions at short distances. Aspects of convergence related to the induced Gaussian dipole model will be explored. Results for polarization work, energy, and force have been derived for the induced Gaussian dipole model, and a discussion of how the model has been implemented into the AMBER molecular dynamics simulation program is provided.

In addition, a method of parameterizing polarizabilities is presented. This method is based on probing a molecule with point charges and fitting polarizabilities to electrostatic potential. In contrast to the generic atom type polarizabilities fit to molecular polarizability tensors, probed polarizabilities are significantly more accurate in terms of reproducing molecular polarizability tensors and electrostatic potential, while retaining conformational transferability. Polarizabilities and atomic partial charges are parameterized for the amino acids, and it is shown that including polarization significantly improves the electrostatic description of point charges over multiple conformations. In addition, a polarizable and non-polarizble model for water and ammonia composed of point charges and induced Gaussian dipoles is presented by fitting to liquid phase heats of vaporization and density. Results are also presented for fitting a polarizable and non-polarizable water model only to ab-initio data, and limitations of the point charge model are discussed.

INDEX WORDS: induced Gaussian dipole, polarization, Gaussian multipole, molecular dynamics, AMBER, GLYCAM

POLARIZABLE FORCE FIELDS

by

DENNY ELKING

M.S. Physics, Washington University 2001

B.S., Physics and Mathematics, University of Missouri-St. Louis 1999

A Dissertation Submitted to the Graduate Faculty of The University of Georgia in Partial Fulfillment of the Requirements for the Degree

DOCTOR OF PHILOSOPHY

ATHENS, GEORGIA

2007

© 2007

Denny Elking

All Rights Reserved

POLARIZABLE FORCE FIELDS

by

DENNY ELKING

Major Professor: Robert J. Woods

Committee: David Landau
Will York

Electronic Version Approved:

Maureen Grasso
Dean of the Graduate School
The University of Georgia
August 2007

ACKNOWLEDGEMENTS

I would like to thank Prof. Robert J. Woods of the University of Georgia and Dr. Tom Darden of the National Institute of Environmental Health Sciences for all of their support and guidance over the past years.

I would also like to acknowledge and thank my committee (Prof. David Landau, Prof. Will York, and Prof. Bob Scott) for their valuable advice. I am grateful to all the people I have worked with from NIEHS and the CCRC including Andres Cisneros, Lalith Perera, Francisco Mendoza Ambrosio, Jean-Philip Piquemal, Lachele Foley, Jorge Outeirino, Jarrod Barnes, Sarah Wittkopp, Austin Yongye, and Ahmed Pathiaseril.

I would also like to acknowledge the Complex Carbohydrate Research Center, the National Institute of Environmental Health Sciences, the Center for Simulational Physics, and the University of Georgia Research Computing Center. Many thanks to Greg Derda at the RCC, Bob Bass at NIEHS, and all of the staff at NIEHS and the CCRC: including Amy Johnson, Sheilah Dixon, Melissa Akins, Lynn Berryman, Lane Guyer, Diane Hermosillo, Karen Howard, Tasashia McCormick, Beverly Chalk, and Lydia Shearer.

TABLE OF CONTENTS

Page

1 Introduction

1.1 Force Fields

In recent years, molecular dynamics simulations have increasingly become a useful tool for studying large molecular systems. Originally, simulations were used to study liquids. As computing power increased, simulations were gradually applied to biomolecular systems such as proteins, carbohydrates, DNA, and lipids. Today, simulations are routinely done on protein crystal structures to gain understanding of how these complicated structures operate.

Typical simulations usually involve $10^3 - 10^6$ atoms. For systems of this magnitude, the CPU requirements render electronic structure based methods impractical. For this reason, force fields have been developed as a set of simplified empirical energy equations capable of handling large molecular systems.

Early force fields were designed using intuitive notions of how atoms and molecules interact. Atoms in a molecule vibrate about their equilibrium positions. Therefore, energy can be expanded in a Taylor series about equilibrium bond lengths r_0 and bond angles θ_0. A truncated Fourier series is employed to describe torsion rotations about bond axes. The force field intramolecular energy, also called the valence energy, is given by eqn 1.1

$$E_{valence} = \sum \frac{1}{2} k(r - r_0)^2 + \frac{1}{2} k(\theta - \theta_0)^2 + \sum_{n=1}^{3} V_n \cos n\omega \qquad 1.1$$

Traditional force fields such as MM3[1-5], AMBER[6-10]/GLYCAM[11-13], and CHARMM[14-19] have this functional form. The valence energy is important in determining molecular geometries and vibrational frequencies. Hagler[20-22] et. al. has shown how to include higher order terms in the Taylor series by fitting to ab-initio conformational energies and

its derivatives. The resulting force field, CVFF, accurately predicts ab-initio geometries and vibrational frequencies for a wide range of molecular systems.

In addition to the valence part, there is a second part of the force field, which models intermolecular interactions. This non-bonded portion includes a long range electrostatic term, a short range exchange/repulsion, and a long range weakly attractive dispersion term. In traditional force fields, electrostatic interactions are commonly modeled by point charges on each atom. The short range repulsion and long range dispersion are often modeled by a 12-6 Lennard Jones potential. The resulting non-bond energy is given by:

$$E_{nonbond} = \sum \frac{q_i q_j}{r_{ij}} + \varepsilon_{ij}\left(\left(\frac{\sigma_{ij}}{r_{ij}}\right)^{12} - 2\left(\frac{\sigma_{ij}}{r_{ij}}\right)^{6}\right)$$

The non-bonded portion of the force field is particularly important because it largely determines condensed phase quantities such as thermodynamic properties of liquids and biomolecular-ligand interactions.

Recently, force fields, such as AMOEBA[23-25], SIBFA[26-28], and GEM[29-31], have been proposed to more accurately model electrostatic interactions. AMOEBA and SIBFA employ point multipoles, while the GEM force field is composed of an explicit charge density fitted using Gaussian basis sets. The multipole and density based force fields are able to more accurately reproduce high-level ab-initio data such as dimer energies and geometries. However, a drawback to these more elaborate force fields is the increase in CPU overhead. As a first estimate, multipole-based force fields such as AMOEBA and SIBFA require $10^1 - 10^2$ more CPU time over point charge force fields, while the density based GEM force field requires $10^1 - 10^3$ more CPU time.

The electrostatic and vdW interactions described above are constant with respect to molecular environment. However, it is known that molecular dipole moments change significantly when transferred from gas to liquid phase. Non-polarizable classical force fields based solely on additive models are not able to capture this effect. Rather, permanent molecular dipole interactions are often enhanced to compensate.

Including an explicit polarization term in the force field is a method to model these multi-body effects in condensed phases, while still being able to correctly calculate gas phase properties, such as dimer geometries and interaction energies. Polarization is likely to be particularly important in accurate descriptions of biomolecular interactions.

One goal of this study is to develop a polarization model suitable for use in the AMBER and GLYCAM force fields. Several polarization models such as the Drude oscillator[32 33], fluctuating charges[34], and induced dipoles[24 35 36] have been suggested for use in water models. This work will focus on the induced dipole polarization model, which places induced dipoles on each atom. In this case, the induced dipole $\vec{\mu}$ on an atom is the product of the total electric field $\vec{E}$ and a scalar atomic polarizability α.

$$\vec{\mu} = \alpha \vec{E} \qquad 1.1$$

The original induced dipole model of Applequist[37] places induced point dipoles on each atom. However, this model suffers from the so called 'polarization catastrophe': when two mutually interacting inducible dipoles with atomic polarizabilities α_1 and α_2 diverge at a finite distance, given by:

$$R = \left(4\alpha_1\alpha_2\right)^{1/6} \qquad 1.2$$

Thole[38] has proposed a solution by applying a damping function to induced dipole – induced dipole interactions. However, a drawback to this model is that it does not

prescribe how induced dipoles and permanent charges interact. Ad-hoc assumptions are needed to define interactions between induced dipoles and other charges for the Thole model.

An interesting question arises: since force fields based on charge density have recently been proposed[29-31] to model electrostatic interactions, is it possible to develop a polarization model based on charge density which does not contain the polarization catastrophe condition? In this work, an induced dipole model based on density will be developed. Before presenting a density based polarization model, it would be useful to first discuss electrostatic models based on charge density.

There is an interesting mathematical relationship between Gaussian functions and point multipoles. Consider a charge density composed of a simple normalized Gaussian function with total charge q:

$$\rho(\vec{r}) = q\left(\frac{\beta}{\sqrt{\pi}}\right)^3 \exp(-\beta^2 r^2) \qquad 1.3$$

For large exponents, the charge distribution becomes singular about the origin and behaves as a point charge or point monopole. For this reason, the charge distribution in 1.3 has been defined as a Gaussian monopole. In chapter two, higher order Gaussian multipoles and their relationship with Cartesian point multipoles are explored. A discussion of Cartesian tensors and Cartesian point multipoles is provided in appendix A. The results for Gaussian multipoles are used in chapter three to develop a polarization model based on induced Gaussian dipoles.

There is an interesting property of the induced Gaussian dipole model which relates to the polarization catastrophe. Since the interaction of two permanent Gaussian charge densities is finite at all distances, it might be expected that the interaction between

two induced Gaussian dipoles is finite at all distances. However, for large Gaussian exponents, the induced Gaussian dipoles behave as induced point dipoles. If the exponent is too large, the interaction is too strong and a polarization catastrophe can occur. A relationship for the maximum size of the Gaussian exponent is derived which will prevent a polarization catastrophe at all distances.

In chapter four, the implementation of induced Gaussian dipoles into the molecular dynamics (MD) simulation program AMBER[39] is presented. Results for polarization energy, work, and force are derived for the induced Gaussian dipole model. The Ewald summation[40-43] method for a system of charges in periodic boundary conditions is described. A brief discussion of the Car-Parinello[44 45] method to propagate induced dipoles during an MD simulation through an extended Lagrangian formalism is provided. Finally, results from simulation output are presented.

Once a polarization model has been established, a procedure for obtaining parameters for the model is needed. In chapter five, procedures to optimize atomic polarizabilities for the induced Gaussian dipole polarization model is discussed. Following Applequist and Thole, a set of atom type atomic polarizabilities are found by fitting to a collection of molecular polarizability tensors for the induced Gaussian dipole model, the Thole model, and the induced point dipole model. The performance of all three induced dipole models is compared. In addition to the conventional method of fitting atomic polarizabilities to molecular polarizability tensors, a second procedure is proposed to generate atomic polarizabilites. This procedure is based on probing a molecule with point charges and calculating the electrostatic potential around the

molecule. The 'probed' atomic polarizabilities are fit to the response potential, which is the potential in the presence of the charge probes minus the potential in vacuum.

In chapter six, probed polarizabilities and atomic point charges are generated for the amino acids. Probed polarizabilities are fit to the response potential through the procedure presented in the previous chapter and atomic point charges are found by the conventional method of fitting to total electrostatic potential of a molecule in vacuum. In order to make equal comparisons, a set of point charges is found with and without polarizability present. By exploring multiple conformations of single amino acids, polarization is shown to make a significant improvement in the electrostatic description of point charges. The charges and polarizabilities are tested on a 10 alanine peptide in the extended and α helical conformations.

In chapter seven, a polarizable and non-polarizable model for water and ammonia is presented. The models are developed by fitting a Lennard Jones repulsion parameter and a charge scale factor to heats of vaporization and density. Effective condensed phase charges for polarizable and non-polarizable force fields are discussed. The models are tested by calculating dimer energies and comparing with ab-initio results. An interesting question arises: can force field parameters be fit only to ab-initio data? In a second procedure, the vdW repulsion parameter, the atomic charges, and the polarizabilities for water are optimized only to ab-initio data. The model is tested by calculating the heats of vaporization and density. Finally, limitations with the point charge model are discussed.

In addition to the work presented in the chapters, background material has been included in appendices. As mentioned earlier, in appendix A, Cartesian tensors[46] are discussed and a derivation of electrostatic interactions in terms of Cartesian point

multipoles[47 48] is provided. In appendix B, a derivation of how a molecule interacts with an external field[49] is presented quantum mechanically through Rayleigh Schrödinger perturbation theory. In appendix C, long range intermolecular perturbation theory[49] is discussed. The intermolecular energy or dimer energy up to second order can be separated into electrostatic, polarization, and dispersion contributions. Finally, in appendix D, a derivation of the Ewald summation[40-43] for point charges and point dipoles is provided.

1.2 References

1 J-H Lii, Y. H. Yuh, and N. L. Allinger, J. Am. Chem. Soc. **111**, 8551 (1989)

2 J-H Lii and N. L. Allinger, J. Am. Chem. Soc. **111**, 8566 (1989a)

3 J-H Lii and N. L. Allinger, J. Am. Chem. Soc. **111**, 8576 (1989b)

4 J-H Lii and N. L. Allinger, J. Comp. Chem. **12**, 186 (1991)

5 J-H Lii and N. L. Allinger, J. Comp. Chem. **19**, 1001 (1998)

6 W. D. Cornell, P. Cieplak, C. I. Bayly, I. R. Gould, K. M. Merz Jr., D. M. Ferguson, D. C. Spellmeyer, T. Fox, J. W. Caldwell, and P. A. Kollman, J. Am. Chem. Soc. **117**, 5179 (1995)

7 D. A. Pearlman, D. A. Case, J. C. Caldwell, G. L. Seibel, U. C. Singh, P. Weiner, and P. A. Kollman, AMBER 4.0, (University of California, San Francisco) (1991)

8 Weiner, P. K., & Kollman, P. A., (1981) AMBER: Assisted Model Building with Energy Refinement. A General Program for Modeling Molecules and Their Interactions, J. Comp. Chem. **2**, 287-303.

[9] Weiner, S.J., Kollman, P.A., Case, D.A., Singh, U.C., Ghio, C., Alagona, G., Profeta, S., Jr., Weiner, P.K. (1984) A new force field for molecular mechanical simulation of nucleic acids and proteins. J. Am. Chem. Soc. **106**, 765-784.

[10] S. J. Weiner, P. A. Kollman, D. T. Nguyen, and D. A. Case, J. Comp. Chem. **7**, 230 (1986)

[11] R. J. Woods, R. A. Dwek, C. J. Edge, and B. Fraserreid, J. Phys. Chem. **99** (**11**), 3832 (1995)

[12] M. Basma, S. Sundara, D. Calgan, T. Vernali, and R. J. Woods, J. Comp. Chem. **22** (**11**), 1125 (2001)

[13] R. J. Woods and R. Chappelle, J. Mol. Struct. **527**, 149 (2000)

[14] Brooks, B.R., Bruccoleri, R.E., Olafson, B.D., States, D.J., Swaminathan, S., Karplus, M. (1983) CHARMM: A program for macromolecular energy, minmimization, and dynamics calculations. J. Comp. Chem. 4, 187-217.

[15] Feller et al., Biophys. J. **73**, 2269 (1997)

[16] A. D. MacKerell, D. Bashford, M. Bellott, R. L. Dunbrack, J. D. Eva seck, M. J. Field, S. Fischer, J. Gao, H. Guo, S. Ha, D. JosephMcCarthy, L. Kuc nir, K. Kuczera, F. T. K. Lau, C. Mattos, S. Michnick, T. Ngo, D. T. Nguyen, B. Pro hom, W. E. Reiher, B. Roux, M. Schlenkrich, J. C. Smith, R. Stote, J. Straub, M. Watanabe, J. Wiorkiewiczkuczera, D. Yin, and M. Karplus, J. Phys. Chem., B **102**, 3586 (1998)

[17] A. D. Mackerell J. Wiorkiewiczkuczera, and M. Karplus, J. Amer. Chem. Soc., **117**, 11946 (1995)

[18] F. A. Momany, and R. Rone, Validation of the General Purpose QUANTA 3.2/CHARMm Force Field, J. Comp. Chem. **13**, 888 (1992)

[19] J. J. Pavelites, J. Gao, P.A. Bash and A. D. Mackerell, Jr. J. Comp. Chem. **18**, 221 (1997)

[20] J. R. Maple, M.-J., Hwang, T. P. Stockfisch, U. Dinur, M. Waldman, C. S. Ewig, and A. T. Hagler, J. Comp. Chem **15**, 162 (1994)

[21] M.–J. Hwang, T. P. Stockfisch, and A. T. Hagler, J. Amer. Chem. Soc., **116**, 2515 (1994)

[22] J. R. Maple, M.-J., Hwang, T. P. Stockfisch, and A. T. Hagler, Israel J. Chem., **34**, 195 (1994b).

[23] P. Ren, A. Grossfield, and J. W. Ponder, AMOEBA Force Field, ftp://dasher.wustl.edu/pub/tinker/params.

[24] P. Ren and J. W. Ponder, J. Phys. Chem. B **107**, 5933 (2003)

[25] P. Ren and J. W. Ponder, J. Comp. Chem. **23**, 1497 (2002)

[26] N. Gresh, P. Claverie, and A. Pullman, Theoret, Chim. Acta, **66**, 1 (1984)

[27] N. Gresh, P. Claverie, and A. Pullman, Int. J. Quantum Chem., **29**, 101 (1986)

[28] N. Gresh, J. Comp. Chem. **16**, 856 (1995)

[29] G. A. Cisneros, J. P. Piquemal, and T. A. Darden, J. Chem. Phys. **125**, 184101 (2006)

[30] J. P. Piquemal, G. A. Cisneros, P. Reinhardt, N. Gresh, and T. A. Darden, J. Chem. Phys. **124**, 104101 (2005)

[31] G. A. Cisneros, J. P. Piquemal, and T. A. Darden, J. Chem. Phys. **123**, 044109 (2005)

[32] G. Lamoureux, A. D. MacKerell, and B. J. Roux, J. Chem. Phys. **119**, 5185 (2003)

[33] H. Yu, T. Hansson, and W.F. van Gunsteren, J. Chem. Phys. **118**, 221 (2003)

[34] S. W. Rick, S.J. Stuart, and B.J. Berne, J. Chem. Phys. **101**, 6141 (1994)

[35] J. Caldwell, L. X. Dang, and P. A. Kollman, J. Am. Chem. Soc. **112**, 9144 (1990)

[36] C. J. Burnham, J. Li, S. S. Xantheas, and M. Leslie, J. Chem. Phys. **110**, 4566 (1999)

[37] J. Applequist, J. R. Carl, and K. K. Fung, J. Am. Chem. Soc. **94**, 2952 (1972)

[38] B. T. Thole, Chem. Phys. **59**, 341 (1981)

[39] D. A. Case, T. A. Darden, T. E. Cheatham III, C. L. Simmerling, J. Wang, R. E. Duke, R. Luo, K. M. Merz, D. A. Pearlman, M. Crowley, R. C. Walker, W. Zhang, B. Wang, S. Hayik, A. Roitberg, G. Seabra, K. F. Wong, F. Paesani, X. Wu, S. Brozell, V. Tsui, H. Gohlke, L. Yang, C. Tan, J. Mongan, V. Hornak, G. Cui, P. Beroza, D. H. Mathews, C. Schafmeister, W. S. Ross, and P. A. Kollman, AMBER 9, University of California, San Francisco (2006)

[40] Ewald P. Ann. Phys. **64**, 253 (1921)

[41] S. W. Leeuw, J. W. Perram, E. R. Smith, Proc. R. Soc. Lond. A. **373**, 27 (1980)

[42] S. W. Leeuw, J. W. Perram, E. R. Smith, Proc. R. Soc. Lond. A. **373**, 57 (1980)

[43] S. W. Leeuw, J. W. Perram, E. R. Smith, Proc. R. Soc. Lond. A. **388**, 177 (1980)

[44] R. Car and M. Parrinello, Phys. Rev. Lett. **55**, 2471 (1985)

[45] A. Toukmaji, C. Sagui, J. Board, and T. A. Darden, J. Chem. Phys. **113**, 10913 (2000)

[46] J. Applequist, J. Math. Phys. **24 (4)**, 736 (1983)

[47] J. Applequist, Chem. Phys. 85, 279-290 (1984)

[48] J. Applequist, J. Chem. Phys. 83, 809-826 (1985)

[49] A. Stone, *Intermolecular Forces*, (Oxford University Press, New York, 1996)

2 Gaussian Multipoles

2.1 Introduction

Cartesian point multipoles (see appendix A) provide an excellent description of electrostatic interactions between charge distributions which are sufficiently far away from one another. However, at smaller separations when the charge distributions overlap, the assumptions used in the point multipole description are no longer valid. An example of when two charge distributions overlap and multipole interactions do not accurately account for the electrostatic interaction is the water dimer. Cisneros[1-3] et. al. fit electron density through auxiliary basis sets to ab-initio electron density calculated at B3LYP/aug-cc-pVTZ by minimizing the Coulomb self energy of the molecule. It was shown that a multipole description up to quadrapoles[1] on each atom predicts an electrostatic interaction energy of -5.9 kcal/mol, while the ab-initio electrostatic energy of the water dimer was calculated to be -8.2 kcal/mol using constrained space orbital variation[4] (CSOV) energy decomposition. It is interesting to note that atomic point charges generated from the conventional method of optimizing to electrostatic potential predict an electrostatic interaction energy of -4.5 kcal/mol.

A more important reason to study density based electrostatic models is simulation stability. Electrostatic models based on point multipoles diverge for small R as R^{-n} for $n \geq 1$. A point multipole model for electrostatic interactions may be justified in empirical force fields by using a strong repulsive vdw potential to counteract the attractive electrostatic potential interactions for small R. However, this argument does not apply to polarization models based on induced point multipoles. In the following chapter, the

induced dipole polarization model is discussed. For small separations, induced point dipole – induced point dipole interactions diverge[5] as $(R - R_0)^{-1}$. Simulations that use the induced point dipole polarization model occasionally encounter 'polarization catastrophes' and fail when two atoms get too close. On the other hand, electrostatic models based on explicit charge density are finite at all distances. It will be shown in the following chapter that polarization interactions based on an induced charge density model is finite at all distances if the charge distribution is sufficiently diffuse.

A model based on charge density is needed to accurately model electrostatic and polarization interactions at short range and provide stability to simulations which use explicit polarization. Recently, force fields and simulations[6-8] have begun to use simple 's' orbital and 'p' orbital Gaussian charge densities to model electrostatic interactions. In this chapter, Gaussian multipole[9] charge distributions will be discussed as a smooth continuous generalization of Cartesian point multipole distributions. At long range, Gaussian multipoles behave as point multipoles[10]. At short range, Gaussian multipoles provide a more realistic description when charge distributions overlap which can be signifcant[11].

Before making a precise definition of a Gaussian multipole charge distribution, a simple example will serve as motivation for what follows. Consider a simple radially symmetric Gaussian charge distribution with exponent β, total charge q, and center $\vec{R}$ given by:

$$\rho^{(0)}(\vec{r};\vec{R}) = q\left(\frac{\beta}{\sqrt{\pi}}\right)^3 \exp(-\beta^2\left|\vec{r}-\vec{R}\right|^2) \qquad 2.1.1$$

For small Gaussian exponents, the charge distribution is diffuse and for large exponents, the charge distribution is sharply localized around the center $\vec{R}$. In section 2.4 and 2.7, the electrostatic potential will be derived for this charge distribution, and the result is given by:

$$\varphi^0(\vec{r};\vec{R}) = q\frac{erf(\beta|\vec{r}-\vec{R}|)}{|\vec{r}-\vec{R}|} \qquad 2.1.2$$

where $erf(x)$[2] is the error function[12] defined by $erf(x) \equiv \frac{2}{\sqrt{\pi}}\int_0^x du \exp(-u^2)$. Notice for large x, $erf(x) \to 1$. Hence for a large Gaussian exponent β, the potential from the simple Gaussian charge distribution becomes:

$$\varphi^0(\vec{r};\vec{R}) \cong q\frac{1}{|\vec{r}-\vec{R}|} \qquad 2.1.3$$

i.e. the potential due to a point charge or point monopole. For this reason, the charge distribution in 2.1.1 is defined as a Gaussian monopole.

In the following section, higher order Gaussian multipole charge distributions are defined, e.g. dipole, quadrapole, etc. In sections 2.3 and 2.4, electrostatic interaction energies are derived between different Gaussian multipole charge distributions. In section 2.5, it will be shown that in the limit of large Gaussian exponents, Gaussian multipoles behave like point multipoles. In section 2.6, the force terms are derived for Gaussian multipoles. This treatment parallels the force derivation for point multipoles given in appendix A.5. In section 2.7, electrostatic potential and fields are derived for Gaussian multipole charge distributions. In appendix A.7, it was shown that interaction energies between point multipoles can be conveniently expressed in terms of electrostatic

potential, field, or field gradient. In order to formally treat Gaussian multipoles in a way that parallels point multipoles, 'effective' electrostatic potential and fields are introduced in section 2.8. As in the case of point multipoles with ordinary potential and fields, interaction energies between Gaussian multipoles can be expressed in terms of 'effective' potentials and fields. Finally, in section 2.9, Hermite Gaussian charge distributions are briefly discussed in the context of electronic structure calculations. The results for electron repulsion integrals using Gaussian basis sets can be compared to electrostatic interaction energies between Gaussian multipoles.

2.2 Gaussian Multipole Charge Distributions

A spherically symmetric charge distribution of a simple Gaussian monopole function with exponent β and charge q centered at $\vec{R}$ was given in 2.1.1 as:

$$\rho^{(0)}(\vec{r};\vec{R}) = q\left(\frac{\beta}{\sqrt{\pi}}\right)^3 \exp(-\beta^2\left|\vec{r}-\vec{R}\right|^2) \qquad 2.2.1$$

One subtle point should be addressed before proceeding. In appendix A.2, Cartesian tensors are discussed in order to express results in condensed form. A common convention that will be used in this treatment is to implicitly sum over repeated indices unless otherwise stated. For example, the center vector $\vec{R}$ can be expressed in component form as $\vec{R} = R_1\hat{x}_1 + R_2\hat{x}_2 + R_3\hat{x}_3 \equiv R_p\hat{x}_p$. For vectors/tensors involving components (p =1,2,3 for x,y,z) or particles (i = 1,.. N), the particle index will usually be denoted (when possible) as a superscript and the component index as a subscript. For example, the position of particle 2 is given by: $\vec{R}^2 = R_p^2\hat{x}_p$. See appendix A.2 for a further discussion of Cartesian vector/tensors.

A Gaussian dipole charge distribution with exponent β and dipole moment $\vec{\mu}$ centered at $\vec{R}$ is defined as:

$$\rho^{(1)}(\vec{r};\vec{R}) = \vec{\mu}\cdot\nabla^{R}\left(\frac{\beta}{\sqrt{\pi}}\right)^{3}\exp(-\beta^{2}\left|\vec{r}-\vec{R}\right|^{2}) \qquad 2.2.2$$

The gradient is respect to the center coordinate, i.e. $\nabla^{R} \equiv \hat{x}_{p}\frac{\partial}{\partial R_{p}}$. Similarly, a Gaussian quadrapole charge distribution with exponent β and Cartesian quadrapole tensor $\Theta \equiv \Theta_{pq}\hat{x}_{p}\hat{x}_{q}$ is defined as

$$\rho^{(2)}(\vec{r};\vec{R}) = \Theta\cdot\nabla^{(2),R}\left(\frac{\beta}{\sqrt{\pi}}\right)^{3}\exp(-\beta^{2}\left|\vec{r}-\vec{R}\right|^{2}) \qquad 2.2.3$$

where $\nabla^{(2)} \equiv \nabla\nabla$ is a second rank gradient tensor, and $\Theta\cdot\nabla^{(2),R} \equiv \Theta_{pq}\frac{\partial^{2}}{\partial R_{p}\partial R_{q}}$ is a tensor contraction of rank 2. More generally, an n^{th} order Gaussian multipole can be defined as an n^{th} rank tensor contraction between an n^{th} rank multipole moment $\Theta^{(n)} \equiv \Theta^{(n)}_{p_1 p_2 \cdots p_n}\hat{x}_{p_1}\hat{x}_{p_2}..\hat{x}_{p_n}$ and an n^{th} rank gradient $\nabla^{(n)} \equiv \nabla\nabla...\nabla$ of a simple normalized Gaussian function:

$$\rho^{(n)}(\vec{r};\vec{R}) = \Theta^{(n)}\cdot\nabla^{(n),R}\left(\frac{\beta}{\sqrt{\pi}}\right)^{3}\exp(-\beta^{2}\left|\vec{r}-\vec{R}\right|^{2}) \qquad 2.2.4$$

The n^{th} rank moment tensor $\Theta^{(n)}$ is symmetric with respect to interchanging component indices, i.e. $\Theta^{(n)}_{..p_i..p_j..} = \Theta^{(n)}_{..p_j..p_i..}$

A motivation for defining these charge densities as Gaussian multipoles is that the n^{th} ranked multipole moment integral[13] (A.3.6) of the charge density $\rho^{(n)}(\vec{r};\vec{R})$ is $\Theta^{(n)}$, i.e.

$$\frac{1}{n!}\int d^3r\,(r-R)^{(n)}\,\rho^{(n)}(\vec{r};\vec{R}) = \Theta^{(n)} \qquad 2.2.5$$

For example, the total charge of $\rho^{(0)}(\vec{r};\vec{R})$ is q, since

$$\int d^3r\,\rho^{(0)}(\vec{r};\vec{R}) = q \qquad 2.2.6$$

This can be seen by using the following integral: $\int_{-\infty}^{\infty}\exp(-\beta^2x^2)dx = \frac{\sqrt{\pi}}{\beta}$. Before proving 2.2.5 by induction, it is noted that 2.2.4 can be expressed in terms of gradients with respect to r.

$$\rho^{(n)}(\vec{r};\vec{R}) = (-1)^n\,\Theta^{(n)}\cdot\nabla^{(n),r}\left(\frac{\beta}{\sqrt{\pi}}\right)^3\exp(-\beta^2\left|\vec{r}-\vec{R}\right|^2) \qquad 2.2.7$$

since $\nabla^R F(\left|\vec{r}-\vec{R}\right|) = -\nabla^r F(\left|\vec{r}-\vec{R}\right|)$. For brevity, suppose $\vec{R}=0$. Let $\Delta^{(n)}$ be the n^{th} rank moment tensor of 2.2.7. It will be shown that if $\Delta^{(n-1)} = \Theta^{(n-1)}$, then $\Delta^{(n)} = \Theta^{(n)}$.

The $(p_1\,p_2\,\ldots p_n)$ component $\Delta^{(n)}$ is given by:

$$\begin{aligned}\Delta_{p_1p_2\ldots p_n} &= \frac{1}{n!}\int d^3r\,r_{p_1}r_{p_2}..r_{p_n}\rho^{(n)}(\vec{r};0)\\ &= \frac{(-1)^n}{n!}\int d^3r\,r_{p_1}r_{p_2}..r_{p_n}\Theta^{(n)}\cdot\nabla^{(n),r}\left(\frac{\beta}{\sqrt{\pi}}\right)^3\exp(-\beta^2r^2) \qquad 2.2.8\\ &= \frac{(-1)^n}{n!}\int d^3r\,r_{p_1}r_{p_2}..r_{p_n}\Theta_{q_1q_2..q_n}\nabla^r_{q_1}\nabla^r_{q_2}..\nabla^r_{q_n}\rho^{(0)}(\vec{r};0)\end{aligned}$$

The integrand can be integrated by parts with respect to $\nabla^r_{q_1}$:

$$\begin{aligned}\Delta_{p_1 p_2 \ldots p_n} = & \frac{(-1)^n}{n!}\int d^3 r\, \nabla^r_{q_1}\{r_{\mathrm{p}_1} r_{\mathrm{p}_2} .. r_{\mathrm{p}_n} \Theta_{q_1 q_2 .. q_n} \nabla^r_{q_2} .. \nabla^r_{q_n} \rho^{(0)}(\vec{r};0)\} + \\ & \frac{(-1)^{n-1}}{n!}\int d^3 r\, (\nabla^r_{q_1} r_{\mathrm{p}_1}) r_{\mathrm{p}_2} .. r_{\mathrm{p}_n} \Theta_{q_1 q_2 .. q_n} \nabla^r_{q_2} .. \nabla^r_{q_n} \rho^{(0)}(\vec{r};0) + \\ & \frac{(-1)^{n-1}}{n!}\int d^3 r\, r_{\mathrm{p}_1} (\nabla^r_{q_1} r_{\mathrm{p}_2}) .. r_{\mathrm{p}_n} \Theta_{q_1 q_2 .. q_n} \nabla^r_{q_2} .. \nabla^r_{q_n} \rho^{(0)}(\vec{r};0) + .. \\ & \frac{(-1)^{n-1}}{n!}\int d^3 r\, r_{\mathrm{p}_1} r_{\mathrm{p}_2} .. (\nabla^r_{q_1} r_{\mathrm{p}_n}) \Theta_{q_1 q_2 .. q_n} \nabla^r_{q_2} .. \nabla^r_{q_n} \rho^{(0)}(\vec{r};0)\end{aligned} \qquad 2.2.9$$

The first term is a surface term and is zero when evaluated at the boundary of 3D space. This can be seen by using the following identity[14]: $\int_V d^3 x \nabla f(x) = \oiint_S f(x) d\vec{S}$, where $f(x)$ is a continuous function, V is an arbitrary volume and S is a closed surface surrounding V.

Since $\nabla^r_{q_1} r_{\mathrm{p}_i} = \delta_{q_1 \mathrm{p}_i}$, 2.2.9 becomes:

$$\begin{aligned}&\Delta_{p_1 p_2 \cdot p_n} \\ &= \frac{(-1)^{n-1}}{n!}\int d^3 r\, \{\delta_{q_1 \mathrm{p}_1} r_{\mathrm{p}_2} .. r_{\mathrm{p}_n} + r_{\mathrm{p}_1} \delta_{q_1 \mathrm{p}_2} .. r_{\mathrm{p}_n} + \\ &\qquad .. r_{\mathrm{p}_1} r_{\mathrm{p}_2} .. \delta_{q_1 \mathrm{p}_n}\} \Theta_{q_1 q_2 .. q_n} \nabla^r_{q_2} .. \nabla^r_{q_n} \rho^{(0)}(\vec{r};0)\Big\}\end{aligned} \qquad 2.2.10$$

Each of the individual terms is moment integral of rank $n - 1$, for which the theorem holds. 2.2.10 then becomes

$$\begin{aligned}\Delta_{p_1 p_2 \cdot p_n} &= \frac{1}{n}(\Theta_{p_1 p_2 .. p_n} + \Theta_{p_2 p_1 .. p_n} + .. \Theta_{p_n p_2 .. p_1}) \\ &= \Theta_{p_1 p_2 .. p_n}\end{aligned} \qquad 2.2.11$$

where the last step made use that $\Theta_{p_1 p_2 .. p_n}$ is symmetric. Therefore, the theorem holds for all n.

2.3 Interaction Energies

The electrostatic interaction energy between an n^{th} order Gaussian multipole $\Theta^{(n),1}$ with exponent β_1 centered at $\vec{R}^1$ and a m^{th} order Gaussian multipole $\Theta^{(m),2}$ with exponent β_2 centered at $\vec{R}^2$ is given by:

$$U_{nm}^{12} = \int\int d^3r\, d^3r' \frac{\rho^n(\vec{r};\vec{R}^1)\rho^m(\vec{r}';\vec{R}^2)}{|\vec{r}-\vec{r}'|}$$

$$= \left(\frac{\beta_1\beta_2}{\pi}\right)^3 \int\int d^3r\, d^3r' \frac{\Theta^{(n),1}\cdot\nabla^{(n),1}\Theta^{(m),2}\cdot\nabla^{(m),2}\exp(-\beta_1^2|\vec{r}-\vec{R}^1|^2-\beta_2^2|\vec{r}'-\vec{R}^2|^2)}{|\vec{r}-\vec{r}'|}$$

The gradients are with respect to center coordinates and can be pulled out of the integral.

$$U_{nm}^{12} = \Theta^{(n),1}\cdot\nabla^{(n),1}\Theta^{(m),2}\cdot\nabla^{(m),2}U_{00} \qquad 2.3.1$$

where U_{00} is the electrostatic energy between two Gaussian monopole charge distributions of unit charge:

$$U_{00}(|\vec{R}^1-\vec{R}^2|) \equiv \left(\frac{\beta_1\beta_2}{\pi}\right)^3 \int\int d^3r\, d^3r' \frac{\exp(-\beta_1^2|\vec{r}-\vec{R}^1|^2-\beta_2^2|\vec{r}'-\vec{R}^2|^2)}{|\vec{r}-\vec{r}'|} \qquad 2.3.2$$

2.4 Evaluation of U_{00}

The following derivation of U_{00} can be found in[15]. U_{00} can be expressed as an integral of electrostatic potential $\varphi^0(\vec{r};\vec{R}^2)$ from a Gaussian monopole with unit charge centered at $\vec{R}^2$ and a second charge Gaussian monopole charge density $\rho^0(\vec{r};\vec{R}^1)$ with unit charge centered at $\vec{R}^1$:

$$U_{00} = \int d^3r \rho^0(\vec{r};\vec{R}^1)\varphi^0(\vec{r};\vec{R}^2) \qquad 2.4.1$$

where:

$$\rho^0(\vec{r};\vec{R}^1) \equiv \left(\frac{\beta_1}{\sqrt{\pi}}\right)^3 \exp(-\beta_1^2\left|\vec{r}-\vec{R}^1\right|^2) \qquad 2.4.2$$

$$\varphi^0(\vec{r};\vec{R}^2) \equiv \left(\frac{\beta_2}{\sqrt{\pi}}\right)^3 \int d^3r' \frac{\exp(-\beta_2^2\left|\vec{r}'-\vec{R}^2\right|^2)}{\left|\vec{r}-\vec{r}'\right|} \qquad 2.4.3$$

The denominator in 2.4.3 can be expressed in terms of a Gaussian integral:

$$\frac{1}{\left|\vec{r}-\vec{r}'\right|} = \frac{2}{\sqrt{\pi}} \int_0^\infty du \exp(-u^2\left|\vec{r}-\vec{r}'\right|^2) \qquad 2.4.4$$

and then inserted back into 2.4.3,

$$\varphi^0(\vec{r};\vec{R}^2) = \left(\frac{\beta_2}{\sqrt{\pi}}\right)^3 \frac{2}{\sqrt{\pi}} \int_0^\infty du \int d^3r' \exp(-\beta_2^2\left|\vec{r}'-\vec{R}^2\right|^2) \exp(-u^2\left|\vec{r}-\vec{r}'\right|^2)$$

$$= \left(\frac{\beta_2}{\sqrt{\pi}}\right)^3 \frac{2}{\sqrt{\pi}} \int_0^\infty du \int d^3r' \exp(-(\beta_2^2+u^2)\left|\vec{r}'-\vec{X}\right|^2) \exp(-\frac{u^2\beta_2^2\left|\vec{r}-\vec{R}^2\right|^2}{u^2+\beta_2^2})$$

where $\vec{X} \equiv \frac{u^2\vec{r}+\beta_2^2\vec{R}}{u^2+\beta_2^2}$. Performing the integration over r' gives:

$$\varphi^0(\vec{r};\vec{R}^2) = \left(\frac{\beta_2}{\sqrt{\pi}}\right)^3 \frac{2}{\sqrt{\pi}} \int_0^\infty du \left(\frac{\pi}{u^2+\beta_2^2}\right)^{3/2} \exp(-\frac{u^2\beta_2^2\left|\vec{r}-\vec{R}^2\right|^2}{u^2+\beta_2^2}) \qquad 2.4.5$$

Transform variables, $x^2 \equiv \frac{u^2\beta_2^2\left|\vec{r}-\vec{R}^2\right|^2}{u^2+\beta_2^2}$

$$\varphi^0(\vec{r};\vec{R}^2) = \frac{1}{\left|\vec{r}-\vec{R}^2\right|} \frac{2}{\sqrt{\pi}} \int_0^{\beta_2\left|\vec{r}-\vec{R}^2\right|} dx \exp(-x^2) \qquad 2.4.6$$

This result can be written in terms of the error function[12].

$$\varphi^0(\vec{r};\vec{R}^2) = \frac{erf(\beta_2\left|\vec{r}-\vec{R}^2\right|)}{\left|\vec{r}-\vec{R}^2\right|} \qquad 2.4.7$$

Before evaluating the electrostatic energy, 2.4.6 can be transformed into another useful form by letting $t \equiv \frac{x}{\left|\vec{r} - \vec{R}^2\right|}$

$$\varphi^0(\vec{r};\vec{R}^2) = \frac{2}{\sqrt{\pi}} \int_0^{\beta_2} dt \exp(-t^2 \left|\vec{r} - \vec{R}^2\right|^2) \tag{2.4.8}$$

The electrostatic energy can be found by inserting 2.4.8 into 2.4.1

$$\begin{aligned} U_{00} &= \left(\frac{\beta_1}{\sqrt{\pi}}\right)^3 \frac{2}{\sqrt{\pi}} \int_0^{\beta_2} dt \int d^3 r \exp(-\beta_1^2 \left|\vec{r} - \vec{R}^1\right|^2) \exp(-t^2 \left|\vec{r} - \vec{R}^2\right|^2) \\ &= \left(\frac{\beta_1}{\sqrt{\pi}}\right)^3 \frac{2}{\sqrt{\pi}} \int_0^{\beta_2} dt \left(\frac{\pi}{\beta_1^2 + t^2}\right)^{3/2} \exp\left(\frac{-\beta_1^2 t^2 \left|\vec{R}^1 - \vec{R}^2\right|^2}{\beta_1^2 + t^2}\right) \end{aligned} \tag{2.4.9}$$

Now let $v^2 \equiv \frac{\beta_1^2 t^2 \left|\vec{R}^1 - \vec{R}^2\right|^2}{\beta_1^2 + t^2}$, U_{00} becomes

$$\begin{aligned} U_{00} &= \frac{1}{R^{12}} \frac{2}{\sqrt{\pi}} \int_0^{\beta_{12} R^{12}} dv \exp(-v^2) \\ &= \frac{erf(\beta_{12} R^{12})}{R^{12}} \end{aligned} \tag{2.4.10}$$

where $\beta_{12} \equiv \frac{\beta_1 \beta_2}{\sqrt{\beta_1^2 + \beta_2^2}}$ and $R^{12} \equiv \left|\vec{R}^1 - \vec{R}^2\right|$.

2.5 Gaussian Multipoles and Point Multipoles

The expression 2.4.10 for U_{00} can now be substituted into 2.3.1 to arrive at the the electrostatic interaction energy U_{nm}^{12} between an n^{th} and m^{th} order Gaussian multipole:

$$\begin{aligned} U_{nm}^{12} &= \Theta^{(n),1} \cdot \nabla^{(n),1} \Theta^{(m),2} \cdot \nabla^{(m),2} \frac{erf(\beta_{12} R^{12})}{R^{12}} \\ &= (-1)^m \Theta^{(n),1} \Theta^{(m),2} \cdot \nabla^{(n+m),1} \frac{erf(\beta_{12} R^{12})}{R^{12}} \end{aligned} \tag{2.5.1}$$

In the last step, ∇^1 does not act on $\Theta^{(m),2}$. In particular, the Gaussian multipole energies up to dipole- dipole are given by:

monopole-monopole $$U_{00}^{12} = q^1 q^2 \frac{erf(\beta_{12} R^{12})}{R^{12}} \qquad 2.5.2.a$$

monopole-dipole $$U_{01}^{12} = -q^1 \vec{\mu}^2 \cdot \nabla^1 \frac{erf(\beta_{12} R^{12})}{R^{12}} \qquad 2.5.2.b$$

dipole-dipole $$U_{11}^{12} = -\vec{\mu}^1 \vec{\mu}^2 \cdot \nabla^{(2),1} \frac{erf(\beta_{12} R^{12})}{R^{12}} \qquad 2.5.2.c$$

If the large exponent limit is applied to the interaction energies in 2.4.1, $\beta_1, \beta_2, \beta_{12} \rightarrow \infty$, and $erf(x) \rightarrow 1$ as $x \rightarrow \infty$, and the n^{th} m^{th} Gaussian multipole interaction energy becomes:

$$U_{nm}^{12} = (-1)^m \Theta^{(n),1} \Theta^{(m),2} \cdot \nabla^{(n+m),1} \frac{1}{R^{12}} \qquad 2.5.3$$

i.e. the interaction energy of point multipoles in A.4.14.

In the expression for Gaussian charge density, the exponent determines how localized or diffuse the density is about the center.

$$\rho_0(\vec{r}; \vec{R}) = q\left(\frac{\beta}{\sqrt{\pi}}\right)^3 e^{-\beta^2 |\vec{r} - \vec{R}|^2} \qquad 2.5.4$$

For small exponents, the charge density is diffuse and spread out in space. For large exponents, the charge density becomes sharply localized near the center. In the large exponent limit, the charge density for the Gaussian monopole becomes that of a point charge.

$$\lim_{\beta \rightarrow \infty} q\left(\frac{\beta}{\sqrt{\pi}}\right)^3 e^{-\beta^2 |\vec{r} - \vec{R}|^2} = q\delta^{(3)}(\vec{r} - \vec{R}) \qquad 2.5.5$$

Use has been made by one of the representations of the 3D Dirac-Delta function[16]

$$\delta^{(3)}(\vec{r}-\vec{R}) = \lim_{\beta\to\infty}\left(\frac{\beta}{\sqrt{\pi}}\right)^3 e^{-\beta^2\left|\vec{r}-\vec{R}\right|^2} \qquad 2.5.6$$

2.6 Force and Torque

The following treatment for forces between Gaussian multipoles is almost identical to the derivation given for point multipoles in appendix A.5 and is summarized here for completeness. The force on particle 1 $\vec{F}^1$ due to the $n^{\text{th}} - m^{\text{th}}$ rank Gaussian multipole interaction between particle 1 and 2 is defined as the negative gradient with respect to particle 1

$$\vec{F}^1 = -\nabla^1 U_{nm}^{12} \qquad 2.6.1$$

The multipole moment $\Theta^{(n),1}$ on each atom can be defined with respect to the constant global reference frame $\hat{x}_1, \hat{x}_2, \hat{x}_3$ or a local (body) coordinate frame $\hat{x}'_1, \hat{x}'_2, \hat{x}'_3$. The local coordinate frame of atom 1 can be defined in terms of atom 1's position $\vec{R}^1$ and also the positions of atom 1's neighbors $\vec{R}^a$ and $\vec{R}^b$. The local frame is related to the global frame by a rotation matrix D_{qp}.

$$\hat{x}'_p \equiv \sum_{q=1}^{3} D_{qp}\hat{x}_q = D_{qp}\hat{x}_q \qquad 2.6.2$$

The components of $\Theta^{(n),1}$ in the global frame ${}^G\Theta^{(n),1}_{pq\ldots r}$ are related to the components in the local (body) frame ${}^B\Theta^{(n),1}_{pq\ldots r}$ by

$${}^G\Theta^{(n),1}_{pq\ldots r} = D_{pp'}D_{qq'}..D_{rr'}\,{}^B\Theta^{(n),1}_{p'q'\ldots r'} \qquad 2.6.3$$

The derivative of $\Theta^{(n),1}$ with respect to ∇^1 was derived in appendix A.5 and is given by:

$$\nabla^1\Theta^{(n),1} = n\hat{x}_v \frac{\partial D_{ps}}{\partial R_v^1} D_{st}^T\,{}^G\Theta^{(n),1}_{tq\ldots r}\hat{x}_p\hat{x}_q..\hat{x}_r \qquad 2.6.4$$

Therefore, the force on atom 1 is given by:

$$\vec{F}_1 = (-1)^{m+1}(\nabla^1\Theta^{(n),1})\Theta^{(m),2}\cdot\nabla^{(n+m),1}\frac{erf(\beta_{12}R^{12})}{R^{12}} + (-1)^{m+1}\Theta^{(n),1}\Theta^{(m),2}\cdot\nabla^{(n+m+1),1}\frac{erf(\beta_{12}R^{12})}{R^{12}} \qquad 2.6.5$$

The first term on the right side of 2.6.5 is a torque term since it is a derivative with respect to orientation. The second term is a derivative of energy with respect to translation of the distance between the two multipoles and is the ordinary translational force term. Finally, it should be noted that the interaction U_{nm}^{12} contributes force terms to atom 1 and atom 2, and also to the neighbors of atom1 and atom 2.

2.7 Electrostatic Potential and Field

The electrostatic potential can be defined in two equivalent ways. In appendix A.6, the electrostatic potential was defined as the variation in energy of a system when an infinitesimal point charge was added to the system, $\varphi \equiv \lim_{\delta q\to 0}\frac{\delta U}{\delta q}$ [14]. Potential can also be defined as a Coulomb integral over charge density $\rho(r)$, given by:

$$\varphi(\vec{r}) \equiv \int d^3r'\,\rho(r')\frac{1}{|\vec{r}-\vec{r}'|} \qquad 2.7.1$$

This definition was used in 2.4.3 for the calculation of φ_0, the electrostatic potential of a Gaussian monopole with unit charge. Using the definition for potential in 2.7.1, the electrostatic potential for a Gaussian multipole with charge density by 2.2.4 is:

$$\begin{aligned}\varphi_m(\vec{r};\vec{R}^2) &= \Theta^{(m),2}\cdot\nabla^{(m),2}\left(\frac{\beta_2}{\sqrt{\pi}}\right)^3\int d^3r'\exp(-\beta_2^2|\vec{r}'-\vec{R}^2|^2)\frac{1}{|\vec{r}-\vec{r}'|} \\ &= \Theta^{(m),2}\cdot\nabla^{(m),2}\varphi^0(\vec{r};\vec{R}^2)\end{aligned} \qquad 2.7.2$$

Using the result for φ^0 in 2.4.7

$$\begin{aligned}\varphi_m(\vec{r};\vec{R}^2) &= \Theta^{(m),2}\cdot\nabla^{(m),2}\frac{erf(\beta_2\left|\vec{r}-\vec{R}^2\right|)}{\left|\vec{r}-\vec{R}^2\right|}\\ &= (-1)^m\Theta^{(m),2}\cdot\nabla^{(m),r}\frac{erf(\beta_2\left|\vec{r}-\vec{R}^2\right|)}{\left|\vec{r}-\vec{R}^2\right|}\end{aligned} \qquad 2.7.3$$

It will prove useful in the next section to apply the other definition of electrostatic potential ($\varphi \equiv \lim_{\delta q\to 0}\frac{\delta U}{\delta q}$) to Gaussian multipoles. From 2.5.1, the interaction energy between a Gaussian monopole (n = 0) and an m^{th} order Gaussian multipole is given by:

$$U_{0m}^{12} = (-1)^m q^1\Theta^{(m),2}\cdot\nabla^{(m),1}\frac{erf(\beta_{12}R^{12})}{R^{12}} \qquad 2.7.4$$

If the large exponent limit is take for the monopole, $\beta_1 \to \infty$, then $\beta_{12} \to \beta_2$ and the Gaussian monopole becomes a point charge, and 2.7.4 becomes

$$U_{0m}^{12} = (-1)^m q^1\Theta^{(m),2}\cdot\nabla^{(m),1}\frac{erf(\beta_2 R^{12})}{R^{12}} \qquad 2.7.5$$

The electrostatic potential is then

$$\begin{aligned}\varphi_m(\vec{R}^1;\vec{R}^2) &= \lim_{\delta q^1\to 0}\frac{\delta U_{0m}^{12}}{\delta q^1}\\ &= (-1)^m\Theta^{(m),2}\cdot\nabla^{(m),1}\frac{erf(\beta_2 R^{12})}{R^{12}}\end{aligned} \qquad 2.7.6$$

which is equivalent to 2.7.3 (if $\vec{R}^1 \equiv \vec{r}$ is the field point).

In appendix A.6.4, the electric field $\vec{E}$ is defined as the negative field gradient of potential: $\vec{E}(\vec{R}^1;\vec{R}^2) \equiv -\nabla^1\varphi(\vec{R}^1;\vec{R}^2)$. Hence, the electric field for an m^{th} rank Gaussian multipole can be found from 2.7.6 to be:

$$\vec{E}_m(\vec{R}^1;\vec{R}^2) = -\nabla^1 \varphi_m(\vec{R}^1;\vec{R}^2)$$
$$= (-1)^m \Theta^{(m),2} \cdot \nabla^{(m+1),1} \frac{erf(\beta_2 R^{12})}{R^{12}} \qquad 2.7.7$$

The n^{th} ranked field gradient[14] of an m^{th} ranked point multipole is defined in A.6.6. For am m^{th} ranked Gaussian multipole, the n^{th} ranked field gradient is given by:

$$E_m^n(\vec{R}^1;\vec{R}^2) = -\nabla^{(n),1} \varphi_m(\vec{R}^1;\vec{R}^2)$$
$$= (-1)^{m+1} \Theta^{(m),2} \cdot \nabla^{(n+m),1} \frac{erf(\beta_2 R^{12})}{R^{12}} \qquad 2.7.8$$

In the point multipole limit, $\beta_2 \to \infty$ and $erf(\beta_2 R^{12}) \to 1$, so that the potential, field, and field gradients become:

$$\varphi_m(\vec{R}^1;\vec{R}^2) = (-1)^m \Theta^{(m),2} \cdot \nabla^{(m),1} \frac{1}{R^{12}} \qquad 2.7.9a$$

$$\vec{E}_m(\vec{R}^1;\vec{R}^2) = (-1)^{m+1} \Theta^{(m),2} \cdot \nabla^{(m+1),1} \frac{1}{R^{12}} \qquad 2.7.9a$$

$$E_m^n(\vec{R}^1;\vec{R}^2) = (-1)^{m+1} \Theta^{(m),2} \cdot \nabla^{(n+m),1} \frac{1}{R^{12}} \qquad 2.7.9c$$

which is equivalent to A.6.3, A.6.5, and A.6.6.

2.8 'Effective' Electrostatic Potential and Field

In section A.6, it was shown that interaction energies for point multipoles could be conveniently expressed in terms of potential and its gradients. In this section, 'effective' electrostatic potential and field are defined. The motivation for this is to be able to express interaction energy between Gaussian multipoles in terms of 'effective' potentials and fields.

The interaction energy of a point monopole ($n = 0$) with a point multipole of rank m is given by A.6.7:

$$U_{0m}^{12} = q^1 \varphi_m(\vec{R}^1; \vec{R}^2)$$

where $\varphi_m(\vec{R}^1; \vec{R}^2) = (-1)^m \Theta^{(m),2} \cdot \nabla^{(m),1} \frac{1}{R^{12}}$ is the potential due to the point multipole of rank *m*. On the other hand, the interaction energy of a Gaussian monopole with a Gaussian multipole of rank *m* is given by:

$$U_{0m}^{12} = (-1)^m q^1 \Theta^{(m),2} \cdot \nabla^{(m),1} \frac{erf(\beta_{12} R^{12})}{R^{12}}$$

However, in the Gaussian multipole case, $U_{0m}^{12} \neq q^1 \varphi_m(\vec{R}^1; \vec{R}^2)$, since

$\varphi_m(\vec{R}^1; \vec{R}^2) = (-1)^m \Theta^{(m),2} \cdot \nabla^{(m),1} \frac{erf(\beta_2 R^{12})}{R^{12}}$ contains the wrong exponent ($\beta_2 \neq \beta_{12}$).

It would be useful to be able to express energy in terms of field and potential for Gaussian multipoles. However, the Gaussian multipole energy is an integral over two charge densities, and the potential/fields are integrals over a single charge density. Therefore, the Gaussian multipole energy can not be expressed in terms of ordinary potential/fields.

In the definition for electrostatic potential in ($\varphi \equiv \lim_{\delta q \to 0} \frac{\delta U}{\delta q}$), the potential is defined as the variation in energy when an infinitesimal point charge is added to the system. If the point charge *q* is replaced with an infinitesimal Gaussian charge $\widetilde{q}$ with exponent β_1, the 'effective' potential $\widetilde{\varphi}$ can be defined as:

$$\begin{aligned} \widetilde{\varphi}_m(\vec{R}^1; \vec{R}^2) &= \lim_{\delta \widetilde{q}^1 \to 0} \frac{\delta U_{0m}}{\delta \widetilde{q}^1} \\ &= (-1)^m \Theta^{(m),2} \cdot \nabla^{(m),1} \frac{erf(\beta_{12} R^{12})}{R^{12}} \end{aligned} \qquad 2.8.1$$

The difference between the true potential in 2.7.6 and the 'effective' potential in 2.8.1, is the exponent $\beta_2 \rightarrow \beta_{12}$. In a similar manner, the n^{th} rank field gradient of the 'effective' potential from an m^{th} order Gaussian multipole is defined as:

$$\begin{aligned} \widetilde{E}_m^{(n)}(\vec{R}^1;\vec{R}^2) &\equiv -\nabla^{1,(n)}\widetilde{\varphi}_m(\vec{R}^1;\vec{R}^2) \\ &= (-1)^{m+1}\Theta^{(m),2}\cdot\nabla^{(n+m),1}\frac{erf(\beta_{12}R^{12})}{R^{12}} \end{aligned} \tag{2.8.2}$$

Now the interaction energy between Gaussian multipoles can be expressed in terms of 'effective' potential and fields. The energy between a Gaussian monopole and an m^{th} order Gaussian multipole is given by:

$$\begin{aligned} U_{0m} &= (-1)^m q^1\Theta^{(m),2}\cdot\nabla^{(m),1}\frac{erf(\beta_{12}R^{12})}{R^{12}} \\ &= q^1\widetilde{\varphi}_m(\vec{R}^1;\vec{R}^2) \end{aligned} \tag{2.8.3}$$

The energy for a Gaussian dipole with an m^{th} order Gaussian multipole is given by:

$$\begin{aligned} U_{1m} &= (-1)^m \vec{\mu}^1\Theta^{(m),2}\cdot\nabla^{(m+1),1}\frac{erf(\beta_{12}R^{12})}{R^{12}} \\ &= -\vec{\mu}^1\cdot\widetilde{\vec{E}}_m^{(1)}(\vec{R}^1;\vec{R}^2) \end{aligned} \tag{2.8.4}$$

In general, the interaction energy for an n^{th} order Gaussian multipole with an m^{th} order Gaussian multipole is given by:

$$\begin{aligned} U_{nm} &= (-1)^m\Theta^{(n),1}\Theta^{(m),2}\cdot\nabla^{(n+m),1}\frac{erf(\beta_{12}R^{12})}{R^{12}} \\ &= -\Theta^{(n),1}\cdot\widetilde{E}_m^{(n)}(\vec{R}^1;\vec{R}^2) \end{aligned} \tag{2.8.5}$$

The main reason for introducing 'effective' potentials is to simplify energy interactions between Gaussian multipoles and to develop a formalism for Gaussian multipoles which parallels that of point multipoles. As mentioned earlier, the general method of evaluating interaction energy between two charge densities involves an integral over two coordinate systems. However, the field involves only a single integral.

The second charge density is implicitly integrated into the 'effective' potential. In the following two chapters, a polarization model based on induced Gaussian dipoles is developed. It is first postulated that 'effective' fields rather than ordinary fields are used to polarize the charge density by inducing a dipole moment on the atom. Later, it is shown that the results for polarization energy, work, and force are greatly simplified when 'effective' fields rather than ordinary fields are used to induce polarization.

2.9 Gradient Tensors

In section A.6, tensor gradients of $\frac{1}{R}$ were evaluated for point multipoles. For Gaussian multipoles, tensor gradients of the form $\nabla^{(n)} \frac{erf(\beta R)}{R}$ are needed. From the definition in A.2.14, the n^{th} ranked tensor gradient of $\frac{erf(\beta R)}{R}$ can be expressed in component form as:

$$\nabla^{(n)} \frac{erf(\beta R)}{R} = \hat{x}_{p_1} \hat{x}_{p_2} .. \hat{x}_{p_n} \frac{\partial^n}{\partial R_{p_1} \partial R_{p_2} .. \partial R_{p_n}} \frac{erf(\beta R)}{R} \tag{2.9.1}$$

The first four tensor gradients are evaluated as:

$$\nabla^{(1)} \frac{erf(\beta R)}{R} = -\vec{R} \beta^3 B_1(x) \tag{2.9.2}$$

$$\nabla^{(2)} \frac{erf(\beta R)}{R} = \hat{x}_p \hat{x}_q \left(R_p R_q \beta^5 B_2(x) - \delta_{pq} \beta^3 B_1(x) \right) \tag{2.9.3}$$

$$\nabla^{(3)} \frac{erf(\beta R)}{R} = \hat{x}_p \hat{x}_q \hat{x}_r \left((\delta_{pq} R_r + \delta_{pr} R_q + \delta_{rq} R_p) \beta^5 B_2(x) - R_p R_q R_r \beta^7 B_3(x) \right) \tag{2.9.4}$$

$$\nabla^{(4)}\frac{erf(\beta R)}{R} = \hat{x}_p\hat{x}_q\hat{x}_r\hat{x}_s\{(\delta_{pq}\delta_{rs} + \delta_{pr}\delta_{qs} + \delta_{rq}\delta_{sp})\beta^5 B_2(x) - (\delta_{pq}R_rR_s + \delta_{pr}R_qR_s + \delta_{rq}R_pR_s + \delta_{ps}R_qR_r + \delta_{qs}R_pR_r + \delta_{rs}R_pR_q)\beta^7 B_3(x) + R_pR_qR_rR_s\beta^9 B_4(x)\} \quad 2.9.5$$

where $x \equiv \beta R$, and the dimensionless $B_n(x)$ [17] [18] functions are defined by:

$B_0(x) \equiv \frac{erf(x)}{x}$, $B_{n+1}(x) \equiv -\frac{1}{x}\frac{dB_n}{dx}$. The first four functions are given by:

$$B_0(x) \equiv \frac{erf(x)}{x}$$
$$B_1(x) \equiv -\frac{dB_0}{dx}\frac{1}{x} = \frac{erf(x)}{x^3} - \frac{2}{\sqrt{\pi}}e^{-x^2}\frac{1}{x^2}$$
$$B_2(x) \equiv -\frac{dB_1}{dx}\frac{1}{x} = \frac{3erf(x)}{x^5} - \frac{2}{\sqrt{\pi}}e^{-x^2}\frac{1}{x^4}\left(3+2x^2\right) \quad 2.9.6$$
$$B_3(x) \equiv -\frac{dB_2}{dx}\frac{1}{x} = \frac{15erf(x)}{x^7} - \frac{2}{\sqrt{\pi}}e^{-x^2}\frac{1}{x^6}\left(15+10x^2+4x^4\right)$$
$$B_4(x) \equiv -\frac{dB_3}{dx}\frac{1}{x} = \frac{105erf(x)}{x^9} - \frac{2}{\sqrt{\pi}}e^{-x^2}\frac{1}{x^8}\left(105+70x^2+28x^4+8x^6\right)$$

In practice, the numerical evaluation of $B_n(x)$ using 2.9.6 is unstable for small *x*. However, $B_n(x)$ is finite and continuously differentiable when *x* is small. Starting with the Taylor series[12] for $erf(x) = \frac{2}{\sqrt{\pi}}\sum_{n=0}^{\infty}\frac{(-1)^n x^{2n+1}}{n!(2n+1)}$, a Taylor series can be derived for $B_n(x)$ and used to approximate $B_n(x)$ when *x* is small:

$$B_n(x) = \frac{2}{\sqrt{\pi}}\sum_{k=0}^{\infty}\frac{(-1)^k x^{2k}}{k!}\frac{2^n}{2(n+k)+1} \quad 2.9.7$$

For large *x*, the asymptotic limit of *erf*(*x*) → 1 holds, and the following relationship can be used to approximate $B_n(x)$ when *x* is large:

$$B_n(x) \cong \frac{(2n-1)!!}{x^{2n+1}} \qquad 2.9.8$$

The Gaussian multipole interaction energies up to dipole-dipole are given by 2.2.5a, 2.2.5b, 2.2.5c. When the results for the tensor gradients are inserted into the energies, the result is:

monopole-monopole $U_{00}^{12} = q^1 q^2 \beta_{12} B_0(x)$ 2.9.9

monopole-dipole $U_{01}^{12} = q^1 \vec{\mu}^2 \cdot \vec{R}^{12} \beta_{12}^3 B_1(x)$ 2.9.10

dipole-dipole $U_{11}^{12} = \vec{\mu}^1 \cdot \vec{\mu}^2 \beta_{12}^3 B_1(x) - \vec{\mu}^1 \cdot \vec{R}^{12} \vec{\mu}^2 \cdot \vec{R}^{12} \beta_{12}^5 B_2(x)$ 2.9.11

The potential at $\vec{R}^1$ for a Gaussian monopole with charge q^2 or dipole $\vec{\mu}^2$ and exponent β_2 located at $\vec{R}^2$ is given by:

$$\varphi_0(\vec{R}^1; \vec{R}^2) = q^2 \beta_2 B_0(\beta_2 R^{12}) \qquad 2.9.12$$

$$\varphi_1(\vec{R}^1; \vec{R}^2) = \vec{\mu}^2 \cdot \vec{R}^{12} \beta_2^3 B_1(\beta_2 R^{12}) \qquad 2.9.13$$

The 'effective' potentials onto a Gaussian particle with exponent β_1 are found by simply by replacing β_2 with β_{12} in 2.9.12 and 2.9.13.

$$\widetilde{\varphi}_0(\vec{R}^1; \vec{R}^2) = q^2 \beta_2 B_0(\beta_{12} R^{12}) \qquad 2.9.14$$

$$\widetilde{\varphi}_1(\vec{R}^1; \vec{R}^2) = \vec{\mu}^2 \cdot \vec{R}^{12} \beta_2^3 B_1(\beta_{12} R^{12}) \qquad 2.9.15$$

The 'effective' fields are found by taken the $n = 1$ and $m = 0, 1$ in 2.8.2

$$\widetilde{\vec{E}}_0(\vec{R}^1; \vec{R}^2) = q^2 \vec{R} \beta^3 B_1(\beta_{12} R^{12}) \qquad 2.9.16$$

$$\widetilde{\vec{E}}_1(\vec{R}^1; \vec{R}^2) \equiv \vec{\mu}^2 \cdot \hat{x}_p \hat{x}_q \left(R_p R_q \beta^5 B_2(\beta_{12} R^{12}) - \delta_{pq} \beta^3 B_1(\beta_{12} R^{12}) \right) \qquad 2.9.17$$

2.10 Relation to Hermite Gaussian Functions

In gas phase electronic structure calculations, Gaussian functions[19] are often used as a basis because all necessary one and two electron integrals have analytic solutions. Two electron Coulomb integrals of the form in 2.10.1 are needed.

$$\left\langle \chi_\mu \chi_\upsilon \middle| \chi_\sigma \chi_\rho \right\rangle \equiv \int\int d^3 r d^3 r' \frac{\chi_\mu^*(r)\chi_\upsilon^*(r')\chi_\sigma(r)\chi_\rho(r')}{\left|\vec{r}-\vec{r}'\right|} \qquad 2.10.1$$

χ_μ is a Cartesian Gaussian basis function of the form:

$$\chi_\mu(\vec{r},\beta,\vec{R}) \equiv N_{pqr}(x_R)^p (y_R)^q (z_R)^r \exp(-\alpha\left|\vec{r}-\vec{R}\right|^2) \qquad 2.10.2$$

where N_{pqr} is a normalization constant, $x_R \equiv x - X$, $y_R \equiv y - Y$, $z_R \equiv z - Z$, and $\vec{R} \equiv X\hat{x} + Y\hat{y} + Z\hat{z}$ is a nuclear center. The set of Cartesian Gaussian functions can be linearly transformed into the set of Hermite Gaussian functions of the form:

$$\Lambda_{tuv}(\vec{r},\beta,\vec{R}) \equiv \left(\frac{\alpha}{\pi}\right)^{\frac{3}{2}} \left(\frac{\partial}{\partial X}\right)^t \left(\frac{\partial}{\partial Y}\right)^u \left(\frac{\partial}{\partial Z}\right)^v \exp(-\alpha\left|\vec{r}-\vec{R}\right|^2) \qquad 2.10.3$$

The Gaussian multipoles $\Theta^{(n)}$ defined in this work are tensor contractions between multipole moments and the set of Hermite Gaussian functions with $t+u+v = n$. One method of evaluating the electron repulsion integrals of 2.10.1 is to first transform the Cartesian Gaussian basis into a Hermite Gaussian basis. The nuclear center derivatives in 2.10.3 can be pulled out of the integral. The integral can then be evaluated in terms of simple s-orbital Gaussian functions or Gaussian monopoles as in the calculation of U_{00}. Recursion relationships, such as the McMurchie-Davidson[20] scheme, are used to evaluate the integrals for higher angular momentum (higher order Gaussian multipoles) in terms of a Boys' function of order n defined by:

$$F_n(x) \equiv \int_0^1 t^{2n} \exp(-xt^2) dt \qquad 2.10.4$$

The following relationship for derivatives holds:

$$F_{n+1} = -\frac{dF_n}{dx} \qquad 2.10.5$$

The zero[th] order Boys' function can be transformed[15] in the *erf*(x) function as:

$$F_0(x) = \sqrt{\frac{\pi}{4}} \frac{erf(\sqrt{x})}{\sqrt{x}} = \sqrt{\frac{\pi}{4}} B_0\left(\sqrt{x}\right) \qquad 2.10.6$$

Using these two relationships, it can be shown that

$$F_n(x) = \frac{1}{2^n} \sqrt{\frac{\pi}{4}} B_n\left(\sqrt{x}\right) \qquad 2.10.7$$

Though the final results are identical, the formalism in this work differs from that used in electronic structure theory. The approach for evaluating the interaction between Gaussian multipoles in this work parallels that of point multipoles, in order for comparisons to be made at each stage. Instead of using McMurchie-Davidson recursion, the treatment here used explicit Cartesian gradients (2.9.2 - 2.9.5). The function $B_n(x)$ in 2.9.6 was used instead of the Boy's functions $F_n(x)$. For more details on electron integral evaluation in electronic structure calculations, see *Molecular Electronic Structure Theory*[15].

2.11 References

[1] G. A. Cisneros, J. P. Piquemal, and T. A. Darden, J. Chem. Phys. **125**, 184101 (2006)

[2] J. P. Piquemal, G. A. Cisneros, P. Reinhardt, N. Gresh, and T. A. Darden, J. Chem. Phys. **124**, 104101 (2005)

[3] G. A. Cisneros, J. P. Piquemal, and T. A. Darden, J. Chem. Phys. **123**, 044109 (2005)

[4] P. S. Bagus, K. Hermann, and C. W. Bauschlicher, Jr., J. Chem. Phys. **80**, 4378 (1984)

[5] J. Applequist, J. R. Carl, and K. K. Fung, J. Am. Chem. Soc. **94**, 2952 (1972)

[6] P. Paricaud, M. Předota, A. A. Chialvo, and P. T. Cummings, J. Chem. Phys. **122**, 244511 (2005)

[7] M. Masia, M. Probst, and R. Rey, J. Chem. Phys. **123**, 164505 (2005)

[8] D. M. York and W. Yang, J. Chem. Phys. **104**, 159 (1996)

[9] R. J. Wheatley, Mol. Phys. **79** (**3**), 597 (1996)

[10] M. Challacombe, E. Schegler, and J. Almlof, *Modern developments in Hartree--Fock theory: Fast methods for computing the Coulomb matrix: Computational Chemistry: Review of Current Trends*, edited by J. Leszczynski, (World Scientific Inc, Singapore, 1996)

[11] M. A. Freitag, M. S. Gordon, J. H. Jensen, and W. J. Stevens, J. Chem. Phys. **112**, 7300 (2000)

[12] N. N. Lebedev, *Special Functions and Their Applications,* (Dover, New York, 1972)

[13] J. Applequist, Chem. Phys. **85**, 279 (1984)

[14] J. D. Jackson, *Classical Electrodynamics*, 3rd edition, (Wiley, New York, 1999)

[15] T. Helgaker, P. Jørgensen, and J. Olsen, *Molecular Electronic Structure Theory*, (Wiley, New York, 2000)

[16] G. B. Arfken and H. J. Weber, *Mathematical Methods for Physicists*, 4th edition, (Academic Press, San Diego, 1995)

[17] A. Toukmaki, C. Sagui, J. Board, and T. A. Darden, J. Chem. Phys. **113 (24)**, 10913 (2000)

[18] W. Smith, CCP5 Quarterly **4**, 13 (1982)

[19] S. F. Boys, Proc. R. Soc. London, Ser. A **200**, 542 (1950)

[20] L. E. McMurchie and E. R. Davidson, J. Comput. Phys. **26**, 218 (1978)

3 Gaussian Polarization Model

3.1 Introduction

In recent years, including polarization in molecular dynamics simulations has been the center of a considerable amount of effort[1-5]. It is known that molecular dipole moments change significantly when transferred from gas to liquid phase; non-polarizable classical force fields based solely on additive models are not able to capture this effect. Rather, permanent molecular dipole interactions are often enhanced to compensate[6].

Including an explicit polarization term in the force field is a method to model these multi-body effects in condensed phases, while still being able to correctly calculate gas phase properties, such as dimer geometries and interaction energies. Polarization is likely to be particularly important in accurate descriptions of biomolecular interactions. A further important advantage of using a polarizable force field relates to parameter development. Polarizable force fields fit to ab-initio data would be expected to do well both in gas and condensed phase.

Several polarization models such as the Drude oscillator[7 8], fluctuating charges[9], and induced dipoles[10 11 12] have been suggested for use in water models. However, the induced dipole model[1 2 4 5] and the fluctuating charge model[2 3 5] seems to have received the most attention in terms of force field development. The simplest induced dipole model places isotropic inducible point dipoles on each atom. If hyperpolarization effects, as might arise from strong electric fields, are absent, then the induced dipole responds linearly with respect to electric field. In this case, the induced dipole $\vec{\mu}$ on an atom is the product of the total electric field $\vec{E}$ and a scalar atomic polarizability α.

$$\vec{\mu} = \alpha \vec{E} \qquad 3.1.1$$

The total electric field is composed of the external electric field from permanent charge sources $\vec{E}^0$ and the contribution from other induced dipoles. In order to reproduce molecular polarizability tensors using isotropic atomic polarizabilities, induced dipoles within the same molecule should interact with one another[13]. Applequist et. al. found parameters for this model by fitting atomic polarizabilities to experimental molecular polarizability tensors[14].

The development of the interacting induced point dipole model was an important step in modeling polarization because it led to accurate calculations of molecular polarizability tensors. The most serious drawback to using the original point dipole model is known as the polarization catastrophe. This phenomenon happens when two mutually interacting inducible dipoles with atomic polarizabilities α_1 and α_2 diverge at a finite distance, given by:

$$R = \left(4\alpha_1\alpha_2\right)^{1/6} \qquad 3.1.2$$

During a molecular dynamics simulation, this situation leads to non-physical forces and velocities causing the simulation to fail. Thole[15 16] remedied this problem by applying a damping function to dipole-dipole interactions. As an added feature, the damped model resulted in an improved fit to the molecular polarizability tensor data relative to the Applequist point dipole model.

An alternative to the damped interaction model by Thole, which was explored in the previous chapter, is to employ interacting Gaussian densities rather than point dipoles[17 18]. An advantage of using a charge distribution model over the Thole model is that it may be readily generalized to other multipole moments. For example, a point

charge could be replaced by a Gaussian 's' orbital, and a dipole could be replaced by a 'p' orbital[19]. It was shown in chapter two that point multipoles are the large exponent limit of Gaussian multipoles. Indeed, multipoles in current force fields[1] could be replaced by Gaussian multipole (Hermite Gaussian) charge densities[20], which effectively damp short range electrostatic interactions and provide a more realistic description of penetration effects, which can be significant in dimer geometries[21 22].

A peculiar aspect of the Gaussian model that relates to the polarization catastrophe should be pointed out. If the inducible point dipoles are replaced by inducible Gaussian dipoles, it might be expected that the interaction remains finite, since the interaction of two permanent Gaussian dipoles is finite at all distances. However for large exponents, the Gaussian dipoles start to behave like point dipoles, which interact strongly. If the exponents are too large, the interaction is too strong and a polarization catastrophe can occur. A relationship between the minimum diffuseness of the Gaussian exponent β and atomic polarizability α, namely:

$$\beta < \frac{1}{\left(\alpha \frac{4}{3\sqrt{8\pi}}\right)^{\frac{1}{3}}} \qquad 3.1.3$$

is derived that will prevent a polarization catastrophe.

A similar analysis was performed on the Thole model[15], $\{\rho(u) = 3a/4\pi\, exp(-au^3)\}$, and the maximum value of the damping parameter a was found to be 1.0.

One focus of this study is to develop an induced Gaussian dipole polarization model. In the following section, results from chapter two pertaining to Gaussian monopoles and dipoles are summarized. In section 3.3, the induced Gaussian dipole

polarization model is introduced as a generalization of the induced point dipole model. The procedure to calculate molecular polarizability tensors from atomic polarizabilities is discussed in this section. In section 3.4, the molecular polarizability tensor is derived explicitly for the important case of a diatomic molecule. In section 3.5, the polarization catastrophe for the Gaussian and Thole model is discussed, and a proof of 3.1.3 is provided. Finally, in section 3.6, an equivalent definition of molecular polarizability as a derivative of molecular dipole with respect to external field is given. As an example, the molecular polarizability tensor is calculated for water using the procedure outlined in 3.4 and also as a numerical derivative of induced molecular dipole with respect to external field.

3.2 Gaussian Model

In chapter two, Gaussian multipoles were discussed. In this section, the results for Gaussian monopoles and dipoles are summarized. In particular, the dipole-dipole interaction matrix is defined and relationships for electric potential and fields needed for the Gaussian polarization model are stated.

It was shown in appendix A.7 that interaction energies between point multipoles can be expressed in terms of potential, field, or field gradient. In order to generalize Gaussian multipoles from point multipoles, ‘effective’ potentials and fields were defined between Gaussian multipoles in section 2.8. Interaction energies between Gaussian multipoles can be expressed in terms of ‘effective’ potential and fields. The ordinary electrostatic potential is defined as the variation in energy when an infinitesimal point charge (or point monopole) is added to the system. The ‘effective’ potential is defined as

the variation in energy when an infinitesimal Gaussian monopole is added to the system. 'Effective' potential between Gaussian multipole charge distributions are convenient because it implicitly takes into account both charge distributions as continuous charge densities. In the following section, it is postulated that 'effective' fields rather than ordinary electric fields are used to induce polarization. In chapter four, it is shown that the use of 'effective' fields greatly simplifies the polarization energy, work, and force.

A Gaussian monopole density with nuclear center at $\vec{R}$, charge q, and exponent β is given by (2.2.1):

$$\rho_0(\vec{r};\vec{R}) = q\left(\frac{\beta^2}{\pi}\right)^{\frac{3}{2}} e^{-\beta^2\left|\vec{r}-\vec{R}\right|^2} \qquad 3.2.1$$

Similarly, a Gaussian dipole density with dipole moment $\vec{\mu}$ is given by (2.2.2):

$$\rho_1(\vec{r};\vec{R}) = \vec{\mu}\cdot\nabla^R\left(\frac{\beta^2}{\pi}\right)^{\frac{3}{2}} e^{-\beta^2\left|\vec{r}-\vec{R}\right|^2} \qquad 3.2.2$$

The interaction energies between Gaussian monopole and dipole densities at $\vec{R}^1$ and $\vec{R}^2$ with exponents β_1 and β_2 are derived in chapter two and given by 2.9.9, 2.9.10, and 2.9.11:

$$U_{00}^{12} = q^1 q^2 \beta_{12} B_0(x) \qquad 3.2.3$$

$$U_{01}^{12} = q^1 \vec{\mu}^2\cdot\vec{R}^{12}\beta_{12}^3 B_1(x) \qquad 3.2.4$$

$$U_{11}^{12} = (\vec{\mu}^1\cdot\vec{\mu}^2)\beta_{12}^3 B_1(x) - (\vec{\mu}^1\cdot\vec{R}^{12})(\vec{\mu}^2\cdot\vec{R}^{12})\beta_{12}^5 B_2(x) \qquad 3.2.5$$

where $\beta_{12} \equiv \dfrac{\beta_1\beta_2}{\sqrt{\beta_1^2+\beta_2^2}}$, $\vec{R}^{12} \equiv \vec{R}^1 - \vec{R}^2$, $R^{12} \equiv \left|\vec{R}^1 - \vec{R}^2\right|$, and $x \equiv \beta_{12}R^{12}$. $B_0(x)$, $B_1(x)$, and $B_2(x)$ are defined by 2.9.6 as:

$$B_0(x) \equiv \frac{erf(x)}{x}$$
$$B_1(x) \equiv -\frac{dB_0}{dx}\frac{1}{x} = \frac{erf(x)}{x^3} - \frac{2}{\sqrt{\pi}} e^{-x^2} \frac{1}{x^2} \qquad 3.2.6$$
$$B_2(x) \equiv -\frac{dB_1}{dx}\frac{1}{x} = \frac{3erf(x)}{x^5} - \frac{2}{\sqrt{\pi}} e^{-x^2} \frac{1}{x^4}\left(3 + 2x^2\right)$$

The Gaussian dipole – dipole energy in 3.2.5 can be expressed in terms of a dipole – dipole interaction matrix $\mathbf{T}^{12}$

$$U_{11}^{12} = -\vec{\mu}^1 \cdot \mathbf{T}^{12} \cdot \vec{\mu}^2, \qquad 3.2.7$$

in which $\mathbf{T}^{12} \equiv \nabla^1 \nabla^1 \frac{erf(\beta_{12} R^{12})}{R^{12}}$ is found from 2.9.3:

$$\begin{aligned} \mathbf{T}^{12} &= \left(R_p^{12} R_q^{12} \beta_{12}^5 B_2(x) - \delta_{pq} \beta_{12}^3 B_1(x)\right) \hat{x}_p \hat{x}_q \\ &= \beta_{12}^3 \left\{ \beta_{12}^2 \vec{R}^{12} \vec{R}^{12} B_2(x) - B_1(x) \mathbf{I} \right\} \end{aligned} \qquad 3.2.8$$

$\vec{R}^{12} \equiv R_p^{12} \hat{x}_p$ and $\mathbf{I} \equiv \delta_{pq} \hat{x}_p \hat{x}_q$ (identity matrix) are expressed in vector/tensor notation (see appendix A.2).

The ordinary potential φ_0 at $\vec{R}^1$ of a Gaussian monopole at $\vec{R}^2$ with charge q^2 and exponent β_2 is given by 2.9.12:

$$\varphi_0(\vec{R}^1) = q^2 \beta_2 B_0(\beta_2 R^{12}) \qquad 3.2.10$$

Similarly, the ordinary potential φ_1 at $\vec{R}^1$ of a Gaussian dipole at $\vec{R}^2$ with dipole $\vec{\mu}^2$ and exponent β_2 can be evaluated from 2.9.13:

$$\varphi_1(\vec{R}^1) = \vec{\mu}^2 \cdot \vec{R}^{12} \beta_2^3 B_1(\beta_2 R^{12}) \qquad 3.2.11$$

In section 2.8, it was shown that interaction energies could be expressed in terms of 'effective' potentials and fields. The 'effective' field of a Gaussian monopole with

charge q^2 and exponent β_2 at $\vec{R}^2$ onto another Gaussian particle with exponent β_1 at $\vec{R}^1$ is given by 2.9.16:

$$\vec{E}_0(\vec{R}^1;\vec{R}^2) = q^2\vec{R}^{12}\beta_{12}^3 B_1(\beta_{12}R^{12}) \qquad 3.2.12$$

The ˜ symbol has been dropped on 'effective' field for clarity. The 'effective' field of a Gaussian dipole with dipole $\vec{\mu}^2$ and exponent β_2 at $\vec{R}^2$ onto another Gaussian particle with exponent β_1 at $\vec{R}^1$ is given by 2.9.17:

$$\begin{aligned}\vec{E}_1(\vec{R}^1;\vec{R}^2) &= \vec{\mu}^2 \cdot \left(\vec{R}^{12}\vec{R}^{12}\beta^5 B_2(\beta_{12}R^{12}) - \mathbf{I}\beta^3 B_1(\beta_{12}R^{12})\right) \\ &= \vec{\mu}^2 \cdot \mathbf{T}^{12}\end{aligned} \qquad 3.2.13$$

The 'effective' fields are used to induce dipoles in the Gaussian dipole polarization model.

3.3 Gaussian Polarization Model

The section follows the treatment of Applequist[12] and Thole[13] by deriving the molecular polarizability tensor for linear isotropic polarizabilities using induced Gaussian dipoles. The main difference between this treatment and that of Applequist or Thole is that the dipole-dipole interaction matrix $\mathbf{T}^{12}$ is given by 3.2.8 and the electric fields used are 'effective' electric fields (3.2.12 and 3.2.13) between Gaussian particles.

The symmetric molecular polarizability tensor α_{pq}^{mol} is defined by:

$$\begin{pmatrix}\mu_x^{\text{mol}}\\ \mu_y^{\text{mol}}\\ \mu_z^{\text{mol}}\end{pmatrix} = \begin{pmatrix}\alpha_{xx}^{\text{mol}} & \alpha_{xy}^{\text{mol}} & \alpha_{xz}^{\text{mol}}\\ \alpha_{yx}^{\text{mol}} & \alpha_{yy}^{\text{mol}} & \alpha_{yz}^{\text{mol}}\\ \alpha_{zx}^{\text{mol}} & \alpha_{zy}^{\text{mol}} & \alpha_{zz}^{\text{mol}}\end{pmatrix}\begin{pmatrix}E_x^0\\ E_y^0\\ E_z^0\end{pmatrix} \qquad 3.3.1$$

where $\vec{\mu}^{\text{mol}}$ is the induced molecular induced dipole and $\vec{E}^0$ is a constant external electric field applied to the molecule. In order to calculate the molecular polarizability

tensor from induced Gaussian dipoles, consider a molecule composed of N atoms each with an isotropic polarizability α_i assigned to it. The induced dipole on particle i $\vec{\mu}^i$ is the product of the atomic polarizability α_i and the total 'effective' field due to permanent charges $\vec{E}^{0,i}$ and the 'effective' field due to other induced dipoles, $\sum_{j\neq i}\mathbf{T}^{ij}\cdot\vec{\mu}^j$.

$$\vec{\mu}^i = \alpha^i\left(\vec{E}^{0,i} + \sum_{j\neq i}\mathbf{T}^{ij}\cdot\vec{\mu}^j\right) \qquad 3.3.2$$

This is a linear equation for $\vec{\mu}^i$, which can be rewritten as

$$\mathbf{A}\overline{\mu} = \overline{E}^0 \qquad 3.3.3$$

where $\overline{\mu}$ and $\overline{E}^0$ are $3N$ column vectors, and $\mathbf{A}$ is a $3N$ *x* $3N$ matrix given by:

$$\mathbf{A} = \begin{bmatrix} (\alpha^1)^{-1} & 0 & \dots & 0 \\ 0 & (\alpha^2)^{-1} & \dots & \dots \\ \vdots & \vdots & \ddots & \dots \\ 0 & 0 & \dots & (\alpha^N)^{-1} \end{bmatrix} - \begin{bmatrix} 0 & \mathbf{T}^{12} & \dots & \mathbf{T}^{1N} \\ \mathbf{T}^{21} & 0 & \dots & \dots \\ \vdots & \vdots & \ddots & \dots \\ \mathbf{T}^{N1} & \mathbf{T}^{N2} & \dots & 0 \end{bmatrix} \qquad 3.3.4$$

or in tensor particle-component notation,

$$A^{ij}_{pq} = \frac{1}{\alpha^i}\delta_{ij}\delta_{pq} - T^{ij}_{pq} \qquad 3.3.5$$

where δ_{ij} is the kronecker delta function, defined by $\delta_{ij} = 1$ ($i = j$) and $\delta_{ij} = 0$ for ($i \neq j$). As in chapter two, for tensors involving components (p =1,2,3 for *x,y,z*) and particles (i = 1,.. N), the particle index will usually be denoted (when possible) as a superscript and the component index as a subscript. Solving for $\overline{\mu}$ in 3.3.3,

$$\overline{\mu} = \mathbf{A}^{-1}\overline{E} \qquad 3.3.6$$

Since the total induced molecular dipole is found by summing the induced atomic dipoles, the calculated molecular polarizability tensor α_{pq}^{mol} is the direct sum of $\mathbf{A}^{-1}$ over particle number.

$$\alpha_{pq}^{\text{mol}} = \sum_{i=1}^{N}\sum_{j=1}^{N} A_{pq}^{-1,ij} \qquad 3.3.7$$

A small technical note should be made regarding 'effective' fields for the external constant field acting upon the molecule in 3.3.1. Since the field is constant, 'effective' field is the same as ordinary field because a constant field can be created by a large point charge a far distance away, i.e. a point charge outside the range of the Gaussian exponents. 'Effective' fields differ from ordinary fields when atoms are close enough that their Gaussian charge distributions overlap.

If the assumption of linear isotropic atomic polarizabilities were generalized to linear anisotropic polarizabilities, α^i becomes a symmetric polarizability matrix α_{pq}^i and the equation for induced dipoles (3.3.2) becomes (in component form):

$$\mu_p^i = \alpha_{pq}^i \left(E_q^{0,i} + \sum_{j\neq i} \mathbf{T}_{qr}^{ij} \cdot \mu_r^j \right) \qquad 3.3.8$$

where repeated component indices *q* and *r* have been summed over. This can be expressed as $\mathbf{A}\overline{\mu} = \overline{E}^0$ where the **A** matrix takes the form:

$$A_{pq}^{ij} = \alpha_{pq}^{-1,i}\delta_{ij} - T_{pq}^{ij} \qquad 3.3.9$$

where $\alpha_{pq}^{-1,i}$ is the inverse of anisotropic atomic polarizability tensor α_{pq}^i for particle *i*. The molecular polarizability can be found by inverting **A** as in 3.3.6 and then taking the direct sum as in 3.3.7.

3.4 Diatomic Molecule

In the case of a diatomic molecule, the molecular polarizability tensor has 2 independent components: one parallel to the bond axis $\alpha_{\parallel}$ and another perpendicular to the bond axis $\alpha_{\perp}$. By considering 2 particles interacting in 1 dimension, these components can be explicitly derived for the Gaussian model by solving for $\vec{\mu}^1$ and $\vec{\mu}^2$ in 3.3.2 using the result for the dipole – dipole interaction matrix $\mathbf{T}^{12}$ (3.2.8).

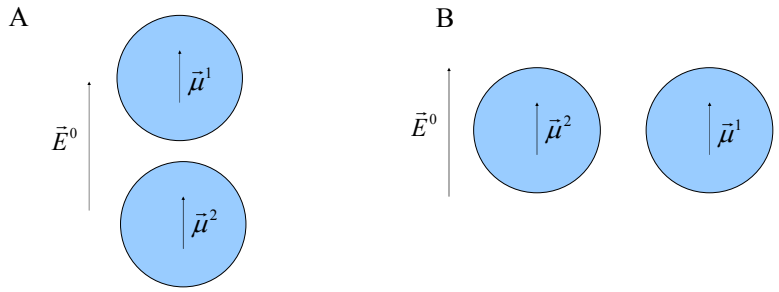

Figure 3.1 Two induced dipoles interacting parallel (**A**) and perpendicular (**B**) to a constant external electric field.

Consider the case of two particles whose bond axis is parallel to the external field in Figure 3.1A. Suppose the external field and the separation is along the $\hat{y}$ axis. In this case, $\vec{\mu}^1 = \mu^1 \hat{y}$, $\vec{\mu}^2 = \mu^2 \hat{y}$, $\vec{R}^{12} = R\hat{y}$, $\vec{E}^{0,1} = \vec{E}^{0,2} = E^0 \hat{y}$, $\mathbf{T}^{12} = \mathbf{T}^{21} = \beta_{12}^3 \left\{ \beta_{12}^2 RRB_2(x)\hat{y}\hat{y} - B_1(x)\mathbf{I} \right\}$. The equation for induced dipoles (3.3.2) becomes:

$$\begin{aligned} \mu^1 \hat{y} &= \alpha^1 \left(E^0 + \beta_{12}^3 F(x) \mu^2 \right) \hat{y} \\ \mu^2 \hat{y} &= \alpha^2 \left(E^0 + \beta_{12}^3 F(x) \mu^1 \right) \hat{y} \end{aligned} \qquad 3.4.1$$

where

$$F(x) \equiv x^2 B_2(x) - B_1(x) \qquad 3.4.2$$

3.4.1 can be solved for μ^1 and μ^2, yielding the following result:

$$\mu^1 = \frac{\alpha^1 + \alpha^1\alpha^2\beta_{12}^3 F(x)}{1-\alpha^1\alpha^2\beta_{12}^6 F(x)F(x)} E^0$$
$$\mu^2 = \frac{\alpha^2 + \alpha^1\alpha^2\beta_{12}^3 F(x)}{1-\alpha^1\alpha^2\beta_{12}^6 F(x)F(x)} E^0 \qquad 3.4.3$$

The total induced dipole along the bond axis is $\mu^{\|} = \mu^1 + \mu^2$, and the molecular polarizability along the bond axis is given by:

$$\alpha_{\|} = \frac{\mu^{\|}}{E^0} = \frac{\alpha^1 + \alpha^2 + 2\alpha^1\alpha^2\beta_{12}^3 F(x)}{1-\alpha^1\alpha^2\beta_{12}^6 F(x)F(x)} \qquad 3.4.4$$

Now consider the case of two particles whose bond axis is perpendicular to the external field as in Figure 3.1B. Suppose the external field is along the $\hat{y}$ axis, and the separation is along the $\hat{x}$ axis. In this case, $\vec{\mu}^1 = \mu^1\hat{y}$, $\vec{\mu}^2 = \mu^2\hat{y}$, $\vec{R}^{12} = R\hat{x}$, $\vec{E}^{0,1} = \vec{E}^{0,2} = E^0\hat{y}$, $\mathbf{T}^{12} = \mathbf{T}^{21} = \beta_{12}^3\left\{\beta_{12}^2 RRB_2(x)\hat{x}\hat{x} - B_1(x)\mathbf{I}\right\}$. The equation for dipoles (3.3.2) becomes:

$$\mu^1\hat{y} = \alpha^1\left(E^0 - \beta_{12}^3 B_1(x)\mu^2\right)\hat{y}$$
$$\mu^2\hat{y} = \alpha^2\left(E^0 - \beta_{12}^3 B_1(x)\mu^1\right)\hat{y} \qquad 3.4.5$$

which can be solved for μ^1 and μ^2, yielding the following result:

$$\mu^1 = \frac{\alpha^1 - \alpha^1\alpha^2\beta_{12}^3 B_1(x)}{1-\alpha^1\alpha^2\beta_{12}^6 B_1(x)B_1(x)} E^0$$
$$\mu^2 = \frac{\alpha^2 - \alpha^1\alpha^2\beta_{12}^3 B_1(x)}{1-\alpha^1\alpha^2\beta_{12}^6 B_1(x)B_1(x)} E^0 \qquad 3.4.6$$

The total induced dipole perpendicular to the bond axis is $\mu^{\perp} = \mu^1 + \mu^2$, and the molecular polarizability perpendicular the bond axis is given by:

$$\alpha_{\perp} = \frac{\mu^{\perp}}{E^0} = \frac{\alpha^1 + \alpha^2 - 2\alpha^1\alpha^2\beta_{12}^3 B_1(x)}{1-\alpha^1\alpha^2\beta_{12}^6 B_1(x)B_1(x)} \qquad 3.4.7$$

In the point dipole limit, $B_1(x) \cong \frac{1}{x^3}$ and $B_2(x) \cong \frac{3}{x^5}$ (2.9.8). Therefore, $F(x) \cong \frac{2}{x^2}$ and the molecular polarizability tensor parallel and perpendicular to the bond axis reduce to:

$$\alpha_{\parallel} \cong \frac{\alpha^1 + \alpha^2 + 2\alpha^1\alpha^2 \frac{2}{R^3}}{1 - \alpha^1\alpha^2 \frac{4}{R^6}} \qquad 3.4.8$$

$$\alpha_{\perp} \cong \frac{\alpha^1 + \alpha^2 - 2\alpha^1\alpha^2 \frac{2}{R^3}}{1 - \alpha^1\alpha^2 \frac{1}{R^6}} \qquad 3.4.9$$

3.5 Polarization Catastrophe

In the introduction, it was stated that the exponent parameter in the Gaussian model should be sufficiently diffuse in order for a polarization catastrophe not to occur. This condition, given by 3.1.3,

$$\beta < \frac{1}{\left(\alpha \frac{4}{3\sqrt{8\pi}}\right)^{\frac{1}{3}}} \qquad 3.5.1$$

will now be proved.

Consider two interacting inducible dipoles with polarizabilities α_1 and α_2 separated by a distance R along the x-axis. Since induced dipoles parallel to the separation axis interact more strongly than dipoles that are perpendicular to their separation axis, it suffices to consider dipoles interacting parallel to their separation axis.

In order for the interaction between two dipoles to be finite, the denominator in 3.4.4 should be positive.

$$\alpha^1 \alpha^2 \beta_{12}^6 F(x) F(x) < 1 \qquad 3.5.2$$

where $F(x)$ is defined in 3.4.2 by:

$$F(x) \equiv x^2 B_2(x) - B_1(x) \qquad 3.5.3$$

and $\beta_{12} \equiv \dfrac{\beta_1 \beta_2}{\sqrt{\beta_1^2 + \beta_2^2}}$ and $x \equiv \beta_{12} R$. $B_1(x)$ and $B_2(x)$ are defined in 3.2.6 and 2.9.6 by:

$B_1(x) = \dfrac{erf(x)}{x^3} - \dfrac{2}{\sqrt{\pi}} e^{-x^2} \dfrac{1}{x^2}$ and $B_2(x) = \dfrac{3erf(x)}{x^5} - \dfrac{2}{\sqrt{\pi}} e^{-x^2} \dfrac{1}{x^4}\left(3 + 2x^2\right)$. $F(x)$ is plotted in Figure 3.2.

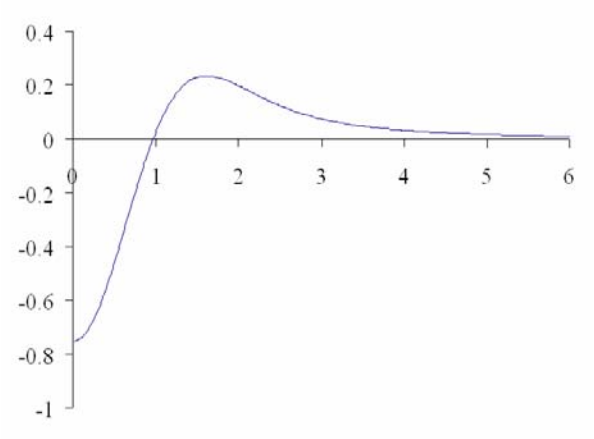

Figure 3.2 Plot of $F(x) = x^2 B_2(x) - B_1(x)$

Let

$$F_0 \equiv \max\left\{\left|F(x)\right|\right\} = \frac{4}{3\sqrt{\pi}} \approx 0.752252778 \qquad 3.5.4$$

be the maximum value of $F(x)$ which occurs at $x = 0$. If β_1 and β_2 are chosen such that

$$\beta_i < \frac{1.0}{\left(\alpha^i \dfrac{4}{3\sqrt{8\pi}}\right)^{\frac{1}{3}}} \quad i = 1,2 \qquad 3.5.5$$

then 3.5.2 is valid for all x.

Proof:

$$\frac{1}{\beta_{12}^2} = \frac{1}{\beta_1^2} + \frac{1}{\beta_2^2} = \left(\frac{1}{\beta_1} - \frac{1}{\beta_2}\right)^2 + \frac{2}{\beta_1\beta_2} \geq \frac{2}{\beta_1\beta_2} \tag{3.5.6}$$

or

$$\beta_{12}^2 \leq \frac{\beta_1\beta_2}{2} \tag{3.5.7}$$

Using 3.5.4 and 3.5.7, 3.5.2 becomes

$$\alpha_1\alpha_2\beta_{12}^6 F(x)F(x) \leq \alpha_1\alpha_2\beta_{12}^6 F_0^2 \leq \alpha^1\alpha^2\left(\frac{\beta_1\beta_2}{2}\right)^3 F_0^2 \tag{3.5.8}$$

Substituting β_i (3.5.5) and F_0 (3.5.4) into 3.5.8 gives:

$$\alpha_1\alpha_2\beta_{12}^6 F(x)F(x) < \alpha^1\alpha^2 \frac{1.0}{8\left(\alpha^1 \frac{4}{3\sqrt{8\pi}}\right)\left(\alpha^2 \frac{4}{3\sqrt{8\pi}}\right)}\left(\frac{4}{3\sqrt{\pi}}\right)^2 = 1 \tag{3.5.9}$$

i.e. 3.5.2 is satisfied.

A similar analysis can be applied to the Thole model. The dipole-dipole interaction is[23]:

$$\mathbf{T}^{Thole} = \frac{1}{R^5}\left\{3\vec{R}\vec{R}(1-(1+au^3)e^{-au^3} - R^2(1-e^{-au^3})\vec{\vec{I}})\right\} \tag{3.5.10}$$

where

$$u \equiv \frac{R}{(\alpha^1\alpha^2)^{\frac{1}{6}}} \tag{3.5.11}$$

In 1 dimension, the molecular polarizability tensor for Thole can be solved for explicitly as in section 3.4:

$$\alpha_{\parallel} = \frac{\alpha^1 + \alpha^2 + 2\sqrt{\alpha^1 \alpha^2}\,\widetilde{F}(u)}{1 - \widetilde{F}(u)^2} \tag{3.5.12}$$

$$\alpha_{\perp} = \frac{\alpha^1 + \alpha^2 - 2\sqrt{\alpha^1 \alpha^2}\,\widetilde{G}(u)}{1 - \widetilde{G}(u)^2} \tag{3.5.13}$$

where $\widetilde{F}(u)$ and $\widetilde{G}(u)$ are defined by:

$$\begin{aligned} \widetilde{F}(u) &\equiv \frac{1}{u^3}(2 - (2 + 3au^3)e^{-au3}) \\ \widetilde{G}(u) &\equiv \frac{1}{u^3}(1 - e^{-au3}) \end{aligned} \tag{3.5.14}$$

A catastrophe doesn't occur as long as the denominator of 3.5.12 is positive.

$$1 - \widetilde{F}(u)^2 > 0 \tag{3.5.15}$$

Let

$$\widetilde{F}_0 \equiv \max\left\{\left|\widetilde{F}(u)\right|\right\} = a \tag{3.5.16}$$

which occurs at $u = 0$. The catastrophe condition then becomes:

$$\widetilde{F}(u)^2 \le \widetilde{F}_0^2 < 1 \tag{3.5.17}$$

i.e. $a < 1.0$.

Finally, in the point dipole case, a polarization catastrophe occurs when the denominator 3.4.8 is zero, i.e. $R = \left(4\alpha^1 \alpha^2\right)^{\frac{1}{6}}$. This was stated in the introduction (3.1.2).

3.6 Results

For small external fields, the induced molecular dipole is linearly related to the external electric field, i.e.

$$\begin{pmatrix} \mu_x^{\text{mol}} \\ \mu_y^{\text{mol}} \\ \mu_z^{\text{mol}} \end{pmatrix} = \begin{pmatrix} \alpha_{xx}^{\text{mol}} & \alpha_{xy}^{\text{mol}} & \alpha_{xz}^{\text{mol}} \\ \alpha_{yx}^{\text{mol}} & \alpha_{yy}^{\text{mol}} & \alpha_{yz}^{\text{mol}} \\ \alpha_{zx}^{\text{mol}} & \alpha_{zy}^{\text{mol}} & \alpha_{zz}^{\text{mol}} \end{pmatrix} \begin{pmatrix} E_x^0 \\ E_y^0 \\ E_z^0 \end{pmatrix} \tag{3.6.2}$$

where E_q^0 a constant external electric field , μ_p^{mol} is the induced molecular dipole, and α_{pq}^{mol} is the dipole-dipole molecular polarizability tensor. This equation can be expressed in tensor form:

$$\mu_p^{\text{mol}} = \alpha_{pq}^{\text{mol}} E_q^0 \tag{3.6.1}$$

For larger external fields, the induced molecular dipole is a power series in external field (B.2.37):

$$\mu_p^{\text{mol}} = \alpha_{pq}^{\text{mol}} E_q^0 + \beta_{pqr}^{\text{mol}} E_q^0 E_r^0 + .. \tag{3.6.2}$$

where β_{pqr}^{mol} is defined as the dipole-dipole-dipole first hyperpolarizability tensor (B.2.31). Therefore, a second definition of molecular polarizability tensor is given by (B.2.23):

$$\alpha_{pq}^{\text{mol}} \equiv \left. \frac{\partial \mu_p^{\text{mol}}}{\partial E_q^0} \right|_{E^0=0} \tag{3.6.3}$$

The procedure for calculating the molecular polarizability tensor outlined in section 3.3 can be tested numerically by calculating a finite difference derivative of induced dipole with external field using 3.5.3.

$$\alpha_{pq}^{\text{mol}} \cong \frac{1}{\Delta E_q} \left(\mu_p^{\text{mol}}(\Delta E_q) - \mu_p^{\text{mol}}(0) \right) \tag{3.6.4}$$

A small constant electric field perturbation ΔE_q is applied to each atom for all three directions (q = 1, 2, 3). The induced dipoles $\mu_p^{\mathrm{i}}(\Delta E_q)$ are then calculated iteratively using 3.3.1 for each atom (i = 1, .. N) in all three directions (p = 1,2,3). $\mu_p^{\mathrm{i}}(0)$ need not be calculated because the induced dipoles are zero for zero external field. The total induced molecular dipole is given by the sum of induced atomic dipoles $\mu_p^{\mathrm{mol}}(\Delta E_q) = \sum_{\mathrm{i}=1}^{N} \mu_p^{\mathrm{i}}(\Delta E_q)$. Finally, the finite difference molecular polarizability tensor in 3.6.4 may be calculated by dividing by ΔE_q.

As an example, atomic polarizabilities (α) and exponents (β) for water were found (by a procedure to be discussed later) to be α_{O} = 0.6830 Å^3, β_{O} = 1.5484 Å^{-1} for oxygen and α_{H} = 0.2515 Å^3, β_{H} = 3.1603 Å^{-1} for hydrogen. In Table 3.1, the molecular polarizability tensor for water is calculated exactly using the procedure from section 3.3, and also numerically using 3.6.4 with $\Delta E_q = 10^{-4}$ eÅ^{-2}. Notice the errors in the finite difference numerical derivative are on the same order as the finite difference 10^{-4} - 10^{-5}.

	α_{XX}	α_{YX}	α_{YY}	α_{ZX}	α_{ZY}	α_{ZZ}
Exact	1.10715	-0.11682	1.18976	0.00000	0.00000	0.84381
Numerical	1.10711	-0.11679	1.18970	0.00000	0.00000	0.84379

Table 3.1 Exact and numerical finite difference molecular polarizability tensor (Å^3) for water calculated using the induced Gaussian dipole polarizability model.

3.7 Conclusions

An induced Gaussian dipole polarization model was developed as a generalization of the induced point dipole model. The main drawback to the original induced point dipole model of Applequist is the polarization catastrophe condition which occurs when

the distance between two induced point dipoles approaches $R = \left(4\alpha^1\alpha^2\right)^{\frac{1}{6}}$ and the polarization interaction diverges. It was shown the interaction between two induced Gaussian dipoles is finite for all distances if the Gaussian exponent β is sufficiently diffuse:

$$\beta < \frac{1}{\left(\alpha \frac{4}{3\sqrt{8\pi}}\right)^{\frac{1}{3}}}$$

As in Applequist and Thole, the procedure to calculate molecular polarizability tensors from induced Gaussian dipoles was outlined in section 2.3. The molecular polarizability tensor was calculated explicitly for the case of a diatomic molecule with induced Gaussian dipoles, induced Thole dipoles, and induced point dipoles. The procedure to calculate the molecular polarizability tensor was also tested numerically by calculating a finite difference derivative of induced dipole with respect to external field.

A drawback to the Thole model is that the model is essentially a damping function between induced dipole – induced dipole interactions. Though it solves the polarization catastrophe problem, it does not prescribe a method to calculate interactions between induced dipoles and permanent charges. Ad hoc assumptions are needed to define interactions between induced dipoles and permanent charges. Moreover, if future studies indicate induced quadrapoles are important, there is no clear path to generalize Thole to include higher order multipoles.

On the other hand, all interactions are well defined in the induced Gaussian dipole model because the Gaussian dipole is based on a charge density. It is straightforward to evaluate the interaction of an induced Gaussian dipole with another induced Gaussian dipole or any other source of permanent charge (e.g. point charges, point multipoles, or

Gaussian multipole charge densities). The main assumption in the induced Gaussian dipole model was the use of 'effective' electric fields rather than ordinary electric fields to induce polarization.

One reason that 'effective' fields rather than ordinary electric fields are used to polarize the induced Gaussian dipole is because the induced Gaussian dipole is a charge density defined over a finite volume. If ordinary electric field is used, it is only defined at a single point; i.e. that of the Gaussian dipole atomic center. 'Effective' fields implicitly integrates out the effect that the induced Gaussian dipole is a charge density delocalized over a finite volume.

3.8 References

1 P. Ren, A. Grossfield, and J. W. Ponder, AMOEBA Force Field, ftp://dasher.wustl.edu/pub/tinker/params.

2 G. A. Kaminski, H. A. Stern, B. J. Berne, R. A. Friesner, Y. X. Cao, R. B. Murphy, R. Zhou, and T. A. Halgren, J. Comp. Chem. **23**, 1515 (2002)

3 S. Patel and C. L. Brooks III, J. Comp. Chem. **25**, 1 (2004)

4 P. Cieplak, J. Caldwell, and P. Kollman, J. Comp. Chem., **22** (**10**), 1048 (2001)

5 K. Palmo, B. Mannfors, N. G. Mirkin, and S. Krimm, Biopolymers **68**, 383 (2003)

6 C. I. Bayly, P. Cieplak, W. D. Cornell, and P. A. Kollman, J. Phys. Chem. **97**, 10269 (1993)

7 G. Lamoureux, A. D. MacKerell, and B. J. Roux, J. Chem. Phys. **119**, 5185 (2003)

[8] H. Yu, T. Hansson, and W.F. van Gunsteren, J. Chem. Phys. 118, 221 (2003)

[9] S. W. Rick, S.J. Stuart, and B.J. Berne, J. Chem. Phys. 101, 6141 (1994)

[10] J. Caldwell, L. X. Dang, and P. A. Kollman, J. Am. Chem. Soc. 112, 9144 (1990)

[11] C. J. Burnham, J. Li, S. S. Xantheas, and M. Leslie, J. Chem. Phys. **110**, 4566 (1999)

[12] P. Ren and J. W. Ponder, J. Phys. Chem. B **107**, 5933 (2003)

[13] L. Silberstein, Phil. Mag. **33**, 92, 215, 521 (1917)

[14] J. Applequist, J. R. Carl, and K. K. Fung, J. Am. Chem. Soc. **94**, 2952 (1972)

[15] B. T. Thole, Chem. Phys. **59**, 341 (1981)

[16] P. Th. van Duijnen, and M. J. Swart, J. Phys. Chem. A **102**, 2399 (1998)

[17] P. Paricaud, M. Předota, A. A. Chialvo, and P. T. Cummings, J. Chem. Phys. **122**, 244511 (2005)

[18] M. Masia, M. Probst, and R. J. Rey, J. Chem. Phys. **123**, 164505 (2005)

[19] D. M. York, W. Yang, J. Chem. Phys. **104**, 159 (1996)

[20] G. A. Cisneros, J. P. Piquemal, and T. A. Darden, J. Chem. Phys. **125**, 184101 (2006)

[21] J. P. Piquemal, N. Gresh, and C. Giessner-Prettre, J. Phys. Chem. A **107**, 10353 (2003)

[22] M. A. Freitag, M. S. Gordon, J. H. Jensen, and W. J. Stevens, J. Chem. Phys. **112**, 7300 (2000)

[23] C. J. Burnham, J. Li, S. S. Xantheas, and M. Leslie, J. Chem. Phys. **110**, 4566 (1999)

4 Implementation of Induced Gaussian Dipoles into Molecular Dynamics Simulations: AMBER

4.1 Introduction

In the previous chapter, the induced Gaussian dipole polarization model was introduced as a generalization of the induced point dipole model. The calculation of molecular polarizability tensors and the polarization catastrophe condition was discussed. This chapter will focus on implementing induced Gaussian dipoles into a molecular dynamics simulation program.

Polarization energy[1 2], work, and force[3] have been derived previously for an induced point dipole interacting with an external field. In this chapter, polarization energy, work, and force are derived for a system of induced Gaussian dipoles interacting with a source of permanent charges. In section 4.2, polarization energy is derived for a collection of induced Gaussian dipoles interacting with one another and an external field source. When a charge distribution becomes polarized due to the presence of an external field, work is done because there is movement of charge. The total polarization energy is composed of the electrostatic interaction energy of the Gaussian dipoles and the work needed to polarize the dipoles. In section 4.3, polarization force is derived as the negative gradient of polarization energy with respect to particle position. It was shown in appendix A.4 and A.5 that permanent dipoles experience a translational force term and an orientation force term due to torque. Since the polarization energy is the sum of the electrostatic energy of the induced dipoles U and the work to polarize the dipoles V, the polarization force can be calculated as the sum of two contributions, F_U and F_V. F_U is the

negative gradient of U with respect to particle position and F_V is the negative gradient of V. It is shown that the torque term from both F_U and F_V exactly cancel so that there is no torque term for induced dipoles. It is interesting to note that the final form of the force on induced Gaussian dipoles is identical to the force on a permanent Gaussian dipole without the orientation torque term.

It was mentioned in the previous chapter that in order to generalize the induced point dipole polarization into the induced Gaussian dipole model, 'effective' electric fields rather than ordinary electric fields are used to induce polarization. One reason to use 'effective' fields is that electrostatic energy can be conveniently expressed in terms of 'effective' potentials and fields (see section 2.8). Another reason to use 'effective' fields to induce polarization is that the dipole-dipole interaction matrix is symmetric with respect to particle interchange. In the following derivation of polarization force, a key assumption is that the dipole-dipole interaction matrix be symmetric with respect to particle interchange. This assumption would not hold if ordinary electric fields between Gaussian particles were used to induce polarization. Finally, ordinary fields act upon a single point, and the induced Gaussian dipole is a charge density delocalized over a finite volume. The 'effective' field implicitly integrates out the effect that the field point is over the induced Gaussian dipole density.

Molecular simulations are frequently performed under periodic boundary conditions. A system with periodic boundary conditions interacts with images of itself replicated over again in all three dimensions. A solid crystal would be an example, of a periodic system. In order to simulate the effects of solvent at long range, simulations of biological systems often use periodic boundary conditions. Long range electrostatic

interactions converge slowly and special techniques such as Ewald summation[4 - 7] or Particle Mesh Ewald[8 - 12] (PME) are used to speed convergence of the electrostatic interactions. A brief derivation of the Ewald summation method for point charges and point dipoles is provided in appendix D. In section 4.4, the results from appendix D are summarized. This is followed by a brief discussion of how a periodic system of point charges and Gaussian dipoles can be calculated as a short range correction to the results for a periodic system of point charges and point dipoles.

In section 3.3, it was noted that the induced dipoles can be calculated by solving a system of linear equations. Typically, this is done by making an initial guess for the induced dipoles and then calculating the induced dipoles (3.3.2) iteratively until self-consistency is achieved. For large systems, this method can be expensive during a molecular dynamics simulation. An alternative method of calculating the induced dipoles is to use a Car-Parinello[13] (CP) extended Lagrangian scheme. Initially, the induced dipoles are calculated exactly by solving the set of linear equations for induced dipoles iteratively. The induced dipoles along with their velocities are then treated as dynamical variables. Equations of motion are derived from a Lagrangian for the induced dipoles so that the induced dipoles propagate in such a way that their values fluctuate around their true values. This method has previously been implemented in molecular dynamics simulations[10 14 - 16]. A brief discussion of the Lagrangian dipole propagation scheme is described in section 3.5.

Finally in section 3.6, simulation results are provided in the form of AMBER output. The force for induced Gaussian dipoles is compared with a finite difference derivative of energy. During a molecular dynamics simulation, the polarization energy as

calculated exactly by the iterative method is compared to the polarization energy from propagating the induced dipoles using the CP Lagrangian scheme for a box of 341 waters simulated in the *NPT* ensemble

4.2 Polarization Energy

In this section, polarization energy is derived for a system of induced Gaussian dipoles interacting with one another and a permanent external field composed of point charges. The electrostatic energy of the system is derived in terms of a permanent – permanent charge interaction, a permanent – polarizable, and a polarizable – polarizable interaction. Following the discussion on electrostatic energy, the polarization work and total polarization energy is derived for the system of induced Gaussian dipoles.

Electrostatic Energy

Consider a system composed of *N* atoms with permanent charges and induced Gaussian dipoles $\vec{\mu}^i$ (i = 1, 2.. N). The permanent charges could be point charges, point multipoles, or Gaussian multipoles. The total electrostatic energy U^{tot} of the system can be expressed as a sum of contributions:

$$U^{tot} = U^{00} + U^{0-pol} + U^{pol-pol} \qquad 4.2.1$$

where U^{00} is the electrostatic energy of permanent charges with permanent charges, U^{0-pol} is the electrostatic energy of permanent charges with induced Gaussian dipoles, and $U^{pol-pol}$ is the electrostatic energy of induced Gaussian dipoles with induced Gaussian dipoles.

The calculation of the permanent charge – permanent charge energy U^{00} follows straightforwardly from the electrostatic model, e.g.

$$U^{00} = \frac{1}{2}\sum_{i\neq j}^{N}\frac{q^i q^j}{R^{ij}} \qquad \text{for point charges}$$

$$U^{00} = \frac{1}{2}\sum_{i\neq j}^{N}\sum_{n,m}\Theta^{(n),i}\Theta^{(m),j}\cdot\nabla^{(n),i}\nabla^{(m),j}\frac{1}{R^{ij}} \qquad \text{for point multipoles}$$

$$U^{00} = \frac{1}{2}\sum_{i\neq j}^{N}\sum_{n,m}\Theta^{(n),i}\Theta^{(m),j}\cdot\nabla^{(n),i}\nabla^{(m),j}\frac{erf(\beta_{ij}R^{ij})}{R^{ij}} \qquad \text{for Gaussian multipoles}$$

The electrostatic energy of an induced Gaussian dipole $\vec{\mu}^i$ with a permanent charge can be expressed in terms of 'effective' field $\vec{E}^{0,j\to i}(\vec{R}^i;\vec{R}^j)$ from the permanent charge at $\vec{R}^j$ onto the induced dipole at $\vec{R}^i$, i.e. (2.8.4) is given by:

$$U_{ij}^{0-pol} = -\vec{\mu}^i\cdot\vec{E}^{0,j\to i}(\vec{R}^i;\vec{R}^j) \qquad 4.2.3$$

where the ˜ symbol on the 'effective' field in 2.8.4 has been dropped for clarity. For example, the 'effective' field from a point charge is given by:

$$\begin{aligned}\vec{E}^{0,j\to i}(\vec{R}^i;\vec{R}^j) &= -\nabla^i q^j\frac{erf(\beta_i R^{ij})}{R^{ij}}\\ &= q^j\vec{R}^{ij}\beta_i^3 B_1(\beta_i R^{ij})\end{aligned} \qquad 4.2.4$$

The total electrostatic energy between a system of induced Gaussian dipoles interacting with permanent charges is given by:

$$U^{0-pol} = -\sum_{i=1}^{N}\vec{\mu}^i\cdot\vec{E}^{0,i}(\vec{R}^i) \qquad 4.2.5$$

where $\vec{E}^{0,i}(\vec{R}^i)$ is the total 'effective' field on induced dipole *i* due to the permanent charges.

$$\vec{E}^{0,i}(\vec{R}^i) = \sum_{j=1}^{N} \vec{E}^{0,j\to i}(\vec{R}^i;\vec{R}^j) \qquad 4.2.6$$

The interaction energy between two Gaussian dipoles is given by (3.2.7): $U_{11}^{12} = -\vec{\mu}^1 \cdot \mathbf{T}^{12} \cdot \vec{\mu}^2$, where $\mathbf{T}^{12} = \beta_{12}^3 \left\{ \beta_{12}^2 \vec{R}^{12}\vec{R}^{12} B_2(x) - B_1(x)\vec{\vec{I}} \right\}$ is the dipole – dipole interaction matrix in 3.2.8. Therefore, the total interaction of a system of Gaussian dipoles is given by:

$$U^{pol-pol} = -\frac{1}{2}\sum_{i\neq j}^{N} \vec{\mu}^i \vec{\mu}^j \cdot \mathbf{T}^{ij} \qquad 4.2.7$$

The permanent – permanent charge interaction energy U^{00} does not affect polarization energy or work, and it need not be considered now. Therefore, the electrostatic energy of polarization U^{pol} is defined as:

$$\begin{aligned} U^{pol} &\equiv U^{0-pol} + U^{pol-pol} \\ &= -\sum_{i=1}^{N} \vec{\mu}^i \cdot \vec{E}^{0,i}(\vec{R}^i) - \frac{1}{2}\sum_{i\neq j}^{N} \vec{\mu}^i \vec{\mu}^j \cdot \mathbf{T}^{ij} \end{aligned} \qquad 4.2.8$$

Polarization Work and Energy

A charge distribution $\rho(\vec{r})$ becomes polarized or perturbed in the presence of an external electric field $\vec{E}$. There is work involved in polarizing a charge distribution because charge is being moved due to the external field. In the case of Gaussian dipoles, the polarizable charge distribution is given by 2.2.2:

$$\rho(\vec{r}) = \vec{\mu} \cdot \nabla^R \left(\frac{\beta}{\sqrt{\pi}} \right)^3 \exp(-\beta^2 \left| \vec{r} - \vec{R} \right|^2) \qquad 4.2.9$$

The total polarization energy *W* is the sum of the polarizable electrostatic interaction energy U^{pol} and the work needed to polarize the charge distribution *V*.

$$W = U^{pol} + V \tag{4.2.10}$$

From 4.2.8, U^{pol} can formally be expressed as a function of the induced dipoles $\vec{\mu}^i$ and the permanent 'effective' fields at the positions of induced dipoles $\vec{E}^{0,i} \equiv \vec{E}^{0,i}(\vec{R}^i)$. Ultimately, $\vec{E}^{0,i}$ is a linear function of the permanent charges q^j (multipole moments, charge densities, etc). However for brevity, U^{pol} may be considered a function of $\vec{\mu}^i$ and $\vec{E}^{0,i}$. Hence, *W* and *V* are also functions of $\vec{\mu}^i$ and $\vec{E}^{0,i}$, i.e.

$$W = W(\vec{\mu}^i, \vec{E}^{0,i}) \tag{4.2.11}$$

The polarizable charge distribution $\rho(\vec{r})$ or dipoles $\vec{\mu}^i$ organizes itself so that *W* is a minimum with respect to variations in $\rho(\vec{r})$ at constant permanent field[1] $\vec{E}^{0,i}$.

$$\left(\frac{\partial W}{\partial \mu_p^i}\right)_{\vec{E}^{0,i}} = 0 \tag{4.2.12}$$

where μ_p^i is any component of $\vec{\mu}^i \equiv \mu_p^i \hat{x}_p$. If the polarizable charge distribution $\rho(\vec{r})$ or dipoles $\vec{\mu}^i$ are held fixed, the charges do not move and the work is zero[1].

$$\left(\frac{\partial V}{\partial E_p^{0,i}}\right)_{\vec{\mu}^i} = 0 \tag{4.2.13}$$

Therefore, the derivative in *W* with respect to $\vec{E}^{0,i}$ at constant $\vec{\mu}^i$ is given by:

$$\left(\frac{\partial W}{\partial E_p^{0,i}}\right)_{\vec{\mu}^i} = \left(\frac{\partial U}{\partial E_p^{0,i}}\right)_{\vec{\mu}^i} + \left(\frac{\partial V}{\partial E_p^{0,i}}\right)_{\vec{\mu}^i} = \left(\frac{\partial U}{\partial E_p^{0,i}}\right)_{\vec{\mu}^i} \tag{4.2.14}$$

For small variations in $\vec{\mu}^i$ and $\vec{E}^{0,i}$, the variation in *W* is given by:

$$dW = \left(\frac{\partial W}{\partial E_p^{0,i}}\right)_{\vec{\mu}^i} d(E_p^{0,i}) + \left(\frac{\partial W}{\partial \mu_p^i}\right)_{\vec{E}^0} d\mu_p^i \tag{4.2.15}$$

Inserting 4.2.14 and 4.2.12 into 4.2.15, yields:

$$dW = \left(\frac{\partial U}{\partial E_p^{0,i}} \right)_{\vec{\mu}^i} d(E_p^{0,i}) \qquad 4.2.16$$

From 4.2.8,

$$\left(\frac{\partial U}{\partial E_p^{0,i}} \right)_{\vec{\mu}^i} = -\mu_p^i \qquad 4.2.17$$

The total polarization energy may be found by integrating 4.2.16 from zero external permanent field to the full permanent field specified by the permanent charges q^j. Suppose $q^j \to \lambda q^j$ where $0 \le \lambda \le 1$, then $E_p^{0,i} \to \lambda E_p^{0,i}$ because the 'effective' field is linearly related to the permanent charges. Therefore, $d(E_p^{0,i}) = E_p^{0,i} d\lambda$, and the total work is given by:

$$W = -\int_0^1 d\lambda \mu_p^i E_p^{0,i} \qquad 4.2.18$$

However, μ_p^i is determined from solving the linear equations (2.4.3):

$$\mathbf{A}\overline{\mu} = \overline{E}^0 \qquad 4.2.19$$

where $\overline{\mu}$ and $\overline{E}^0$ are vectors of size 3N and $A_{qr}^{jk} \equiv \frac{1}{\alpha^j}\delta_{jk}\delta_{qr} - T_{qr}^{jk}$ is a 3N x 3N matrix defined in 3.3.5 (or 3.3.9 for anisotropic atomic polarizabilities). Solving for $\overline{\mu}$ in 4.2.19

$$\overline{\mu} = \mathbf{A}^{-1}\overline{E}^0 \qquad 4.2.20$$

or in component form, $\mu_p^i = A_{pq}^{-1,ij} E_q^{0,j}$. This can be inserted into 4.2.18 with $E_p^{0,i} \to \lambda E_p^{0,i}$:

$$
\begin{aligned}
W &= -\int_0^1 \lambda d\lambda (A_{pq}^{-1,ij} E_q^{0,j}) E_p^{0,i} \\
&= -\frac{1}{2} A_{pq}^{-1,ij} E_q^{0,j} E_p^{0,i} = \frac{1}{2} \mu_p^i E_p^{0,i} \\
&= -\frac{1}{2} \sum_{i=1}^{N} \vec{\mu}^i \cdot \vec{E}^{0,i}
\end{aligned}
\tag{4.2.21}
$$

The work needed to polarize the system can be found by:

$$
\begin{aligned}
V &= W - U^{pol} \\
&= -\frac{1}{2} \sum_{i=1}^{N} \vec{\mu}^i \cdot \vec{E}^{0,i} + \sum_{i=1}^{N} \vec{\mu}^i \cdot \vec{E}^{0,i} + \frac{1}{2} \sum_{i,j=1}^{N} \vec{\mu}^i \vec{\mu}^j \cdot \mathbf{T}^{ij} \\
&= \frac{1}{2} \sum_{i=1}^{N} \vec{\mu}^i \cdot \vec{E}^{0,i} + \frac{1}{2} \sum_{i,j=1}^{N} \vec{\mu}^i \vec{\mu}^j \cdot \mathbf{T}^{ij} \\
&= \frac{1}{2} \sum_{i=1}^{N} \vec{\mu}^i \cdot \vec{E}^i
\end{aligned}
\tag{4.2.22}
$$

where $\vec{E}^i$ is the total 'effective' electric field on induced dipole *i* given by:

$$
\vec{E}^i \equiv \vec{E}^{0,i} + \sum_{j=1}^{N} \vec{\mu}^j \cdot \mathbf{T}^{ij} \tag{4.2.23}
$$

4.3 Polarization Force

In the previous section, the polarization energy $W = -\frac{1}{2} \sum_{j=1}^{N} \vec{\mu}^j \cdot \vec{E}^{0,j}$ (4.2.21) was derived for a system of induced Gaussian dipoles $\vec{\mu}^i$ interacting with one another and an 'effective' field $\vec{E}^{0,i}$ due to permanent charges (4.2.6). In tensor component notation, *W* is given by (where repeated indices are summed over):

$$
W = -\frac{1}{2} \mu_q^j E_q^{0,j} \tag{4.3.1}
$$

The polarization force on particle *i* is defined as the negative gradient of polarization energy *W* (4.3.1) with respect to the coordinates of particle *i*.

$$F_p^i = -\frac{\partial W}{\partial x_p^i} = \frac{1}{2}\left(\frac{\partial \mu_q^j}{\partial x_p^i} E_q^{0,j} + \mu_q^j \frac{\partial E_q^{0,j}}{\partial x_p^i} \right) \qquad 4.3.2$$

In order to calculate the first term in 4.3.2, $\frac{\partial \mu_q^j}{\partial x_p^i}$ must be evaluated. The induced dipoles μ_p^i are linearly related to external field $E_q^{0,j}$, by (4.2.20) :

$$\mu_p^i = A_{pq}^{-1,ij} E_q^{0,j} \qquad 4.3.3$$

where A_{qr}^{jk} is defined in 3.3.5 (and in 3.3.9 for anisotropic atomic polarizabilities):

$$A_{qr}^{jk} \equiv \frac{1}{\alpha^j} \delta_{jk} \delta_{qr} - T_{qr}^{jk} \qquad 4.3.4$$

Before proceeding, it should first be noted that the dipole dipole interaction matrix $T_{qr}^{jk} \equiv \frac{\partial}{\partial x_q^j} \frac{\partial}{\partial x_r^j} \frac{erf(\beta_{jk} R^{jk})}{R^{jk}}$ is symmetric with respect to particle interchange $T_{qr}^{jk} = T_{qr}^{kj}$ and component interchange $T_{qr}^{jk} = T_{rq}^{jk}$. Therefore, A_{qr}^{jk} in 4.3.4 is also symmetric. It is straightforward to show that if a matrix $\mathbf{A}$ is symmetric and has an inverse, then the inverse $\mathbf{A}^{-1}$ is also symmetric. Therefore, $A_{qr}^{-1,jk}$ in 4.3.3 is also symmetric, i.e. $A_{qr}^{-1,jk} = A_{qr}^{-1,kj} = A_{rq}^{-1,jk} = A_{rq}^{-1,kj}$.

The derivative of 4.3.3 is given by:

$$\frac{\partial \mu_q^j}{\partial x_p^i} = \frac{\partial A_{qr}^{-1,jk}}{\partial x_p^i} E_r^{0,k} + A_{qr}^{-1,jk} \frac{\partial E_r^{0,k}}{\partial x_p^i} \qquad 4.3.5$$

$\frac{\partial A_{qr}^{-1,jk}}{\partial x_p^i}$ can be found by first noting that for any matrix $\mathbf{A}$ which has an inverse, $\mathbf{A}^{-1}$

$$\mathbf{A}\mathbf{A}^{-1} = \mathbf{I}$$

$$\frac{\partial \mathbf{A}}{\partial x}\mathbf{A}^{-1} + \mathbf{A}\frac{\partial \mathbf{A}^{-1}}{\partial x} = 0 \qquad 4.3.6$$

$$\frac{\partial \mathbf{A}^{-1}}{\partial x} = -\mathbf{A}^{-1}\frac{\partial \mathbf{A}}{\partial x}\mathbf{A}^{-1}$$

Therefore, $A_{qr}^{jk} A_{rs}^{-1,kl} = \delta_{jl}\delta_{qs} \Rightarrow \frac{\partial A_{qr}^{-1,jk}}{\partial x_p^i} = -A_{qs}^{-1,jl}\frac{\partial A_{st}^{lm}}{\partial x_p^i} A_{tr}^{-1,mk}$. This result can be inserted into 4.3.5 and then into 4.3.2 with the result:

$$\begin{aligned} F_p^i &= \frac{1}{2}\left(\left(\frac{\partial A_{qr}^{-1,jk}}{\partial x_p^i} E_r^{0,k} + A_{qr}^{-1,jk}\frac{\partial E_r^{0,k}}{\partial x_p^i}\right)E_q^{0,j} + \mu_q^j \frac{\partial E_q^{0,j}}{\partial x_p^i}\right) \\ &= \frac{1}{2}\left(\left(-A_{qs}^{-1,jl}\frac{\partial A_{st}^{lm}}{\partial x_p^i} A_{tr}^{-1,mk} E_r^{0,k} + A_{qr}^{-1,jk}\frac{\partial E_r^{0,k}}{\partial x_p^i}\right)E_q^{0,j} + \mu_q^j \frac{\partial E_q^{0,j}}{\partial x_p^i}\right) \\ &= \frac{1}{2}\left(-\mu_s^l \frac{\partial A_{st}^{lm}}{\partial x_p^i}\mu_k^m + \mu_r^k \frac{\partial E_r^{0,k}}{\partial x_p^i} + \mu_q^j \frac{\partial E_q^{0,j}}{\partial x_p^i}\right) \\ &= -\frac{1}{2}\mu_q^j \frac{\partial A_{qr}^{jk}}{\partial x_p^i}\mu_r^k + \mu_q^j \frac{\partial E_q^{0,j}}{\partial x_p^i} \end{aligned} \qquad 4.3.7$$

In 4.3.7, it was noted that $A_{qr}^{-1,jk}$ is symmetric and therefore, $\mu_q^j = A_{rq}^{-1,kj} E_r^{0,k}$. From 4.3.4, $\frac{\partial A_{qr}^{jk}}{\partial x_p^i} = -\frac{\partial T_{qr}^{jk}}{\partial x_p^i}$, so that 4.3.7 becomes:

$$F_p^i = \frac{1}{2}\mu_q^j \frac{\partial T_{qr}^{jk}}{\partial x_p^i}\mu_r^k + \mu_q^j \frac{\partial E_q^{0,j}}{\partial x_p^i} \qquad 4.3.8$$

Note that *i* must be equal to *j* or *k*. 4.3.8 becomes:

$$\begin{aligned} F_p^i &= \frac{1}{2}\left(\mu_q^i \frac{\partial T_{qr}^{ik}}{\partial x_p^i}\mu_r^k + \mu_q^j \frac{\partial T_{qr}^{ji}}{\partial x_p^i}\mu_r^i\right) + \mu_q^j \frac{\partial E_q^{0,j}}{\partial x_p^i} \quad \text{(no sum over i)} \\ &= \frac{1}{2}\mu_q^i \mu_r^j \left(\frac{\partial T_{qr}^{ij}}{\partial x_p^i} + \frac{\partial T_{rq}^{ji}}{\partial x_p^i}\right) + \mu_q^j \frac{\partial E_q^{0,j}}{\partial x_p^i} \\ &= \mu_q^i \mu_r^j \frac{\partial T_{qr}^{ij}}{\partial x_p^i} + \mu_q^j \frac{\partial E_q^{0,j}}{\partial x_p^i} \quad \text{(since T is symmetric)} \end{aligned} \qquad 4.3.9$$

It is straightforward to evaluate $\frac{\partial T_{qr}^{ij}}{\partial x_p^i}$ from $\nabla^{(3)} \frac{erf(\beta R)}{R}$ in 2.9.4:

$$\frac{\partial T_{qr}^{ij}}{\partial x_p^i} = (\delta_{pq} R_r^{ij} + \delta_{pr} R_q^{ij} + \delta_{rq} R_p^{ij}) \beta_{ij}^5 B_2(x) - R_p R_q R_r \beta_{ij}^7 B_3(x) \qquad 4.3.10$$

$\frac{\partial E_q^{0,j}}{\partial x_p^i}$ is the gradient of the 'effective' field from permanent charges. As an example, for point charges $\frac{\partial E_q^{0,j}}{\partial x_p^i}$ can be found from 4.2.4 and 4.2.6 to be:

$$\begin{aligned} \frac{\partial E_q^{0,j}}{\partial x_p^i} &= -\nabla^i{}_p \nabla^j{}_q \sum_{k=1}^{N} q^k \frac{erf(\beta_j R^{jk})}{R^{jk}} \\ &= -\delta_{ij} \sum_{k=1}^{N} q^k \nabla^i{}_p \nabla^i{}_q \frac{erf(\beta_j R^{jk})}{R^{jk}} + (1-\delta_{ij}) q^i \nabla^i{}_p \nabla^i{}_q \frac{erf(\beta_j R^{ij})}{R^{ij}} \end{aligned} \qquad 4.3.11$$

4.3.11 can be evaluated further by expressing the gradient tensors in terms of $B_n(x)$ as in 2.9.2 – 2.9.6. Equations 4.3.10 and 4.3.11 can be used to evaluate the force in 4.3.7 for a system of induced Gaussian dipoles and point charges.

It is interesting to note that if ordinary electric fields and not 'effective' electric fields were used to induced the Gaussian dipoles, $T_{qr}^{jk} \equiv \frac{\partial}{\partial x_q^j} \frac{\partial}{\partial x_r^k} \frac{erf(\beta_k \left| \vec{R}^j - \vec{R}^k \right|)}{\left| \vec{R}^j - \vec{R}^k \right|}$ would not be symmetric with respect to particle interchange, $T_{qr}^{jk} \neq T_{qr}^{kj}$. Therefore, A_{qr}^{jk} and $A_{qr}^{-1,jk}$ would also not be symmetric for particle interchange, and the assumptions used in 4.3.7 to derive the force would not be valid. If anisotropic atomic polarizabilities were used, A_{qr}^{jk} would still be symmetric for particle number and component number, and the results for polarization energy, work, and force would still hold.

It is also interesting to note that the final equation for polarization force (4.3.8) is the same result for a permanent Gaussian dipole interacting with a permanent field if the torque term $\frac{\partial \mu_q^j}{\partial x_p^i}$ was neglected. The reason is that if the force were derived in terms of electrostatic energy U and work components V, the torque terms exactly cancel. To illustrate this, matrix notation is used in the following derivation for clarity and brevity. Let $\overline{\mu}$, $\overline{E}^0$, and $\overline{E}$ be $3N$ column vectors for induced dipoles, external permanent 'effective' field, and total 'effective' field. Furthermore, let **T** and **A** be $3N$ *x* $3N$ symmetric matrices defined in 3.3.4. In this notation, the electrostatic interaction energy U^{pol} (4.2.8) and work V (4.2.22) becomes:

$$U^{pol} = -\overline{\mu} \cdot \overline{E}^0 - \frac{1}{2} \overline{\mu} \cdot \mathbf{T} \cdot \overline{\mu} \qquad 4.3.12$$

$$V = \frac{1}{2} \overline{\mu} \cdot \overline{E} \qquad 4.3.13$$

The total field $\overline{E}$ can be expressed in terms of $\overline{E}^0$, $\overline{\mu}$, and **T** from 4.2.23 as:

$$\overline{E} = \overline{E}^0 + \mathbf{T} \cdot \overline{\mu} \qquad 4.3.14$$

The induced dipole is related to total electric field through the atomic polarizabilities, i.e. $\vec{\mu}^i = \alpha^i \vec{E}^i$ (and $\vec{\mu}^i = \boldsymbol{\alpha}^i \cdot \vec{E}^i$ for anisotropic atomic polarizabilities). This can be expressed in matrix notation by:

$$\overline{\mu} = \boldsymbol{\alpha} \cdot \overline{E} \qquad 4.3.15$$

where $\boldsymbol{\alpha}$ is a $3N$ *x* $3N$ diagonal matrix containing the atomic polarizabilities (block diagonal symmetric matrix containing atomic polarizability tensors for the anistropic model). The work in 4.3.13 can then be expressed in terms of $\overline{\mu}$ and $\boldsymbol{\alpha}^{-1}$:

$$V = \frac{1}{2}\,\overline{\mu}\cdot\boldsymbol{\alpha}^{-1}\cdot\overline{\mu} \qquad 4.3.16$$

The force contributions from U^{pol} and V are given by the negative gradients of 4.3.12 and 4.3.16, respectively:

$$\begin{aligned} F^{U} &\equiv -\frac{\partial U^{pol}}{\partial x} \\ &= \frac{\partial\overline{\mu}}{\partial x}\cdot\overline{E}^{0} + \overline{\mu}\cdot\frac{\partial\overline{E}^{0}}{\partial x} + \frac{\partial\overline{\mu}}{\partial x}\cdot\mathbf{T}\cdot\overline{\mu} + \frac{1}{2}\overline{\mu}\cdot\frac{\partial\mathbf{T}}{\partial x}\cdot\overline{\mu} \\ &= \frac{\partial\overline{\mu}}{\partial x}\cdot\overline{E} + \overline{\mu}\cdot\frac{\partial\overline{E}^{0}}{\partial x} + \frac{1}{2}\overline{\mu}\cdot\frac{\partial\mathbf{T}}{\partial x}\cdot\overline{\mu} \end{aligned} \qquad 4.3.17$$

$$\begin{aligned} F^{V} &\equiv -\frac{\partial V}{\partial x} \\ &= -\frac{1}{2}\frac{\partial\overline{\mu}}{\partial x}\cdot\boldsymbol{\alpha}^{-1}\cdot\overline{\mu} - \frac{1}{2}\overline{\mu}\cdot\boldsymbol{\alpha}^{-1}\cdot\frac{\partial\overline{\mu}}{\partial x} = -\frac{\partial\overline{\mu}}{\partial x}\cdot\boldsymbol{\alpha}^{-1}\cdot\overline{\mu} \\ &= -\frac{\partial\overline{\mu}}{\partial x}\cdot\overline{E} \end{aligned} \qquad 4.3.18$$

Therefore, the total force is given as the sum of 4.3.17 and 4.3.18

$$\begin{aligned} F^{W} &\equiv F^{U} + F^{V} \\ &= \frac{\partial\overline{\mu}}{\partial x}\cdot\overline{E} + \overline{\mu}\cdot\frac{\partial\overline{E}^{0}}{\partial x} + \frac{1}{2}\overline{\mu}\cdot\frac{\partial\mathbf{T}}{\partial x}\cdot\overline{\mu} - \frac{\partial\overline{\mu}}{\partial x}\cdot\overline{E} \\ &= \overline{\mu}\cdot\frac{\partial\overline{E}^{0}}{\partial x} + \frac{1}{2}\overline{\mu}\cdot\frac{\partial\mathbf{T}}{\partial x}\cdot\overline{\mu} \end{aligned} \qquad 4.3.19$$

which agrees with 4.3.8. Notice the torque term $\frac{\partial\overline{\mu}}{\partial x}\cdot\overline{E}$ exactly cancels when F^{U} is added to F^{V}.

The above analysis suggests that a possible method of implementing polarization energy, work, and force is given as follows: First calculate the purely electrostatic energy of the permanent charges and induced dipoles. Calculate the total ('effective') electric field (4.3.14) and the force on the dipoles (4.3.8 or 4.3.19). Then add the polarization

work $V = \frac{1}{2}\overline{\mu} \cdot \overline{E}$ to the total electrostatic energy. This is essentially the algorithm that was previously implemented in AMBER for point charges and induced point dipoles.

4.4 Extension to Periodic Systems: Ewald Summation

As mentioned in the introduction, molecular dynamics simulations are often run under periodic boundary conditions in order to remove the artificial boundary from the sides of a simulation box or unit cell. The electrostatic interaction energy of the unit cell with itself and all periodic images of itself is given by:

$$U_{point} = \frac{1}{2}\sum_i \sum_j \left(q^i + \vec{\mu}^i \cdot \nabla^i\right)\left(q^j - \vec{\mu}^j \cdot \nabla^i\right)\sum_{\vec{n}}{}^{*} \frac{1}{\left|\vec{R}^{ij} + \vec{n}\right|} \qquad 4.4.1$$

where the sides of the box are $\vec{a}_r$ and $\vec{n} = n_1\vec{a}_1 + n_2\vec{a}_2 + n_3\vec{a}_3$ is a unit cell translation vector (n_i are integers). The * indicates that if $\vec{n} = 0$, omit the $i = j$ term and any other terms in the 'masked list', e.g. do not count 1-2 or 1-3 Coulomb interactions between atoms that are bonded to or near each other.

Coulomb interactions decay slowly as 1/*r*. Consequently, the sum in 4.4.1 is a conditionally convergent series. In practice, the series converges very slowly. The Ewald summation method was devised in order to significantly speed the convergence of 4.4.1 for periodic systems. In the Ewald method, the Coulomb energy is separated into parts. A Fourier series called the reciprocal sum is used to calculate the slowly varying periodic part of the Coulomb energy. The other part of the energy, called the direct sum energy, converges rapidly with distance. The direct sum energy is mainly due to particle interactions which are near one another and can be truncated at a specified non-bonded cutoff, typically ~8Å. In addition, there is also a self-interaction correction to the energy

and an energy correction to account for the 'masked pairs', which are interaction pairs purposely not included in 4.4.1 (e.g. 1-2 or 1-3 Coulomb interactions). A brief derivation of the Ewald summation method of point charges and point dipoles is provided in appendix D. The result for energy is given by D.13 and D.14:

$$U = U_{rec} + U_{dir} + U_{adj} + U_{self} \tag{4.4.2}$$

$$\begin{aligned}
U_{rec} &\equiv \frac{1}{2}\sum_i \sum_j \left(q^i + \vec{\mu}^i \cdot \nabla^i\right)\left(q^j - \vec{\mu}^j \cdot \nabla^i\right)\sum_{\vec{m}\neq 0} \frac{1}{V_{cell}\pi\, m^2} e^{-\frac{m^2\pi^2}{\beta^2}} e^{2\pi i \vec{m}\cdot\vec{r}^{ij}} \\
U_{dir} &\equiv \frac{1}{2}\sum_i \sum_j \left(q^i + \vec{\mu}^i \cdot \nabla^i\right)\left(q^j - \vec{\mu}^j \cdot \nabla^i\right)\sum_{\vec{n}}{}^{*} \frac{erfc\left(\beta\left|\vec{r}^{ij} + \vec{n}\right|\right)}{\left|\vec{r}^{ij} + \vec{n}\right|} \\
U_{adj} &\equiv \frac{1}{2}\sum_{(i,j)\in M} \left(q^i + \vec{\mu}^i \cdot \nabla^i\right)\left(q^j - \vec{\mu}^j \cdot \nabla^i\right)\frac{erfc\left(\beta r^{ij}\right) - 1}{r^{ij}} \\
U_{self} &\equiv \frac{1}{2}\sum_i \sum_j \left(q^i + \vec{\mu}^i \cdot \nabla^i\right)\left(q^j - \vec{\mu}^j \cdot \nabla^i\right)\lim_{\substack{\vec{r}^i \to \vec{r}^j \\ i\to j}} \frac{erfc\left(\beta r^{ij}\right) - 1}{r^{ij}}
\end{aligned} \tag{4.4.3}$$

where $erfc(x) \equiv 1 - erf(x) = \frac{2}{\sqrt{\pi}}\int_x^\infty du \exp(-u^2)$ is the complementary error function which decays rapidly for $x > 1$. U_{rec} is the reciprocal sum energy, which is calculated in Fourier space. U_{dir} is the direct sum energy which converges quickly in coordinate space and is truncated outside a non-bond cutoff, typically 8Å. U_{adj} is the correction for the 'masked pairs', e.g. 1-2 or 1-3 Coulomb interactions. U_{self} is the self-interaction correction, i.e. it is a correction for the $i = j$ term for $\vec{n} = 0$. There are also reciprocal, direct, self, and adjusted terms to the potential, field, and force (see appendix D).

The Ewald summation method was devised to speed convergence of the sum (4.4.1), and the method is essentially exact. The energy for a periodic system of point charges and point dipoles is given in 4.4.2. In a periodic system of point charges and Gaussian dipoles, the exact electrostatic interaction energy is given by:

$$U_{Gauss} = \frac{1}{2}\sum_i \sum_j q^i q^j \sum_{\vec{n}}{}^* \frac{1}{r^{ij,n}} - \sum_i \sum_j q^i \vec{\mu}^j \cdot \nabla^i \sum_{\vec{n}}{}^* \frac{erf(\beta_i r^{ij,n})}{r^{ij,n}}$$
$$- \frac{1}{2}\sum_i \sum_j \vec{\mu}^i \vec{\mu}^j \cdot \nabla^i \nabla^i \sum_{\vec{n}}{}^* \frac{erf(\beta_{ij} r^{ij,n})}{r^{ij,n}} \qquad 4.4.4$$

where $\vec{r}^{\,ij,n} \equiv \vec{r}^{\,ij} + \vec{n}$. The difference between U_{Gauss} in 4.4.4 and U_{point} in 4.4.1 is a correction

$$\begin{aligned} U_{corr} &= U_{Gauss} - U_{point} \\ &= \sum_i \sum_j q^i \vec{\mu}^j \cdot \nabla^i \sum_{\vec{n}}{}^* \frac{erfc(\beta_i r^{ij,n})}{r^{ij,n}} \\ &+ \frac{1}{2}\sum_i \sum_j \vec{\mu}^i \vec{\mu}^j \cdot \nabla^i \nabla^i \sum_{\vec{n}}{}^* \frac{erfc(\beta_{ij} r^{ij,n})}{r^{ij,n}} \end{aligned} \qquad 4.4.5$$

Since *erfc*(*x*) decays rapidly for $x > 1$, the correction for Gaussian dipoles also decays rapidly in distance. The force correction $\vec{F}^i_{corr}$ can be found by taking the negative gradient of 4.4.5, (without the $\frac{\partial \mu}{\partial x}$ torque term).

$$\vec{F}^i_{corr} = \sum_j \left(q^j \vec{\mu}^i - q^i \vec{\mu}^j\right) \cdot \nabla^i \nabla^i \sum_{\vec{n}}{}^* \frac{erfc(\beta_i r^{ij,n})}{r^{ij,n}}$$
$$- \sum_j \vec{\mu}^j \vec{\mu}^i \cdot \nabla^i \nabla^i \nabla^i \sum_{\vec{n}}{}^* \frac{erfc(\beta_{ij} r^{ij,n})}{r^{ij,n}} \qquad 4.4.6$$

The electrostatic potential for a periodic system of point charges and point dipoles is given by:

$$\varphi_{point}(\vec{r}^{\,i}) = \sum_j \left(q^j - \vec{\mu}^j \cdot \nabla^i\right) \sum_{\vec{n}'}{}^* \frac{1}{r^{ij,n}} \qquad 4.4.7$$

The 'effective' electrostatic potential on a Gaussian dipole *i* for a periodic system of point charges and Gaussian dipoles is given by:

$$\varphi_{Gauss}(\vec{r}^{\,i}) = \sum_j q^j \sum_{\vec{n}'}{}^* \frac{erf(\beta_i r^{ij,n})}{r^{ij,n}} - \sum_j \vec{\mu}^j \cdot \nabla^i \sum_{\vec{n}'}{}^* \frac{erf(\beta_{ij} r^{ij,n})}{r^{ij,n}} \qquad 4.4.8$$

Therefore, the correction to the 'effective' potential for Gaussian dipole *i* is given by the difference between φ_{Gauss} and φ_{point}:

$$\begin{aligned} \varphi_{corr}(\vec{r}^{\,i}) &= \varphi_{Gauss}(\vec{r}^{\,i}) - \varphi_{point}(\vec{r}^{\,i}) \\ &= -\sum_j q^j \sum_{\vec{n}'}{}^* \frac{erfc(\beta_i r^{ij,n})}{r^{ij,n}} \\ &\quad + \sum_j \vec{\mu}^j \cdot \nabla^i \sum_{\vec{n}'}{}^* \frac{erfc(\beta_{ij} r^{ij,n})}{r^{ij,n}} \end{aligned} \qquad 4.4.9$$

The correction to the total 'effective' field on Gaussian dipole *i* is given by the negative gradient of 4.4.9:

$$\begin{aligned} \vec{E}_{corr}(\vec{r}^{\,i}) &= -\nabla^i \varphi_{corr}(\vec{r}^{\,i}) \\ &= \sum_j q^j \nabla^i \sum_{\vec{n}'}{}^* \frac{erfc(\beta_i r^{ij,n})}{r^{ij,n}} - \sum_j \vec{\mu}^j \cdot \nabla^i \nabla^i \sum_{\vec{n}'}{}^* \frac{erfc(\beta_{ij} r^{ij,n})}{r^{ij,n}} \end{aligned} \qquad 4.4.10$$

The gradient tensors $\nabla^{(n)} \frac{erfc(\beta r)}{r}$ are evaluated in D.2.24 – D.2.26.

The algorithm implemented into AMBER is given by the following:

1) Calculate point charge and point dipole Ewald terms for electrostatic energy, force, and field. There is no dipole torque term to the force (see discussion at the end of section 4.3).
2) Calculate the Gaussian dipole correction for energy, force, and total 'effective' field.
3) The induced dipoles are calculated using the total corrected field.
4) The polarization work is calculated from the induced dipoles and the total field. This work is then added to the electrostatic interaction energy of the Gaussian dipoles to yield the total polarization energy.

4.5 Induced Dipole Iterative Methods

The induced dipoles (3.3.2) can be calculated exactly by solving a system of linear equations. Typically, this is accomplished by making an initial guess of the induced dipole and calculating a new set of induced dipoles from the field of the old set of induced dipoles. This procedure is done iteratively until self-consistency is achieved. In matrix notation, the predicted set of induced dipoles at the $(k+1)^{th}$ iteration is given by:

$$\overline{\mu}_{k+1} = \boldsymbol{\alpha}\left(\overline{E}^{0} + \mathbf{T} \cdot \overline{\mu}_{k}\right) \qquad 4.5.1$$

It was found that in some cases, the dipoles did not converge, but fluctuated about mean values. In order to dampen the fluctuations in solving systems of linear equations through iterative algorithms, Successive Over-Relaxation (SOR) methods[17] take a weighted average over the predicted and previous induced dipole:

$$\overline{\mu}_{k+1} = \Omega\boldsymbol{\alpha}\left(\overline{E}^{0} + \mathbf{T} \cdot \overline{\mu}_{k}\right) + (1-\Omega)\overline{\mu}_{k} \qquad 4.5.2$$

Ponder and Ren[18] have recommended a value for Ω of 0.7.

4.6 Lagrangian Dipole Propagation

As noted in the introduction, the iterative method of solving for the induced dipoles can be expensive during a molecular dynamics simulation. An alternative to the iterative procedure is to use a Car-Parrinello[13] (CP) extended Lagragian method[10 14-16]. Originally, the CP method was developed for density functional molecular dynamics. The electronic ground state of the system is initially calculated. The electronic ground state follows the nuclear motion adiabatically through equations of motion that are derived from a Lagrangian. A similar scheme has been developed for propagating

induced dipoles. This CP dipole propagation scheme has previously been implemented into AMBER[10] for induced point dipoles.

In this scheme, the induced dipoles $\vec{\mu}^i$ and atomic positions $\vec{r}^{\,i}$ along with their velocities $\dot{\vec{\mu}}^i$ and $\dot{\vec{r}}^{\,i}$ are treated as dynamical variables. The Lagrangian of the system is given by:

$$L \equiv \frac{1}{2}\sum_{i=1}^{N} m_i \dot{\vec{r}}^{\,i} \cdot \dot{\vec{r}}^{\,i} + \frac{1}{2}\sum_{i=1}^{N} M\dot{\vec{\mu}}^i \cdot \dot{\vec{\mu}}^i - U \qquad 4.6.1$$

where m_i is the mass of the particle and M is the fictitious mass of the induced dipole. U is the sum of the permanent – permanent charge energies, the electrostatic energy of the dipoles, and the work to polarize the dipoles expressed by:

$$U = U^{00} - \sum_{j=1}^{N} \vec{\mu}^j \cdot \vec{E}^{0,j} - \frac{1}{2}\sum_{j=1}^{N}\sum_{k=1}^{N} \vec{\mu}^j \cdot \mathbf{T}^{jk} \cdot \vec{\mu}^k + \frac{1}{2}\sum_{i=1}^{N} \frac{\vec{\mu}^i \cdot \vec{\mu}^i}{\alpha^i} \qquad 4.6.2$$

The Lagrangian equations of motion for the atomic positions are given by:

$$\begin{aligned} \frac{d}{dt}\left(\frac{\partial L}{\partial \dot{\vec{r}}^{\,i}}\right) &= \frac{\partial L}{\partial \vec{r}^{\,i}} \\ m_i \ddot{\vec{r}}^{\,i} &= -\frac{\partial U^{00}}{\partial \vec{r}^{\,i}} + \sum_{j=1}^{N} \vec{\mu}^j \cdot \frac{\partial \vec{E}^{\,j}}{\partial \vec{x}^{\,i}} \\ &= \vec{F}^{\,00,i} + \sum_{j=1}^{N} \vec{\mu}^j \cdot \frac{\partial \vec{E}^{\,0,j}}{\partial \vec{x}^{\,i}} + \frac{1}{2}\sum_{j=1}^{N}\sum_{k=1}^{N} \vec{\mu}^j \cdot \frac{\partial \mathbf{T}^{jk}}{\partial \vec{x}^{\,i}} \cdot \vec{\mu}^k \\ &= \vec{F}^{\,00,i} + \vec{F}^{\,pol,i} \end{aligned} \qquad 4.6.3$$

where $\vec{F}^{00,i}$ is the force due to permanent charges and $\vec{F}^{\,pol,i}$ is the polarization force given by 4.3.8. The Lagrangian equations of motion for the induced dipoles are given by:

$$\frac{d}{dt}\left(\frac{\partial L}{\partial \dot{\vec{\mu}}^i}\right) = \frac{\partial L}{\partial \vec{\mu}^i}$$

$$M\ddot{\vec{\mu}}^i = \vec{E}^{0,i} + \sum_{j=1}^{N} \mathbf{T}^{ij} \cdot \vec{\mu}^j - \frac{\vec{\mu}^i}{\alpha^i} \qquad 4.6.4$$

$$= \vec{E}^i - \frac{\vec{\mu}^i}{\alpha^i}$$

The dipoles $\vec{\mu}^i$ fluctuate about the mean value $\alpha^i \vec{E}^i$ which is the true value of the dipoles.

The dipole velocities $\dot{\vec{\mu}}^i$ are maintained at a constant temperature which is small using a Berendsen[19] thermostat. If $T = \frac{2}{3k}\frac{1}{2}\sum_{i=1}^{N} M\dot{\vec{\mu}}^i \cdot \dot{\vec{\mu}}^i$ is the current temperature of the dipoles (k is Boltzmann's constant) and the T_0 is the reference temperature, then the dipole velocities $\dot{\vec{\mu}}^i$ are scaled at each time step by

$$\left[1 + \frac{\Delta t}{\tau}\left(\frac{T_0}{T} - 1\right)\right]^{\frac{1}{2}} \qquad 4.6.5$$

where Δt is the time step and τ is a time constant. The reference temperature is kept small T_0 = 1K so that the dipole velocities $\dot{\vec{\mu}}^i$ and accelerations $\ddot{\vec{\mu}}^i$ are small, and therefore, the dipoles are kept close to their true values. The dipole mass M is also kept small so that the dipoles can quickly adjust to the nuclear motion. However, if M is too small, the dynamics quickly become unstable. For a 1fs time step, it has been empirically determined[10] that M = 0.3 leads to a stable simulation for induced point dipoles. When the CP algorithm was tested with the induced Gaussian dipoles, it was found that for many liquids that τ = 1.0 ps leads to stable simulations with averaged polarization energies near their true values. For strongly polar systems, τ had to be smaller at 0.1 ps.

For larger values of τ, gradual heating occurred in the simulations, which was indicated by an increase in average polarization energy over time.

4.7 Results

This section will present some results of the induced Gaussian dipole implementation into AMBER. From a CPU cost perspective, the cost of the induced Gaussian dipole correction is only slightly more expensive than the previously existing induced point dipole scheme. The main reason for this is that the energy correction in 4.4.5 decays rapidly with distance. A typical value of the Gaussian exponent for the induced dipoles is 1.0 $Å^{-1}$. At this value, the non-bond cutoff for the energy correction is around 4.89 Å for a tolerance of 10^{-12}. This leads to an overall CPU overhead of the induced Gaussian dipole polarization model over the previous induced point dipole polarization model of approximately 30%.

During the implementation of induced Gaussian dipoles, numerous tests were done on gas phase dimers. In Table 4.1, analytic forces are compared to numerical forces obtained by a finite difference approximation.

F (analytic) = -1.09908219 0.42747651 0.00000000
F (numerical) = -1.09908099 0.42747700 -0.00000100

F (analytic) = -0.20124978 0.01732015 0.00000000
F (numerical) = -0.20125099 0.01732000 -0.00000000

F (analytic) = -0.33547487 0.18759862 -0.14361461
F (numerical) = -0.33547499 0.18759799 -0.14361500

Table 4.1 Exact and Numerical finite difference forces for the induced Gaussian dipole polarization model in AMBER.

The CP Lagrangian dipole propagation scheme, which was previously implemented into AMBER, was test on the new induced Gaussian polarization model. A box of 341 polarizable waters (the Force Field parameters of the water will be discussed in chapter seven) was simulated for 500 ps in the *NPT* ensemble. The temperature and pressure were monitored using a Berendsen[19] thermostat with temperature and pressure coupling constants, τ_T = 1.0 ps, and τ_P = 1.0 ps, respectively. The atomic positions and velocities were integrated through the Velocity Verlet algorithm, with constraints placed on bond lengths through the SHAKE[20 21] algorithm. The induced dipoles were propagated with the CP Lagrangian method with temperature coupling constants for the induced dipoles, τ = 1.0 ps and 0.1 ps. The induced dipoles were also calculated iteratively with a tolerance of 10^{-5} D for RMSD of the dipoles between successive iterations. The average number of iterations per time step at this tolerance is 4.35.

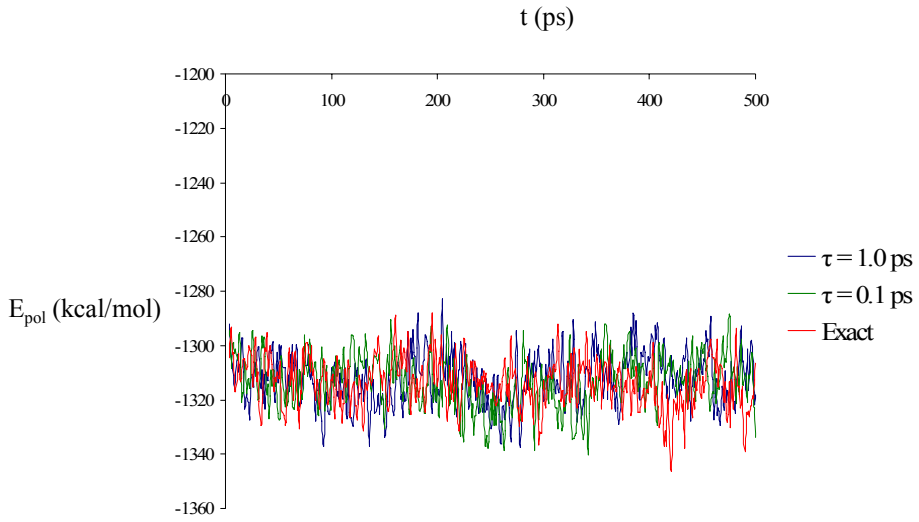

Figure 4.1 Plot of polarization energy versus time for a simulation using iterative (exact) calculation for induced dipoles and Lagrangian propagation with τ = 1.0 ps and τ = 0.1 ps.

In Figure 4.1, the exact polarization energy as calculated by the iterative method is compared to the polarization energy as calculated using the CP induced Gaussian dipoles for τ = 1.0 ps and τ = 0.1 ps on the box of 341 polarizable waters. The average polarization energies and fluctuations (in kcal/mol) are -1312.12 ± 13.61, -1313.12 ± 13.76, -1314.72 ± 13.56 for the simulations with CP induced dipoles (τ = 1.0), CP induced dipoles (τ = 0.1 ps), and the iterative (exact) method, respectively. Notice the average polarization energy (-1312.12) for the CP dipoles with the long coupling constant to temperature τ = 1.0 ps is slightly higher energy than the polarization energy (-1313.12) for CP dipoles with the short coupling constant to temperature τ = 0.1 ps. Both average polarization energies with CP induced dipoles are higher in energy than the average polarization with exact induced dipoles (-1314.72). This should be expected because the

CP induced dipoles were designed to fluctuate around the exact induced dipoles, and the polarization energy is a minimum at the exact induced dipoles (4.2.12). Therefore, any deviation from the exact induced dipoles will yield a higher polarization energy. Therefore, the CP induced dipoles with the larger coupling constant with temperature (τ = 1.0) fluctuated more and had a higher polarization energy than the CP induced dipoles with the smaller coupling constant (τ = 0.1). However, the difference in polarization energies between the CP induced dipoles and the exact induced dipoles is small, and it appears that using CP induced dipoles is a good approximation.

4.8 Conclusions

The induced Gaussian dipole polarization model has been implemented into the AMBER molecular dynamics program. The polarization work, energy, and force has been derived for a system of induced Gaussian dipoles interacting with one another and an external field from permanent charges. Previous derivations of polarization work, energy, and force were given for an induced point dipole interacting with an external field due to permanent charges only.

Simulations are frequently performed under periodic boundary conditions. A brief discussion of the Ewald summation method for point charges and point dipoles was provided and a derivation of the method can be found in appendix D. It was shown that a periodic system of point charges and induced Gaussian dipoles can be treated as a short range correction to a periodic system of point charges and induced point dipoles. The nonbond cutoff for the short range correction was found to be ~5 Å.

During a molecular dynamics simulation, the induced dipoles can be calculated exactly by solving a system of linear equations iteratively. For strongly interacting systems, Successive Over-Relaxation (SOR) methods can be applied to converge the system of linear equations. This method can be expensive during a molecular dynamics simulation. Alternatively, it was shown that the CP Lagrangian method can be used to propagate induced dipoles. The polarization energies from CP induced dipoles were found to be only slightly higher (-1312.12, -1313.12 kcal/mol) than the polarization energies calculated from exact induced dipoles (-1314.72). This is explained by the fact that the polarization energy is a minimum when the exact induced dipoles are used.

4.9 References

1 J. Applequist, Chem. Phys. **85**, 279 (1984)

2 C. J. Bottcher, *Theory of Electric Polarization: Dielectrics in Static Fields,* 2nd edition, revised (Elsevier, New York, 1993)

3 J. G. Ángyán, F. Colonna-Cesari, O. Tapia, Chem. Phys. Lett. **166**, 180 (1990)

4 Ewald P. Ann. Phys. **64**, 253 (1921)

5 S. W. Leeuw, J. W. Perram, E. R. Smith, Proc. R. Soc. Lond. A. **373**, 27 (1980)

6 S. W. Leeuw, J. W. Perram, E. R. Smith, Proc. R. Soc. Lond. A. **373**, 57 (1980)

7 S. W. Leeuw, J. W. Perram, E. R. Smith, Proc. R. Soc. Lond. A. **388**, 177 (1980)

8 T. A. Darden, D. York, and L. Pedersen, J. Chem. Phys. **9**8 (12) 10089 (1993)

9 U. Essmann, L. Perera, M. L. Berkowitz, T. Darden, H. Lee, and L. G. Pedersen, J. Chem. Phys. **103** (19) 8577

[10] A. Toukmaji, C. Sagui, J. Board, and T. A. Darden, J. Chem. Phys. **113**, 10913 (2000)

[11] C. Sagui and T. A. Darden, J. Chem. Phys. **114** (15) 6578 (2001)

[12] C. Sagui, L. G. Pedersen, and T. A. Darden, J. Chem. Phys. **120** (1), 73 (2004)

[13] R. Car and M. Parrinello, Phys. Rev. Lett. **55**, 2471 (1985)

[14] M. L. Saboungi, A. Rahman, J. W. Halley, and M. Blander, J. Chem. Phys. **88**, 5818 (1988)

[15] M. Sprik and M. Klein, J. Chem. Phys. 89, 7556 (1988)

[16] M. Wilson and P. A. Madden, J. Phys.: Condens. Matter **5**, 2687 (1993)

[17] R. L. Burden and J. D. Faires, *Numerical Analysis,* 6th edition, revised (Brooks/Cole Publishing Co, Pacific Grove, CA, 1997)

[18] P. Ren, A. Grossfield, and J. W. Ponder, AMOEBA Force Field, ftp://dasher.wustl.edu/pub/tinker/params.

[19] H. J. C. Berendsen, J. P. M. Postma, W. F. van Gunsteren, A. DiNola, and J. R Haak, J. Chem. Phys. **81** (**8**), 3684 (1984)

[20] J. P. Ryckaert, G. Ciccotti, and H.J.C. Berendsen, J.Comput. Phys. **23,** 327 (1977)

[21] S. Miyamoto and P.A. Kollman, J. Comput. Chem. **13,** 952 (1992)

5 Gaussian Dipole Polarizabilities

5.1 Introduction

In this chapter, the Gaussian induced dipole model is compared with the damped Thole[1] model and the Applequist[2] point dipole model. In the same spirit as Thole and Applequist, transferable atom type polarizabilities will be found for all three models by fitting to molecular polarizability tensors calculated at the B3LYP/cc-pVTZ level.

Polarizabilities generated by fitting to molecular polarizability tensor data are convenient in that they are transferable among related molecular classes, however they are limited in accuracy because they rely on the assumption of atom types. For example, all oxygen atoms are grouped into one class and assigned the same polarizability, regardless of the neighboring environment. In this work, an independent procedure for generating atomic polarizabilities will be presented. It is based on probing a molecule with point charges[3 4] or external electric fields[5] and calculating the response electrostatic potential. The response electrostatic potential is the potential generated by the molecule in the external field of the point charge probes minus the potential of the molecule in vacuum. Atomic polarizabilities are then fit to this response potential on a grid of points encompassing the molecule. Just as atomic charges fit to the electrostatic potential are found to reproduce molecular dipole moments[6 7 8], probed polarizabilities fit to the electrostatic response potential are found to reproduce molecular polarizability tensors. In contrast to atom type polarizabilities, probed polarizabilities are optimized for specific molecules improving accuracy.

While non-transferable, Gaussian probed polarizabilities are readily computed. Like fitted atomic partial charges, probed polarizabilities are not transferable between

molecules. However, probed polarizabilities are conformationally invariant which is important for electrostatics of flexible molecules.

In the next section 5.2, methods used to optimize atomic polarizabilities are discussed. The procedure to fit a set of atom type polarizabilities to a large number of molecular polarizability tensors is described. The alternative method of fitting polarizabilities to response potential generated by probing a molecule with point charges and then sampling the electrostatic potential is then discussed. In section 5.3, results from both fitting methods are presented. The atom type polarizabilities fit to the tensor are given for the Gaussian model, the Thole model, and the Applequist point dipole model. The performance of all three models is examined by comparing the results for atom type polarizabilities. Following the discussion on atom type polarizabilities fit to the tensor, results of probed polarizabilities fit to the response potential are presented. Gaussian probed polarizabilites were found for a variety of organic molecules and compared with Gaussian atom type polarizabilities by examining the quality of fit for molecular polarizability tensor and response potential. Results of molecules with highly anisotropic molecular polarizability tensors are given, and limitations in assuming isotropic atomic polarizabilities are discussed. Finally, probed polarizabilities are generated for a flexible molecule at one conformation. This set of polarizabilities is tested on many other conformations to investigate how transferable the polarizabilities are with respect to different geometries of a molecule.

5.2 Methods

Atom Type Polarizability Parameterization

In order to compare the Gaussian model with other induced dipole models, a set of atom type (AT) specific atomic polarizabilities has been optimized by fitting to molecular polarizability tensors as in Thole[1] and Applequist[2]. The geometries were optimized, and molecular polarizability tensors were calculated at the B3LYP/cc-pVTZ level for a training set of 127 organic molecules. In this work all ab initio calculations were performed at the B3LYP/cc-pVTZ level using Gaussian 98[9]. Atomic polarizabilities were fit to this data using the Gaussian Model, the damped Thole model, and the Applequist point dipole model. For the Gaussian Model, the exponents β were fit with a single adjustable parameter a.

$$\beta = \frac{a}{\left(\alpha \frac{4}{3\sqrt{8\pi}}\right)^{\frac{1}{3}}} \qquad 5.2.1$$

The Thole model studied in this work is the same as that implemented in the AMOEBA force field[10].

$$\rho(u) = \frac{3a}{4\pi}\exp(-au^3) \qquad 5.2.2$$

As in the Gaussian model, the parameter a in the Thole model was also allowed to vary. For both the Gaussian and Thole model, the polarization condition (see section 3.5) requires

$$a \leq 1 \qquad 5.2.3$$

The atomic polarizabilities were fit to the six independent components of the molecular polarizability tensor $(\alpha_{xx}^{\text{mol}}, \alpha_{yx}^{\text{mol}}, \alpha_{yy}^{\text{mol}}, \alpha_{zx}^{\text{mol}}, \alpha_{zy}^{\text{mol}}, \alpha_{zz}^{\text{mol}})$ over the molecular training set.

The root mean squared deviation (RMSD) in the tensor elements for a given molecule, α_{rmsd}, is defined by:

$$\alpha_{\text{rmsd}} \equiv \sqrt{\frac{1}{6}\sum_{p,q}^{6}\left(\alpha_{pq}^{\text{mol}} - \alpha_{pq}^{0,\text{mol}}\right)^2} \qquad 5.2.4$$

where α_{pq}^{mol} is the tensor calculated by the model and $\alpha_{pq}^{0,\text{mol}}$ is the ab initio reference tensor. The fitting function χ^2 is defined as the sum of the squares of individual molecular tensor RMSDs:

$$\chi^2 \equiv \frac{1}{N}\sum_{i=1}^{N}\alpha_{\text{rmsd},i}^2 \qquad 5.2.5$$

where N is the number of molecules. The total RMSD over the data training set is then $\sqrt{\chi^2}$. χ^2 was optimized using the non-linear least squares Levenberg-Marquardt algorithm[11]. Tensor errors $\Delta\alpha$ are defined for each molecule as the tensor RMSD divided by the average eigenvalue of the molecular polarizability tensor α_{eigen}.

$$\Delta\alpha \equiv \frac{\alpha_{\text{rmsd}}}{\alpha_{\text{eigen}}} \qquad 5.2.6$$

Probed Polarizability Parameterization Algorithm

Molecules were probed with point charges positioned around the molecule. For each probe charge, the electrostatic potential is computed on a grid of points encompassing the molecule. The atomic polarizabilities along with the exponent parameter a were fit to the response electrostatic potential comprised of the probed electrostatic potentials minus the vacuum electrostatic potential.

The ChelpG[8] electrostatic grid was used with a grid spacing of 0.3 Å and an outer grid radius of 2.8 Å for each atom. The inner grid radii used were 1.45 Å for H, 1.5 Å for

C, 1.7 Å for N, O, F, and 2.3 Å for second and third row elements. Point charges were placed along bond axes outside the vdW surface of the molecule defined by probe radii on each atom. The probe radii were chosen to be large enough to be outside the vdW radii of each atom, but close enough to adequately sample the polarization response. The probe radii were set to 2.0 Å for H, 2.5 Å for first row atoms (C, N, O, F), 3.0 Å for second row atoms (P, S, Cl) and 3.5 Å for third row atoms (Br). For each bond, both atoms comprising the bond were probed separately. A single probe charge was set along the bond axis as in Figure 5.1A. Initially the probe was placed on the bond axis at the probe radii distance. However, if the probe charge happened to be inside any other atom's probe radius, the distance along the axis was increased in increments of 0.3 Å up to a maximum of 5.0 Å. If at 5.0 Å the probe charge was still inside another atom's probe radii, the probe charge was discarded. For sp^2 hybridized atoms or atoms containing lone pairs, an additional point charge was placed above and below the plane at the same distances from the nuclei as the bond axis probes as in Figure 5.1B.

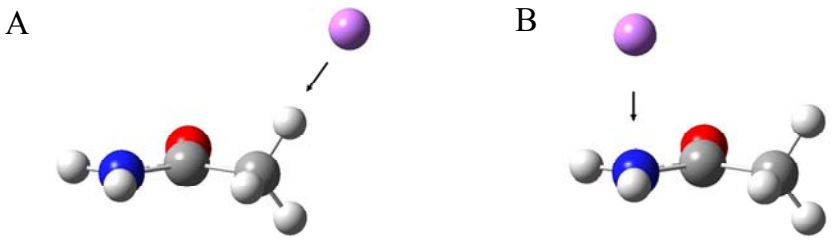

Figure 5.1 Probe Charge on Acetamide: Bond axis probe on C-H (**A**) and out of plane amide probe on amido N (**B**).

While the molecular polarizability tensor error depends weakly on the magnitude of the probe charge, it depends strongly on the sign of the charge. Thus, it was found that

both positive and negative charges at each probe position are necessary. The probe charge magnitudes needed to be large enough to cause a measurable response in the electric potential, but not so large that hyperpolarization effects occur. In Figure 5.2, the error in molecular polarizability tensor $\Delta\alpha$ is plotted against probe charge magnitude for some sp^3 and sp^2 first row molecules. Optimal probe charges of ± 0.8e for first row sp^3 atoms (C, H, O, N, F), ± 0.5e for sp^2 first row atoms (C, O, N), and ± 1.1e for second and third row atoms (P, S, Cl, Br) were inferred from the tensor errors.

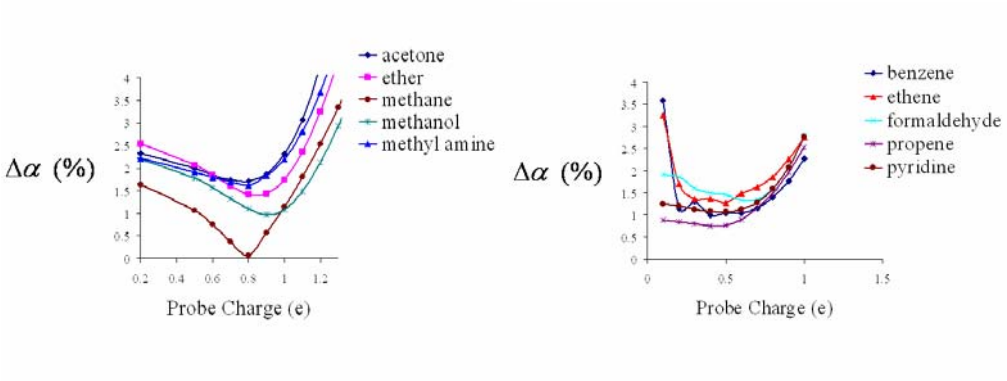

Figure 5.2 Tensor Error Dependence $\Delta\alpha$ on Probe Charge Magnitudes for: sp^3 C,N,O,H (Left) and sp^2 C,N,O (Right).

As an example, consider the probe positioning procedure for water in Figure 5.3. For each OH bond, a separate positive probe is placed next to both atoms making up the bond. This gives 4 bond axis probes. Since water has an atom with lone pairs, positive probes are also placed above and below the plane containing the lone pair atom, giving 2 out of plane probes and 6 positive probes altogether. Negative charge probes are also placed at the same positions as the positive probes, giving 12 probe charges total. Another example is methane with 4 bonds and no lone pair or sp^2 atoms. The number of probe charges for methane is therefore 16.

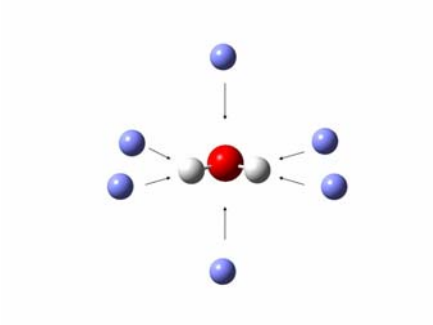

Figure 5.3 Positions of Probe Charges for Water

Probed polarizabilities for the Gaussian model were simultaneously fit to each grid of response electrostatic potentials generated by the point charge probes. The response electrostatic potential is the probed potential minus the vacuum potential. This response potential is directly compared with the potential arising from the Gaussian dipoles (3.2.11):

$$\varphi_1(\vec{R}^1) = \vec{\mu}^2 \cdot \vec{R}^{12} \beta_2^3 B_1(\beta_2 R^{12}) \qquad 5.2.7$$

The induced dipoles were allowed to interact through 'effective' electric fields with one another (3.2.13):

$$\begin{aligned} \vec{E}_1(\vec{R}^1;\vec{R}^2) &= \vec{\mu}^2 \cdot \left(\vec{R}^{12}\vec{R}^{12}\beta^5 B_2(\beta_{12}R^{12}) - \mathbf{I}\beta^3 B_1(\beta_{12}R^{12})\right) \\ &= \vec{\mu}^2 \cdot \mathbf{T}^{12} \end{aligned} \qquad 5.2.8$$

and the external probe charges (3.2.12):

$$\vec{E}_0(\vec{R}^1;\vec{R}^2) = q^2 \vec{R}^{12} \beta_{12}^3 B_1(\beta_{12} R^{12}) \qquad 5.2.9$$

. The induced dipoles were determined iteratively using 3.3.2.:

$$\vec{\mu}^i = \alpha^i \left(\vec{E}^{0,i} + \sum_{j \neq i} \mathbf{T}^{ij} \cdot \vec{\mu}^j \right) \qquad 5.2.10$$

For each molecule, the optimizable parameters were the atomic polarizabilities and a single Gaussian exponent parameter *a* (5.2.1). If *M* is the number of grid of points from the ChelpG scheme and *P* is the number of charge probes, the fitting function χ^2 is defined by:

$$\chi^2 = \frac{1}{M \cdot P} \sum_{i=1}^{M} \sum_{j=1}^{P} (\varphi_{ij}^{\text{Gauss}} - \Delta\varphi_{ij}^{\text{QM}})^2 \qquad 5.2.11$$

where $\varphi_{ij}^{\text{Gauss}}$ (5.2.7) is the induced Gaussian dipole potential and $\Delta\varphi_{ij}^{\text{QM}}$ is the ab initio response potential at the i^{th} grid point of the j^{th} probe charge, respectively. The response potential $\Delta\varphi_{ij}^{\text{QM}}$ is given by:

$$\Delta\varphi_{ij}^{\text{QM}} \equiv \varphi_{ij}^{\text{QM}} - \varphi_{i}^{\text{QM}}(\text{vacuum}) \qquad 5.2.12$$

where φ_{ij}^{QM} is the ab initio potential at the i^{th} grid point with the j^{th} probe charge and φ_{i}^{QM} (vacuum) is the ab initio vacuum potential at the i^{th} grid point. χ^2 was optimized using the non-linear least squares Levenberg-Marquardt algorithm[11]. The RMSD in response potential φ_{rmsd} is given by the square root of χ^2.

$$\Delta V_{\text{rmsd}} = \sqrt{\chi^2} \qquad 5.2.13$$

Since the induced dipoles are linearly related to external electric field $\overline{\mu} = \mathbf{A}^{-1}\overline{E}$ (3.3.6), the contribution from intra-molecular polarization is constant and only the response potential need be considered. By subtracting the vacuum potential from the total potential, the only contribution to the response potential is from induced dipoles arising from the external point charge source. The Gaussian inducible dipoles are allowed to interact with one another and the probe charge. In this way, the computed polarizabilities are unaffected by either the intramolecular polarization or the choice of

the permanent electrostatic model (e.g. point charges[6 7 8], point multipoles[1 12], Hermite Gaussian functions[13] (Gaussian multipoles)). Thus, the permanent electrostatic model may be selected and optimized subsequent to the derivation of the polarizabilities[13].

5.3 Results

Tensor Fit Atom Type Polarizabilities

The Gaussian, Thole, and Point Dipole models were fit to ab initio molecular polarizability tensors for selected atom types as described in section 5.2.1. For both the Gaussian and Thole models, the optimized parameters included the atomic polarizabilities and a single adjustable variable *a*, which represents the diffuseness or strength of the interactions. Generally, the larger the value of *a*, the stronger the induced dipole – induced dipole interactions. The optimized value of *a* for the Gaussian model (0.957), and for the Thole model (0.662) were both below 1.0, satisfying the catastrophe condition (See Appendix). The point dipole model has no damping correction, which is equivalent to allowing $a \rightarrow \infty$ in either the Thole or Gaussian models.

As in the original Thole[1] paper, the atom types were generally the elements. An extra atom type was also set aside for an aromatic/alkene carbon atom. In order to study ionic parameters relevant to amino acids, ammonium N and H and carboxylate O atom types were also added. The optimized parameters, the RMSD values for the fits, and the errors for all three models are given in Table 5.1. For the 127 molecules studied, the Gaussian model (3.67 % avg. error) performed slightly better than the Thole model (3.81 % error) and much better than the point dipole model (7.78% error).

Atom Type	Gaussian $a = 0.957$	Thole $a = 0.662$ (0.572)[a]	Applequist $a \to \infty$
H	0.381	0.416 (0.427)[a]	0.181 (0.135)[b]
HP (ammonium H^+)	0.141	0.119	0.051
C	1.090	1.010 (1.334)[a]	0.727 (0.878)[b]
C (aromatic, alkene)	1.362	1.407	0.620
N	0.801	0.709 (1.073)[a]	0.456 (0.530)[b]
NP (ammonium N^+)	0.408	0.387	0.470
O	0.612	0.605 (0.837)[a]	0.303 (0.465)[b]
O2 (acid O^-)	1.025	1.207	0.413
F	0.315	0.283	0.311 (0.320)[b]
Cl	1.921	1.844	1.778 (1.91)[b]
Br	2.934	2.791	2.734 (2.88)[b]
S	2.742	2.461	2.152
P	1.545	1.282	1.787
α_{rmsd} (Å^3)	0.260	0.280	0.615
$\Delta\alpha$ (%)	3.67	3.81	7.78

Table 5.1 Atom type (AT) polarizabilities (Å^3) for Gaussian, Thole, and Applequist Point dipole models
[a]Values in parenthesis taken from Ref[1]
[b]Values in parenthesis taken from Ref[2].

The original polarizabilities found by Thole[1] and Applquist[2] in Table 5.1 were optimized by fitting to experimental gas phase molecular polarizability tensors. In general, these polarizabilities should be larger in magnitude than those fit from the B3LYP/cc-pVTZ data. Diffuse functions were not included in the cc-pVTZ basis set, in order to underestimate the gas phase polarizability to better approximate what is believed to be the liquid state polarizability[15 16 17].

The point dipole polarizabilities are smaller than the damped Thole or Gaussian polarizabilities. Point dipoles interact more strongly, because there is no damping and the parameters are smaller to compensate. A similar trend also exists between the Thole and Gaussian model; for most atom types, the polarizabilities in Thole are slightly smaller than in the Gaussian model. The reason for this is probably due to the fact that the Thole model density $\rho \sim \exp(-\beta r^3)$ decays faster than the Gaussian density

$\rho \sim \exp(-\beta r^2)$. This would imply that the damping in the Thole model decays quicker than in the Gaussian model. Therefore, the Thole model is slightly more similar to the point dipole model than is the Gaussian model. To compensate for this behavior, the Thole polarizabilities and the damping parameter *a* are smaller than in the Gaussian model (*a* was defined in both models so that the polarization catastrophe occurs at *a* = 1.0).

The molecular polarizability tensor calculated from ab initio (QM) and the three models (Gauss, Thole, Point Dipole) are given, along with percent errors, for the illustrative case of benzene in Table 5.2. The results for the Gaussian model are almost identical to the Thole model, both with a tensor error $\Delta\alpha$ of 2.7%. For the point dipole model, $\Delta\alpha$ is significantly larger at 11.0%. Benzene was chosen as an example because aromatic compounds are a well-known case in which the point dipole model does not adequately reproduce the molecular polarizability tensor. Specifically, the component of the tensor perpendicular (z) to the molecular plane (xy) is underestimated. This is due to weak point dipole parameters interacting strongly with each other in the plane but not perpendicular to the plane.

	XX	YX	YY	ZX	ZY	ZZ	$\Delta\alpha$ (%)
Gauss	11.86	0.00	11.86	0.00	0.00	4.78	2.7
Thole	11.85	0.00	11.85	0.00	0.00	4.74	2.7
Applquist	10.67	0.00	10.67	0.00	0.00	2.75	11.0
QM	11.45	0.00	11.45	0.00	0.00	5.01	

Table 5.2 Molecular polarizability tensor ($Å^3$) using atom type (AT) polarizabilities for benzene

Though the Gaussian model gave a better fit than did the Thole model, the performance difference between the two models is small. This is in agreement with Thole's original work, in which seven different damping functions all gave similar

RMSD fits to the data. As stated earlier, the main advantage of the Gaussian model over the Thole model is that point multipoles can be readily generalized to Gaussian multipole charge densities.

Comparison of Probed Polarizabilities with Atom Type Polarizabilities

The probed method was applied to several test organic molecules. For each molecule, the error in the molecular polarizability tensor $\Delta\alpha$ (5.2.6) and the RMSD in the response field ΔV_{rmsd} (5.2.9) are calculated using the probed polarizabilities and presented in Table 5.3. In order to compare with the generic atom type (AT) parameters, $\Delta\alpha$ and ΔV_{rmsd} are also calculated using the set of AT polarizabilities. In virtually all cases, $\Delta\alpha$ and ΔV_{rmsd} are significantly smaller for the molecule specific probed polarizabilities than the transferable AT polarizabilities.

Since the probed polarizabilities are fit to the response field, it is not surprising that these parameters perform significantly better than the AT parameters. For example, the ΔV_{rmsd} (in 10^{-3}e/Å) for water is 1.02 using the probe polarizabilities and 3.02 using the AT polarizabilities. Another example is ammonia, in which ΔV_{rmsd} is 1.67 using the probe polarizabilities and 2.72 using the AT parameters. The average of ΔV_{rmsd} over all 28 molecules was found to be 2.01 for the probed polarizabilities and 3.04 for the AT polarizabilities. In other words, the RMSD in the response potential was on average 50% larger using the AT polarizabilities over the probed polarizabilities.

As can be seen from Table 5.3, the probed polarizabilities also resulted in much better tensor fits $\Delta\alpha$ than did the AT polarizabilities. The probed parameters had an average tensor error of 1.37% with a maximum error of 2.65%. This can be compared

with the transferable AT parameters, which had an average error of 6.42% and a maximum error of 21.76%. This is remarkable since the AT parameters were fit to the tensor, while the probed polarizabilities used no tensor information in the fit.

The AT parameters do reasonably well if the molecule of interest was included in the atom type training set. As an example from Table 5.3, the probed polarizabilities gave a tensor error $\Delta\alpha$ of 1.44% for dimethyl ether and 1.79% for dimethyl sulfide. The AT parameters gave acceptable results for both molecules (2.32% and 2.99% errors respectively). However, both of these molecules were used in the atom type (AT) training sets. On the other hand, sulfate and sulfuric acid were not included in the AT training set. For sulfate, $\Delta\alpha$ = 20.77% and for sulfuric acid, $\Delta\alpha$ = 21.76% using the AT parameters. This can be compared with the results using the probe polarizabilities: $\Delta\alpha$ = 0.88% for sulfate and $\Delta\alpha$ = 1.15% for sulfuric acid. The large errors in the AT parameters can be understood by examining the sulfur (S) polarizability. The probed parameters predicted α = 1.2 Å^3 for S in sulfate, while the AT parameters used a generic sulfur value of α = 2.7 Å^3. The AT polarizability for S of 2.7 Å^3 might be appropriate for thiols, however sulfate S is oxidized which should shift much of the electron density to the oxygens thereby lowering the polarizability of S. Of course, a new atom type could be added for sulfate S, and the parameters refit. An advantage of the probed molecule approach is that it eliminates the need to arbitrarily assign atom types or refit parameters.

	a	$\Delta\alpha$ (%) Probed	$\Delta\alpha$ (%) Atom Type	ΔV_{rmsd} (10^{-3} e/Å) Probed	ΔV_{rmsd} (10^{-3} e/Å) Atom Type
Acetamide	0.906	1.30	2.33	1.61	2.06
Acetate Anion	0.942	1.99	4.72	3.30	4.18
Acetic Acid	0.920	1.55	7.04	1.61	2.30
Acetone	0.919	1.70	2.62	1.84	1.95
Ammonia	0.851	2.22	8.47	1.67	2.72
Ammonium Cation	0.901	0.10	16.83	0.63	2.50
Benzene	0.966	0.85	2.33	2.24	2.58
Butadiene	0.984	2.45	7.13	2.45	2.85
Dimethyl Ether	0.955	1.44	2.32	2.19	2.25
Dimethyl Sulfide	0.948	1.79	2.99	2.50	2.91
Ethane	0.939	1.10	1.28	1.89	1.94
Ethene	0.961	2.65	6.39	2.19	2.65
Formaldehyde	0.974	2.13	2.83	2.22	2.33
Formamide	0.937	1.45	2.89	1.54	2.03
Hydrogen Sulfide	0.893	1.78	13.20	3.68	5.55
Methane	0.901	0.05	2.21	1.89	2.03
Methanethiol	0.943	2.14	5.61	2.42	3.19
Methanol	0.948	1.10	5.30	1.79	2.36
Methyl Amine	0.931	1.68	3.20	2.13	2.46
N-methyl formamide	0.935	1.33	2.72	1.90	2.21
Phosphate	0.799	1.02	0.72	2.79	3.51
Phosphoric Acid	0.891	0.12	8.63	1.65	3.43
Propene	0.952	0.88	4.31	2.11	2.37
Pyridine	0.955	0.95	1.90	2.14	2.55
Pyrole	0.868	1.60	6.26	2.08	2.96
Sulfate	0.955	0.88	20.77	1.58	7.43
Sulfuric Acid	0.958	1.15	21.76	1.38	6.84
Water	0.877	2.09	15.04	1.02	3.02
Average	0.926	1.37	6.42	2.01	3.04

Table 5.3 Comparison of probed and atom type polarizabilities

The AT parameters were fit over a large collection of data to get the overall optimal molecular polarizability tensors. It is possible that the fitting procedure for the AT parameterization incorrectly assigned the atomic polarizabilities, but is still able to reproduce the tensor. As an example, the probed and AT atomic polarizabilities are given for acetamide in Figure 5.4. In Table 5.4, the molecular polarizability tensor is given for both models and compared with the reference ab initio (QM) value. Since $\Delta\alpha$ = 1.30%

for the probed and $\Delta\alpha$ = 2.33% for the AT parameters, both sets are able to reproduce the tensor. However, the AT polarizabilities are 20% smaller than probed polarizabilities for the amido C, N, and O atoms while the AT polarizabilities on the polar H atoms are 30% larger to compensate. The probed polarizabilities suggest that the amido C (α_C = 1.20 Å^3) is more polarizable than the methyl C (α_C = 1.08 Å^3). In general, the probe polarizabilities find that sp^2 C is more polarizable than sp^3 C (e.g. α_C = 1.05 Å^3 for ethane and α_C = 1.40 Å^3 for ethene).

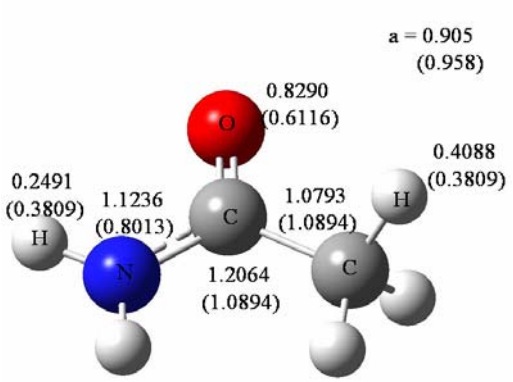

Figure 5.4 Probed and (Atom Type) polarizabilities in Å^3 for acetamide

	XX	YX	YY	ZX	ZY	ZZ	$\Delta\alpha$ (%)
Probe	6.07	-0.03	5.80	0.00	0.00	3.88	1.3
AT	6.12	-0.15	5.87	0.00	0.00	3.68	2.3
QM	6.08	0.11	5.77	0.00	0.00	3.79	

Table 5.4 Molecular polarizability tensor (Å^3) for acetamide calculated by B3LYP/cc-pVTZ (QM) and probed polarizabilities (Probe) and atom type Polarizabilities (AT) for the Gaussian model

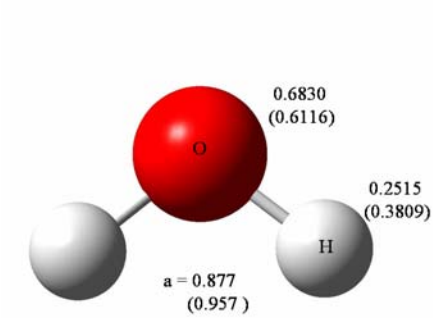

Figure 5.5 Probed and (Atom Type) Polarizabilities in Å^3 for water

	XX	YX	YY	ZX	ZY	ZZ	$\Delta\alpha$ (%)
Probe	1.11	-0.12	1.19	0.00	0.00	0.84	2.1
AT	1.32	-0.25	1.50	0.00	0.00	0.88	15.0
QM	1.14	-0.09	1.20	0.00	0.00	0.82	

Table 5.4 Molecular polarizability tensor (Å^3) for water calculated by B3LYP/cc-pVTZ (QM) and probed polarizabilities (Probe) and atom type Polarizabilities (AT) for the Gaussian model

A final example of the performance of the probed polarizabilities is given by the important case of water. The atomic polarizabilities are given in Figure 5.5 and the molecular polarizability tensors are given in Table 5.5. The tensor error $\Delta\alpha$ is 2.09 % using the probed polarizabilities and 15.04% for AT parameters. As noted earlier, the RMSD in response potential ΔV_{rmsd} (10^{-3}e/Å) is three times smaller using the probed polarizabilities (1.02) than the AT parameters (3.02). The poor results for water using the AT parameters are somewhat surprising since water was included in the AT training set. Furthermore, when two new AT polarizabilities were added specifically for water, α_{O} and α_{H}, and these polarizabilities were fit only to the tensor for water, then $\Delta\alpha$ was found to be 2.02% (the exponent parameter a was constrained to 0.879 to avoid overfitting). This would imply that the probed polarizabilities with $\Delta\alpha$ = 2.09% is near the limit which would best reproduce the molecular polarizability tensor in the context of the isotropic induced Gaussian dipole model.

Limitations with the Isotropic Model

The probed polarizability scheme works well for ordinary organic molecules containing C, O, N, H, S and P. The optimized exponent parameter *a* had an average value of 0.926, which is below the polarization catastrophe upper bound of 1.0. In general, sp^3 hybridized molecules performed slightly better than sp^2 molecules, (e.g. $\Delta\alpha$ = 1.10 % for ethane, $\Delta\alpha$ = 2.65 % for ethene). A possible reason for this is that the isotropic atomic polarizability model studied in this paper assumes spherically symmetric induced dipoles on each atom. The electron density around an sp^3 hybridized molecule should be more spherically isotropic than a molecule which is sp^2 hybridized. Further evidence suggest that highly symmetric molecules give better results than molecules of lower symmetry, (e.g. $\Delta\alpha$ = 0.10% for ammonium cation, $\Delta\alpha$ = 2.22% for ammonia).

Diatomic	$\alpha_{\parallel}$		$\alpha_{\perp}$		$\Delta\alpha$ (%)
	QM	Probe	QM	Probe	
F_2	1.567	1.197	0.431	0.722	27.9
Cl_2	5.519	5.140	2.370	2.663	6.7
Br_2	8.350	7.938	3.777	4.050	4.3

Table 5.6 $\alpha_{\parallel}$ and $\alpha_{\perp}$ in $Å^3$ for diatomic halides using probed polarizabilities. In all cases, $a \rightarrow \infty$, indicating point dipole behavior.

To further test the limits of the isotropic atomic polarizability Gaussian model, polarizabilities were computed for diatomic halides (Table VI.). During the optimization, the exponent parameter *a* diverged to infinity implying point dipole behavior, and large errors occurred in the molecular polarizability tensors. These discrepancies can be rationalized by looking at the two independent tensor components: $\alpha_{\parallel}$ (3.4.4) which is the tensor component parallel to the bond axis and $\alpha_{\perp}$ (3.4.7) which is perpendicular to

the bond axis. In the diatomic halides, $\alpha_{\parallel}$ is too small and $\alpha_{\perp}$ is too large. For example in F_2, the ab initio values are $\alpha_{\parallel} = 1.567$ and $\alpha_{\perp} = 0.431$, and the optimized model values are $\alpha_{\parallel} = 1.197$ and $\alpha_{\perp} = 0.722$. In a purely additive polarization model, in which the isotropic induced dipoles do not interact with each other, the molecular polarizability tensor is isotropic, e.g. $\alpha_{\parallel} = \alpha_{\perp}$ in the diatomic case. It is the interaction between the isotropic induced dipoles that causes anisotropy in the tensor, and $\alpha_{\parallel} > \alpha_{\perp}$ in the diatomic molecule case. The larger the interaction, the greater the difference between $\alpha_{\parallel}$ and $\alpha_{\perp}$. The largest possible interaction is that of no field damping or induced point dipoles. For the diatomic halides, even point dipoles did not provide a sufficiently strong interaction to accurately reproduce $\alpha_{\parallel}$ and $\alpha_{\perp}$. The worst case is F_2, with $\Delta\alpha = 27.9\%$. These large differences between ab initio and derived values for $\alpha_{\parallel}$ and $\alpha_{\perp}$ implies that isotropic atomic polarizabilities on atoms alone are not a good approximation for diatomic halides or any other highly anisotropic molecule. If anisotropic atomic polarizabilities were used[10], then the atomic polarizability tensor could have different components parallel and perpendicular to the bond axis. This would allow for the possibility of correctly calculating $\alpha_{\parallel}$ and $\alpha_{\perp}$ for the molecule even in the absence of induced dipole - induced dipole interactions. Anisotropic induced dipoles would be necessary to reproduce the tensor correctly for highly anisotropic molecules such as F_2. Anisotropic induced dipoles can be represented by generalizing the scalar atomic polarizability α to an atomic polarizability tensor α_{pq}.

The poor performance of the isotropic Gaussian model for the diatomic halides is due to a limitation in assuming isotropic atomic polarizabilities and not to the Gaussian model or the probed polarizabilities. To illustrate this, polarizabilities were fit solely to the tensor of F_2 for the point dipole, Gaussian and Thole models in Table 5.7. For the Gaussian and Thole models, the exponent parameter *a* was constrained to the maximum value of 1.0. The tensor errors $\Delta\alpha$ were 26.8 % for the point dipole model, 27.2 % for the Thole model, and 30.3 % for the Gaussian model. The Thole model agreed more with the point dipole model than did the Gaussian model. This is further evidence that the Thole model behaves slightly more like point dipoles than the Gaussian model.

	$\alpha_{\parallel}$	$\alpha_{\perp}$	$\Delta\alpha$ (%)
Point Dipole ($a \rightarrow \infty$)	1.340	0.771	26.8 %
Thole (a = 1.0)	1.325	0.772	27.2 %
Gauss (a = 1.0)	1.232	0.784	30.3 %
QM	1.566	0.430	

Table 5.7 $\alpha_{\parallel}$ and $\alpha_{\perp}$ in $Å^3$ for F_2 using polarizabilities fit to the tensor for the Point Dipole, Thole, and Gaussian models.

However, the results for the diatomic halides mentioned above do not pose a serious limitation to the isotropic induced Gaussian model. Reasonable results were obtained when the probed method was applied to acid halides and halogenated organic molecules in Table 5.8. The exponent parameter *a* for the non-halide atoms was allowed to optimize (except for HF) while the halide exponent parameter was constrained to the maximum value of 1.0. The tensor errors $\Delta\alpha$ are much smaller for these halogen containing compounds cases (0.6% – 4.4%). Other anisotropic molecules not presented in Table 5.8 were also studied, many of which gave reasonable results for $\Delta\alpha$: 2.0% for N_2, 5.1% for CN^-, 3.2% for CO, 2.4% for ethyne, 2.3% for CO_2, and 2.0% for CS_2.

	$a_{H,C}$	$\Delta\alpha$ (%)
CH_3F	0.954	0.6
CH_3Cl	0.933	3.3
CH_3Br	0.922	3.6
HF	1.000	4.4
HCl	0.834	1.5
HBr	0.779	1.0

Table 5.8 Tensor error $\Delta\alpha$ and exponent parameter a for halogenated molecules. $a = 1.0$ for F, Cl, Br and a was allowed to optimize for C and H (except for HF)

Effects of Molecular Conformation

It would be highly desirable if the probed atomic polarizabilities could be fit to a single molecular conformation. To examine the extent to which polarizabilities were sensitive to conformation, probed polarizabilities optimized for a single geometry were tested on other conformations generated by rotating internal torsion angles. It was found that probed polarizabilities generated from a single geometry could reproduce both the molecular polarizability tensor and also the response potential.

The effects of multiple torsion conformations on molecular polarizability tensor using a single set of atomic polarizabilities were tested on glycine dipeptide in Figure 5.6. The torsion angles $\varphi \equiv$ C1-N1-C2-C3 and $\psi \equiv$ N1-C2-C3-N2 along the main axis were considered. The geometry was fully optimized at the B3LYP/cc-pVTZ level (φ,ψ = 180°, 180°), and atomic polarizabilities were generated for this single geometry using the probed method. The torsion angles φ and ψ were then rotated from 45° to 315° in increments of 30°. The two angles were constrained to the rotated values, while the rest of the geometry was allowed to relax. The molecular polarizability tensors for these constrained geometries were then calculated using the probed atomic polarizabilities generated from the single optimized geometry (φ,ψ = 180°, 180°) and then compared with the reference ab initio values at those rotated geometries. The error in the tensor $\Delta\alpha$

is presented for φ and ψ in Figure 5.7. Over the conformational space, the variation in the tensor between the optimized and the rotated geometries reached as high as 17.2% and averaged to 12.8%. Despite the large variation in the tensor, the error in the tensor $\Delta\alpha$ never increased above 1.5%, and the average of $\Delta\alpha$ over all conformations was found to be 0.87%. Similar results were found by rotating a single torsion angle along the X-C-C-Y axis for ethylene glycol, fluoropropane, and $NH_2CH_2CH_2CO_2^-$.

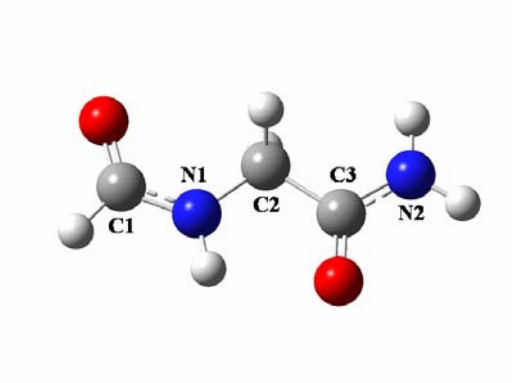

Figure 5.6 Glycine Dipeptide. $\varphi \equiv$ C1-N1-C2-C3 and $\psi \equiv$ N1-C2-C3-N2

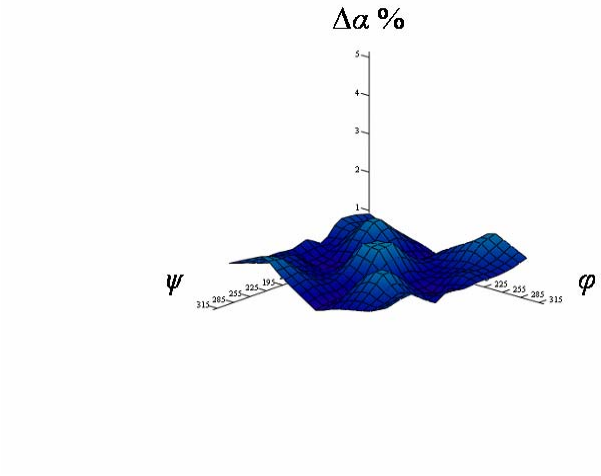

Figure 5.7 Tensor error $\Delta\alpha$ (%), dependence on φ and ψ for glycine dipeptide

The RMSD in the response potential ΔV_{rmsd} was also found to be essentially invariant across multiple torsion conformations. The geometry of $NH_2CH_2CH_2CO_2^-$ was optimized and a set of probed polarizabilities were generated for this geometry, α^0. At the fully optimized geometry, the torsion angle along the main axis of $NH_2CH_2CH_2CO_2^-$, ω_{NCCC}, was found to be 65.9°. ω_{NCCC} was then rotated and constrained to 0°, 60°, 120°, and 180° while the rest of the geometry was allowed to relax. Four new sets of probed polarizabilities were generated at each new torsion configurations, α^i (i = 1..4).

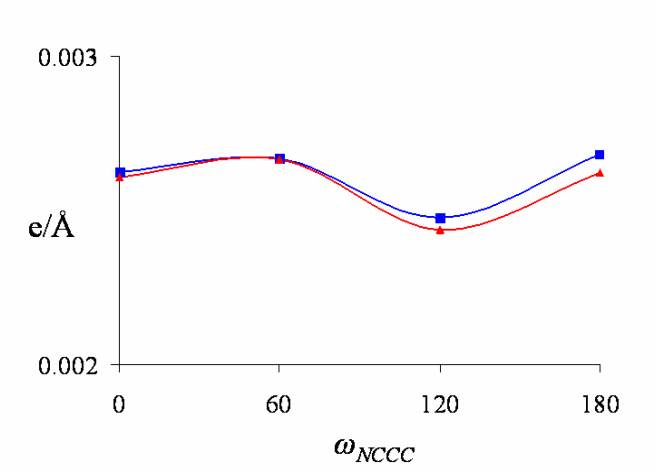

Figure 5.8 ΔV_{rmsd} dependence on torsion angle for $NH_2CH_2CH_2CO_2^-$ angles using probed polarizabilities generated at the fully optimized geometry (blue, ■) and polarizabilities generated specifically for each torsion geometry (red, ▲).

In Figure 5.8, the response field RMSD ΔV_{rmsd} was plotted for each of the rotated geometries using the optimized geometry set of polarizabilities, α^0, and also the set of polarizabilities generated specifically for that geometry, α^i. It was found the relative error for ΔV_{rmsd} between the two sets of polarizabilities was less than 1.0 % for all 4 torsion geometries (Figure 5.8). This can be compared with an average relative error for

ΔV_{rmsd} between the probed and the AT polarizabilities of ~50% (Table 5.3). Similar results were also found for ethylene glycol and fluoropropane.

5.4 Conclusions

The Gaussian polarization model has been examined as an alternative to the Thole model. Originally, the Thole model was designed to fix the polarization catastrophe problem associated with the point dipole model. In the Thole model, a damping function is applied to keep short-range induced dipole - induced dipole interactions finite. It was proved in section 3.5 that the induced Gaussian dipole model also avoids the polarization catastrophe if the Gaussian exponent is sufficiently 'diffuse'. A relationship on the maximum size of the Gaussian exponent and the polarizability was derived. A similar condition was also derived for the Thole model. In both the Gaussian and Thole models, the catastrophe condition is satisfied if the exponent parameter *a* is less than 1.0 (5.2.1 and 5.2.2).

The performance of the point dipole, Thole, and Gaussian isotropic induced dipole models have been compared by optimizing atom type atomic polarizabilities to molecular polarizability tensors calculated at the B3LYP/cc-pVTZ level on a data set of 127 organic molecules. The Gaussian model (3.67% avg. tensor error) performed slightly better the Thole model (3.81%) and much better than point dipole model (7.78%). The limits of using isotropic atomic polarizabilities can be seen by analyzing highly anisotropic molecules such as diatomic halides. For these examples, the parameters tended towards strongly interacting point dipoles. To better represent these less common cases, anisotropic atomic polarizabilities are needed.

When atom type polarizabilities are derived by fitting to a data set of molecular polarizability tensors, a question arises: how transferable are these atom type parameters. Here, it was found that atom type polarizabilities are transferable only to the extent that the atom types are appropriately identified. An alternative method of optimizing polarizabilities, which is molecule specific, was also presented. It is based on probing a molecule with point charges and fitting the polarizabilities to the response field. The approach is similar to the derivation of atomic partial charges by electrostatic potential fitting, and many of the ideas were borrowed from the well-known ChelpG method. The probed polarizabilities were tested against atom type polarizabilities over 28 molecules. In all cases, the probed polarizabilities showed a significant improvement over the transferable atom type parameters. The probed method gave an average tensor error $\Delta\alpha$ of 1.41% and a maximum tensor error of 2.7%. This can be compared with the transferable atom type polarizabilities which yielded an average tensor error of 6.5% and a maximum error of 21.8%. The probed polarizabilities also predicted the response potential significantly better than the transferable atom type parameters. The average of response potential RMSD ΔV_{rmsd} (in 10^{-3}e/Å) over the 28 molecules was 2.01 for the probed polarizabilities and 3.04 for the AT polarizabilities.

The probe charge method is capable of generating polarizabilities that are specific to the molecule and are therefore sensitive to each atoms chemical environment. For example, it was found that the polarizability on the carbon atom for methane, methanol, and fluoromethane was found to be 1.05, 0.85, and 0.75 Å^3, respectively. These values agree with chemical intuition in that electron withdrawing groups should lower the electron density and therefore the polarizability on the carbon atom. In general, it would

be difficult to arrive at this level of sensitivity by fitting to tensor data alone because the molecular polarizability tensor has at most six independent components. In most cases, polarizabilities for a single molecule containing many atom types cannot be fit to the tensor alone because there is simply not enough data. Notably, it may be possible to use the probe method to derive transferable atom type polarizabilities. The probed charge method could be carried out separately on a large collection of molecules. The resulting parameters could be compared and generalizations relating atom types could then be made. However, if atom specific partial charges are used, it would seem natural to also assume atom specific polarizabilities.

It was also found that atomic polarizabilities are not sensitive to geometric rotations about torsion angles, as shown in the glycine dipeptide and $NH_2CH_2CH_2CO_2^-$. Both the molecular polarizability tensor and the response potential could be accurately reproduced over multiple conformations using a single set of probed polarizabilities. This very fortunate result is important in the construction or application of force fields for molecular simulation.

The atomic polarizabilities presented in this work are independent of the permanent electrostatic model used. The atom type polarizabilities were fit to molecular polarizability tensors and the probed polarizabilities were fit to the response electrostatic potential. Intramolecular polarization effects can be accounted for later when the permanent electrostatic model is fit. In this way, the atomic polarizabilities generated could be used in any electrostatic model; for example, point charges, point multipoles or Gaussian multipole charge densities.

Both the Thole and Gaussian isotropic polarizability models perform well for most organic molecules. Although the Gaussian model did slightly better than the Thole model over the 127 molecule atom type training set, the difference between the two in terms of performance is small. Although it was not tested, the probed procedure could be applied to the Thole model and still be expected to generate accurate results. The Thole model is somewhat arbitrary, since in the original Thole paper, seven different damping functions performed equally well in terms of fitting to tensor data. The main advantage of the Gaussian model over the Thole model is the possible generalization of other point multipoles to Gaussian charge densities.

5.5 References

1 B. T. Thole, Chem. Phys. **59**, 341 (1981)

2 J. Applequist, Chem. Phys. **85**, 279 (1984)

3 G. A. Kaminski, H. A. Stern, B. J. Berne, R. A. Friesner, Y. X. Cao, R. B. Murphy, R. Zhou, and T. A. Halgren, J. Comp. Chem. **23**, 1515-1531 (2002)

4 J. G.Ángyán, C. Chipot, F. Dehez, C. Hättig, G. Jansen, and C. J. Millot, J. Comp. Chem. **24**, 997 (2000)

5 K. Palmo, B. Mannfors, N. G. Mirkin, and S. Krimm, Biopolymers **68**, 383 (2003)

6 C. I. Bayly, P. Cieplak, W. D. Cornell, and P. A. Kollman, Phys. Chem. **97**, 10269 (1993)

7 R. J. Woods, M. Khalil, W. Pell, S. H. Moffat, and V. H. Smith Jr., J. Comp. Chem. **11**, 297 (1990)

[8] C. M. Breneman and K. B. Wiberg, J. Comp. Chem. **11**, 361-373 (1990)

[9] Gaussian 98, Revision A.11.3, M. J. Frisch, G. W. Trucks, H. B. Schlegel, G. E. Scuseria, M. A. Robb, J. R. Cheeseman, V. G. Zakrzewski, J. A. Montgomery, Jr., R. E. Stratmann, J. C. Burant, S. Dapprich, J. M. Millam, A. D. Daniels, K. N. Kudin, M. C. Strain, O. Farkas, J. Tomasi, V. Barone, M. Cossi, R. Cammi, B. Mennucci, C. Pomelli, C. Adamo, S. Clifford, J. Ochterski, G. A. Petersson, P. Y. Ayala, Q. Cui, K. Morokuma, N. Rega, P. Salvador, J. J. Dannenberg, D. K. Malick, A. D. Rabuck, K. Raghavachari, J. B. Foresman, J. Cioslowski, J. V. Ortiz, A. G. Baboul, B. B. Stefanov, G. Liu, A. Liashenko, P. Piskorz, I. Komaromi, R. Gomperts, R. L. Martin, D. J. Fox, T. Keith, M. A. Al-Laham, C. Y. Peng, A. Nanayakkara, M. Challacombe, P. M. W. Gill, B. Johnson, W. Chen, M. W. Wong, J. L. Andres, C. Gonzalez, M. Head-Gordon, E. S. Replogle, and J. A. Pople, Gaussian, Inc., Pittsburgh PA, 2002

[10] P. Ren, A. Grossfield, and J. W. Ponder, AMOEBA Force Field ftp://dasher.wustl.edu/pub/tinker/params

[11] W. H. Press, B. P. Flannery, B. P., S. A. Teukolsky, and W. T. Vetterling, *Numerical Recipes in C: The Art of Scientific Computing*, 2nd edition, (Cambridge University Press; Cambridge, 1992)

[12] A. Stone J. J. Mol. Phys. **56**, 1047 (1985)

[13] J. P. Piquemal, G. A. Cisneros, P. Reinhardt, N. Gresh, and T. A. Darden, J. Chem. Phys. **124**, 104101 (2006)

[14] P. Ren and J. W. Ponder, J. Comp. Chem. **23**, 1497 (2002)

[15] G. A. Kaminski, H. A. Stern, B. J. Berne, and R. A. Friesner, J. Phys. Chem. A **108**, 621 (2004)

[16] R. A. Friesner, R. B. Murphy, M. D. Beachy, M. N. Ringnalda, W. T. Pollard, B. D. Dunietz, and Y. X. Cao, J. Phys. Chem. A. **103**, 1913 (1999)

[17] T. J. Giese and D. M. York, J. Chem. Phys. **120**, 9903 (2004)

6 Amino Acid Atomic Polarizabilities/Partial Charges

6.1 Introduction

Including polarization in protein force fields has received a considerable amount of attention. Kollman[1-3] et. al. has introduced induced point dipoles of Applequist into the AMBER force field. Brooks[4-6] et. al. and Freisner[7 8] et. al. has developed fluctuating charge protein polarizable force fields for use in the CHARMM force field. Ponder[9-11] et. al. has developed the AMOEBA polarizable protein force field employing induced Thole dipoles for the polarization model and point multipoles to represent permanent electrostatic interactions. This chapter will focus on developing probe polarizabilities for the induced Gaussian dipole model and atomic point charges for the amino acids.

In the preceding chapter, a method to parameterize atomic polarizabilities was presented. The method is based on probing a molecule with point charges and calculating the electrostatic potential through electronic structure calculations. The probe polarizabilities are then fit to the response electrostatic potential. Probed polarizabilities were tested on a variety of organic molecules and shown to consistently yield significantly lower RMSD fits for both molecular polarizability tensor and response field as compared to the conventional method of fitting atom type polarizabilities to molecular polarizability tensors. In this chapter, results will be presented for probed polarizabilities generated for the amino acids.

The polarization model determines the electrostatic properties of a molecule in the presence of external electric fields, while the permanent electrostatic model determines the electrostatic properties of a molecule in vacuum, i.e. in the absence of an external

field. For large molecules, such as amino acids or nucleic acids, it should be expected that a molecule can polarize itself as its conformation changes. Rules for intramolecular polarization can be developed to account for how the permanent charge distribution affects the polarizable charge distribution in a flexible molecule. It was remarked in chapter 5, that polarizabilities can be fit by removing the effect of intramolecular polarization. By fitting to response electrostatic potential (the probed potential minus the vacuum potential), the contribution from the permanent electrostatic model is exactly canceled for linear polarizable models. Hence, the probed polarizabilities are independent of electrostatic model. Once polarizabilities have been determined, the electrostatic model can then be fit in the presence of polarization using rules for intramolecular polarization.

Though results have been derived for the more general cases of point multipoles and Gaussian multipole charge densities, atom centered point charges will be the permanent electrostatic model in this study. Point charges have been optimized for the amino acids using the conventional method of fitting to electrostatic potential (ESP) surrounding the molecule[12-14]. The point charges are simultaneously fit to multiple geometric conformations in order to investigate the effects of intramolecular polarization.

A commonly used rule to treat intramolecular polarization is to neglect[3 9 11 15] or screen[4-8] short range interactions between atoms that are bonded to one another. In AMBER[3 15], 1-5 and greater charge – induced dipole interactions at calculated at full strength, the 1-4 charge – induced dipole interactions are scaled, and the 1-2 and 1-3 interactions are neglected. A 1-2 interaction is defined as a pair of atoms that are bonded to each other. A 1-3 interaction is defined as a pair of atoms that share a bond with a

middle atom. Similarly, a 1-4 interaction is a pair of atoms that is separated by two middle atoms, and a 1-5 interaction is a pair of atoms separated by three atoms. In earlier studies, the optimal 1-4 scaling factor has not been precisely defined. Suggested values have ranged from 0.5 to 0.8. By treating the 1-4 scaling factor as an optimizable parameter during the calculations, a value is reported here which improves the ESP fits for single amino acids over multiple conformations.

In addition to generating amino acid charges/polarizabilities for use in future simulations, another goal of this study is to investigate how inclusion of polarizability improves the electrostatic description of force fields. It will be shown that inclusion of polarization significantly improves dipole moments and electrostatic potential of single amino acids over multiple conformations. The effect of polarizability becomes greater for larger molecules and systems. As a final test of polarization, the ESP was calculated for a 10-alanine peptide in the idealized fully extended and α-helical conformations. The charges fit to a single alanine amino acid were tested on the 10 alanine peptide conformation with and without polarization included. It will be shown that polarizability significantly improves the ESP potential, particularly when the peptide is in the α-helix conformation when amide groups in close proximity to one another become polarized.

6.2 Methods

Probed Polarizabilities

The method to fit probed polarizabilities is described extensively in section 5.2. In this section, a discussion of how probed polarizabilities were generated for amino

acids will be provided. Single amino acid structures were constructed with an acetate (ACE) cap on the N-terminus end and an N-methyl (NME) group cap on the C-terminus end as in figure 6.1. The geometry of each amino acid structure was initially optimized at the B3LYP/cc-pVTZ level. Since probed polarizabilities were found to be conformationally invariant (see 5.3.4), probed polarizabilities were generated at B3LYP/cc-pVTZ level of theory at the B3LYP/cc-pVTZ optimized geometry. All ab-initio calculations were performed with Gaussian 98[16].

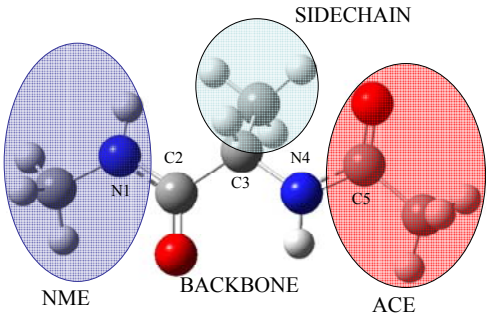

Figure 6.1 Amino Acid (alanine) with the N-methyl (NME) and acetate (ACE) caps. $\varphi \equiv$ C2-C3-N4-C5 and $\psi \equiv$ N1-C2-C3-N4

Once probed polarizabilities have been determined for each of the individual amino acid structures, the polarizabilities for the amino acid backbone, the ACE cap, and the NME cap were averaged over all amino acids. Probed polarizabilities for the side-chains were re-optimized with the averaged polarizabilities for the backbone, the ACE cap, and the NME cap constrained to their averaged values. The measured results are the RMSD in the response field ΔV_{rmsd} (5.2.13), the error in molecular polarizability tensor $\Delta\alpha$ (5.2.6), and the average of the eigenvalues of the molecular polarizability tensor α_{eigen}.

Point Charges

After the polarizabilities have been established, optimization of the point charges can proceed. In order to account for intramolecular polarization, a 1-4 charge – induced dipole scaling factor was also allowed to be a freely optimizable parameter. The point charges along with the 1-4 scaling factor were optimized to electrostatic potential (ESP) on a ChelpG grid. As discussed in section 5.2, a ChelpG[13] grid consists of a rectangular grid of points with a 0.3 Å spacing. Points in between an outer and inner radius for each atom were kept, while points outside the radii were discarded. The outer radii were set to 2.8 Å for each atom. The inner radii were set to 1.45 Å for H, 1.5 Å for C, 1.7 Å for N and O, and 2.3 Å for S.

Several geometric conformations were used during the fit. The different geometries were found by rotating the (φ ,ψ) torsion angles of the amino acid backbone (see Figure 6.1). The range of (φ ,ψ) torsion angles were selected to be representative of populated regions from a Ramachandran plot. Two sets of (φ ,ψ) coupled torsion angles were used. In the first set, φ = -120°, -105°, -90°, -75° and ψ = 90°, 105°, 120°, 135°, 150°, 165° (in increments of 15°). The second set of (φ ,ψ) was φ = -120°, -105°, -90°, -75° and ψ = -60°, -45°. Additionally, uncoupled single torsion rotations were added for amino acids with long polar sidechains in order to better sample the conformation space. The rotated torsion angles were constrained to their respective values while the rest of the molecule was free to relax at the B3LYP/cc-pVTZ level.

For each amino acid, the point charges and the 1-4 scaling factor were optimized to electrostatic potential calculated at B3LYP/cc-pVTZ for all the conformations. The fitting function is given by:

$$\chi^2 = \frac{1}{M \cdot N} \sum_{i=1}^{M} \sum_{j=1}^{N} (V_{ij} - V_{ij}^{QM})^2 \qquad 6.2.1$$

where V_{ij} is the electrostatic potential due to the point charges and induced Gaussian dipoles and V_{ij}^{QM} is the B3LYP/cc-pVTZ electrostatic potential at the i^{th} grid point of the j^{th} geometry. The RMSD in electrostatic potential ΔV_{rmsd}^{tot} is the square root of χ^2.

$$\Delta V_{rmsd}^{tot} = \sqrt{\chi^2} \qquad 6.2.2$$

The electrostatic potential is a linear function of charges. However, the potential is a quadratic function when considering both the charges and the 1-4 scaling factor. Therefore, the non-linear least squares Levenberg-Marquardt algorithm has been used to optimize the parameters. In addition, constraints for total charge were used in the optimization. The total charge on each of the ACE, NME, and protein backbone units was constrained to have a net charge of zero, while the total charge of the sidechains was constrained to have a net charge of that particular amino acid: -1, 0, or +1.

A well known artifact of fitting point charges to electrostatic potential (ESP) is the large artificial charges that develop on methyl or CH_2 groups. For example, a simple ChelpG calculation (at the B3LYP/cc-pVTZ level) predicts the charges on carbon and hydrogen to be -0.320 and +0.080, respectively for methane and 0.0132e and -0.0044e for ethane. Notice the sign change on the carbon in going from methane to ethane. At long range, electrostatic interactions between alkanes are small due to their apolar nature. For example, the permanent molecular dipole of isopropane is 0.132 D (Debye) (calculated at B3LYP/cc-pVTZ) while the molecular dipole of isopropanol is 1.54 D.

The combined charge of the alkyl group is more stable that the actual charges on the alkyl group. For example, a ChelpG calculation of methyl amine predicts the alkyl

carbon and hydrogen charge to be 0.312e and -0.035e, respectively. The RMSD in ESP is 7.06 (10^{-3} e/Å). Notice the combined charge on the entire CH_3 group is 0.207e. If the alkyl hydrogen charge is constrained to be zero, the charge on the carbon now optimizes to 0.182e, and the RMSD in ESP is 7.14 (10^{-3} e/Å). Since the new carbon charge of 0.182e is close to the CH_3 group charge of 0.207e, and since the RMSD in ESP did not increase significantly, it can be concluded that the charges on alkyl hydrogens are not significant. For this reason, all alky hydrogen point charges were constrained to be zero.

The performance of the charges was judged on the basis of the RMSD in total electrostatic potential ΔV_{rmsd}^{tot} and the molecular dipole $\vec{d}$ for each conformation given by:

$$\vec{d} = \sum_{i=1}^{K} q^i \vec{r}^{\,i} + \vec{\mu}^i \qquad 6.2.3$$

where K is the number of atoms and q^i is the charge, $\vec{r}^{\,i}$ is the position of atom i, and $\vec{\mu}^i$ is the induced Gaussian dipole of atom i. The induced Gaussian dipoles were allowed to interact with one another and the permanent charges through scaled 1-4 interactions and full strength 1-5 and greater interactions. For each conformation, the molecular dipole $\vec{d}$ can be directly compared with the molecular dipole calculated at B3LYP/cc-pVTZ. If $\vec{d}^{\,a}$ is the molecular dipole for conformation a predicted by the model and ${}^{QM}\vec{d}^{\,a}$ is the B3LYP/cc-pVTZ molecular dipole, then the RMSD for the permanent dipole at conformation a is given by:

$$\Delta d_{rmsd}^{a} = \sqrt{(\vec{d}^{\,a} - {}^{QM}\vec{d}^{\,a})^2} \qquad 6.2.4$$

For each amino acid, the dipole RMSD's were averaged over each conformation and given by $\Delta\overline{d}_{rmsd}$:

$$\Delta\bar{d}_{rmsd} \equiv \frac{1}{N}\sum_{a=1}^{N}\Delta d^{a}_{rmsd} \qquad 6.2.5$$

In order to compare the magnitude of the molecular dipoles with the RMSD fits for the dipole, an averaged dipole magnitude for each amino acid was also calculated as:

$$\left|\vec{d}\right| \equiv \frac{1}{N}\sum_{a=1}^{N}\left|\vec{d}^{\,a}\right| \qquad 6.2.6$$

In addition to the amino acid charges fit in the presence of polarizability, a second set of amino acid charges were optimized using an identical procedure without polarizabilitiy present (i.e. the polarizabilities were set to zero). The second set of charges optimized without polarizability was generated in order to investigate how much polarization improves the force field.

10-Alanine Test Case

In order to test the effect of polarization in a protein, a 10-alanine peptide was constructed in two conformations. The first conformation is in an idealized α-helix with each (φ ,ψ) angle set to (-60°, -60°) as in Figure 6.2A. The second geometry is an idealized fully extended conformation with each (φ ,ψ) angle set to (180°, 180°) as in Figure 6.2B.

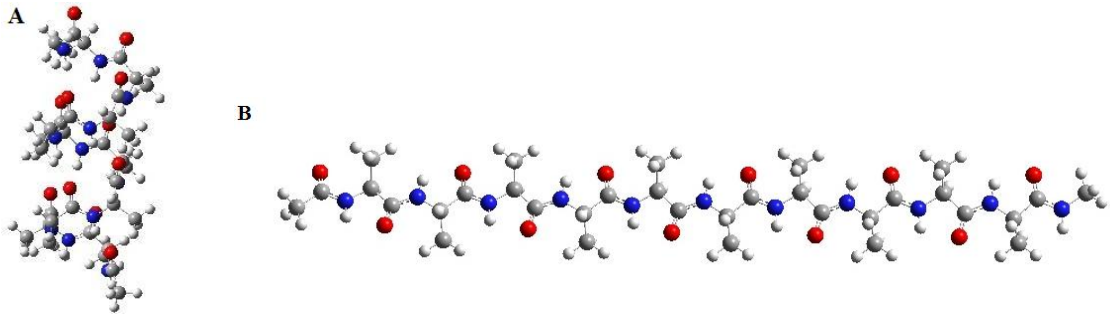

Figure 6.2 10-alanine peptides in α-helix form (**A**) with (φ ,ψ) = (-60°, -60°) and extended conformation (**B**) with (φ ,ψ) = (180°, 180°)

For both conformations, the (φ ,ψ) angles were constrained to their respective values while the rest of the geometry was allowed to relax at the B3LYP/6-31G* level. The electrostatic potential was calculated at the B3LYP/cc-pVTZ level on the B3LYP/6-31G* optimized geometries. The charges that were fit to a single alanine with and without polarizability present were tested on the 10-alanine peptide to see how well it reproduces electrostatic potential.

6.3 Results

Probed Polarizabilities

Probed polarizabilities were calculated for the amino acids with ACE and NME caps. Once the initial probed polarizabilities were found, the polarizabilities on the amino acid backbone, the ACE cap, and the NME cap were averaged over all the amino acids. The actual values of the averaged polarizabilities are given in Figure 6.3. The polarizabilities ($Å^3$) on the sp^2 hybridized amide groups are larger than their sp^3 hybridized counterparts. For example, the polarizabilities on the sp^2 backbone carbonyl

oxygen and the ACE cap carbonyl oxygen are 0.829 and 0.826, respectively. From previous calculations on small organic molecules not listed, the probe polarizabilities on the sp^3 hybridized oxygen atom in methanol, dimethyl ether, and water are 0.710, 0.749, and 0.684, respectively. The polarizabilities on the sp^2 backbone amide nitrogen and NME cap amide nitrogen are 1.365 and 1.349, respectively. This can be compared to the polarizabilities on sp^3 nitrogen of 1.107 and 1.080 for methyl amine and ammonia, respectively. As a final observation, the polarizabilities on the alkyl carbons directly attached to amide nitrogen are smaller in magnitude than the polarizabilities on alkyl carbons not attached to electronegative atoms. The polarizabilities on the alkyl carbons directly attached to the amide nitrogen are 0.694 (on the NME cap) and 0.728 (sp^3 backbone α-carbon), while the polarizabilities on the ACE cap methyl carbon is 1.042. The amide group is an electronegative electron withdrawing group and has the effect of reducing the polarizability on alkyl carbon. In general, this level of sensitivity in polarizability parameters would not be possible if conventional atom type polarizabilities fit to molecular polarizability tensors were used.

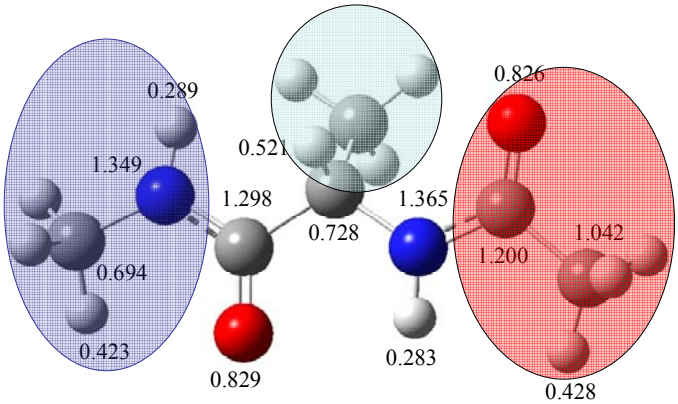

Figure 6.3 Averaged polarizabilities for the amino acid backbone, ACE cap, and NME cap.

The RMSD and errors in the fits are presented in Table 6.1 for each amino acid. In order to see the relative magnitudes of the molecular polarizability tensor, the average eigenvalues α_{eigen} of the molecular polarizability tensor are calculated at the B3LYP/cc-pVTZ level and listed in column 2 of Table 6.1. In general, the magnitude of the molecular polarizability tensor is proportional to the size of the amino acid. In column 3 of Table 6.1, the error in the molecular polarizability tensor is listed for the probed polarizabilities. The maximum error is 2.9% for GLU and the average error is 0.92%.

Amino Acid	α_{eigen} (Å^3)	$\Delta\alpha$ (%) All Free	$\Delta\alpha$ (%) Averaged Backbone	ΔV_{rmsd} (10^{-3} e/Å) All Free	ΔV_{rmsd} (10^{-3} e/Å) Averaged Backbone
ALA	13.68	0.85	1.14	1.52	1.53
ARG (+)	21.93	0.78	1.80	1.46	1.48
ASN	16.82	1.04	1.04	1.40	1.42
ASP (–)	17.02	1.15	0.96	1.80	1.85
CYS	16.53	0.82	1.07	1.79	1.83
GLN	18.64	0.62	0.88	1.42	1.43
GLU (–)	18.97	2.90	0.87	2.99	3.10
GLY	11.86	0.45	1.74	1.52	1.62
HIS	20.27	1.20	1.02	1.64	1.68
ILE	19.04	0.58	0.67	1.61	1.62
LEU	19.11	0.56	0.71	1.61	1.62
LYS^+ (+)	20.02	1.26	1.49	1.58	1.58
MET	20.35	0.99	1.19	1.66	1.67
PHE	23.22	0.91	0.93	1.63	1.63
SER	14.26	0.77	1.06	1.45	1.46
THR	16.07	0.60	0.86	1.45	1.45
TRP	27.80	0.97	1.45	1.80	1.89
TYR	24.12	0.85	0.89	1.57	1.58
VAL	17.26	0.68	0.78	1.56	1.56
Average		0.92	1.01	1.66	1.69

Table 6.1 Probed Polarizabilities for the Amino Acids. Probed Polarizabilities for the Amino Acids. In column 2, α_{eigen} is the average eigenvalues of the molecular polarizability tensor. Columns 3 and 4 contains the error in the polarizability tensor for the freely optimizable polarizabilities and constrained backbone polarizabilities, respectively. Column 5 and 6 contains the RMSD in response potential for the freely optimizable polarizabilities and constrained backbone polarizabilities, respectively.

After the initial probed polarizabilities of the amino acids have been established, the polarizabilities for the backbone, the ACE cap, and the NME cap were averaged over all the amino acids. The polarizabilities for the side-chains were then refit while the backbone, the ACE cap, and the NME cap polarizabilities were constrained to their averaged values. In column 4, the errors in molecular polarizability tensor for the averaged backbone polarizabilities are given. It is interesting to note that the errors do not increase significantly when using averaged backbone polarizabilities. The average error in the tensor was 0.92% when the polarizabilities on all the atoms were free to optimize and 1.01% when the polarizabilities were constrained to the averaged backbone values. The RMSD in response potential ΔV_{rmsd} follows a similar trend. The average value ΔV_{rmsd} over the amino acids was 1.66 (10^{-3} e/Å) using the initial set of polarizabilities which were all free to optimize, while the average of ΔV_{rmsd} using the averaged backbone polarizabilities is 1.69. Since the polarizabilities were fit to the response field, ΔV_{rmsd} is always larger for the averaged backbone polarizabilities because there are fewer parameters to fit. However, the effect is small. The average of ΔV_{rmsd} for the amino acids (1.66 or 1.69 10^{-3} e/Å) can be compared to the average of ΔV_{rmsd} (2.01 10^{-3} e/Å) for the test set of organic molecules in Chapter 5. The results indicate that the polarizabilities on the backbone, ACE, and NME groups on all the amino acids are quite similar to one another.

Point Charges

Point charges were fit to the total electrostatic potential over several conformations of single amino acids with ACE and NME caps with and without polarizability present. The set of probed polarizabilities used was the set whose amino acid backbone, ACE cap, and NME cap were averaged over the amino acids while the sidechains were refit. In addition, a 1-4 charge – induced dipole scaling factor was treated as an optimizable parameter for the charge optimization with polarization present. In Table 6.2, the optimized 1-4 charge-induced dipole scale is given for each amino acid. The values ranged from 0.07 to 0.21. The average value over the amino acids was found to be 0.13. Similar results were obtained for other organic molecules not listed, such as fluoropropane, ethylene glycol, and $H_2NCH_2CH_2COO^-$. For this reason, the 1-4 charge – induced dipole scaling factor was set to 0.1 and kept at that value for the rest of the calculations.

Amino Acid	1-4 Charge-Induced Dipole Scale	Amino Acid	1-4 Charge-Induced Dipole Scale
ALA	0.071	LEU	0.099
ARG (+)	0.210	LYS^+ (+)	0.138
ASN	0.182	MET	0.108
ASP (–)	0.134	PHE	0.136
CYS	0.213	SER	0.068
GLN	0.108	THR	0.108
GLU (–)	0.102	TRP	0.169
GLY	0.084	TYR	0.168
HIS	0.093	VAL	0.115
ILE	0.171		
Average			0.13

Table 6.2 Optimal 1-4 Charge-Induced Dipole Scale Factors for each amino acid.

Point charges were refit with polarizability present using the 1-4 scaling factor of 0.1. In addition, a set of point charges was optimized without polarizability present, i.e. the polarizabilities were set to 0.0. Once the charges have been initially determined for each amino acid individually, the charges on the amino acid backbone, the ACE cap, and the NME cap were averaged over all the amino acids. The averaged charges with and without polarizability present are given in Figure 6.4.

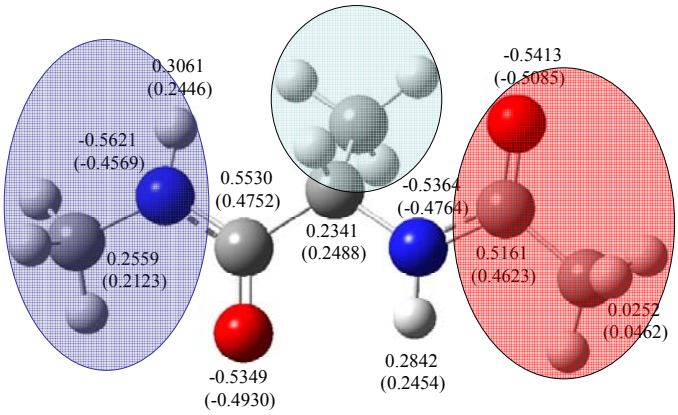

Figure 6.4 Averaged charges with and (without) polarizability for the amino acid backbone, ACE cap, and NME cap.

The RMSD for total electrostatic potential ΔV_{rmsd}^{tot} (6.2.2) over all of the conformations is listed in column 3 of Table 6.3 for the charges fit without polarizability and in column 5 for the charges fit with polarizability. In all cases, ΔV_{rmsd}^{tot} is lower for charges optimized with polarizability than without. The average of ΔV_{rmsd}^{tot} over all amino acids is 6.70 (10^{-3} e/Å) without polarizability and 5.81 (10^{-3} e/Å) with polarizability.

In order to see the relative magnitudes of the potential, the absolute value of the potential $|\overline{V}|$ was averaged over all the conformations and given in column 1 of Table

6.3. For the charged amino acids ARG, ASP, GLU, and LYS^+, $|\overline{V}|$ is larger by an order of magnitude than the uncharged amino acids.

		Non_polarizable		Polarizable	
Amino Acid	$\|\overline{V}\|$	ΔV_{rmsd}^{tot} (All Free)	ΔV_{rmsd}^{tot} (Average Backbone)	ΔV_{rmsd}^{tot} (All Free)	ΔV_{rmsd}^{tot} (Average Backbone)
ALA	25.45	5.67	7.02	5.11	5.14
ARG (+)	185.13	7.07	9.69	4.96	4.98
ASN	29.69	6.27	7.27	5.52	6.33
ASP (–)	207.07	9.76	18.31	6.48	6.64
CYS	26.93	7.61	9.22	7.15	7.82
GLN	29.86	5.49	6.26	4.81	4.85
GLU (–)	200.43	8.57	17.43	5.94	7.02
GLY	27.89	6.12	7.57	5.25	5.38
HIS	29.67	6.94	8.05	6.36	6.54
ILE	21.41	5.39	6.55	5.23	5.36
LEU	21.43	5.50	6.62	5.13	5.21
LYS^+ (+)	187.48	7.05	9.07	4.87	4.94
MET	24.66	6.80	7.60	6.41	6.46
PHE	23.29	6.99	7.94	6.60	6.63
SER	28.20	6.29	7.62	5.73	5.94
THR	27.69	6.21	7.55	5.97	6.15
TRP	26.35	7.32	8.40	6.97	7.13
TYR	25.95	7.20	8.22	6.59	6.67
VAL	22.60	5.57	7.09	5.43	5.62
Average		6.70	8.72	5.81	6.03

Table 6.3 Results for total electrostatic potential. Column 2 contains the average of the absolute value of total electrostatic potential. Column 3 and column 5 contain the RMSD in total electrostatic potential ΔV_{rmsd}^{tot} for the optimized charges for amino acids with and without polarizability present. Column 4 and column 6 contain ΔV_{rmsd}^{tot} for the optimized charges with and without polarizability present for averaged backbone charges.

As in the case for the polarizabilities, the backbone charges were averaged over the amino acids and then the sidechains refit. Columns 4 and 6 contain ΔV_{rmsd}^{tot} for the backbone averaged charges without and with polarizability, respectively. The effect of using averaged backbone charges without polarizability is more severe for the charged

amino acids ASP and GLU. ΔV^{tot}_{rmsd} nearly doubles in both cases: 9.76 → 18.31 for ASP and 8.57 → 17.43 for GLU. For charges optimized with polarizability, the effect of averaging backbone charges is less drastic. ΔV^{tot}_{rmsd} increases modestly for the charged amino acids: 6.48 → 6.64 for ASP and 5.94 → 7.02 for GLU. In going from all optimizable charges to averaged backbone charges, the average of ΔV^{tot}_{rmsd} over all the amino acids changes from 6.70 → 8.72 for charges without polarizability and 5.81 → 6.03 for charges with polarizability.

Another electrostatic property that can be used to make comparisons is molecular dipole moment. In order to see the relative sizes of the molecular dipole, the average magnitude of the molecular dipole (6.2.6) calculated at the B3LYP/cc-pVTZ level is given in column 2 of Table 6.4. For the charged amino acids, the total molecular dipole depends on the origin of the reference coordinate system and is omitted. The dipole moments are calculated at each conformation using the optimized point charge and induced Gaussian dipole model (6.2.3). The conformation averaged RMSD in dipole moment $\Delta\bar{d}_{rmsd}$ (6.2.5) is given in column 3 and column 5 of Table 6.4 for the optimized point charges without and with polarizability, respectively. Polarizability decreases the RMSD for dipoles by a factor of two or more in most cases. The average of $\Delta\bar{d}_{rmsd}$ over amino acids was 0.421 D for charges without polarizability and 0.186 D for charges with polarizability. Similar results were obtained for the backbone averaged charges. In this case, the average of $\Delta\bar{d}_{rmsd}$ was 0.987 D for backbone averaged charges without polarizability and 0.258 D for charges with polarizability.

Amino Acid	$\lvert \vec{d} \rvert$	Non_polarizable		Polarizable	
		$\Delta\bar{d}_{rmsd}$ (All Free)	$\Delta\bar{d}_{rmsd}$ (Average Backbone)	$\Delta\bar{d}_{rmsd}$ (All Free)	$\Delta\bar{d}_{rmsd}$ (Average Backbone)
ALA	2.89	0.216	0.714	0.124	0.139
ARG (+)	*	0.712	1.468	0.225	0.250
ASN	4.28	0.478	0.831	0.168	0.462
ASP (–)	*	0.909	2.933	0.299	0.303
CYS	3.35	0.337	0.763	0.286	0.531
GLN	3.44	0.365	0.591	0.140	0.140
GLU (–)	*	0.804	2.830	0.276	0.755
GLY	2.93	0.251	0.760	0.109	0.172
HIS	5.50	0.385	0.804	0.142	0.171
ILE	2.81	0.222	0.625	0.116	0.142
LEU	2.82	0.269	0.620	0.120	0.175
LYS^+ (+)	*	0.562	1.231	0.202	0.264
MET	3.07	0.302	0.610	0.149	0.216
PHE	3.11	0.464	0.718	0.235	0.184
SER	3.68	0.309	0.742	0.171	0.248
THR	4.12	0.285	0.676	0.177	0.211
TRP	4.00	0.523	0.788	0.221	0.147
TYR	3.48	0.476	0.696	0.185	0.136
VAL	2.83	0.214	0.773	0.178	0.325
Average		0.421	0.987	0.186	0.258

Table 6.4 Dipole moment (D) of the amino acids. Column 2 contains the magnitude of the B3LYP/cc-pVTZ molecular dipole averaged over conformations. Column 3 and 5 contain the RMSD of the dipole averaged over conformations for the charges fit with and without polarizability. Contain 4 and 6 contain the same quantity with averaged backbone charges.

Alanine Decapeptide

In order to test the effect of polarization in a large peptide, a 10 alanine peptide was constructed in the α-helix and fully extended conformation as in Figure 6.1. The charges optimized to a single alanine (with and without polarizability present) were tested on the 10 alanine peptide. As mentioned in section 6.2, the (φ ,ψ) angles were constrained to (-60°, -60°) for the idealized α-helix and (180°, 180°) for the idealized fully extended conformation, while the rest of the geometry was optimized at the B3LYP/6-31G* level. The electrostatic potential (ESP) around the 10 alanine peptide

was calculated as the same level of theory used to optimize the charges, B3LYP/cc-pVTZ.

In the center of the α-helix, polarization is expected to be particularly important because of hydrogen bonds between amide groups in adjacent turns of the helix. A non-polarizable force field would not be expected to perform well in environments where polarization is important unless effective charges that compensate for the lack of polarization are used. A method to find effective charges is to simply scale the gas phase charges. The charges fit for a single alanine were scaled by λ = 1.00, 1.05, 1.10, .. 1.30 and then tested on the 10 alanine peptide in both conformations. In Figure 6.5, the RMSD in potential V_{rmsd} for the α-helix is plotted at different charge scaling factors using the set of charges optimized to a single alanine with and without polarizability present. In order to compare these fits to what would be the best possible fit, a third set of 'best' charges was optimized specifically for the 10 alanine in the α-helix conformation. The RMSD in potential V_{rmsd} for the 'best' charges was found to be 6.12 (10^{-3} e/Å). When the charge scale factor λ was 1.0, i.e. charges optimized to a single alanine, V_{rmsd} = 18.38 (10^{-3} e/Å) for the charges without polarizability, and V_{rmsd} = 14.40 for the charges with polarizability. As the charge scaling factor was increased, V_{rmsd} for both sets of charges decreased. The optimal charge scale factor for charges without polarizability was found to be 1.25. In other words, the gas phase non-polarizable charges had to be scaled up by 25% to best reproduce the electrostatic potential for an α-helix. This number can be compared to the ratio between the gas phase dipole of water 1.8 D and what is believed to be the liquid phase dipole of 2.2-2.7 D, i.e. the dipole is scaled by 1.2 to 1.5. It is interesting to note that the charges with polarizability also should be scaled to best

reproduce the condensed phase ESP for the α-helix . Though as expected, the optimal scale factor for charges with polarizability (1.15) is less than the optimal scale factor for charges without polarizability (1.25). For charges with polarizability, V_{rmsd} = 8.15 (10^{-3} e/Å) at the optimal charge scale factor 1.15, and V_{rmsd} = 9.67 (10^{-3} e/Å) at the optimal charge scale factor 1.25 for charges without polarizability.

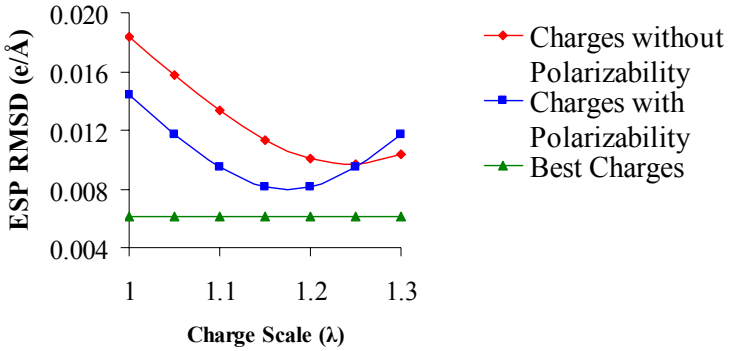

Figure 6.5 V_{rmsd} for 10 alanine α-helix using scaled charges optimized to a single alanine.

In a perfect electrostatic/polarization model, it would be expected that the charges would not need to be scaled. Therefore, either the polarization model or the polarizing field of the electrostatic model is underestimating the polarization effect. It was recently shown that the ab-initio electrostatic energy of a water dimer calculated at B3LYP/6-31G* is -8.32 kcal/mol[17]. If point charges were optimized to the electrostatic potential calculated at the B3LYP/6-31G* level, the point charges predict a dimer electrostatic energy of -5.31 kcal/mol. Point charges significantly underestimate the electrostatic energy at short range dimer distances. It would be expected that the point charges also underestimate the electric fields at short range dimer distances. At long range, the dominant electrostatic interaction is between the permanent molecular dipoles of the molecule (if the molecular dipoles are not zero). Since point charges optimized to

electrostatic potential reproduce molecular dipole moments, point charges accurately reproduce electrostatic interactions at long range. In the α-helix, amide groups in close proximity to one another are the main source of polarization. At short range, the polarizing electric field due to the point charges is underestimated and this is the reason why the charges need to be scaled by 15%.

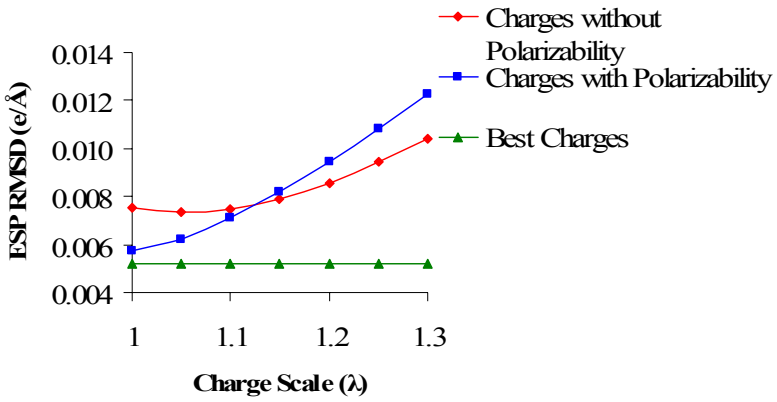

Figure 6.6 V_{rmsd} for 10 alanine in the fully extended conformation using scaled charges optimized to a single alanine.

The other conformation that was studied is the fully extended conformation when all of the (φ, ψ) angles are (180°, 180°), (see Figure 6.1). V_{rmsd} was plotted at different charge scales in Figure 6.6 for charges with and without polarizability. For charges with polarizability, a charge scaling factor λ of 1.0 (no charge scaling) excellently reproduces the ESP. For λ = 1.0, the RMSD in ESP is 5.75 (10^{-3} e/Å) for the charges with polarizability and 7.52 for charges without polarizability. These numbers can be compared with V_{rmsd} = 5.18 for the 'best' possible set of charges optimized specifically to the extended 10 alanine. In this conformation, the polarization response is adequately reproduced because the strongly polarizing amide groups are separated by a much farther

distance. At the longer distances, the polarizing fields due to the point charges can be expected to be more accurate than at short distances.

6.4 Conclusions

Probed polarizabilities were determined for the amino acids, the NME cap, and the ACE cap. The average error in the molecular polarizability tensor over the amino acids is 0.92% and the average error in the response potential is 1.66 10^{-3} e/Å. The effect of averaging the polarizability on the amino acid backbone, the NME cap, and the ACE cap is not significant. When the polarizabilities on the sidechains were refit with the averaged backbone, NME cap, and ACE cap polarizabilities kept constant, the averaged error in the molecular polarizability tensor increased to 1.01% and the error in the response field increased to 1.69 10^{-3} e/Å. This can be compared to an average error in the molecular polarizability tensor of 1.37% and an error in the response potential of 2.01 10^{-3} e/Å for the test set of organic molecules in Table 5.3. The results indicate that averaging atomic polarizabilities over amino acid backbones is a good approximation. This suggests that atomic polarizabilities for other biomolecules, such as saccharides, can be found by generating probed polarizabilities for a set of structures and then averaging the polarizabilities over related atom types.

Atomic point charges were fit to the total ESP for the amino acids over multiple conformations with and without polarizability present. In each case, polarizability improved the error in the total ESP and also the error in the total molecular dipole. The error in the total electrostatic potential averaged over the amino acids was found to be 6.70 10^{-3} e/Å without polarizability present and 5.81 10^{-3} e/Å with polarizability present.

When the charges were averaged over the amino acid backbones and the sidechain charges reoptimized, the error in the total ESP increased to 8.72 10^{-3} e/Å without polarizability present and 6.03 10^{-3} e/Å with polarizability present. A similar improvement was found with the molecular dipole moment. The error in the molecular dipole averaged over amino acids was found to be 0.421 D without polarizability present and 0.186 D with polarizability present. When the backbone charges were averaged and the sidechain charges refit, the error in the dipole moment increase to 0.987 D without polarizability present and 0.258 D with polarizability present.

The results discussed above indicate that polarization improves the electrostatic description of single amino acids over multiple conformations. The polarizabilities and atomic charges fit to the single amino acids were tested on a 10-alanine peptide in an idealized fully extended and α-helical conformation. The ESP was calculated using the charges optimized to a single alanine with and without polarizability present. In the α-helical conformation, the results indicate that point charges without polarizability should be scaled larger by 25% and that point charges with polarizability should be scaled larger by 15%. A possible reason why the charges with polarizability need to be scaled by 15% is that point charges underestimate electric fields at short distances. The field applied to the induced dipoles is too weak. In the fully extended conformation, the point charges with polarizability adequately reproduce the ESP and do not need to be scaled. These results indicate that further improvements can be made if more sophisticated electrostatic models, e.g. point multipoles or Gaussian multipole charge densities are used in place of point charges.

6.5 References

[1] A. E. Howard, U. C. Singh, M. Billeter, and P. A. Kollman, J. Am. Chem. Soc. **110**, 6984 (1988)

[2] J. Caldwell, L. X. Dang, and P. A. Kollman, J. Am. Chem. Soc. **112**, 9144 (1990)

[3] P. Cieplak, J. Caldwell, and P. A. Kollman, J. Comp. Chem. **22** (**10**), 1048 (2001)

[4] S. Patel and C. L. Brooks III, J. Comp. Chem. **25**, 1 (2004)

[5] S. Patel, A. D. MacKerell Jr., and C. L. Brooks 25, 1504 (2004)

[6] S. Patel and C. L. Brooks III, Mol. Sim. **32** (**3-4**), 231 (2006)

[7] G. A. Kaminski, H. A. Stern, B. J. Berne, R. A. Friesner, Y. X. Cao, R. B. Murphy, R. Zhou, and T. A. Halgren, J. Comp. Chem. **23**, 1515 (2002)

[8] G. A. Kaminski, H. A. Stern, B. J. Berne, and R. A. Friesner, J. Phys. Chem. A **108**, 621 (2004)

[9] P. Ren, A. Grossfield, and J. W. Ponder, AMOEBA Force Field, ftp://dasher.wustl.edu/pub/tinker/params.

[10] P. Ren and J. W. Ponder, J. Phys. Chem. B **107**, 5933 (2003)

[11] P. Ren and J. W. Ponder, J. Comp. Chem. **23**, 1497 (2002)

[12] C. I. Bayly, P. Cieplak, W. D. Cornell, and P. A. Kollman, Phys. Chem. **97**, 10269 (1993)

[13] C. M. Breneman and K. B. Wiberg, J. Comp. Chem. **11**, 361 (1990)

[14] R. J. Woods, M. Khalil, W. Pell, S. H. Moffat, and V. H. Smith Jr., J. Comp. Chem. **11**, 297 (1990)

[15] A. Toukmaji, C. Sagui, J. Board, and T. A. Darden, J. Chem. Phys. **113**, 10913 (2000)

[16] Gaussian 98, Revision A.11.3, M. J. Frisch, G. W. Trucks, H. B. Schlegel, G. E. Scuseria, M. A. Robb, J. R. Cheeseman, V. G. Zakrzewski, J. A. Montgomery, Jr., R. E. Stratmann, J. C. Burant, S. Dapprich, J. M. Millam, A. D. Daniels, K. N. Kudin, M. C. Strain, O. Farkas, J. Tomasi, V. Barone, M. Cossi, R. Cammi, B. Mennucci, C. Pomelli, C. Adamo, S. Clifford, J. Ochterski, G. A. Petersson, P. Y. Ayala, Q. Cui, K. Morokuma, N. Rega, P. Salvador, J. J. Dannenberg, D. K. Malick, A. D. Rabuck, K. Raghavachari, J. B. Foresman, J. Cioslowski, J. V. Ortiz, A. G. Baboul, B. B. Stefanov, G. Liu, A. Liashenko, P. Piskorz, I. Komaromi, R. Gomperts, R. L. Martin, D. J. Fox, T. Keith, M. A. Al-Laham, C. Y. Peng, A. Nanayakkara, M. Challacombe, P. M. W. Gill, B. Johnson, W. Chen, M. W. Wong, J. L. Andres, C. Gonzalez, M. Head-Gordon, E. S. Replogle, and J. A. Pople, Gaussian, Inc., Pittsburgh PA, 2002

[17] G. A. Cisneros, J. P. Piquemal, and T. A. Darden, J. Chem. Phys. **125**, 184101 (2006)

7 Optimization of van der Waals Parameters: Water and Ammonia

7.1 Introduction

In biomolecular force fields such as AMBER[1-6]/GLYCAM[7-9] and CHARMM[10-15], the non-bond energy is composed of an electrostatic term, a recently added polarization term, and a van der Waals (vdW) term. The vdW term is modeled by a 12-6 Lennard-Jones potential of the form:

$$V(r) = \frac{A_{ab}}{r^{12}} - \frac{C_{ab}}{r^{6}} \qquad 7.1.1$$

The r^{-12} term models the short range exchange/repulsion part of the non-bond energy and the r^{-6} term models the attractive long range dispersion contribution.

Many groups have devoted a significant amount of time in developing parameters for the vdW potential. Jorgensen[16-19] et. al. has created the OPLS force field by fitting atom type point charges and vdW parameters to liquid phase heats of vaporization and density for pure solvents calculated through Monte Carlo simulations. MacKerell[20-22] et. al. has developed a two step hybrid approach of fitting vdW parameters to ab-initio data and then adjusting the resulting parameters to match heats of vaporization and density for pure solvents.

In terms of force field parameter development, fitting to ab-initio data is ideal because of the wealth of information available. When optimizing to experimental data, typically there are a few measured experimental quantities in which to fit to. For example, when fitting to heats of vaporization and density, there are two experimentally measured data points per solvent. On the other hand, MacKerell has fit Lennard-Jones parameters to ab-initio dimer data by probing molecules with He and Ne atoms. Many

data points can be obtained for interaction energy by probing different atoms and extending the probe trajectory.

However, there are two major obstacles in fitting vdW parameters to ab-initio data. The first problem is accuracy of the ab-initio method. It has been shown that extremely high ab-initio methods[23 24], e.g. CCSD(T)/aug-cc-pV5Z, are needed to accurately calculate dispersion energies between the noble gases. This level of theory is perhaps too expensive to fit an entire force field. York and Giese[25 26] have proposed an empirical method of obtaining high quality ab-initio data for weakly attractive dimer systems. The method takes a linear combination of ab-initio energies calculated at lower levels of theory and, by using basis set extrapolation techniques, predicts dimer energies at the CCSD(T) level. The small dimer energies for noble gases are the result of weak dispersion interactions. For example, the Ar-Ar dimer energy[23] is 0.270 kcal/mol. On the otherhand, interactions between hydrogen bonded dimers are dominated by electrostatic interactions. For example, an accurate estimate[27] of the water dimer energy is 5.02 kcal/mol. Lower levels of ab-initio theory[28], e.g. MP2/6-311++G(3d,p) and B3LYP/6-311++G(3d,p), can be used to reasonably estimate dimer energies and geometries of hydrogen bonded systems. MacKerell[20] has fit Lennard-Jones parameters to MP3/6-311++G(3d,3p), which appears to be a reasonable compromise between accuracy and CPU expense.

However, a more important question arises: is the functional form of the force field with point charges and a Lennard-Jones potential accurate enough that ab-initio data can be used? This work will attempt to answer this question by finding vdW parameters for water by two different approaches. In the first approach, vdW parameters are found

for water with and without polarizability present by optimizing to heats of vaporization and density through molecular dynamics (MD) simulations. The resulting vdW parameters are tested on dimer energies calculated at the MP2/cc-pVTZ level with the counterpoise correction[29] utilized to account for basis set superposition error (BSSE). It is shown that polarizability makes a significant improvement in reproducing ab-initio dimer energies. However, it would be interesting to check how well vdW parameters optimized to ab-initio dimer data reproduce liquid phase properties. In the second procedure, vdW parameters for water are found by fitting to dimer energies calculated at the BSSE corrected MP2/cc-pVTZ level. The heats of vaporization and density are calculated from the ab-initio optimized parameters. Though polarization makes a significant improvement, it is shown the ab-initio optimized parameters poorly reproduce the liquid phase properties. In the last section, dimer energies on the water dimer potential energy surface are explored. Pure electrostatic contributions[30] to the ab-initio dimer energy are compared to the electrostatic interactions predicted by point charges. The results indicate that the errors in fitting vdW parameters to ab-initio data for water is not due to a limitation in the level of ab-initio theory (BSSE corrected MP2/cc-pVTZ), but a fundamental limitation in assuming atom centered point charges and a 12-6 Lennard-Jones vdW potential.

In earlier studies[1-23], the vdW parameters A_{ab} and C_{ab} are usually expressed in terms of σ and ε.

$$V(r) = \varepsilon_{ab}\left(\left(\frac{\sigma_{ab}}{r}\right)^{12} - 2\left(\frac{\sigma_{ab}}{r}\right)^{6}\right) \qquad 7.1.2$$

In this case, $A_{ab} = \varepsilon_{ab}\sigma_{ab}^{12}$ and $C_{ab} = 2\varepsilon_{ab}\sigma_{ab}^{6}$. For a given atom type *a*, vdW parameters σ_a and ε_a are assigned. The combining rule for vdW parameters between two different atom types *a* and *b* in AMBER or CHARMM is $\sigma_{ab} = \sigma_a + \sigma_b$ and $\varepsilon_{ab} = \sqrt{\varepsilon_a \varepsilon_b}$. The minimum of $V(r)$ in 7.1.2 occurs at σ_{ab}, and $V(\sigma_{ab}) = \varepsilon_{ab}$ is the well-depth at the minimum. This functional form is particularly convenient for determining vdW parameters of noble gases. For example, the dimer distances σ_{aa} and well-depths ε_{aa} for He-He, Ne-Ne, and Ar-Ar dimers calculated[23] at the CCSD(T)/t-aug-cc-pV5Z level are 3.00, 3.16, and 3.80 Å, respectively for the minimum energy separation distance and 0.020, 0.080, and 0.262 kcal/mol for the well-depth, respectively.

In our studies, it was found that the parameter surface of fitting σ and ε for carbon and hydrogen to heats of vaporization and density of alkanes, alkenes, and aromatic compounds has a flat surface or shallow minimum. In other words, multiple sets of significantly different parameters yielded similar quality of fits to heats of vaporization and density for carbon and hydrogen containing compounds. In order to reduce the number of parameters, a different combining rule for A_{ab} and C_{ab} is employed in this study. Molecular dipole-dipole dispersion coefficients C_{AB}^{mol} have been determined experimentally[31-36]. The molecular dispersion coefficient between a pair of molecules *A* and *B* C_{AB}^{mol} can be modeled as a pairwise sum of atom-atom contributions, i.e. $C_{AB}^{mol} = \sum_{a \in A}\sum_{b \in B} C_{ab}$. Parameters for C, H, N, O have been fit to the experimental molecular dispersion coefficients[37 38] through the Slater-Kirkwood[39] combination rule (see appendix C.3 for a derivation)

$$C_{ab} = \frac{2\alpha^a(0)\alpha^b(0)C_{aa}C_{bb}}{\alpha^b(0)^2 C_{aa} + \alpha^a(0)^2 C_{bb}} \qquad 7.1.3$$

In 7.1.3, C_{ab} is the dispersion coefficient between atom *a* and atom *b*, and α^a and α^b are the atomic polarizabilities for atom *a* and atom *b*, respectively. In this study, the dispersion parameters C_{aa} and α^a determined by Yang and Wu[38] for the Slater-Kirkwood combination rule are employed in the Lennard-Jones potential. The repulsion parameter A_{ab} is expressed in terms of atom type repulsion parameters A_a and A_b by the following combination rule:

$$A_{ab} = A_a A_b \qquad 7.1.4$$

The atom type repulsion parameters A_a are optimized to heats of vaporization and density.

The choice of atomic point charges is particularly important to condensed phase properties. In non-polarizable force fields, charges optimized to the electrostatic potential (ESP) calculated at the HF/6-31G* level[40] have been employed because they overestimate the gas phase dipole by ~20-30%. For example, the experimental gas phase molecular dipole of water is 1.85 D, while HF/6-31G* predicts the molecular dipole to be 2.19 D. Another example is ammonia. The experimental and HF/6-31G* molecular dipoles of ammonia are 1.5 D and 1.95 D, respectively. It is interesting to note that the B3LYP/cc-pVTZ level, which has been employed throughout this work, predicts the molecular dipole of water and ammonia to be 1.91 D and 1.58 D, respectively. In this study, atomic point charges are found for water and ammonia by optimizing to the ESP calculated at the B3LYP/cc-pVTZ level. In order to account for condensed phase effects in the atomic charges, a charge scale factor λ_{ch} is an optimizable parameter in the vdW

optimizations. Hence, the atom type repulsion parameter A_a and the charge scale factor λ_{ch} are optimized to heats of vaporization density.

7.2 Methods

Dispersion Parameters C_{ab}

As mentioned in the introduction, the Slater Kirkwood combination rule along with the parameters optimized by Yang and Wu were employed for the calculation of the C_{ab} dispersion term in the Lennard-Jones potential 7.1.1. In the published values, the atomic polarizabilities α^a have been transformed into 'effective' number of electrons N_a: $N_a \equiv 16{C_{aa}}^2 / 9{\alpha^a}^2$ (7.1.3) with a similar expression for N_b. In terms of N_a and N_b, the Slater-Kirkwood equation is given by:

$$C_{ab} = \frac{2\left({C_{aa}}^2 {C_{bb}}^2 N_a N_b\right)^{\frac{1}{3}}}{\left(C_{aa} {N_b}^2\right)^{\frac{1}{3}} + \left(C_{bb} {N_a}^2\right)^{\frac{1}{3}}} \qquad 7.2.1$$

These parameters have been used, with a caveat. The vdW parameters on polar hydrogens (i.e. hydrogens attached to O or N) are either zero or set to small values in OPLS. Simulations of liquid water have indicated that small vdW parameters on the polar hydrogens are preferred when considering heats of vaporization and density. Ab-initio calculations of water dimers also have indicated that vdW parameters on polar hydrogen should be small. For this reason, the dispersion coefficients for polar hydrogens C_{HH} were set to zero. All of the dispersion contribution is placed on the oxygen C_{OO} and nitrogen C_{NN} atom types. Therefore, two new atom types were introduced: OH2 for oxygen with 2 attached hydrogens, and NH3 for nitrogen with 3 attached hydrogens. C_{aa} and N_a parameters were found for the two new atom types by

fitting to molecular dispersion coefficients calculated by the model of Yang and Wu. The standard non-linear least squares Levenberg-Marquardt algorithm[41] has been employed to optimize the parameters.

Force Field Parameters

Point charges were optimized to the ESP and probed polarizabilities were optimized to the response ESP calculated at the B3LYP/cc-pVTZ level for water and ammonia. All ab-initio calculations were performed with Gaussian 98[42]. The charges, polarizabilities, and polarizability exponents are given in Table 7.1 for water and Table 7.2 for ammonia. The rigid TIP3P[43] water geometry, with a fixed bond length of 0.9572 Å and a fixed bond angle of 104.52°, was employed in the water model. The ammonia bond lengths were constrained to 1.01 Å with the SHAKE[44] algorithm, while the AMBER[6] force field was employed to model the flexible bond angles. The H-N-H equilibrium bond angle and force constant are 109.50° and 35.0 kcal/mol/°, respectively.

Element	Charge q (e)	Polarizability α (Å^3)	Exponent β (Å^{-1})
O	-0.6936	0.6822	1.548
H	0.3468	0.2522	2.156

Table 7.1 Initial charges, polarizabilities, and polarizability exponents for water optimized at the B3LYP/cc-pVTZ level.

Element	Charge q (e)	Polarizability α (Å^3)	Exponent β (Å^{-1})
N	-0.8871	1.0865	1.2866
H	0.2957	0.29731	1.9817

Table 7.2 Initial charges, polarizabilities, and polarizability exponents for ammonia optimized at the B3LYP/cc-pVTZ level.

Calculation of Heats of Vaporization and Density

Molecular dynamics (MD) simulations were performed through the sander module of AMBER[6]. Simulations were run with a 1 fs time steps in both the *NVT* and *NPT* ensembles, which were maintained in those conditions with a Berendsen[45] thermostat. A non-bond cutoff of 8Å with Particle Mesh Ewald (PME)[46] and a continuum correction for the Lennard-Jones potential were employed to calculate long range interactions. In the simulations with polarization, induced dipoles were propagated by the Car-Parinello Lagrangian scheme[46] (see section 4.6), with coupling constant τ_μ = 0.1 ps. The protocol to calculate the heat of vaporization and density from molecular dynamics simulation is given by:

1) Equilibrate the solvent with 50ps of simulation in the *NVT* ensemble, with Berendsen temperature coupling constant, τ_T = 0.1 ps.
2) Equilibrate the solvent with 150ps in the *NPT* ensemble with Berendsen temperature and pressure coupling constants, τ_T = 0.1 ps and τ_P = 0.1 ps.
3) Simulate the solvent for 300ps in the *NPT* ensemble with Berendsen temperature and pressure coupling constants, τ_T = 1.0 ps and τ_P = 1.0 ps. Average the density and non-bond energy E_{liq} over the simulation and write the coordinates of the solvent box to an output file every 2 ps. The coordinates of the solvent molecules are used to calculate the intra-molecular non-bond energy E_{intra}. The intra-molecular non-bond energy is averaged over solvent molecules and time.

The heat of vaporization is calculated by:

$$H_{vap} = \left\langle E_{liquid} \right\rangle - \left\langle E_{intra} \right\rangle + RT \qquad 7.2.3$$

Optimization to Heats of Vaporization and Density

The repulsion parameters A_{aa} and the charge scale λ_{ch} parameter were optimized to heats of vaporization H_{vap} and density d using the non-linear least squares Levenberg-Marquardt algorithm[41]. Since the simulation averaged properties H_{vap} and d are accurate to the second or third decimal place, numerical derivatives of heat of vaporization H_{vap} and density d were estimated by a fit to the data. The parameters were perturbed forward and backward, and a derivative was fit to a straight line passing through the three points. The derivative step size is 0.01*X, where X is the current value of the parameter. Fully automated code was written to optimize the parameters and keep track of the simulations on multiple processor computer clusters.

Ab-initio Dimer Test

Three configurations of the water dimer illustrated in Figure 7.1 were optimized at the MP2/cc-pVTZ level. After the initial optimization, the relative geometries of the waters were translated along the directions of the arrows in Figure 7.1. Ab-initio energies of the dimer geometries were calculated along the trajectory at the MP2/cc-pVTZ level with BSSE accounted for through the counterpoise correction[29]. The dimer energy between two molecules A and B is the energy of the A-B complex minus the energy of A and B, i.e. $E_{\text{dimer}} = E(AB) - E(A) - E(B)$.

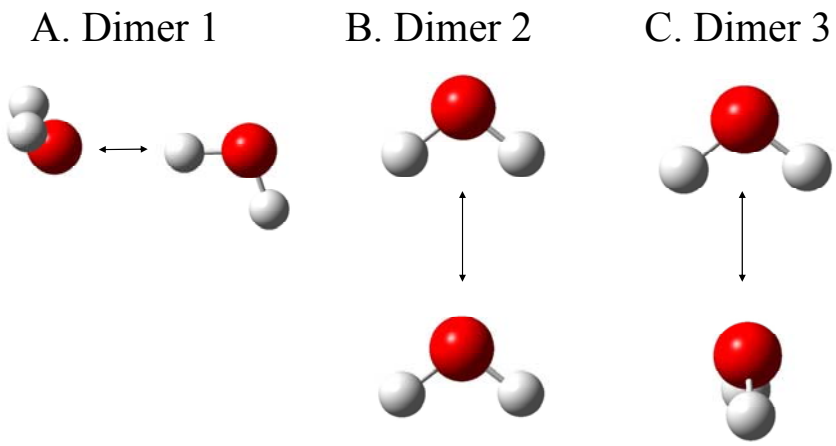

Figure 7.1 Water dimer geometries.

Optimization to Ab-initio Energy

The vdW repulsion parameter A_O for water was optimized to the ab-initio water dimer energies calculated along the trajectories in Figure 7.1 at the BSSE corrected MP2/cc-pVTZ level. As mentioned earlier, the charges and probed polarizabilities were calculated at the B3LYP/cc-pVTZ level. However, the difference between charges and polarizabilities fit to data calculated at the MP2/cc-pVTZ level and the B3LYP/cc-pVTZ level are neglible. In order to illustrate this, the charges and polarizabilites optimized at the MP2/cc-pVTZ level and the B3LYP/cc-pVTZ level are given in Table 7.3. Notice the charge on oxygen is -0.6992 at the MP2/cc-pVTZ level and -0.6936 at the B3LYP/cc-pVTZ level. This difference does not significantly affect the results.

Element	Charge q (e)	Polarizability α (Å^3)	Exponent β (Å^{-1})
O	-0.6992 (-0.6936)	0.6847 (0.6822)	1.5326 (1.548)
H	0.3496 (0.3468)	0.2385 (0.2522)	2.1783 (2.156)

Table 7.3 Charges, polarizabilities, and polarizability exponents for water calculated at the MP2/cc-pVTZ and (B3LYP/cc-pVTZ) level.

The charge scale factor was set to 1.0 in order to reproduce dimer energies at long range. The parameters were optimized through the standard non-linear least squares Levenberg-Marquardt algorithm. Only energies within 5kcal/mol of the dimer energy minimum were used in the fit, in order to discard points at short range when large exchange repulsion energies dominate the ab-initio dimer energy and the 12-6 potential function is not expected to accurately account for this.

7.3 Results

C_{ab} Dispersion Optimization

The parameters C_{aa} and N_a for the atom types: H, C(sp^3), C(sp^2), C(sp), N, O(sp^3), and O(sp^2) are taken from the model of Yang and Wu[38], and are listed in Table 7.4. The new atom type parameters for OH2 and NH3 were fit to 504 pairs of molecular dispersion coefficients calculated using the parameters of Yang and Wu as reference data. The OH2 and NH3 parameters are also listed in Table 7.4. Notice the parameters for OH2 and NH3 are larger than the parameters for N, O(sp^3), and O(sp^2) because the OH2 and NH3 parameters implicitly take into account hydrogen.

Atom Type	C_{aa}	N_a
H[a]	39.00	0.80
C(sp^3)[a]	303.7	2.49
C(sp^2)[a]	377.0	2.49
C(sp)[a]	409.8	2.49
N[a]	265.5	2.82
O(sp^3)[a]	160.0	3.15
O(sp^2)[a]	175.3	3.15
OH2	624.3	4.46
NH3	1224.0	5.16

Table 7.4 Dispersion parameters for Slater-Kirkwood combination rule.
[a]Values taken from reference[35].

Some examples of molecular dispersion coefficients calculated from the new OH2 and NH3 parameters are compared to the molecular dispersion coefficients using the parameters of Yang and Wu in Table 7.5. Notice the molecular dispersion coefficients calculated from the new optimized parameters match the model of Yang and Wu to the 4-5 significant figures. The RMSD fit to the Yang and Wu model for the 504 molecular pairs is 0.0209 kcal/mol/Å^6. The experimental values (if available) are also given for comparison. The main reason for not fitting directly to experimental data was to avoid the possibility of over-fitting parameters to insufficient experimental data.

Pair	New Model	Yang Model[a]	Experiment[b]
H_2O – H_2O	624.262	624.293	624.1
H_2O – methane	1054.501	1054.493	1051.9
H_2O – NH_2CH_3	1616.691	1616.657	-
H_2O – CO_2	1140.734	1140.829	1168.0
H_2O – benzene	3823.546	3823.601	3822.4
H_2O – NH_3	872.332	872.312	872.6
NH_3 – NH_3	1223.980	1223.969	1226.8
NH_3 – methane	1482.584	1482.583	1479.9
NH_3 – benzene	5380.787	5380.803	5390.5
NH_3 – CO_2	1593.235	1593.270	1630.1
NH_3 – phenol	5816.642	5816.648	-
H_2O – dimethyl ether	2112.946	2112.983	-

Table 7.5 Molecular Dispersion Coefficients in (kcal/mol/Å^6). [a] Calculated values using parameters from reference[38]. [b]Experimental values taken from references[31-36 38].

Optimization of Water to Heats of Vaporization and Density

The dispersion parameter for water was placed on the oxygen (C_{OO} = 624.3) as described in the previous section, while the hydrogen dispersion parameter was set to zero (C_{HH} = 0.0). The repulsion parameter on hydrogen A_H was set to 1.0, while the repulsion parameter on oxygen A_O and the charge scale factor λ_{ch} factor were optimized to heats of vaporization and density for a range of temperatures: 273°, 298°, 323°, and 348°. The optimized parameters are given for the models with and without polarizability in Table 7.6. The original non-polarizable TIP3P[43 46] water model is also given for comparison. In order to illustrate the actual size of the repulsion parameter in terms of an atomic radius, the repulsion and dispersion term were converted in terms of σ and ε, i.e. $\sigma_O = \frac{1}{2}\left(\frac{2A_O A_O}{B_{OO}}\right)^{\frac{1}{6}}$ and $\varepsilon_O = \frac{{B_{OO}}^2}{4A_O A_O}$. As expected, the charge scale factor is smaller for parameters optimized with polarizability (λ_{ch} = 1.130) than without (λ_{ch} = 1.255). The charge scale factors agree with the results from the 10 alanine peptide in chapter 6. The non-polarizable charges optimized to a single alanine had to be scaled up by 25% to best reproduce the electrostatic potential for 10 alanine in the α helical conformation, while the charges with polarizability need only be scaled up by 15%. In the model with polarizability, the repulsion parameter is larger with σ_O = 1.86 Å than in the model without polarizability σ_O = 1.76 Å. The non-polarizable model can be compared with the TIP3P water model, which was also fit to heats of vaporization and density. The non-polarizable model charges are slightly larger than TIP3P and the repulsion parameter is slightly smaller than TIP3P. It should be noted that TIP3P was optimized with a 9Å non-bond cutoff and no long range corrections for electrostatic or Lennard-Jones potential,

while the new optimized models employed both PME and continuum corrections to the Lennard-Jones.

	Polarizable	Non-Polarizable	TIP3P[a]
σ_O (Å)	1.860	1.756	1.768
ε_O (kcal/mol)	0.118	0.167	0.152
A_{OO} (10^{-3} kcal/molÅ^{12})	822.0	581.4	582.
A_{HH} (10^{-3} kcal/molÅ^{12})	1.0	1.0	0.0
C_{OO} (kcal/molÅ^6)	624.3	624.3	595.
C_{HH} (kcal/molÅ^6)	0.0	0.0	0.0
λ_{ch}	1.130	1.255	1.203
q_O	-0.7836	-0.8704	-0.834
q_H	0.3918	0.4352	0.417

Table 7.6 Optimized parameters for water with and without polarizability present. [a]Values taken from reference[47].

The actual values of the heats of vaporization are given in Table 5.4 and the densities are given Table 7.7. Notice the density *d* is a monotonically decreasing function of temperature. This is indicative of the simple atom centered point charge water model that is studied here. The values of the parameters are fit in such a way that the error in density is balanced for the different temperatures. For example, at a temperature of 248° K, the density in the non-polarizable model (d = 1.0252 g/ml) is overestimated compared to experiment (d = 0.9896 g/ml). However, at a temperature of 348° K, the density (d = 0.9466 g/ml) is underestimated compared to experiment (d = 0.9748 g/ml). Similar trends follow in the polarizable water model and in the TIP3P water model.

T (K°)	H_{vap} (no polarizability)	H_{vap} (polarizability)	H_{vap} (experiment)
273	10.93	11.054	10.76
298	10.68	10.701	10.51
323	10.42	10.360	10.25
348	10.18	10.032	9.991
RMSD	0.175	0.185	

Table 7.7 Heats of vaporization (kcal/mol) for optimized water models with and without polarizability.

T (K°)	*d* (no polarizability)	*d* (polarizability)	*d* (TIP3P[a])	*d* (experiment)
248	1.0252	1.0263	1.049	0.9896
273	1.0108	1.0179	1.023	0.9998
298	0.9921	0.9956	1.002	0.9970
323	0.9710	0.9729	0.977	0.9880
348	0.9466	0.9479	0.953	0.9748
RMSD	0.0223	0.0229	0.0306	

Table 7.8 Density (g/ml) for optimized water models with and without polarizability. [a]Values taken from reference[44].

The performance of the non-polarizable water model is similar to that of TIP3P. The heat of vaporization at T = 298° K is 10.68 (kcal/mol) for the non-polarizable model, 10.45 for TIP3P[42], and 10.51 for the experimental result. The RMSD in density over the temperatures from 248-348° K is 0.0223 g/ml for the non-polarizable model, 0.0229 g/ml for the polarizable model, and 0.0306 g/ml for TIP3P. This is interesting because the two proposed models had 2 optimizable parameters (A_O and λ_{ch}), while the TIP3P model had 3 optimizable parameters, (σ_O, ε_O, and λ_{ch}). This can be partially explained by the dispersion parameter C_{OO} between the proposed model (624.3) and TIP3P (595) are similar (see Table 7.6). However, it also indicates the possibility of over-fitting too many vdW parameters to the data. Both the charge scale λ_{ch} and well-depth parameter ε model the attractive interaction between the molecules. When considering heat of vaporization

and density only, there is perhaps not enough information to uniquely assign both λ_{ch} and ε.

The effect of placing a repulsion parameter on the water hydrogen was also investigated. In table 7.9, the repulsion parameter on hydrogen A_H was varied from 0.01 to 20, while the charge scale λ_{ch} and the oxygen repulsion parameter σ_O (A_O) were optimized. As the hydrogen repulsion parameter increased, the repulsion on oxygen decreased and the charge scale λ_{ch} increased to compensate. It appears that the lowest error in both heat of vaporization and density occurred for the smallest value of hydrogen repulsion parameter. This is perhaps the reason why TIP3P[32 47], TIP4P[43 47], and TIP5P[49] models do not have vdW parameters on the polar hydrogen. A small, but non-zero repulsion parameter was placed on hydrogen $A_H = 1.0$ for purposes of simulational stability.

$A_H = (A_{HH})^{1/2}$	σ_O	λ_{ch}	d (RMSD)	H_{vap} (RMSD)
0.01	1.770	1.227	0.0218	0.2782
0.1	1.767	1.229	0.0218	0.2855
0.5	1.761	1.241	0.0215	0.3029
1.0	1.756	1.255	0.0224	0.3158
5.0	1.724	1.320	0.0292	0.3531
10.0	1.693	1.360	0.0345	0.3617
20.0	1.628	1.397	0.0399	0.3497

Table 7.9 Optimization results for water without polarizability are given for different repulsion parameters on hydrogen.

vdW Optimization of Ammonia

A model for ammonia was optimized with and without polarizability to heats of vaporization and density through a procedure similar to that employed for water described earlier. The optimized parameters for ammonia are given in Table 7.10. In this

case, the charge scale λ_{ch} is 1.214 without polarizability and 1.104 with polarizability. This can be compared with the scale factors for water, 1.255 without polarizability and 1.130 with polarizability.

	Non-Polarizable	Polarizable
σ_N (Å)	1.858	1.8785
ε_N (kcal/mol Å^6)	0.225	0.211
A_{NN} (10^{-3} kcal/molÅ^{12})	1661.1	1773.7
A_{HH} (10^{-3} kcal/molÅ^{12})	25.0	25.0
C_{NN} (kcal/molÅ^6)	1224.0	1224.0
C_{HH} (kcal/molÅ^6)	0.0	0.0
λ_{ch}	1.214	1.104
q_N	-1.3191	-1.1991
q_H	0.4397	0.3997

Table 7.10 Optimized parameters for ammonia with and without polarizability present.

As in the case for water, the repulsion parameter for polar hydrogen A_H was varied, while the charge scale λ_{ch} and the nitrogen repulsion parameter A_N (σ_N) were optimized for the non-polarizable ammonia model. The hydrogen repulsion parameter A_H was varied from 0.1 to 50, and the results are given in Table 7.11. In contrast to water model, the RMSD errors in both heat of vaporization and density decreased when repulsion is placed on the polar hydrogen of the non-polarizable ammonia model. A value of A_H = 5.0 was selected as a value to study ammonia. The heats of vaporization and density are given in Tables 7.12 and 7.13, respectively. It is interesting to note that RMSD errors for heat of vaporization and density are higher in the polarizable model than in the non-polarizable model with the repulsion parameter A_H = 5.0.

$A_H = (A_{HH})^{1/2}$	σ_N (Å)	λ_{ch}	d (RMSD) (g/ml)	H_{vap} (RMSD) (kcal/mol)
0.1	1.915	1.205	0.01344	0.0934
1.0	1.901	1.203	0.01124	0.0686
5.0	1.858	1.214	0.00798	0.0401
10	1.809	1.222	0.00810	0.0300
20	1.711	1.226	0.00743	0.0164
50	1.435	1.202	0.00737	0.0087

Table 7.11 Effect of placing a repulsion parameter A_H on the polar hydrogen of ammonia. Average RMSD errors in heats of vaporization and density for simulations without polarizability.

T (K°)	H_{vap} (no polarizability)	H_{vap} (polarizability)	H_{vap} (experiment)
233	5.713	5.803	5.648
243	5.537	5.611	5.531
253	5.431	5.406	5.408
263	5.240	5.221	5.277
273	5.096	5.036	5.140
RMSD	0.040	0.094	

Table 7.12 Heats of vaporization (kcal/mol) for optimized parameters for ammonia with and without polarizability.

T (K°)	d (no polarizability)	d (polarizability)	d (experiment)
233	0.6997	0.7043	0.6896
243	0.6810	0.6847	0.6775
253	0.6676	0.6625	0.6649
263	0.6446	0.6414	0.6519
273	0.6266	0.6193	0.6385
RMSD	0.00799	0.0123	

Table 7.13 Density (g/ml) for optimized parameters for ammonia models with and without polarizability.

Ab-initio Dimer Test

The polarizable and non-polarizable water models obtained by optimizing the charge scale λ_{ch} and oxygen repulsion parameter A_O (σ_O) to heats of vaporization and density were tested on ab-initio dimer energies. The dimer energies were calculated at the BSSE corrected MP2/cc-pVTZ level along the three trajectories illustrated in Figure

7.1. In Figure 7.2, the dimer energy calculated by ab-initio, the polarizable model, and the non-polarizable model are plotted as the O..H distance is varied for dimer 1 in Figure 7.1A. Similarly the dimer energies along the trajectories for dimer 2 in Figure 7.1B and dimer 3 in Figure 7.1C are given in Figure 7.3 and Figure 7.4, respectively.

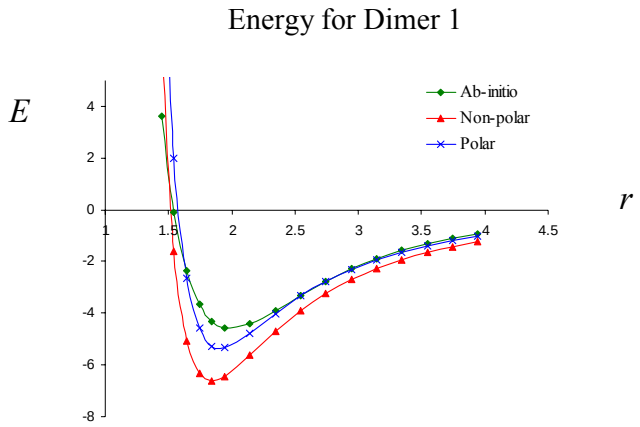

Figure 7.2 Polarization Energy (kcal/mol) for Dimer 1 in Figure 1A. *r* (Å) is the O..H distance.

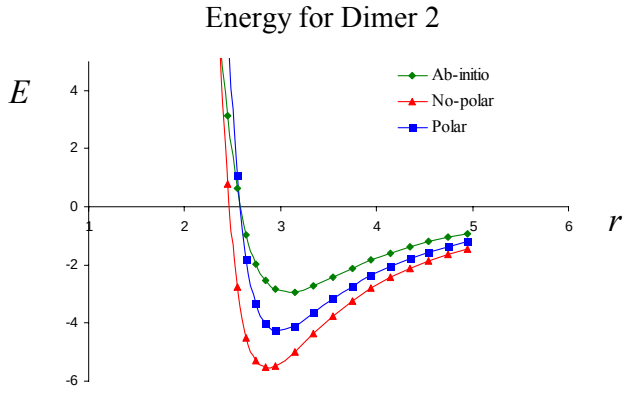

Figure 7.3 Polarization Energy (kcal/mol) for Dimer 2 in Figure 1B. *r* is the O..O distance.

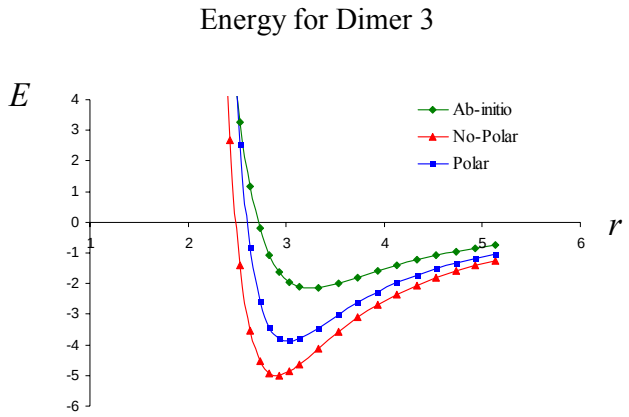

Figure 7.4 Polarization Energy (kcal/mol) for Dimer 3 in Figure 1C. *r* is the O..O distance.

The minimum dimer energies and distances at the minimum energy along the trajectory are given in Table 7.14 and Table 7.15, respectively. Both the polarizable and non-polarizable water models have dimer energies which are lower than the ab-initio dimer energy for all three trajectories. For dimer 1, the minimum along the trajectory for the ab-initio dimer energy is E = -4.61 kcal/mol which occurs at the O..H distance r = 1.94 Å. This can be compared to the dimer energy along the trajectory for the non-polarizable water model E = -6.63 kcal/mol at r = 1.85 and for the polarizable water model E = -5.34 kcal/mol at r = 1.92. The non-polarizable water model agrees with the dimer energy for TIP3P[43] of -6.50 kcal/mol. The larger dimer energy for the non-polarizable model as compared to the polarizable model can be attributed to a larger charge scale and a smaller repulsion parameter. Similar results occur for the other two water dimers. The errors in the dimer energies for the polarizable model range from 0.73 kcal/mol to 1.73 kcal/mol, while in the non-polarizable model the errors in dimer energy range from 2.02 to 2.84 kcal/mol.

	Dimer 1	Dimer 2	Dimer 3
Ab-initio	-4.61	-2.94	-2.15
Polarizable Model	-5.34	-4.29	-3.88
Non-Polarizable Model	-6.63	-5.54	-4.99

Table 7.14 Minimum energies (kcal/mol) along trajectories in Figure 7.1 for water parameters (Table 7.6) optimized to ab-initio data.

	Dimer 1 r = O..H	Dimer 2 r = O..O	Dimer 3 r = O..O
Ab-initio	2.01	3.11	3.27
Polarizable Model	1.92	2.88	3.03
Non-Polarizable Model	1.85	3.00	2.91

Table 7.15 Distances of minimum dimer energy r (Å) along trajectories in Figure 7.1 for water parameters (Table 7.6) optimized to ab-initio data.

Optimization to Dimer Energies

The vdW repulsion parameter for oxygen A_O (σ_O) was optimized to the ab-initio energies for all three dimer trajectories in Figure 7.1, and the charge scale factor λ_{ch} was set to 1.0. The optimized parameters for A_O (σ_O) are given in Table 7.16.

	Polarizable	Non-Polarizable
σ_O (Å)	1.800	1.742
ε_O (kcal/mol)	0.143	0.175
A_{OO} (10^{-3} kcal/molÅ^{12})	679.2	557.8
A_{HH} (10^{-3} kcal/molÅ^{12})	1.0	1.0
C_{OO} (kcal/molÅ^6)	624.3	624.3
C_{HH} (kcal/molÅ^6)	0.0	0.0
λ_{ch}	1.0	1.0
q_O	-0.6936	-0.6936
q_H	0.3468	0.3468

Table 7.16 Ab-initio energy optimized parameters for water with and without polarizability present.

The ab-initio, polarizable model, and non-polarizable model dimer energies for dimer 1, dimer 2, and dimer 3 are plotted in Figures 7.5, 7.6, and 7.6, respectively. The minimum

dimer energies and distances at the minimum energy along the trajectory are given in Table 7.17 and Table 7.18, respectively.

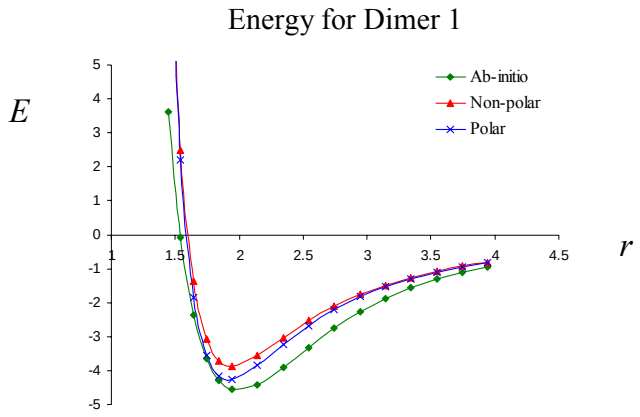

Figure 7.5 Dimer energies along dimer 1 in Figure 7.1A for the models optimized to ab-initio dimer energy.

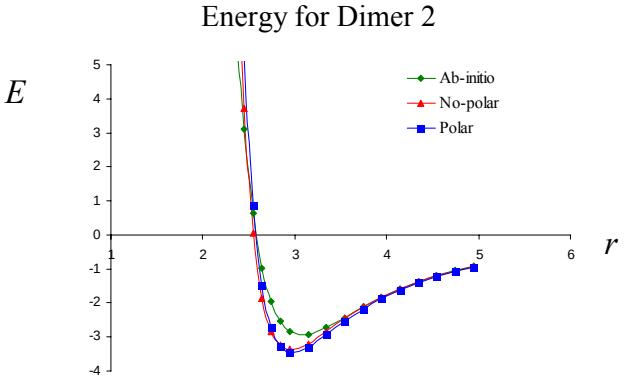

Figure 7.6 Dimer energies along dimer 2 in Figure 7.1B for the models optimized to ab-initio dimer energy.

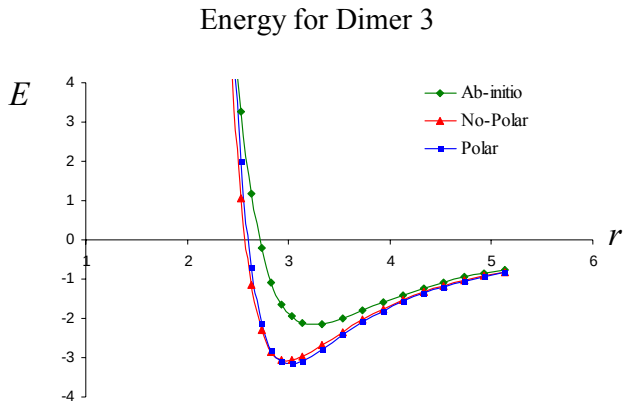

Figure 7.7 Dimer energies along dimer 3 in Figure 7.1C for the models optimized to ab-initio dimer energy.

	Dimer 1	Dimer 2	Dimer 3
Ab-initio	-4.61	-2.94	-2.15
Polarizable Model	-4.26	-3.47	-3.15
Non-Polarizable Model	-3.88	-3.37	-3.06

Table 7.17 Minimum energies (kcal/mol) along trajectories in Figure 7.1 for water parameters (Table 7.6) optimized to heats of vaporization and density.

	Dimer 1 r = O..H	Dimer 2 r = O..O	Dimer 3 r = O..O
Ab-initio	2.01	3.11	3.27
Polarizable Model	1.94	3.00	3.02
Non-Polarizable Model	1.97	2.98	3.00

Table 7.18 Distances of minimum dimer energy r (Å) along trajectories in Figure 7.1 for water parameters (Table 7.6) optimized to heats of vaporization and density.

At long range, the dimer energy is largely determined by the interaction between permanent molecular dipoles. Since the electrostatic potential (ESP) optimized point charges reproduce permanent molecular dipole moments, the ab-initio optimized parameters reproduces the long range dimer energy for all three dimers in Figures 7.5 – 7.7 because the charge scale λ_{ch} was set to 1.0. Notice in dimer 1 (Table 7.17), the ab-initio dimer energy (E = -4.61 kcal/mol) is lower than the non-polarizable model dimer

energy (E = -3.88 kcal/mol), while the ab-initio energy in dimer 2 (E = -2.94 kcal/mol) and dimer 3 (E = -2.15 kcal/mol), is greater than the non-polarizable model energy in dimer 2 (E = -3.37 kcal/mol) and dimer 3 (E = -3.06 kcal/mol). A similar result holds for the polarizable model. At short range, the repulsion parameter for oxygen A_O (σ_O) was optimized so that the difference between the model and ab-initio dimer energy is a minimum for all three dimers.

The ab-initio optimized vdW parameters were tested in simulations by calculating heats of vaporization and density. In Table 7.17, the heats of vaporization are given for the models optimized to ab-initio dimer energies. Notice the non-polarizable vdW underestimate the heat of vaporization by 50% with an RMSD of 4.95 kcal/mol. The polarizable vdW parameters perform significantly better with an RMSD of 2.58 kcal/mol. However, both sets of parameters optimized to ab-initio data perform poorly when compared to the water models optimized to the liquid data: heats of vaporization and density. Recall the RMSD for heat of vaporization for the water models optimized to the liquid data is 0.175 kcal/mol and 0.185 kcal/mol for the non-polarizable and polarizable models, respectively.

T (K°)	H_{vap} (no polarizability)	H_{vap} (polarizability)	H_{vap} (experiment)
273	5.83	8.25	10.76
298	5.58	7.95	10.51
323	5.31	7.66	10.25
348	4.99	7.36	9.991
RMSD	4.95	2.58	

Table 7.19 Heats of vaporization (kcal/mol) for optimized water models with and without polarizability.

In Table 7.18, the densities are given for the water models optimized to ab-initio data. The RMSD in density for the ab-initio optimized parameters are 0.251 and 0.0515 g/ml for the non-polarizable and polarizable water models, respectively. This can be compared to the RMSD in density for the water models optimized to liquid data, 0.0223 and 0.0229 g/ml for the non-polarizable and polarizable water models, respectively.

T (K°)	*d* (no polarizability)	*d* (polarizability)	*d* (experiment)
248	0.8943	1.0236	0.9896
273	0.8497	0.9928	0.9998
298	0.7989	0.9608	0.9970
323	0.7391	0.9275	0.9880
348	0.6616	0.8905	0.9748
RMSD	0.215	0.0515	

Table 7.20 Density (g/ml) for optimized water models with and without polarizability.

Water Dimer Potential Energy Surface

A set of 10 water dimers[27] has been proposed as a test for water models[49]. The dimers are illustrated in Figure 7.8. Cisneros[30] et. al. has calculated the pure electrostatic component of the ab-initio dimer energies at the BSSE corrected B3LYP/aug-cc-pVTZ and B3LYP/6-31G* levels through the Constrained Orbital Variation (CSOV) method[51]. The electrostatic energies due to a set of point charges optimized to the ESP calculated at the B3LYP/6-31G* level were tested on the geometries provided by Cisneros.

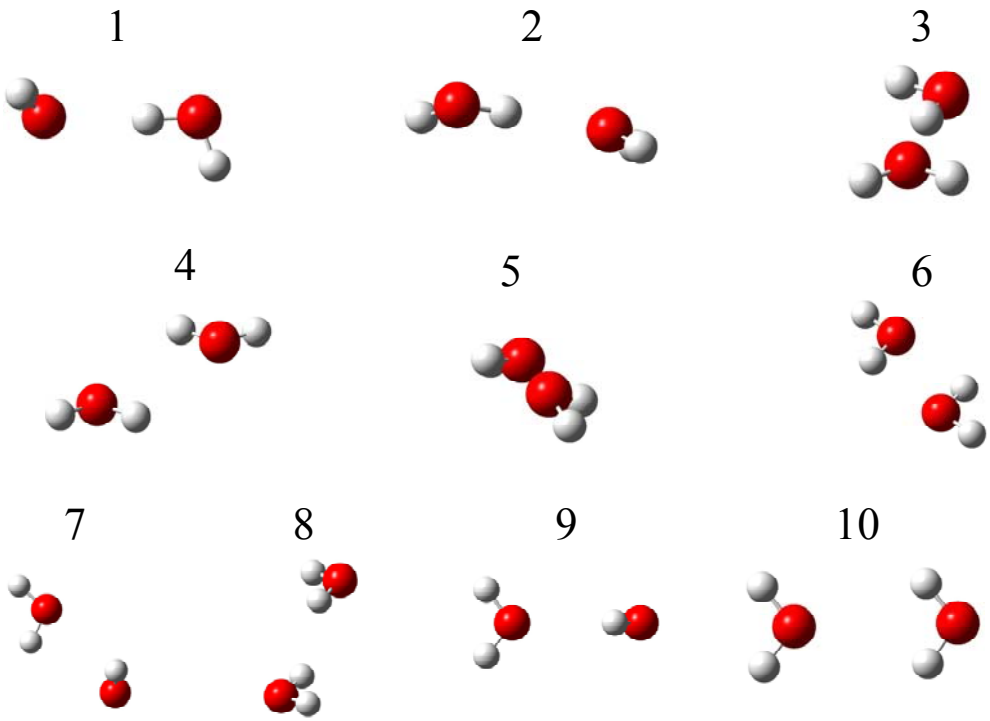

Figure 7.8 10 Water Dimers employed in water model tests.

Dimer Number	Point Charge	CSOV Electostatic Energy[a]	Total Dimer Energy[a]
1	-5.31	-8.32	-5.62
2	-4.90	-7.02	-4.94
3	-5.08	-7.00	-4.91
4	-4.66	-6.23	-4.20
5	-4.33	-5.59	-3.80
6	-4.51	-5.43	-3.73
7	-3.57	-4.35	-3.07
8	-0.99	-1.31	-1.20
9	-4.07	-4.79	-3.07
10	-3.22	-3.09	-2.33

Table 7.21 Dimer energies for 10 water dimers in Figure 7.8. The CSOV electrostatic energy and total dimer energy is calculated at the BSSE corrected B3LYP/6-31G* level. The point charges were fit to the ESP calculated at the B3LYP/6-31G* level.
[a]Values taken from reference[30].

For each of the 10 dimers, the total ab-initio dimer energies, the CSOV electrostatic dimer energies, and the point charge electrostatic dimer energies are given in Table 7.21. In dimer 1, the CSOV electrostatic energy is -8.32 kcal/mol, while the point charge electrostatic energy is -5.31 kcal/mol. The large discrepancy between the correct electrostatic energy and the electrostatic energy the point charges predict is observed for most of the other dimer geometries. However, it is interesting to note that the point charge electrostatic energy is very close to the total dimer energy. For example, in dimer 1, the point charge energy is -5.31 kcal/mol and the total dimer energy is -5.62 kcal/mol. A similar trends holds for the other 9 dimers, i.e. the point charge electrostatic energy is within 1 kcal/mol of the total dimer energy. This remarkable coincidence has also been pointed out by Dunitz and Gavezzotti[52] when calculating dimer energies between hydrogen bonded systems.

7.4 Conclusions

A polarizable and non-polarizable model for water and ammonia has been proposed by fitting a single vdW repulsive parameter (A_O for water and A_N for ammonia) and a charge scale factor λ_{ch} to experimental heats of vaporization and density. The dispersion parameters were fit separately to experimental molecular dispersion coefficients. The performance of the water models is similar to the performance of the TIP3P water model. The non-polarizable charge scale factor λ_{ch} (relative to charges optimized to the ESP calculated at the B3LYP/cc-pVTZ level) was found to be 1.255 for water and 1.214 for ammonia. The polarizable charge scale factor λ_{ch} was found to be 1.130 for water and 1.104 for ammonia. From chapter 6, the charge scale factor needed

to scale single alanine charges to best reproduce the electrostatic potential around a 10 alanine peptide in the α helical conformation was 1.25 for non-polarizable charges and 1.15 for polarizable charges. More research is required, but this suggests that atomic point charges can be found by fitting to the ESP calculated at the B3LYP/cc-pVTZ level and then scaling up by 20-25% for a non-polarizable force field and scaling up by 10-15% for a polarizable force field.

The polarizable and non-polarizable water models optimized to heats of vaporization and density were tested on dimer energies calculated at the BSSE corrected MP2/cc-pVTZ level along three water dimer trajectories. The errors in the dimer energies for the polarizable model range from 0.73 kcal/mol to 1.73 kcal/mol, while in the non-polarizable model the errors in dimer energy range from 2.02 to 2.84 kcal/mol.

The reverse procedure was also tested. The vdW repulsion parameter A_O was fit to the ab-initio dimer data and the charge scale factor λ_{ch} was set to 1.0 to reproduce ab-initio dimer energies at long range. The resulting ab-initio optimized parameters were tested by calculating heats of vaporization and density. Though polarization made a significant improvement, large errors were found for these quantities. The non-polarizable ab-initio water model underestimated the heat of vaporization by 50%. The RMSD for heat of vaporization was 4.95 kcal/mol for the non-polarizable model and 2.58 for the polarizable model. This can be compared to the model optimized to heat of vaporization and density. The RMSD for this model was 0.175 kcal/mol and 0.185 kcal/mol for the non-polarizable and polarizable models, respectively. Similar trends were also found for the density.

The point charge model was tested on a series of 10 water dimers. Significant errors occurred in the point charge electrostatic dimer energies with respect to the CSOV electrostatic component of the ab-initio dimer energies. For example in dimer 1 of Figure 7.8, the point charge model predicted a dimer energy of -5.31 kcal/mol, while the CSOV electrostatic component of the dimer energy was found to be -8.32 kcal/mol. Similar results were found for the other dimers. This is interesting because it explains why the polarizable point charges need to be scaled by 10-15%. If the point charge model underestimates the magnitude of the electrostatic energy at short range, then it can be expected that the electric fields due to the point charges are also underestimated. Therefore, in order to accurately account for the polarization effect, the point charges need to be scaled up. Another interesting property of the point charge model was found for the water dimers. The electrostatic dimer energy of the point charges is very similar to the total dimer energy. Other reports have indicated that this strange coincidence holds for other hydrogen bonded systems.

7.5 References

[1] W. D. Cornell, P. Cieplak, C. I. Bayly, I. R. Gould, K. M. Merz Jr., D. M. Ferguson, D. C. Spellmeyer, T. Fox, J. W. Caldwell, and P. A. Kollman, J. Am. Chem. Soc. **117**, 5179 (1995)

[2] D. A. Pearlman, D. A. Case, J. C. Caldwell, G. L. Seibel, U. C. Singh, P. Weiner, and P. A. Kollman, AMBER 4.0, (University of California, San Francisco) (1991)

[3] Weiner, P. K., & Kollman, P. A., (1981) AMBER: Assisted Model Building with Energy Refinement. A General Program for Modeling Molecules and Their Interactions, J. Comp. Chem. **2**, 287-303.

[4] Weiner, S.J., Kollman, P.A., Case, D.A., Singh, U.C., Ghio, C., Alagona, G., Profeta, S., Jr., Weiner, P.K. (1984) A new force field for molecular mechanical simulation of nucleic acids and proteins. J. Am. Chem. Soc. **106**, 765-784.

[5] S. J. Weiner, P. A. Kollman, D. T. Nguyen, and D. A. Case, J. Comp. Chem. **7**, 230 (1986)

[6] D. A. Case, T. A. Darden, T. E. Cheatham III, C. L. Simmerling, J. Wang, R. E. Duke, R. Luo, K. M. Merz, D. A. Pearlman, M. Crowley, R. C. Walker, W. Zhang, B. Wang, S. Hayik, A. Roitberg, G. Seabra, K. F. Wong, F. Paesani, X. Wu, S. Brozell, V. Tsui, H. Gohlke, L. Yang, C. Tan, J. Mongan, V. Hornak, G. Cui, P. Beroza, D. H. Mathews, C. Schafmeister, W. S. Ross, and P. A. Kollman, AMBER 9, University of California, San Francisco (2006)

[7] R. J. Woods, R. A. Dwek, C. J. Edge, and B. Fraserreid, J. Phys. Chem. **99** (**11**), 3832 (1995)

[8] M. Basma, S. Sundara, D. Calgan, T. Vernali, and R. J. Woods, J. Comp. Chem. **22** (**11**), 1125 (2001)

[9] R. J. Woods and R. Chappelle, J. Mol. Struct. **527**, 149 (2000)

[10] Brooks, B.R., Bruccoleri, R.E., Olafson, B.D., States, D.J., Swaminathan, S., Karplus, M. (1983) CHARMM: A program for macromolecular energy, minmimization, and dynamics calculations. J. Comp. Chem. **4**, 187-217.

[11] Feller et al., Biophys. J. **73**, 2269 (1997)

[12] A. D. MacKerell, D. Bashford, M. Bellott, R. L. Dunbrack, J. D. Eva seck, M. J. Field, S. Fischer, J. Gao, H. Guo, S. Ha, D. JosephMcCarthy, L. Kuc nir, K. Kuczera, F. T. K. Lau, C. Mattos, S. Michnick, T. Ngo, D. T. Nguyen, B. Pro hom, W. E. Reiher, B. Roux, M. Schlenkrich, J. C. Smith, R. Stote, J. Straub, M. Watanabe, J. Wiorkiewiczkuczera, D. Yin, and M. Karplus, J. Phys. Chem., B **102**, 3586 (1998)

[13] A. D. Mackerell J. Wiorkiewiczkuczera, and M. Karplus, J. Amer. Chem. Soc., **117**, 11946 (1995)

[14] F. A. Momany, and R. Rone, Validation of the General Purpose QUANTA 3.2/CHARMm Force Field, J. Comp. Chem. **13**, 888 (1992)

[15] J. J. Pavelites, J. Gao, P.A. Bash and A. D. Mackerell, Jr. J. Comp. Chem. **18**, 221 (1997)

[16] W. L. Jorgensen, J. Am. Chem. Soc. **103**, 335 (1981)

[17] W. L. Jorgensen, J. D. Madura, and C. J. Swenson, J. Am. Chem. Soc. **106**, 6638 (1984)

[18] W. L. Jorgensen, D. S. Maxwell, J. Tirado-Rives, J. Am. Chem. Soc. **118**, 11225 (1996)

[19] R. C. Rizzo and W. L. Jorgensen, J. Am. Chem. Soc. **121**, 4827, (1999)

[20] D. Yin and A. D. MacKerell, Jr., J. Phys. Chem., **100**, 2588, (1996)

[21] D. Yin and A. D. MacKerell, Jr., J. Comp. Chem. **19** (**3**), 334 (1998)

[22] I. J. Chen, D. Yin, and A. D. MacKerell, Jr., J. Comp. Chem. **23**, 199 (2002)

[23] D. E. Woon, J. Chem. Phys. **100** (**4**), 2838 (1994)

[24] T. P. Haley and S. M. Cybulski, J. Chem. Phys. **119** (**11**), 5487 (2003)

[25] T. J. Giese and D. M. York, Int. J. Quantum Chem. **98**, 388 (2004)

[26] T. J. Giese and D. M. York, J. Chem. Phys. **120** (**2**), 590 (2004)

[27] G. S. Tschumper, M. L. Leininger, B. C. Hoffman, E. F. Valeev, H. F. Schaeffer, and M. Quack, J. Chem. Phys. **116** (**2**), 690 (2002)

[28] P. R. Rablen, J. W. Lockman, and W. L. Jorgensen, J. Phys. Chem. A, **102**, 3782 (1998)

[29] S. F. Boys and F. Bernardi, Mol. Phys. **19**, 553 (1970)

[30] G. A. Cisneros, J. P. Piquemal, and T. A. Darden, J. Chem. Phys. **123**, 044109 (2005)

[31] D. J. Margoliash and W. J. Meath, J. Chem. Phys. **68** (**4**), 1426 (1978)

[32] B. L. Jhanwar and W. J. Meath, Mol. Phys. **41** (**5**), 1061 (1980)

[33] B. L. Jhanwar and W. J. Meath, Chem. Phys. **67**, 185 (1982)

[34] A. Kumar and W. J. Meath, Mol. Phys. **54** (**4**), 823 (1985)

[35] A. Kumar and W. J. Meath, Mol. Phys. **75** (**2**), 311 (1992)

[36] A. Kumar and W. J. Meath, Mol. Phys. **90** (**3**), 389 (1997)

[37] T. A. Halgren, J. Am. Chem. Soc. **114**, 7827 (1992)

[38] Q. Wu and W. Yang, J. Chem. Phys. **116** (**2**), (2002)

[39] J. C. Slater and J. G. Kirkwood, Phys. Rev. **37**, 682 (1931)

[40] C. I. Bayly, P. Cieplak, W. D. Cornell, and P. A. Kollman, Phys. Chem. **97**, 10269-10280 (1993)

[41] W. H. Press, B. P. Flannery, B. P., S. A. Teukolsky, and W. T. Vetterling, *Numerical Recipes in C: The Art of Scientific Computing*, 2nd edition, (Cambridge University Press; Cambridge, 1992)

[42] Gaussian 98, Revision A.11.3, M. J. Frisch, G. W. Trucks, H. B. Schlegel, G. E. Scuseria, M. A. Robb, J. R. Cheeseman, V. G. Zakrzewski, J. A. Montgomery, Jr., R. E. Stratmann, J. C. Burant, S. Dapprich, J. M. Millam, A. D. Daniels, K. N. Kudin, M. C. Strain, O. Farkas, J. Tomasi, V. Barone, M. Cossi, R. Cammi, B. Mennucci, C. Pomelli, C. Adamo, S. Clifford, J. Ochterski, G. A. Petersson, P. Y. Ayala, Q. Cui, K. Morokuma, N. Rega, P. Salvador, J. J. Dannenberg, D. K. Malick, A. D. Rabuck, K. Raghavachari, J. B. Foresman, J. Cioslowski, J. V. Ortiz, A. G. Baboul, B. B. Stefanov, G. Liu, A. Liashenko, P. Piskorz, I. Komaromi, R. Gomperts, R. L. Martin, D. J. Fox, T. Keith, M. A. Al-Laham, C. Y. Peng, A. Nanayakkara, M. Challacombe, P. M. W. Gill, B. Johnson, W. Chen, M. W. Wong, J. L. Andres, C. Gonzalez, M. Head-Gordon, E. S. Replogle, and J. A. Pople, Gaussian, Inc., Pittsburgh PA, 2002

[43] W. L. Jorgensen, J. Chandrasekhar, J. D. Madura, R. W. Impey, and M. L. Klein, J. Chem. Phys. **79** (**2**), 926 (1983)

[44] J. P. Ryckaert, G. Ciccotti, and H.J.C. Berendsen, J.Comput. Phys. **23,** 327 (1977)

[45] H. J. C. Berendsen, J. P. M. Postma, W. F. van Gunsteren, A. DiNola, and J. R Haak, J. Chem. Phys. **81** (**8**), 3684 (1984)

[46] A. Toukmaji, C. Sagui, J. Board, and T. A. Darden, J. Chem. Phys. **113**, 10913-10927 (2000)

[47] W. L. Jorgensen and C. Jenson, J. Comp. Chem. **19** (**10**), 1179 (1998)

[48] W. L. Jorgensen and J. D. Madura, Mol. Phys. **56** (**6**), 1381 (1985)

[49] M. W. Mahoney and W. L. Jorgensen, J. Chem. Phys. **112** (**20**), 8910 (2000)

[50] J. G. C. M. van Duijneveldt-van de Rijdt, W. T. M. Mooij, and F. B. D. Duijneveld, Phys. Chem. Chem. Phys. **5**, 1169 (2003)

[51] P. S. Bagus, K. Hermann, and C. W. Bauschlicher, Jr., J. Chem. Phys. **80**, 4378 (1984)

[52] J. D. Dunitz and A. Gavezzotti, Angew. Chem. Int. Ed. **44**, 1766 (2005)

8 Conclusions

8.1 Concluding Remarks

A polarization model based on induced Gaussian dipoles has been developed for the AMBER[1-5]/GLYCAM[6-8] force field. The induced Gaussian dipole model is based on induced charge density and overcomes the polarization catastrophe problem of the original induced point dipole model if the Gaussian exponent is sufficiently diffuse. For an induced Gaussian dipole with polarizability α and exponent β, it was shown that the maximum size of the Gaussian exponent is given by:

$$\beta < \frac{1}{\left(\alpha \frac{4}{3\sqrt{8\pi}}\right)^{\frac{1}{3}}}$$

Gaussian multipoles charge distributions were presented as a continuous generalization of point multipoles. Interaction energies, forces, electrostatic potential, electric field, and electric field gradients were derived between interacting Gaussian multipole charge densities. Gaussian multipole charge densities (Hermite Gaussian functions) are currently being employed to create more sophisticated force fields[9-11] based on electron charge density. The results obtained for Gaussian multipoles were used in the development of the induced Gaussian dipole polarization model.

The implementation of the induced Gaussian dipole model into the molecular dynamics (MD) simulation program AMBER[12] was discussed. Polarization energy, work, and force were derived for a system of induced Gaussian dipoles interacting with a set of permanent charges. It was shown that induced Gaussian dipoles can be implemented as a short range correction to the induced point dipole model with a non-bond cutoff of 5Å. MD simulations are often performed under periodic boundary

conditions, and the Ewald summation method was derived in appendix D for a periodic system of point charges and point dipoles. During an MD simulation, the induced dipoles can be found either by solving for the induced dipoles iteratively until self consistency is achieved or by propagating the induced dipoles through the Car-Parinello[13 14] (CP) method. In the CP method, the induced dipoles and their velocities are treated as dynamical variables and propagated in time through equations of motion. The CP method has been shown to be a good approximation with induced Gaussian dipoles for the case of water. Average polarization energies from a box of 341 waters calculated by the CP method (E_{pol} = -1313.12 kcal/mol) do not significantly differ from results obtained by solving for the induced dipoles exactly (E_{pol} = -1314.72 kcal/mol).

In order to obtain parameters for the induced Gaussian dipole model, two methods of generating atomic polarizabilities were presented. In the first method originally employed by Applequist[15] and Thole[16], a set of atom type polarizabilities was fit to a large collection of molecular polarizability tensors. Atom type atomic polarizabilities were found for the Gaussian model, the Thole model, and the Applequist point dipole model. It was shown that the Gaussian model performed slightly better than Thole in terms of fitting to molecular polarizability tensors. However, both the Gaussian model and the Thole model performed significantly better than the point dipole model. A second method of generating atomic polarizabilities was presented. This method is based on probing a molecule with point charges and calculating the electrostatic potential around the molecule. Atomic polarizabilities were fit to the response potential, which is the potential of the molecule in the presence of the charge probes minus the potential of the molecule in vacuum. Probed polarizabilities were shown to be significantly more

accurate than the atom type polarizabilities. For a set of organic molecules, the average RMSD error in molecular polarizability was found to be 1.37% for probed polarizabilities and 6.42% for atom type polarizabilities. The average RMSD in response potential was found to be 2.01 (10^{-3} e/Å) for probed polarizabilities and 3.04 for atom type polarizabilities. In addition, molecules with a high degree of anisotropy in the molecular polarizability tensor were investigated. Limitations with assuming isotropic atomic polarizabilities were found for the special case of F_2. However, for the sp^2 and sp^3 hybridized organic molecules investigated, the isotropic induced Gaussian dipole model performed well. Probed polarizabilities were also found to be conformationally invariant, i.e. probed polarizabilities generated in one geometry reproduced the molecular polarizability tensor and response potential in other geometries found by rotating torsion angles.

Probed polarizabilities were generated for the amino acids. When the polarizabilities on the backbone of all the amino acids were constrained to have the same value, the average RMSD in response potential increased from 1.66 (10^{-3} e/Å) to 1.69 (10^{-3} e/Å), and the RMSD error in molecular polarizability tensor increased from 0.92% to 1.01%. These results suggest the probe method can be used to find accurate atomic polarizabilities which are transferable between molecules similar to one another.

Atomic point charges were optimized for the amino acids with and without polarizability present. By fitting to multiple conformations of the amino acids, including polarization was shown to significantly improve the electrostatic properties of the amino acids. The RMSD in total electrostatic potential averaged over the amino acids was found to be 6.70 (10^{-3} e/Å) without polarizability present and 5.81 (10^{-3} e/Å) with

polarizability present. When the amino acid backbone charges were constrained to have the same value for all amino acids, the averaged RMSD in total electrostatic potential was 8.72 (10^{-3} e/Å) without polarizability present and 6.03 (10^{-3} e/Å) with polarizability present. The effect of including polarizability was also tested on molecular dipole moments. The RMSD of molecular dipole moment was averaged over conformations and found to be 0.421 D for charges without polarizability and 0.186 D for charges with polarizability. When the backbone charges were averaged over amino acids, the RMSD of molecular dipole moment was found to be 0.987 D for charges without polarizability and 0.258 D for charges with polarizability. The charges optimized to a single alanine were tested on a 10 alanine peptide in the extended and α helical conformation. In order to best reproduce the electrostatic potential of the 10 alanine in the α helical conformation, the single alanine charges had to be scaled up by 25% without polarizability and 15% with polarizability.

A polarizable and non-polarizable model has been found for water and ammonia by fitting the repulsive vdW parameter and a charge scale factor to heats of vaporization and density. The non-polarizable charge scale factor (relative to charges optimized to B3LYP/cc-pVTZ) was found to be 1.255 for water and 1.214 for ammonia. The polarizable charge scale factor was found to be 1.130 for water and 1.104 for ammonia. These results and the results for 10 alanine in the α helical conformation suggest that charges fit to the electrostatic potential calculated at the B3LYP/cc-pVTZ level should be scaled by 20-25% if polarizability is not present and 10-15% when polarizability is present.

The water models optimized to heats of vaporization and density were tested on dimer energies calculated at the BSSE corrected MP2/cc-pVTZ level. The dimer energies (along the trajectory in Figure 7.1A) were found to be -4.61 kcal/mol for ab-initio, -5.34 kcal/mol for the polarizable model, and -6.63 kcal/mol for the non-polarizable model. The dimer energy of the non-polarizable model agrees with the dimer energy of the non-polarizable TIP3P[17] water model of -6.50 kcal/mol. The lower dimer energy of both the non-polarizable and polarizable water models is due to the charges being scaled up.

A second question was asked during the fitting of vdW parameters: How well would water parameters optimized to ab-initio data reproduce the liquid phase heats of vaporization and density? The charge scale factor was set to 1.0 in order to reproduce dimer energies at long range, and the vdW repulsion parameter was fit to ab-initio water dimer data along three trajectories with and without polarizability present. The non-polarizable model optimized to ab-initio data underestimated the heat of vaporization by 50%, with an RMSD of 4.95 kcal/mol. The polarizable model performed better with an RMSD in the heat of vaporization of 2.58 kcal/mol. However, both models performed poorly when compared to the models optimized to heat of vaporization and density. The RMSD in the heat of vaporization for the models optimized to liquid data was 0.175 kcal/mol and 0.185 kcal/mol for the non-polarizable and polarizable models, respectively. Similar trends were also found for density. The discrepancies can be attributed to the scale factor. In order to accurately reproduce liquid properties, the point charges on the water model should be enhanced relative to the gas phase by 1.255 without polarizability and 1.130 with polarizability.

The limitations of the point charge model were tested by comparing to the ab-initio electrostatic energy by CSOV[18] decomposition for 10 water dimers[19 20] calculated at the B3LYP/6-31G* level[9]. For the water dimer in Figure 7.8 (1), the ab-initio electrostatic energy was found to be -8.32 kcal/mol, while the point charge interaction energy was found to be -5.31 kcal/mol. However, the point charge energy is coincidently similar to the total dimer energy of -5.62 kcal/mol. A similar result holds for the other 9 water dimers. Since the point charges underestimate the electrostatic interaction energy at short range, it can also be expected that the point charges also underestimate the electric field at short range. This explains why a charge scaling factor of 10-15% was necessary in order to reproduce liquid properties for the water and ammonia point charge models with polarization included. It would be expected that the charge scaling factor should be smaller for more sophisticated electrostatic models (e.g. point multipoles and Gaussian multipoles) which more accurately accounts for interactions at short range.

8.2 References

1 W. D. Cornell, P. Cieplak, C. I. Bayly, I. R. Gould, K. M. Merz Jr., D. M. Ferguson, D. C. Spellmeyer, T. Fox, J. W. Caldwell, and P. A. Kollman, J. Am. Chem. Soc. **117**, 5179 (1995)

2 D. A. Pearlman, D. A. Case, J. C. Caldwell, G. L. Seibel, U. C. Singh, P. Weiner, and P. A. Kollman, AMBER 4.0, (University of California, San Francisco) (1991)

3 Weiner, P. K., & Kollman, P. A., (1981) AMBER: Assisted Model Building with Energy Refinement. A General Program for Modeling Molecules and Their Interactions, J. Comp. Chem. **2**, 287-303.

[4] Weiner, S.J., Kollman, P.A., Case, D.A., Singh, U.C., Ghio, C., Alagona, G., Profeta, S., Jr., Weiner, P.K. (1984) A new force field for molecular mechanical simulation of nucleic acids and proteins. J. Am. Chem. Soc. **106**, 765-784.

[5] S. J. Weiner, P. A. Kollman, D. T. Nguyen, and D. A. Case, J. Comp. Chem. **7**, 230 (1986)

[6] R. J. Woods, R. A. Dwek, C. J. Edge, and B. Fraserreid, J. Phys. Chem. **99** (**11**), 3832 (1995)

[7] M. Basma, S. Sundara, D. Calgan, T. Vernali, and R. J. Woods, J. Comp. Chem. **22** (**11**), 1125 (2001)

[8] R. J. Woods and R. Chappelle, J. Mol. Struct. **527**, 149 (2000)

[9] G. A. Cisneros, J. P. Piquemal, and T. A. Darden, J. Chem. Phys. **125**, 184101 (2006)

[10] J. P. Piquemal, G. A. Cisneros, P. Reinhardt, N. Gresh, and T. A. Darden, J. Chem. Phys. **124**, 104101 (2005)

[11] G. A. Cisneros, J. P. Piquemal, and T. A. Darden, J. Chem. Phys. **123**, 044109 (2005)

[12] D. A. Case, T. A. Darden, T. E. Cheatham III, C. L. Simmerling, J. Wang, R. E. Duke, R. Luo, K. M. Merz, D. A. Pearlman, M. Crowley, R. C. Walker, W. Zhang, B. Wang, S. Hayik, A. Roitberg, G. Seabra, K. F. Wong, F. Paesani, X. Wu, S. Brozell, V. Tsui, H. Gohlke, L. Yang, C. Tan, J. Mongan, V. Hornak, G. Cui, P. Beroza, D. H. Mathews, C. Schafmeister, W. S. Ross, and P. A. Kollman, AMBER 9, University of California, San Francisco (2006)

[13] R. Car and M. Parrinello, Phys. Rev. Lett. **55**, 2471 (1985)

[14] A. Toukmaji, C. Sagui, J. Board, and T. A. Darden, J. Chem. Phys. **113**, 10913-10927 (2000)

[15] J. Applequist, J. R. Carl, and K. K. Fung, J. Am. Chem. Soc. **94**, 2952-2960 (1972)

[16] B. T. Thole, Chem. Phys. **59**, 341-350 (1981)

[17] W. L. Jorgensen, J. Chandrasekhar, J. D. Madura, R. W. Impey, and M. L. Klein, J. Chem. Phys. **79** (**2**), 926 (1983)

[18] P. S. Bagus, K. Hermann, and C. W. Bauschlicher, Jr., J. Chem. Phys. **80**, 4378 (1984)

[19] G. S. Tschumper, M. L. Leininger, B. C. Hoffman, E. F. Valeev, H. F. Schaeffer, and M. Quack, J. Chem. Phys. **116** (**2**), 690 (2002)

[20] J. G. C. M. van Duijneveldt-van de Rijdt, W. T. M. Mooij, and F. B. D. Duijneveld, Phys. Chem. Chem. Phys. **5**, 1169 (2003)

Appendix A. Cartesian Point Multipoles

A.1 Introduction

In this appendix, electrostatic interactions are expressed in terms of Cartesian point multipoles[1-3]. Cartesian multipoles are defined as moments over charge density. Interaction energies, forces, potential, fields, and field gradients are derived between two arbitrary charge distributions and expressed in terms of Cartesian point multipoles by expanding $1/R$ in a Taylor series about the centers of both charge distributions. The notation and formalism used here is similar to that given by Applequist[4 5]. Many of the results can also be found in[6-9].

The main motivation for reviewing Cartesian point multipoles is to introduce Gaussian multipoles in chapter two. A Gaussian multipole charge distribution can be viewed as a smooth continuous generalization of a point multipole charge distribution which is non-zero only at a single point. In chapter two, it is shown that point multipoles are the large exponent of Gaussian multipoles. The results for Gaussian multipoles derived in chapter two parallels the treatment given here for point multipoles.

In the following section A.2, the notation, conventions, and definitions for Cartesian vectors and tensors are briefly discussed. In section A.3, point multipoles are defined for charge distributions, and interaction energies between two charge distributions are derived in terms of Cartesian point multipoles. The next section A.4 contains a brief discussion of local and global coordinate systems. A multipole moment for a particle is defined in terms of a local coordinate system for that particle. The local coordinate system is commonly defined in terms of the particle and its attached neighbors. Using the results for transforming between local and global coordinate

system, the force and torque terms are derived in terms of point multipoles in section A.5. In section A.6, matrix elements of Cartesian gradient tensors of $1/R$ are evaluated explicitly up to fourth order. Electrostatic potential, fields, and field gradients are derived in section A.7. It is shown that multipole interaction energies can be expressed in terms of electrostatic potential and fields. Finally, a different method of treating multipoles based on spherical harmonics rather than Cartesian tensors is briefly discussed in section A.8.

A.2 Cartesian Vectors and Tensors

Cartesian point multipoles are formulated in the language of Cartesian tensors[10]. This section will briefly discuss some conventions and properties of Cartesian tensors. Let the Cartesian coordinate basis vectors $\hat{x}, \hat{y}, \hat{z}$ be denoted by $\hat{x}_1, \hat{x}_2, \hat{x}_3$. A vector $\vec{A}$ can be expressed in terms of these basis functions:

$$\vec{A} \equiv A_1\hat{x}_1 + A_2\hat{x}_2 + A_3\hat{x}_3 \qquad \text{A.2.1}$$

This can be more compactly written as $\vec{A} = \sum_{p=1}^{3} A_p\hat{x}_p \equiv A_p\hat{x}_p$, where the common practice of summing over repeated indices is used.

A vector $\vec{A}$ can also be defined as a Cartesian tensor of rank 1 $A^{(1)}$.

$$A^{(1)} \equiv A_p\hat{x}_p \qquad \text{A.2.2}$$

Similarly, a Cartesian tensor of rank 2 $A^{(2)}$ (sometimes referred to as a dyadic[11 12]) has two components and is defined as:

$$A^{(2)} \equiv A_{pq}\hat{x}_p\hat{x}_q \qquad \text{A.2.3}$$

A Cartesian tensor of rank n $A^{(n)}$ has n components and is defined as:

$$A^{(n)} \equiv A_{p_1 p_2 \cdots p_n} \hat{x}_{p_1} \hat{x}_{p_2} .. \hat{x}_{p_n} \qquad \text{A.2.4}$$

An inner or dot product between Cartesian basis vectors is defined as:

$$\hat{x}_p \cdot \hat{x}_q = \delta_{pq} \qquad \text{A.2.5}$$

where δ_{pq} is the kronecker-delta symbol defined as $\delta_{pq} = 1$ for $p = q$ and $\delta_{pq} = 0$ for $p \neq q$.

The dot product between two vectors $\vec{A}$ and $\vec{B}$ or tensors of rank 1 is given by:

$$\vec{A} \cdot \vec{B} \equiv A_p B_q \hat{x}_p \cdot \hat{x}_q = A_p B_q \delta_{pq} = A_p B_p$$

Similarly, a tensor dot product or contraction between two tensors of rank n is defined as:

$$\begin{aligned} A^{(n)} \cdot B^{(n)} &\equiv A_{p_1 p_2 \cdots p_n} \hat{x}_{p_1} \hat{x}_{p_2} .. \hat{x}_{p_n} \cdot B_{q_1 q_2 \cdots q_n} \hat{x}_{q_1} \hat{x}_{q_2} .. \hat{x}_{q_n} \\ &= A_{p_1 p_2 \cdots p_n} B_{q_1 q_2 \cdots q_n} \delta_{p_1 q_n} \delta_{p_2 q_{n-1}} ... \delta_{p_n q_1} \\ &= A_{p_1 p_2 \cdots p_n} B_{p_n .. p_2 p_1} \end{aligned} \qquad \text{A.2.6}$$

A Cartesian tensor is symmetric if for any pair of components

$$A_{..i..j..} = A_{..j..i..} \qquad \text{A.2.7}$$

The tensors that are used in this work are all symmetric, so that the contraction in A.2.6 becomes

$$A^{(n)} \cdot B^{(n)} = A_{p_1 p_2 \cdots p_n} B_{p_1 p_2 \cdots p_n} \qquad \text{A.2.8}$$

The gradient operator is a vector derivative operator defined by:

$$\nabla \equiv \hat{x}_p \frac{\partial}{\partial x_p} \qquad \text{A.2.9}$$

Similarly a gradient tensor of rank n is defined as:

$$\begin{aligned} \nabla^{(n)} &\equiv \nabla \nabla .. \nabla \\ &= \hat{x}_{p_1} \hat{x}_{p_2} .. \hat{x}_{p_n} \frac{\partial}{\partial x_{p_1}} \frac{\partial}{\partial x_{p_2}} .. \frac{\partial}{\partial x_{p_n}} \end{aligned} \qquad \text{A.2.10}$$

In the above definitions for tensors and vectors, the components (p = 1,2,3) were denoted as subscripts. Superscripts will be used to denote particle number for vectors/tensors (when possible). For example, the position of particle i is given by:

$$\vec{R}^i \equiv R_1^i \hat{x}_1 + R_2^i \hat{x}_2 + R_3^i \hat{x}_3 = R_p^i \hat{x}_p \qquad \text{A.2.11}$$

and the gradient for particle j is given by:

$$\nabla^j \equiv \hat{x}_1 \frac{\partial}{\partial R_1^j} + \hat{x}_2 \frac{\partial}{\partial R_2^j} + \hat{x}_3 \frac{\partial}{\partial R_3^j} = \hat{x}_p \frac{\partial}{\partial R_p^j} = \hat{x}_p \nabla_p^j \qquad \text{A.2.12}$$

where the p^{th} component of ∇^j is given by $\nabla_p^j \equiv \frac{\partial}{\partial R_p^j}$. Finally, the n^{th} rank tensor generalizations of $\vec{R}^i$ and ∇^j are:

$$\begin{aligned} R^{(n),i} &\equiv \vec{R}^i \vec{R}^i .. \vec{R}^i \\ &= R_{p_1}^i R_{p_2}^i .. R_{p_n}^i \hat{x}_{p_1} \hat{x}_{p_2} .. \hat{x}_{p_n} \end{aligned} \qquad \text{A.2.13}$$

and

$$\begin{aligned} \nabla^{(n),j} &\equiv \nabla^j \nabla^j .. \nabla^j \\ &= \nabla_{p_1}^j \nabla_{p_2}^j .. \nabla_{p_n}^j \hat{x}_{p_1} \hat{x}_{p_2} .. \hat{x}_{p_n} \\ &= \frac{\partial}{\partial R_{p_1}^j} \frac{\partial}{\partial R_{p_2}^j} \cdots \frac{\partial}{\partial R_{p_n}^j} \hat{x}_{p_1} \hat{x}_{p_2} .. \hat{x}_{p_n} \end{aligned} \qquad \text{A.2.14}$$

A.3 Cartesian Point Multipoles

Consider a two charge distribution; the first charge distribution $\rho^1(\vec{r};\vec{R}^1)$ is centered around particle 1 at $\vec{R}^1$, and the second distribution $\rho^2(\vec{r};\vec{R}^2)$ is centered around particle 2 at $\vec{R}^2$. The electrostatic interaction energy between the two charge distributions is given by[13]:

$$U = \int\int d^3r\, d^3r' \frac{\rho^1(\vec{r};\vec{R}^1)\rho^2(\vec{r};\vec{R}^2)}{\left|\vec{r}-\vec{r}'\right|} \qquad \text{A.3.1}$$

where both integrals are over all space. A simple change of variables can be made by translating the coordinate systems to the centers of $\vec{R}^1$ and $\vec{R}^2$: $\vec{r} = \vec{x} + \vec{R}^1$ and $\vec{r}' = \vec{x}' + \vec{R}^2$, so that A.3.1 becomes:

$$U = \int\int d^3x\, d^3x' \frac{\rho^1(\vec{x}-\vec{R}^1;\vec{R}^1)\rho^2(\vec{x}'-\vec{R}^2;\vec{R}^2)}{\left|\vec{x}+\vec{R}^1-\vec{x}'-\vec{R}^2\right|} \qquad \text{A.3.2}$$

The denominator can be expanded in a Taylor series for $\vec{x}$ about $\vec{R}^1$ [3,4]:

$$\begin{aligned}
\frac{1}{\left|\vec{x}+\vec{R}^1-\vec{x}'-\vec{R}^2\right|} &= \frac{1}{\left|\vec{R}^1-\vec{R}^2-\vec{x}'\right|} + \vec{x}\cdot\nabla^x \frac{1}{\left|\vec{x}+\vec{R}^1-\vec{x}'-\vec{R}^2\right|}\Bigg|_{x=0} \\
&\quad + \frac{1}{2!}\vec{x}\vec{x}\cdot\nabla^x\nabla^x \frac{1}{\left|\vec{x}+\vec{R}^1-\vec{x}'-\vec{R}^2\right|}\Bigg|_{x=0} + \ldots \\
&= \{1 + \vec{x}\cdot\nabla^x + \frac{1}{2!}\vec{x}\vec{x}\cdot\nabla^x\nabla^x + ..\} \frac{1}{\left|\vec{x}+\vec{R}^1-\vec{x}'-\vec{R}^2\right|}\Bigg|_{x=x'=0} \\
&= \sum_{n=0}^{\infty} \frac{1}{n!}\vec{x}^{(n)}\cdot\nabla^{(n),x} \frac{1}{\left|\vec{x}+\vec{R}^1-\vec{x}'-\vec{R}^2\right|}\Bigg|_{x=x'=0}
\end{aligned} \qquad \text{A.3.3}$$

where ∇^x is a gradient with respect to $\vec{x}$, $\vec{x}^{(n)} \equiv \vec{x}\vec{x}...\vec{x}$ is an n^{th} rank symmetric Cartesian tensor, $\nabla^{(n),x} \equiv \nabla^x\nabla^x..\nabla^x$ is an n^{th} rank symmetric Cartesian tensor gradient, and $\vec{x}^{(n)}\cdot\nabla^{(n),x} \equiv x_{p_1}x_{p_2}..x_{p_n}\frac{\partial}{\partial x_{p_1}}\frac{\partial}{\partial x_{p_2}}..\frac{\partial}{\partial x_{p_n}}$. If ∇^1 is the gradients with respect to $\vec{R}^1$, then

$$\nabla^1 \frac{1}{\left|\vec{x}+\vec{R}^1-\vec{x}'-\vec{R}^2\right|} = -\frac{(\vec{x}+\vec{R}^1-\vec{x}'-\vec{R}^2)}{\left|\vec{x}+\vec{R}^1-\vec{x}'-\vec{R}^2\right|^3} = \nabla^x \frac{1}{\left|\vec{x}+\vec{R}^1-\vec{x}'-\vec{R}^2\right|}$$

and A.3.3 becomes:

$$\frac{1}{\left|\vec{x}+\vec{R}^1-\vec{x}'-\vec{R}^2\right|}=\sum_{n=0}^{\infty}\frac{1}{n!}\vec{x}^{(n)}\cdot\nabla^{(n),1}\frac{1}{\left|\vec{R}^1-\vec{R}^2-\vec{x}'\right|} \qquad \text{A.3.4}$$

Similarly, A.3.4 can then be expanded in a Taylor series about $\vec{x}'$

$$\frac{1}{\left|\vec{x}+\vec{R}^1-\vec{x}'-\vec{R}^2\right|}=\sum_{n=0}^{\infty}\sum_{m=0}^{\infty}\frac{1}{n!}\frac{1}{m!}\vec{x}^{(n)}\cdot\nabla^{(n),1}\vec{x}'^{(m)}\cdot\nabla^{(m),2}\frac{1}{\left|\vec{R}^1-\vec{R}^2\right|} \qquad \text{A.3.5}$$

A.3.5 can be inserted into A.3.2:

$$U=\sum_{n=0}^{\infty}\sum_{m=0}^{\infty}\frac{1}{n!}\frac{1}{m!}\int\int d^3x\,d^3x'\,\rho^1(\vec{x}+\vec{R}^1;\vec{R}^1)\rho^2(\vec{x}'+\vec{R}^2;\vec{R}^2)\vec{x}^{(n)}\cdot\nabla^{(n),1}\vec{x}'^{(m)}\cdot\nabla^{(m),2}\frac{1}{\left|\vec{R}^1-\vec{R}^2\right|}$$

Now define multipole moment tensors $\Theta^{(n),1}$ and $\Theta^{(m),2}$ for charge distributions 1 and 2, respectively by:

$$\begin{aligned}\Theta^{(n),1}&\equiv\frac{1}{n!}\int d^3x\;\vec{x}^{(n)}\rho^1(\vec{x}+\vec{R}^1;\vec{R}^1)\\ \Theta^{(m),2}&\equiv\frac{1}{m!}\int d^3x'\;\vec{x}'^{(m)}\rho^2(\vec{x}'+\vec{R}^2;\vec{R}^2)\end{aligned} \qquad \text{A.3.6}$$

The first few moments are the total charge (monopole) q^1, dipole $\vec{\mu}^1$, and quadrapole $\Theta^{(2),1}$:

$$\begin{aligned}q^1&\equiv\Theta^{(0),1}=\int d^3x\;\rho^1(\vec{x}+\vec{R}^1;\vec{R}^1)\\ \vec{\mu}^1&\equiv\Theta^{(1),1}=\int d^3x\;\vec{x}\rho^1(\vec{x}+\vec{R}^1;\vec{R}^1)\\ \Theta^1&\equiv\Theta^{(2),1}=\frac{1}{2!}\int d^3x\;\vec{x}\vec{x}\rho^1(\vec{x}+\vec{R}^1;\vec{R}^1)\end{aligned} \qquad \text{A.3.7}$$

The interaction energy now becomes:

$$U=\sum_{n=0}^{\infty}\sum_{m=0}^{\infty}\Theta^{(n),1}\cdot\nabla^{(n),1}\Theta^{(m),2}\cdot\nabla^{(m),2}\frac{1}{R^{12}} \qquad \text{A.3.8}$$

where $R^{12} \equiv \left|\vec{R}^1 - \vec{R}^2\right|$. Therefore, the interaction energy U_{nm}^{12} between an n^{th} rank Cartesian point multipole of particle 1 and an m^{th} rank Cartesian point multipole of particle 2 is given by:

$$U_{nm}^{12} = \Theta^{(n),1} \cdot \nabla^{(n),1} \Theta^{(m),2} \cdot \nabla^{(m),2} \frac{1}{R^{12}} \qquad \text{A.3.9}$$

The explicit interaction energies up to dipole-dipole are:

monopole-monopole $$U_{00}^{12} = q^1 q^2 \frac{1}{R^{12}} \qquad \text{A.3.10a}$$

monopole-dipole $$U_{01}^{12} = q^1 \vec{\mu}^2 \cdot \nabla^2 \frac{1}{R^{12}} \qquad \text{A.3.10b}$$

dipole-dipole $$U_{11}^{12} = \vec{\mu}^1 \cdot \nabla^1 \vec{\mu}^2 \cdot \nabla^2 \frac{1}{R^{12}} \qquad \text{A.3.10c}$$

A.4 Local and Global Coordinate Systems

The interaction energy between an n^{th} and m^{th} point multipole is given by A.3.9

$$U_{nm} = \Theta^{(n),1} \cdot \nabla^{(n),1} \Theta^{(m),2} \cdot \nabla^{(m),2} \frac{1}{\left|\vec{R}^1 - \vec{R}^2\right|}$$

In general, $\Theta^{(n),1}$ is not a constant with respect to $\vec{R}^1$, and $\Theta^{(m),2}$ is not constant with respect to $\vec{R}^2$. The reason is that orientation is not defined for a single point particle. However, in a molecule, each atom is bonded to other atoms. The neighboring atoms can be used to define a local (body) reference frame $\hat{x}_1', \hat{x}_2', \hat{x}_3'$ with respect to the global reference frame $\hat{x}_1, \hat{x}_2, \hat{x}_3$ [14 15 16].

For example, suppose atom *a* and atom *b* are neighbors of atom 1. A local $\hat{x}_1'$ axis can be defined for atom 1, in the direction of $\vec{R}^a - \vec{R}^1$, i.e.

$$\hat{x}_1' \equiv \frac{\vec{R}^a - \vec{R}^1}{\left|\vec{R}^a - \vec{R}^1\right|} \qquad \text{A.4.2}$$

A local $\hat{x}_2'$ axis for atom 1 can be defined to be orthogonal to $\hat{x}_1'$ using Gram-Schmidt orthogonalization, with the component orthogonal to $\hat{x}_1'$ in the direction of $\vec{R}^c - \vec{R}^1$:

$$\vec{Y} \equiv \vec{R}^c - \vec{R}^1 - (\vec{R}^c - \vec{R}^1) \cdot \hat{x}_1'$$
$$\hat{x}_2' \equiv \frac{\vec{Y}}{\left|\vec{Y}\right|} \qquad \text{A.4.3}$$

The final local axis $\hat{x}_3'$ for atom 1 can be defined to be the cross product of $\hat{x}_1'$ and $\hat{x}_2'$, in order for the local coordinate system to be right-handed:

$$\hat{x}_1' \equiv \hat{x}_2' \otimes \hat{x}_3' \qquad \text{A.4.4}$$

To summarize, a local coordinate system $\hat{x}_1', \hat{x}_2', \hat{x}_3'$ for atom 1 has been defined in terms of the position of atom 1 $\vec{R}^1$ and the positions of its neighbors $\vec{R}^a$ and $\vec{R}^c$.

An orthogonal rotation matrix D_{qp} is used to rotate the global coordinate system $\hat{x}_1, \hat{x}_2, \hat{x}_3$ into the local coordinate system $\hat{x}_1', \hat{x}_2', \hat{x}_3'$. The rotation matrix D_{qp} is defined as:

$$\hat{x}_p' \equiv \sum_{q=1}^{3} D_{qp} \hat{x}_q = D_{qp} \hat{x}_q \qquad \text{A.4.5}$$

where $\hat{x}_1 \equiv (1,0,0)$, $\hat{x}_2 \equiv (0,1,0)$, $\hat{x}_3 \equiv (0,0,1)$. In matrix form, *D* is composed of the column vectors $\hat{x}_p'$.

$$\begin{pmatrix} D_{11} & D_{12} & D_{13} \\ D_{21} & D_{22} & D_{23} \\ D_{31} & D_{32} & D_{33} \end{pmatrix} \equiv \begin{pmatrix} \hat{x}_1' & \hat{x}_2' & \hat{x}_3' \\ \downarrow & \downarrow & \downarrow \\ & & \end{pmatrix} \qquad \text{A.4.6}$$

The rotation matrix D_{qp} is a function of the local unit vectors $\hat{x}_1', \hat{x}_2', \hat{x}_3'$, which are functions of $\vec{R}^1, \vec{R}^a, \vec{R}^c$, i.e. $D_{qp} = D_{qp}(\vec{R}^1, \vec{R}^a, \vec{R}^c)$.

Multipole moments $\Theta^{(n),1}$ are functions of orientation of atom 1 and its neighbors, i.e. $\vec{R}^1, \vec{R}^a, \vec{R}^c$. $\Theta^{(n),1}$ can be expressed in the local (body) reference frame or in the global frame. In the local frame, the components of the tensor ${}^{B}\Theta^{(n),1}_{pq...r}$ are constants, while the local frame unit vectors $\hat{x}_1', \hat{x}_2', \hat{x}_3'$ vary with position. In the global frame, the components of the tensor ${}^{G}\Theta^{(n),1}_{pq...r}$ vary with position, while the unit vectors $\hat{x}_1, \hat{x}_2, \hat{x}_3$ are constants. $\Theta^{(n),1}$ is expressed in either reference frame as:

$$\begin{aligned}\Theta^{(n),1} &= {}^{G}\Theta^{(n),1}_{pq..r}\hat{x}_p\hat{x}_q..\hat{x}_r \\ &= {}^{B}\Theta^{(n),1}_{pq..r}\hat{x}'_p\,\hat{x}'_q..\hat{x}'_r\end{aligned} \qquad \text{A.4.7}$$

If A.4.5 is inserted into A.4.7, the components of the global frame tensor ${}^{G}\Theta^{(n),1}_{pq...r}$ can be expressed in terms of the local frame tensor ${}^{B}\Theta^{(n),1}_{pq...r}$

$${}^{G}\Theta^{(n),1}_{pq...r} = D_{pp'}D_{qq'}..D_{rr'}\,{}^{B}\Theta^{(n),1}_{p'q'...r'} \qquad \text{A.4.8}$$

Inserting A.4.8 into A.4.7, $\Theta^{(n),1}$ becomes:

$$\Theta^{(n),1} = D_{pp'}D_{qq'}..D_{rr'}\,{}^{B}\Theta^{(n),1}_{p'q'...r'}\hat{x}_p\hat{x}_q..\hat{x}_r \qquad \text{A.4.9}$$

Since ${}^{B}\Theta^{(n),1}_{pq...r}$ and $\hat{x}_1, \hat{x}_2, \hat{x}_3$ are constants, and since ${}^{B}\Theta^{(n),1}_{pq...r}$ is symmetric, the derivative of $\Theta^{(n),1}$ with respect to any variable x in $\vec{R}^1, \vec{R}^a, \vec{R}^c$ can be expressed in terms of derivatives of D_{qp},

$$\frac{\partial^G \Theta^{(n),1}}{\partial x} = \left\{ \frac{\partial D_{pp'}}{\partial x} D_{qq'} .. D_{rr'}{}^B \Theta^{(n),1}_{p'q'...r'} + \right.$$
$$D_{pp'} \frac{\partial D_{qq'}}{\partial x} .. D_{rr'}{}^B \Theta^{(n),1}_{p'q'...r'} + ...$$
$$\left. D_{pp'} D_{qq'} .. \frac{\partial D_{rr'}}{\partial x}{}^B \Theta^{(n),1}_{p'q'...r'} \right\} \hat{x}_p \hat{x}_q .. \hat{x}_r \qquad \text{A.4.10}$$
$$= n \frac{\partial D_{pp'}}{\partial x} D_{qq'} .. D_{rr'}{}^B \Theta^{(n),1}_{p'q'...r'} \hat{x}_p \hat{x}_q .. \hat{x}_r$$

where *x* can be any position component that was used to form $\hat{x}'_p$, i.e. $\vec{R}^1, \vec{R}^a, \vec{R}^c$, and use

D is an orthogonal matrix with the property; $I = DD^T = D^T D$ where *I* is the identity matrix and D^T is the transpose of *D*. In tensor form, this condition is: $D_{ts} D_{tp'} = \delta_{sp'}$. Therefore, A.4.10 becomes:

$$\frac{\partial^G \Theta^{(n),1}}{\partial x} = n \frac{\partial D_{pp'}}{\partial x} D_{qq'} .. D_{rr'}{}^B \Theta^{(n),1}_{p'q'...r'} \hat{x}_p \hat{x}_q .. \hat{x}_r$$
$$= n \frac{\partial D_{ps}}{\partial x} \delta_{sp'} D_{qq'} .. D_{rr'}{}^B \Theta^{(n),1}_{p'q'...r'} \hat{x}_p \hat{x}_q .. \hat{x}_r \qquad \text{A.4.11}$$
$$= n \frac{\partial D_{ps}}{\partial x} D_{ts} D_{tp'} D_{qq'} .. D_{rr'}{}^B \Theta^{(n),1}_{p'q'...r'} \hat{x}_p \hat{x}_q .. \hat{x}_r$$
$$= n \frac{\partial D_{ps}}{\partial x} D^{T\ G}_{st} \Theta^{(n),1}_{tq...r} \hat{x}_p \hat{x}_q .. \hat{x}_r$$

In the interaction energy, $U^{12}_{nm} = \Theta^{(n),1} \cdot \nabla^{(n),1} \Theta^{(m),2} \cdot \nabla^{(m),2} \frac{1}{R^{12}}$, $\Theta^{(n),1}$ is not a constant with respect to ∇^1. However, $\Theta^{(m),2}$ is a constant with respect to ∇^1 (as long atom 2 is not the neighbor of atom1 defining the local coordinate system of atom 1). Therefore, the interaction energy becomes:

$$U^{12}_{nm} = \Theta^{(n),1} \Theta^{(m),2} \cdot \nabla^{(n),1} \nabla^{(m),2} \frac{1}{R^{12}} \qquad \text{A.4.13}$$

Now consider a function of R^{12}, $f(R^{12})$. The gradient of f with respect to $\vec{R}^1$ is the negative of the gradient with respect to $\vec{R}^2$.

$$\nabla^1 f(R^{12}) = \frac{df}{dR^{12}} \frac{\vec{R}^1 - \vec{R}^2}{\left|\vec{R}^1 - \vec{R}^2\right|} = -\nabla^2 f(R^{12}) \qquad \text{A.4.14}$$

The interaction energy now can be written as:

$$U_{nm}^{12} = (-1)^m \Theta^{(n),1} \Theta^{(m),2} \cdot \nabla^{(n+m),1} \frac{1}{R^{12}} \qquad \text{A.4.15}$$

A.5 Force and Torque for Point Multipoles

The force on particle 1 $\vec{F}^1$ due to the $n^{\text{th}} - m^{\text{th}}$ rank point multipole interaction between particle 1 and 2 is defined as the negative gradient with respect to particle 1

$$\vec{F}^1 = -\nabla^1 U_{nm}^{12} \qquad \text{A.5.1}$$

However, since $\Theta^{(n),1}$ is not a constant with respect to ∇^1,

$$\begin{aligned} \vec{F}_1 = (-1)^{m+1} (\nabla^1 \Theta^{(n),1}) \Theta^{(m),2} \cdot \nabla^{(n+m),1} \frac{1}{R^{12}} + \\ (-1)^{m+1} \Theta^{(n),1} \Theta^{(m),2} \cdot \nabla^{(n+m+1),1} \frac{1}{R^{12}} \end{aligned} \qquad \text{A.5.2}$$

where

$$\nabla^1 \Theta^{(n),1} = n\hat{x}_v \frac{\partial D_{ps}}{\partial R_v^1} D_{st}^{T\ G} \Theta_{tq\ldots r}^{(n),1} \hat{x}_p \hat{x}_q \ldots \hat{x}_r \qquad \text{A.5.3}$$

The first term in A.5.2 is a derivative with respect to orientation and can be termed a torque contribution. The second term is a derivative of energy with respect to translation of the distance between the two multipoles and is the ordinary force term. Finally, it

should be noted that the interaction U_{nm}^{12} contributes force terms to atom 1 and atom 2, and also to the neighbors of atom1 and atom 2.

A.6 Gradient Tensors

Tensor gradients of the form $\nabla^{(n)} \frac{1}{R}$ will now be evaluated for reference. From the definition in A.2.14, the n^{th} ranked tensor gradient of $\frac{1}{R}$ can be expressed in component form as:

$$\nabla^{(n)} \frac{1}{R} = \hat{x}_{p_1} \hat{x}_{p_2} ..\hat{x}_{p_n} \frac{\partial^n}{\partial R_{p_1} \partial R_{p_2} ..\partial R_{p_n}} \frac{1}{R} \qquad \text{A.6.1}$$

The first four tensor gradients are evaluated as:

$$\nabla^{(1)} T = -\hat{x}_p \frac{R_p}{R^3} \qquad \text{A.6.2}$$

$$\nabla^{(2)} T = \hat{x}_p \hat{x}_q \left(R_p R_q \frac{3}{R^5} - \delta_{pq} \frac{1}{R^3} \right) \qquad \text{A.6.3}$$

$$\nabla^{(3)} T = \hat{x}_p \hat{x}_q \hat{x}_r \left((\delta_{pq} R_r + \delta_{pr} R_q + \delta_{rq} R_p) \frac{3}{R^5} - R_p R_q R_r \frac{15}{R^7} \right) \qquad \text{A.6.4}$$

$$\begin{aligned} \nabla^{(4)} T = \hat{x}_r \hat{x}_p \hat{x}_q \hat{x}_s \{ & (\delta_{pq} \delta_{rs} + \delta_{pr} \delta_{qs} + \delta_{rq} \delta_{sp}) \frac{3}{R^5} \\ & - (\delta_{pq} R_r R_s + \delta_{pr} R_q R_s + \delta_{rq} R_p R_s + \delta_{ps} R_q R_r + \delta_{qs} R_p R_r + \delta_{rs} R_p R_q) \frac{15}{R^7} \\ & + R_p R_q R_r R_s \frac{105}{R^9} \} \end{aligned} \qquad \text{A.6.5}$$

A.7 Electric Potential and Field

Electrostatic potential can be defined as the variation in energy when an infinitesimal point charge is added to the system[13].

$$\varphi \equiv \lim_{\delta q \to 0} \frac{\delta U}{\delta q} \tag{A.7.1}$$

From A.4.14, the interaction energy between a point monopole ($n = 0$) and an m^{th} order point multipole is given by:

$$U_{0m}^{12} = (-1)^m q^1 \Theta^{(m),2} \cdot \nabla^{(m),1} \frac{1}{R^{12}} \tag{A.7.2}$$

Therefore, the electrostatic potential at the field point $\vec{R}^1$ due to an m^{th} order point multipole located at $\vec{R}^2$ is found from A.7.1 and A.7.2.

$$\begin{aligned} \varphi_m(\vec{R}^1;\vec{R}^2) &= \lim_{\delta q^1 \to 0} \frac{\delta U_{0m}}{\delta q^1} \\ &= (-1)^m \Theta^{(m),2} \cdot \nabla^{(m),1} \frac{1}{R^{12}} \end{aligned} \tag{A.7.3}$$

The electric field $\vec{E}$ is defined as the negative field gradient of potential.

$$\vec{E}(\vec{R}^1;\vec{R}^2) \equiv -\nabla^1 \varphi(\vec{R}^1;\vec{R}^2) \tag{A.7.4}$$

The gradient with respect to an m^{th} rank point multipole can be found from A.7.3 as

$$\begin{aligned} \vec{E}_m(\vec{R}^1;\vec{R}^2) &= -\nabla^1 \varphi_m(\vec{R}^1;\vec{R}^2) \\ &= -\nabla^1 (-1)^m \Theta^{(m),2} \cdot \nabla^{(m),1} \frac{1}{R^{12}} \\ &= (-1)^{m+1} \Theta^{(m),2} \cdot \nabla^{(m+1),1} \frac{1}{R^{12}} \end{aligned} \tag{A.7.5}$$

This last step is valid, since the field point gradient ∇^1 has no effect on $\Theta^{(m),2}$, because $\Theta^{(m),2}$ is a function of atom 2 and its neighbors. The n^{th} ranked field gradient of a point multipole of rank m is defined as[4]:

$$E_m^{(n)}(\vec{R}^1;\vec{R}^2) = -\nabla^{(n),1}\varphi_m(\vec{R}^1;\vec{R}^2)$$
$$= (-1)^{m+1}\Theta^{(m),2}\cdot\nabla^{(n+m),1}\frac{1}{R^{12}} \qquad \text{A.7.6}$$

Point multipole interaction energies can be written in terms of potential or field gradients of potential. From A.7.2, the interaction energy between a point monopole (n = 0) and an m^{th} order point multipole is given by:

$$U_{0m}^{12} = (-1)^m q^1\Theta^{(m),2}\cdot\nabla^{(m),1}\frac{1}{R^{12}}$$
$$= q^1\varphi_m(\vec{R}^1;\vec{R}^2) \qquad \text{A.7.7}$$

i.e. the interaction energy is the product of point charge and potential. The interaction energy of a point dipole with an m^{th} order point multipole is given by A.4.14 (with n = 1):

$$U_{1m}^{12} = (-1)^m\vec{\mu}^1\cdot\Theta^{(m),2}\cdot\nabla^{(m+1),1}\frac{1}{R^{12}}$$
$$= -\vec{\mu}^1\cdot\vec{E}_m(\vec{R}^1;\vec{R}^2) \qquad \text{A.7.8}$$

where A.7.5 was used. The interaction energy of point multipole of rank n with a point multipole of rank m is given by A.4.14:

$$U_{nm}^{12} = (-1)^m\Theta^{(n),1}\Theta^{(m),2}\cdot\nabla^{(n+m),1}\frac{1}{R^{12}}$$
$$= -\Theta^{(n),1}\cdot E_m^{(n)}(\vec{R}^1;\vec{R}^2) \qquad \text{A.7.9}$$

i.e. U_{nm}^{12} is an n^{th} rank tensor contraction between $\Theta^{(n),1}$ and the n^{th} rank field gradient of the potential from $\Theta^{(m),2}$.

A.8 Spherical Multipoles

The language of spherical harmonics can also be used to formulate multipole interactions in terms of spherical multipoles[7 14 17 18]. Spherical multipoles have an advantage over Cartesian multipoles because there are fewer tensor components at the

quadrapole level and beyond. A symmetric Cartesian multipole tensor of order l has $(l+1)(l+2)/2$ independent components, while a spherical multipole tensor has $2l+1$ independent components. At the monopole ($l = 0$) and dipole ($l = 1$) level, the number of components between Cartesian and spherical multipoles are the same. However, at the quadrapole level ($l = 2$), there are 6 independent Cartesian tensor components, while only 5 independent components using spherical tensors. In practice, this does not present a serious limitation to modeling or simulation applications, since most treatments use multipole tensors up to the dipole or quadrapole level[15]. Throughout this work, only Cartesian point multipoles and Cartesian Gaussian multipoles are considered.

A.9 References

1 L. Jansen, Phys. Rev. **110,** 661 (1958)

2 A. D. Buckingham, Adv. Chem. Phys. **12**, 107 (1967)

3 S. Kielich, Physica **31**, 444 (1965)

4 J. Applequist, Chem. Phys. 85, 279 (1984)

5 J. Applequist, J. Chem. Phys. 83, 809 (1985)

6 C. J. Bottcher, *Theory of Electric Polarization: Dielectrics in Static Fields,* 2nd edition, revised (Elsevier, New York, 1993)

7 A. Stone, *Intermolecular Forces*, (Oxford University Press, New York, 1996)

8 C. G. Gray and K. E. Gubbins, *Theory of Molecular Fluids Volume 1: Fundamentals*, (Oxford University Press, New York, 1984)

[9] G. C. Maitland, M. Rigby, E. B. Smith, and W. A. Wakeham, *Intermolecular Forces, Their Origin and Determination*, (Oxford University Press, New York, 1981)

[10] J. Applequist, J. Math. Phys. **24 (4)**, 736 (1983)

[11] C. T. Tai, *General Vector and Dyadic Analysis: Applied Mathematics in Field Theory*, 2nd edition revised, (IEEE Press, New York, 1997)

[12] G. B. Arfken and H. J. Weber, Mathematical Methods for Physicists, 4th edition revised, (Academic Press, San Diego, 1995)

[13] J. D. Jackson, *Classical Electrodynamics*, (Wiley, New York, 1999)

[14] P. L. A. Popelier and A. J. Stone, *Mol. Phys*. **82** (**2**), 411

[15] P. Ren, J. Ponder, J. Phys. Chem. B **107**, 5933 (2003)

[16] C. Sagui, L. G. Pedersen, and T. A. Darden, J. Chem. Phys. **120** (1), 73 (2004)

[17] A. J. Stone and R. J. A. Tough, Chem. Phys. Lett. **110** (**2**), 123 (1984)

[18] J. Schwinger, L. L. DeRaad, Jr, K. A. Milton, and W. Tsai, *Classical Electrodynamics*, (Perseus Books, Reading, Massachusetts, 1998)

Appendix B. Perturbation Theory of a Molecule in an External Field

B.1 Introduction

Molecular polarization can be discussed quantum mechanically by applying an external potential onto a molecule. The external potential is treated as a perturbation while the initial non-interacting system is taken to be the molecule in vacuum. The external potential perturbation is expanded in Cartesian point multipoles using the formalism from appendix A. For further references on quantum and classical treatments of polarization, see[1-5].

In the following section, time independent perturbation theory is used to calculate energy corrections between the molecule and the external potential up to third order. The first order correction is shown to be the interaction energy of the permanent molecular multipoles with the external potential. The second order energy correction is the interaction energy of the external field with the permanent multipoles polarized to first order (linear polarization) by the external field. The third order energy correction is shown to be the interaction energy of the external field with the permanent multipoles polarized to second order (first hyperpolarization) by the external field. In addition to the familiar dipole-dipole polarization, higher order multipole moment polarization (e.g. dipole-quadrapole) will also be discussed.

In section B.3, a periodic time-dependent external potential is applied to the molecule. Time-dependent perturbation theory is aplied to first order to calculate the induced multipole moments as periodic functions of time. From the time-varying multipole moments, frequency dependent molecular polarizabilitiy tensors are calculated.

The frequency dependent polarizability tensors are needed in appendix C when perturbation theory is applied to the interaction between two molecules. In particular, long range intermolecular electrostatic, polarization, and dispersion energies are calculated. An interesting relationship is derived between dispersion energy and frequency dependent polarizability tensors calculated at imaginary frequencies.

B.2 Time Independent Field

Consider a molecule in its ground state $|0\rangle$, with non-interacting Hamiltonian $\hat{H}^0$, and energy E_0, i.e.

$$\hat{H}^0|0\rangle = E_0|0\rangle \qquad \text{B.2.1}$$

Similarly, let the excited states of $\hat{H}^0$ be given by $|\alpha\rangle$ with energies E_α.

$$\hat{H}^0|\alpha\rangle = E_\alpha|\alpha\rangle \qquad \text{B.2.2}$$

Now suppose the molecule is subjected to an external potential $V(r)$. The perturbed interacting Hamiltonian is given by:

$$\hat{H}^1 = \sum_a e_a \hat{V}(\vec{r}_a) \qquad \text{B.2.3}$$

where the sum index a is over both electrons and nuclei. If the center of the molecule is located at $\vec{R}$, the external potential at each particle can be expanded in a Taylor series around $\vec{R}$.

$$\begin{aligned}\hat{V}(\vec{r}_a) &= \hat{V}(R) + (\vec{r}_a - \vec{R}) \cdot \nabla_R \hat{V}(R) + .. \frac{1}{n!}(\vec{r}_a - \vec{R})^{(n)} \cdot \nabla^{(n),R} \hat{V}(R) \\ &= \sum_{n=0}^{\infty} \frac{1}{n!}(\vec{r}_a - \vec{R})^{(n)} \cdot \nabla^{(n),R} \hat{V}(R) \\ &= \sum_{n=0}^{\infty} \frac{1}{n!}(\vec{r}_a - \vec{R})^{(n)} \cdot \hat{V}^{(n)}(R)\end{aligned} \qquad \text{B.2.4}$$

where

$$\hat{V}^{(n)} \equiv \nabla^{(n),R} \hat{V} \qquad \text{B.2.5}$$

is the n^{th} rank field gradient of potential. The perturbed Hamiltonian $\hat{H}^1$ becomes

$$\begin{aligned}\hat{H}^1 &= \sum_a \sum_{n=0}^{\infty} \frac{1}{n!}(\vec{r}_a - \vec{R})^{(n)} \cdot e_a \hat{V}^{(n)}(R) \\ &= \sum_{n=0}^{\infty} \hat{M}^{(n)} \cdot \hat{V}^{(n)}(R)\end{aligned} \qquad \text{B.2.6}$$

where

$$\hat{M}^{(n)} \equiv \sum_a e_a \frac{1}{n!}(\vec{r}_a - \vec{R})^{(n)} \qquad \text{B.2.7}$$

is the n^{th} rank Cartesian multipole moment operator.

From perturbation theory, the first order energy correction is given by:

$$\begin{aligned}E_0^{(1)} &= \langle 0 | \hat{H}^1 | 0 \rangle \\ &= \sum_{n=0}^{\infty} \langle 0 | \hat{M}^{(n)} | 0 \rangle \cdot \hat{V}^{(n)}(R) \\ &= \sum_{n=0}^{\infty} \Theta_0^{(n)} \cdot \hat{V}^{(n)}(R)\end{aligned} \qquad \text{B.2.8}$$

where

$$\Theta_0^{(n)} \equiv \langle 0 | \hat{M}^{(n)} | 0 \rangle \qquad \text{B.2.9}$$

is the permanent n^{th} rank multipole moment tensor of the molecule. The first order energy correction is the electrostatic energy of the permanent molecular multipole

moments interacting with the external potential, field, and field gradients. If q_0 is the total molecular charge, $\vec{\mu}_0$ the vacuum molecular dipole, and $\Theta_0^{(2)}$ the vacuum molecular quadrapole, the first order energy correction becomes:

$$E_0^{(1)} = q_0 \hat{V}(R) - \vec{\mu}_0 \cdot \vec{E} - \Theta_0^{(2)} \cdot \vec{E}^{(2)} + .. \qquad \text{B.2.10}$$

where

$$\vec{E} \equiv \vec{E}^{(1)} \equiv -\hat{V}^{(1)} = -\nabla^R V(R) \qquad \text{B.2.11}$$

is the external electric field and

$$\vec{E}^{(n)} \equiv -\hat{V}^{(n)} = -\nabla^{(n),R} V(R) \qquad \text{B.2.12}$$

are the electric field gradients for n ≥1.

The second order energy correction is given by:

$$\begin{aligned} E_0^{(2)} &= -\sum_{\alpha \neq 0} \frac{\langle 0|\hat{H}^1|\alpha\rangle\langle\alpha|\hat{H}^1|0\rangle}{E_\alpha - E_0} \\ &= -\sum_{\alpha \neq 0} \sum_{n=1}^{\infty} \sum_{m=1}^{\infty} \frac{\langle 0|\hat{M}^{(n)}|\alpha\rangle\langle\alpha|\hat{M}^{(m)}|0\rangle}{E_{\alpha 0}} \cdot V^{(n)} V^{(m)} \\ &= -\sum_{\alpha \neq 0} \sum_{n=1}^{\infty} \sum_{m=1}^{\infty} \frac{\hat{M}_{0\alpha}^{(n)} \hat{M}_{\alpha 0}^{(m)}}{E_{\alpha 0}} \cdot V^{(n)} V^{(m)} \end{aligned} \qquad \text{B.2.13}$$

where

$$\begin{aligned} E_{\alpha 0} &\equiv E_\alpha - E_0 \\ \hat{M}_{0\alpha}^{(n)} &\equiv \langle 0|\hat{M}^{(n)}|\alpha\rangle \end{aligned} \qquad \text{B.2.14}$$

and. Notice the $n = 0$ and $m = 0$ terms were omitted in B.2.13 because the excited states are assumed to be orthonormal to the ground state, i.e. $\langle 0|\hat{M}^{(0)}|\alpha\rangle = q\langle 0|\alpha\rangle = 0$. $E_0^{(2)}$ can be rewritten as:

$$E_0^{(2)} = -\frac{1}{2}\sum_{\alpha\neq 0}\sum_{n=1}^{\infty}\sum_{m=1}^{\infty}\frac{\hat{M}_{0\alpha}^{(n)}\hat{M}_{\alpha 0}^{(m)} + \hat{M}_{0\alpha}^{(m)}\hat{M}_{\alpha 0}^{(n)}}{E_{\alpha 0}}\cdot V^{(n)}V^{(m)}$$
$$= -\frac{1}{2}\sum_{n=1}^{\infty}\sum_{m=1}^{\infty}\alpha^{(n)(m)}\cdot V^{(n)}V^{(m)} \qquad \text{B.2.15}$$

where the $n^{\text{th}} - m^{\text{th}}$ pole polarizability tensor $\alpha^{(n)(m)}$ is defined by

$$\alpha^{(n)(m)} \equiv \sum_{\alpha\neq 0}\frac{\hat{M}_{0\alpha}^{(n)}\hat{M}_{\alpha 0}^{(m)} + \hat{M}_{0\alpha}^{(m)}\hat{M}_{\alpha 0}^{(n)}}{E_{\alpha 0}} \qquad \text{B.2.16}$$

Notice $\alpha^{(n)(m)}$ is symmetric with respect to n and m, i.e. $\alpha^{(n)(m)} = \alpha^{(m)(n)}$. The first term in B.2.15 is the familiar dipole-dipole polarizability contribution:

$$E_0^{(2)} = -\frac{1}{2}\alpha^{(1)(1)}\cdot\vec{E}\vec{E} + \ldots \qquad \text{B.2.17}$$

where the molecular dipole-dipole polarizability tensor is given by:

$$\alpha^{(1)(1)} = \sum_{\alpha\neq 0}\frac{\langle 0|\hat{\mu}|\alpha\rangle\langle\alpha|\hat{\mu}|0\rangle}{E_{\alpha 0}} + \frac{\langle 0|\hat{\mu}|\alpha\rangle\langle\alpha|\hat{\mu}|0\rangle}{E_{\alpha 0}}$$
$$= 2\sum_{\alpha\neq 0}\frac{\langle 0|\hat{\mu}|\alpha\rangle\langle\alpha|\hat{\mu}|0\rangle}{E_{\alpha 0}} \qquad \text{B.2.18}$$

If the external field is a constant, then the field gradient $\vec{E}^{(2)} \equiv -\nabla^{(2),R}V(R) \equiv -V^{(2)}(R)$ and its higher derivatives are zero. In this case, the dipole-dipole polarizability contribution is the only term in the second order energy correction. If the external field varies over the size of the molecule, the field gradient is not zero and the next term in the second order energy series is the dipole-quadrapole polarization term given by:

$$-\frac{1}{2}\left(\alpha^{(1)(2)}\cdot\vec{E}\vec{E}^{(2)} - \alpha^{(2)(1)}\cdot\vec{E}^{(2)}\vec{E}\right) = -\alpha^{(1)(2)}\cdot\vec{E}\vec{E}^{(2)} \qquad \text{B.2.19}$$

where the dipole-quadrapole polarizability tensor is given by:

$$\alpha^{(1)(2)} = \sum_{\alpha\neq 0}\frac{\langle 0|\hat{\mu}|\alpha\rangle\langle\alpha|\hat{\Theta}^{(2)}|0\rangle}{E_{\alpha 0}} + \frac{\langle 0|\hat{\Theta}^{(2)}|\alpha\rangle\langle\alpha|\hat{\mu}|0\rangle}{E_{\alpha 0}} \qquad \text{B.2.20}$$

The total interaction energy up to second order is the sum of

$$\begin{aligned} E &= E_0^{(1)} + E_0^{(2)} \\ &= q_0 V(R) + \sum_{n=1}^{\infty} \Theta_0^{(n)} \cdot V^{(n)} - \frac{1}{2} \sum_{n=1}^{\infty} \sum_{m=1}^{\infty} \alpha^{(n)(m)} \cdot V^{(n)} V^{(m)} \end{aligned} \quad \text{B.2.21}$$

The derivative of energy E with respect to potential gradient $V^{(n)}$ ($n \geq 1$) is given by:

$$\begin{aligned} \frac{\partial E}{\partial V^{(n)}} &= \Theta_0^{(n)} - \sum_{m=1}^{\infty} \alpha^{(n)(m)} \cdot V^{(m)} \\ &= \Theta_0^{(n)} + \sum_{m=1}^{\infty} \alpha^{(n)(m)} \cdot \vec{E}^{(m)} \end{aligned} \quad \text{B.2.22}$$

This quantity is the total molecular moment $\Theta^{(n),tot}$ in the presence of external fields.

$$\Theta^{(n),tot} \equiv \frac{\partial E}{\partial V^{(n)}} = \Theta_0^{(n)} + \sum_{m=1}^{\infty} \alpha^{(n)(m)} \cdot \vec{E}^{(m)} \quad \text{B.2.23}$$

For example, the induced dipole is given by its permanent dipole moment, the dipole-dipole polarizability contribution and the dipole-quadrapole polarizability contribution:

$$\vec{\mu}^{tot} = \vec{\mu}_0 + \alpha^{(1)(1)} \cdot \vec{E} + \alpha^{(1)(2)} \cdot \vec{E}^{(2)} + \ldots \quad \text{B.2.24}$$

If the external field is constant over the size of the molecule, the gradient of field $\vec{E}^{(2)}$ is zero and the total dipole moment is given by:

$$\vec{\mu}^{tot} = \vec{\mu}_0 + \alpha^{(1)(1)} \cdot \vec{E} \quad \text{B.2.25}$$

The total molecular moment $\Theta^{(n),tot}$ can also be found by first calculating the perturbative corrections to the wavefunction and then evaluating the expectation value of the moment operator $\hat{M}^{(n)}$. For example, suppose the exact ground state $|\Psi_0\rangle$ is written as a perturbation series as:

$$|\Psi_0\rangle = |0^0\rangle + |0^1\rangle + |0^2\rangle + \ldots \quad \text{B.2.26}$$

where $\left|0^0\right\rangle \equiv \left|0\right\rangle$ is the zero[th] order solution and $\left|0^1\right\rangle$ is the first order correction. From perturbation theory the first order correction is given by:

$$\begin{aligned}\left|0^1\right\rangle &= -\sum_{\alpha\neq 0}\frac{\left|\alpha\right\rangle\left\langle\alpha\right|\hat{H}^1\left|0\right\rangle}{E_{\alpha 0}} \\ &= -\sum_{\alpha\neq 0}\sum_{m=1}^{\infty}\left|\alpha\right\rangle\frac{\hat{M}^{(m)}_{\alpha 0}\cdot V^{(m)}}{E_{\alpha 0}}\end{aligned} \qquad \text{B.2.27}$$

Therefore, the expectation value of the moment operator $\hat{M}^{(n)}$ up to first order is given by:

$$\begin{aligned}\left\langle 0^0+0^1\right|\hat{M}^{(n)}\left|0^0+0^1\right\rangle &= \Theta_0^{(n)} - \sum_{\alpha\neq 0}\sum_{m=1}^{\infty}\frac{\hat{M}^{(n)}_{0\alpha}\hat{M}^{(m)}_{\alpha 0}+\hat{M}^{(m)}_{0\alpha}\hat{M}^{(n)}_{\alpha 0}}{E_{\alpha 0}}\cdot V^{(m)} \\ &= \Theta_0^{(n)} - \sum_{m=1}^{\infty}\alpha^{(n)(m)}\cdot V^{(m)} \\ &= \Theta_0^{(n)} + \sum_{m=1}^{\infty}\alpha^{(n)(m)}\cdot E^{(m)}\end{aligned} \qquad \text{B.2.28}$$

which is equivalent to B.2.23.

Notice that the induced molecular moments are linear in external field in the above analysis. At small electric fields strengths, the induced moments are approximately linear in external field. For larger external fields, the induced moments behave as a non-linear function of external field. This effect is termed hyperpolarization. Hyperpolarization terms can be found by deriving the perturbational energy corrections following second order, i.e. first order hyperpolarization arises from third order perturbational theory and second order hyperpolarization arises from fourth order perturbation theory. In the analysis below, the first order hyperpolarization terms will be derived from the third order energy correction.

The third order energy correction is given by

$$E_0^{(3)} = \sum_{\alpha,\beta\neq 0} \frac{\langle 0|\hat{H}^1|\alpha\rangle\langle\alpha|\hat{H}^1|\beta\rangle\langle\beta|\hat{H}^1|0\rangle}{E_{\alpha 0}E_{\beta 0}} - \langle 0|H_1|0\rangle \sum_{\alpha\neq 0} \frac{\langle 0|\hat{H}^1|\alpha\rangle\langle\alpha|\hat{H}^1|0\rangle}{E_{\alpha 0}} \qquad \text{B.2.29}$$

When the perturbational Hamiltonian (B.2.6) is inserted into B.2.29, the third order energy correction becomes:

$$E_0^{(3)} = \sum_{n=1}^{\infty}\sum_{m=1}^{\infty}\sum_{p=1}^{\infty}\left\{ \sum_{\alpha,\beta\neq 0} \frac{\hat{M}_{0\alpha}^{(n)}\hat{M}_{\alpha\beta}^{(m)}\hat{M}_{\beta 0}^{(p)}}{E_{\alpha 0}E_{\beta 0}} - \hat{M}_{00}^{(n)} \sum_{\alpha\neq 0} \frac{\hat{M}_{0\alpha}^{(m)}\hat{M}_{\alpha 0}^{(p)}}{E_{\alpha 0}} \right\} \cdot V^{(n)}V^{(m)}V^{(p)} \qquad \text{B.2.30}$$

The hyperpolarizability tensor is defined as a symmetric sum of the above bracketed term over permuted indices n, m, p:

$$\beta^{(n)(m)(p)} \equiv P^{nmp}\left\{ \sum_{\alpha,\beta\neq 0} \frac{\hat{M}_{0\alpha}^{(n)}\hat{M}_{\alpha\beta}^{(m)}\hat{M}_{\beta 0}^{(p)}}{E_{\alpha 0}E_{\beta 0}} - \hat{M}_{00}^{(n)} \sum_{\alpha} \frac{\hat{M}_{0\alpha}^{(m)}\hat{M}_{\alpha 0}^{(p)}}{E_{\alpha 0}} \right\} \qquad \text{B.2.31}$$

where the symmetric permutation operator P^{nmp} is defined as:

$$P^{nmp}(A^{nmp}) \equiv A^{nmp} + A^{npm} + A^{mnp} + A^{mpn} + A^{pnm} + A^{pmn} \qquad \text{B.2.32}$$

The third order energy correction in B.2.30 becomes:

$$E_0^{(3)} = \frac{1}{3!}\sum_{n=1}^{\infty}\sum_{m=1}^{\infty}\sum_{p=1}^{\infty}\beta^{(n)(m)(p)} \cdot V^{(n)}V^{(m)}V^{(p)} \qquad \text{B.2.33}$$

The total energy up to third order becomes:

$$\begin{aligned} E &= E_0^{(1)} + E_0^{(2)} + E_0^{(3)} \\ &= q_0 V(R) + \sum_{n=1}^{\infty}\Theta_0^{(n)} \cdot V^{(n)} - \frac{1}{2}\sum_{n=1}^{\infty}\sum_{m=1}^{\infty}\alpha^{(n)(m)} \cdot V^{(n)}V^{(m)} \\ &+ \frac{1}{3!}\sum_{n=1}^{\infty}\sum_{m=1}^{\infty}\sum_{p=1}^{\infty}\beta^{(n)(m)(p)} \cdot V^{(n)}V^{(m)}V^{(p)} \end{aligned} \qquad \text{B.2.34}$$

The total molecular moment $\Theta^{(n),tot}$ becomes a quadratic function of field.

$$\begin{aligned}\Theta^{(n),tot} \equiv \frac{\partial E}{\partial V^{(n)}} &= \Theta_0^{(n)} - \sum_{m=1}^{\infty} \alpha^{(n)(m)} \cdot V^{(m)} + \frac{1}{2!}\sum_{m=1}^{\infty}\sum_{p=1}^{\infty} \beta^{(n)(m)(p)} \cdot V^{(m)} V^{(p)} \\ &= \Theta_0^{(n)} + \sum_{m=1}^{\infty} \alpha^{(n)(m)} \cdot \vec{E}^{(m)} + \frac{1}{2!}\sum_{m=1}^{\infty}\sum_{p=1}^{\infty} \beta^{(n)(m)(p)} \cdot \vec{E}^{(m)} \vec{E}^{(p)}\end{aligned} \qquad \text{B.2.35}$$

For a large constant external field $\vec{E}$ (quadrapole and higher order multipole effects are zero), the total molecular moment is given by:

$$\Theta^{(n),tot} = \Theta_0^{(n)} + \alpha^{(n)(1)} \cdot \vec{E}^{(1)} + \frac{1}{2!}\beta^{(n)(1)(1)} \cdot \vec{E}^{(1)} \vec{E}^{(1)} \qquad \text{B.2.36}$$

As an example, the total molecular dipole (up to first order hyperpolarizability) is given by:

$$\vec{\mu}^{tot} = \vec{\mu}_0 + \alpha^{(1)(1)} \cdot \vec{E} + \frac{1}{2}\beta^{(1)(1)(1)} \cdot \vec{E}\vec{E} \qquad \text{B.2.37}$$

B.3 Time-Dependent Field

Now suppose the perturbing Hamiltonian $\hat{\tilde{H}}^1(t) \equiv \hat{H}^1 f(t)$ has a periodic time dependence attached to it, i.e.

$$\begin{aligned}\hat{\tilde{H}}^1(t) &= \cos(\omega t)\exp(\varepsilon t)\hat{H}^1 \\ &= \cos(\omega t)\exp(\varepsilon t)\sum_a e_a \hat{V}(\vec{r}_a)\end{aligned} \qquad \text{B.3.1}$$

The term $\exp(\varepsilon t)$ is a convergence factor included to make the time perturbation go to zero in the distant past. Once this accomplished, the limit $\varepsilon \to 0$ is taken. As in section B.2, suppose a non-interacting molecule in vacuum has unperturbed Hamiltonian $\hat{H}^0$, $|0\rangle$ as its ground state with energy E_0, and $|\alpha\rangle$ as its excited states with energies E_α. The time independent part of $\hat{\tilde{H}}^1(t)$ can be expressed in terms of multipole moment operators as in B.2.6,

$$\begin{aligned}\hat{\tilde{H}}^1(t) &\equiv \cos(\omega t)\exp(\varepsilon t)\hat{H}^1 \\ &= \cos(\omega t)\exp(\varepsilon t)\sum_{n=0}^{\infty}\hat{M}^{(n)}\cdot\hat{V}^{(n)}(R)\end{aligned} \qquad \text{B.3.2}$$

where $\hat{M}^{(n)} \equiv \sum_a e_a \frac{1}{n!}(\vec{r}_a - \vec{R})^{(n)}$ (B.2.7) is the n^{th} rank Cartesian multipole moment operator, and $\hat{V}^{(n)} \equiv \nabla^{(n),R}\hat{V}$ (B.2.5) is the n^{th} rank field gradient of potential.

If the molecule is initially in its ground eigenstate $|0\rangle$, then the state $|\Psi\rangle$ at a later time is given by:

$$|\Psi\rangle = \exp(-i\omega_0 t)|0\rangle + \sum_\alpha a_\alpha(t)\exp(-i\omega_\alpha t)|\alpha\rangle \qquad \text{B.3.3}$$

where $\omega_\alpha \equiv \frac{E_\alpha}{\hbar}$. To first order, the coefficient $a_\alpha(t)$ is given by:

$$a_\alpha(t) = \frac{-i}{\hbar}H^1_{\alpha 0}\int_{-\infty}^{t}\cos(\omega t')\exp(\varepsilon t')\exp(i\omega_{\alpha 0}t')dt' \qquad \text{B.3.4}$$

where $H^1_{\alpha 0} \equiv \langle\alpha|H^1|0\rangle$. After letting $\varepsilon \to 0$, B.3.4 is evaluated to be

$$a_\alpha(t) = \frac{-H^1_{\alpha 0}}{2\hbar}\left[\frac{\exp(i(\omega_{\alpha 0}+\omega)t)}{\omega_{\alpha 0}+\omega} + \frac{\exp(i(\omega_{\alpha 0}-\omega)t)}{\omega_{\alpha 0}-\omega}\right] \qquad \text{B.3.5}$$

The state to first order becomes

$$|\Psi\rangle = \exp(-i\omega_0 t)|0\rangle - \sum_\alpha \frac{H^1_{\alpha 0}}{2\hbar}\left[\frac{\exp(i(\omega-\omega_0)t)}{\omega_{\alpha 0}+\omega} + \frac{\exp(-i(\omega+\omega_0)t)}{\omega_{\alpha 0}-\omega}\right]|\alpha\rangle \qquad \text{B.3.6}$$

The multipole moment $\Theta^{(n),tot}$ is given by:

$$\Theta^{(n),tot} = \langle\Psi|\hat{M}^{(n)}|\Psi\rangle \qquad \text{B.3.7}$$

If B.3.6 is inserted into B.3.7, the multipole moment becomes:

$$\Theta^{(n),tot} = \Theta_0^{(n)} - \cos(\omega t)\sum_\alpha \frac{\omega_{\alpha 0}}{\hbar(\omega_{\alpha 0}^2 - \omega^2)}\left[M_{0\alpha}^{(n)} H_{\alpha 0}^1 + H_{0\alpha}^1 M_{\alpha 0}^{(n)}\right] + i\sin(\omega t)\sum_\alpha \frac{\omega}{\hbar(\omega_{\alpha 0}^2 - \omega^2)}\left[M_{0\alpha}^{(n)} H_{\alpha 0}^1 - H_{0\alpha}^1 M_{\alpha 0}^{(n)}\right] \quad \text{B.3.8}$$

where $M_{0\alpha}^{(n)} \equiv \left\langle 0 \middle| \hat{M}^{(n)} \middle| \alpha \right\rangle$. It has been argued[1] that if the molecule is in a non-degenerate and therefore, real state, then $M_{0\alpha}^{(n)} H_{\alpha 0}^1 = H_{0\alpha}^1 M_{\alpha 0}^{(n)}$, and the imaginary $\sin(\omega t)$ term is zero.

$$\Theta^{(n),tot} = \Theta_0^{(n)} - \cos(\omega t)\sum_\alpha \frac{\omega_{\alpha 0}}{\hbar(\omega_{\alpha 0}^2 - \omega^2)}\left[M_{0\alpha}^{(n)} H_{\alpha 0}^1 + H_{0\alpha}^1 M_{\alpha 0}^{(n)}\right] \quad \text{B.3.9}$$

Using the expression for H^1 (B.2.5), $H_{\alpha 0}^1$ becomes

$$H_{\alpha 0}^1 = \left\langle \alpha \middle| \sum_{n=0}^{\infty} \hat{M}^{(n)} \cdot \hat{V}^{(n)} \middle| 0 \right\rangle = \sum_{n=1}^{\infty} \hat{M}_{\alpha 0}^{(n)} \cdot \hat{V}^{(n)} \quad \text{B.3.10}$$

$H_{\alpha 0}^1$ can then be inserted into B.3.9 to give:

$$\Theta^{(n),tot} = \Theta_0^{(n)} - \cos(\omega t)\sum_{m=1}^{\infty}\sum_\alpha \frac{\omega_{\alpha 0}}{\hbar(\omega_{\alpha 0}^2 - \omega^2)}\left[M_{0\alpha}^{(n)} \hat{M}_{\alpha 0}^{(m)} + \hat{M}_{0\alpha}^{(m)} M_{\alpha 0}^{(n)}\right] \cdot \hat{V}^{(m)} = \Theta_0^{(n)} + \cos(\omega t)\sum_{m=1}^{\infty} \alpha^{(n)(m)}(\omega) \cdot \vec{E}^{(m)} \quad \text{B.3.11}$$

where $\vec{E}^{(m)} = -V^{(m)}$ and

$$\alpha^{(n)(m)}(\omega) \equiv \sum_\alpha \frac{\omega_{\alpha 0}}{\hbar(\omega_{\alpha 0}^2 - \omega^2)}\left[M_{0\alpha}^{(n)} \hat{M}_{\alpha 0}^{(m)} + \hat{M}_{0\alpha}^{(m)} M_{\alpha 0}^{(n)}\right] \quad \text{B.3.12}$$

is the frequency dependent molecular polarizability tensor. This result will be needed in the following appendix when dispersion is discussed.

B.4 References

[1] A. Stone, *Intermolecular Forces*, (Oxford University Press, New York, 1996)

[2] C. G. Gray and K. E. Gubbins, *Theory of Molecular Fluids Volume 1: Fundamentals*, (Oxford University Press, New York, 1984)

[3] G. C. Maitland, M. Rigby, E. B. Smith, and W. A. Wakeham, *Intermolecular Forces, Their Origin and Determination*, (Oxford University Press, New York, 1981)

[4] C. J. Bottcher, *Theory of Electric Polarization : Dielectrics in Static Fields,* 2nd edition, revised (Elsevier , New York, 1993)

[5] C. J. Bottcher**,** *Theory of Electric Polarization : Dielectrics in Time-Dependent Fields,* 3rd edition, revised (Elsevier, New York, 1996)

Appendix C Intermolecular Perturbation Theory

C.1 Introduction

In this appendix, the interaction between two molecules is studied using Intermolecular Perturbation Theory (IMPT)[1 2]. The non-interacting system is the two molecules isolated from one another. The perturbation is taken to be the electrostatic interaction between the two molecules, and the perturbational Hamiltonian is expanded in terms of Cartesian point multipoles. The molecules are assumed to be separated at long range in order to neglect antisymmetrization effects between the two molecules. The first few orders of perturbation theory lead to a natural decomposition of the intermolecular energy into electrostatic, polarization, and dispersion contributions[3-6]

In the following section, energy corrections up to second order will be calculated for the interaction between two molecules. The first order energy correction is shown to be the purely electrostatic energy between the two molecules while their wavefunctions are frozen in their non-interacting states. The first order energy is expressed as the interaction energy between the molecules of the permanent multipole moments. The IMPT first order energy can be compared to the first order correction energy of a molecule interacting with an external potential in appendix B.2, which was found to be the interaction energy of the permanent electrostatic moments (calculated from the non-interacting molecular state) with the external potential.

The second order energy correction to the intermolecular interaction energy between two molecules (*A* and *B*) is found to be composed of three parts: the energy of *A* polarizing *B*, the energy of *B* polarizing *A*, and the dispersion energy when both *A* and *B*

are mutually polarized. The second order intermolecular energy correction can be compared to the second order energy correction of a molecule interacting with an external field. In the molecule-external field case, the second order energy is purely polarization energy. Dispersion is absent because the field does not get polarized.

The dispersion energy is an interesting purely quantum mechanical effect. In classical models based on polarizable charge density, two mutually interacting polarizable charge densities do not interact if there is not an external permanent field which can polarize the system. In other words, a source of external charges needs to be present in order for classical polarization to happen. An example is two argon atoms. There is no permanent multipole moment on the argon atoms. If two argon atoms are sufficiently separated so that their charge distributions do not overlap, the electrostatic interaction energy is zero. Classically, the polarization energy between the two molecules should also be zero. However quantum mechanically, there is a small attractive energy in which the charge densities on the two argons spontaneously polarize each other in the absence of a permanent field. In section C.3, the dispersion is discussed as the energy in which the two molecules spontaneously polarize one another. The dispersion energy can be expressed in terms of an integral of molecular polarizability tensor over imaginary frequencies. This is used to derive the empirical Slater-Kirkwood model for dispersion interactions between atoms.

As mentioned earlier, the discussion on IMPT in this appendix assumes the molecules are interacting at long range in order to neglect antisymmetrization effects. At short range, enforcing antisymmetrization between the interacting molecules introduces exchange/repulsion terms to the energy. Other energy decomposition schemes such as

Morokuma-Kitaura decomposition[7], Constrained Orbital Variation (CSOV) method[8], and Symmetry Adapted Perturbation Theory[9] were designed to include antisymmetrization effects which make a significant contribution at short range. These other energy decomposition schemes are derived for specific ab-initio methods of calculating or approximately calculating the wave-function for the interacting molecules.

C.2 Perturbational Expansion

Consider two interacting molecules *A* and *B* interacting at long range. The interacting perturbing Hamiltonian $\hat{H}^1$ is the electrostatic interaction between molecules *A* and *B*.

$$H^1 = \sum_{a\in A}\sum_{b\in B}\frac{e_a e_b}{\left|\vec{r}^{\,a} - \vec{r}^{\,b}\right|} \qquad \text{C.2.1}$$

Suppose the center of mass of *A* and *B* are located at $\vec{R}^{\,A}$ and $\vec{R}^{\,B}$, respectively. The denominator can be expanded in terms of Cartesian multipoles as in Appendix A:

$$\frac{1}{\left|\vec{r}^{\,a} - \vec{r}^{\,b}\right|} = \sum_{n=0}^{\infty}\sum_{m=0}^{\infty}\frac{1}{n!}\frac{1}{m!}(\vec{r}^{\,a} - \vec{R}^{\,A})^{(n)}(\vec{r}^{\,b} - \vec{R}^{\,B})^{(m)} \cdot \nabla^{(n),A}\nabla^{(m),B}\frac{1}{\left|\vec{R}^{\,A} - \vec{R}^{\,B}\right|} \qquad \text{C.2.2}$$

C.2.2 can be inserted into C.2.1 and $\hat{H}^1$ can be expressed in terms of moments:

$$\hat{H}^1 = \sum_{n=0}^{\infty}\sum_{m=0}^{\infty}\hat{M}^{(n),A}\hat{M}^{(m),B} \cdot \nabla^{(n),A}\nabla^{(m),B}\frac{1}{\left|\vec{R}^{\,A} - \vec{R}^{\,B}\right|} \qquad \text{C.2.3}$$

where the moment operator for *A* is defined as in B.2.7: $\hat{M}^{(n),A} \equiv \frac{1}{n!}\sum_{a\in A} e_a(\vec{r}^{\,a} - \vec{R}^{\,A})^{(n)}$.

$\hat{M}^{(m),B}$ is defined in a similar manner.

Let $\hat{H}^0$ be the non-interacting Hamiltonian given by:

$$\hat{H}^0 = \hat{H}^{0,A} + \hat{H}^{0,B} \qquad \text{C.2.4}$$

where $\hat{H}^{0,A}$ is the Hamiltonian for molecule A in vacuum and $\hat{H}^{0,B}$ is the Hamiltonian for molecule B in vacuum. Let $|\alpha\rangle$ be the eigenstates of $\hat{H}^{0,A}$ with eigenvalue E_α^{A} and $|\beta\rangle$ represent the eigenstates of $\hat{H}^{0,B}$ with eigenvalue E_β^{B}. At long range, antisymmetrization effects are unimportant, and therefore, the product states $|\alpha\beta\rangle$ represent the states accessible to the interacting molecular dimer A-B. The ground state energy of the isolated systems is given by $|00\rangle$ with energy $E_0^{\mathrm{A}} + E_0^{\mathrm{B}}$. Using Raleigh-Schrodinger perturbation theory, the total dimer energy E_0 for the ground state can be expanded in a series.

$$E_0 = E_0^0 + E_0^1 + E_0^2 + \ldots \qquad \text{C.2.5}$$

The zeroth[th] order contribution is the expectation value of the non-interacting Hamiltonian $\hat{H}^0$ with the ground state $|00\rangle$.

$$E_0^0 = \langle 00|\hat{H}^0|00\rangle = E_0^{\mathrm{A}} + E_0^{\mathrm{B}} \qquad \text{C.2.6}$$

i.e. the sum of the non-interacting monomer energies. The first-order correction is given by:

$$\begin{aligned} E_0^1 &= \langle 00|\hat{H}^1|00\rangle \\ &= \sum_{n=0}^{\infty}\sum_{m=0}^{\infty}\langle 00|\hat{M}^{(n),A}\hat{M}^{(m),B}|00\rangle \cdot \nabla^{(n),A}\nabla^{(m),B}\frac{1}{\left|\vec{R}^A - \vec{R}^B\right|} \\ &= \sum_{n=0}^{\infty}\sum_{m=0}^{\infty}\Theta_0^{(n),A}\Theta_0^{(m),B} \cdot \nabla^{(n),A}\nabla^{(m),B}\frac{1}{\left|\vec{R}^A - \vec{R}^B\right|} \end{aligned} \qquad \text{C.2.7}$$

where

$$\Theta_0^{(n),A} \equiv \left\langle 0 \left| \hat{M}^{(n),A} \right| 0 \right\rangle$$
$$\Theta_0^{(m),B} \equiv \left\langle 0 \left| \hat{M}^{(m),B} \right| 0 \right\rangle \qquad \text{C.2.8}$$

are the permanent vacuum multipoles of A and B, respectively. The first-order energy correction is the pure electrostatic energy of the unperturbed molecules (see eqn A.3.9).

The second order energy E_0^2 is given by:

$$E_0^2 = -\sum_\alpha \sum_\beta {}^* \frac{\left\langle 00 \left| \hat{H}^1 \right| \alpha\beta \right\rangle \left\langle \alpha\beta \left| \hat{H}^1 \right| 00 \right\rangle}{E_{\alpha 0}^{\mathrm{A}} + E_{\beta 0}^{\mathrm{B}}} \qquad \text{C.2.9}$$

where $E_{\alpha 0}^{\mathrm{A}} \equiv E_\alpha^{\mathrm{A}} - E_0^{\mathrm{A}}$ and the * means omit the $|00\rangle$ term in the double sum. The second order energy can be separated into three contributions: energy of B polarizing A $U_{\mathrm{pol}}^{\mathrm{A}}$, energy of A polarizing B $U_{\mathrm{pol}}^{\mathrm{B}}$, and the dispersion energy between A and B $U_{\mathrm{disp}}^{\mathrm{AB}}$.

$$U_{\mathrm{pol}}^{\mathrm{A}} = -\sum_{\alpha \neq 0} \frac{\left\langle 00 \left| H^1 \right| \alpha 0 \right\rangle \left\langle \alpha 0 \left| H^1 \right| 00 \right\rangle}{E_{\alpha 0}^{\mathrm{A}}} \qquad \text{C.2.10}$$

$$U_{\mathrm{pol}}^{\mathrm{B}} = -\sum_{\beta \neq 0} \frac{\left\langle 00 \left| H^1 \right| 0\beta \right\rangle \left\langle 0\beta \left| H^1 \right| 00 \right\rangle}{E_{\beta 0}^{\mathrm{B}}} \qquad \text{C.2.11}$$

$$U_{\mathrm{disp}}^{\mathrm{AB}} = -\sum_{\alpha \neq 0} \sum_{\beta \neq 0} \frac{\left\langle 00 \left| H^1 \right| \alpha\beta \right\rangle \left\langle \alpha\beta \left| H^1 \right| 00 \right\rangle}{E_{\alpha 0}^{\mathrm{A}} + E_{\beta 0}^{\mathrm{B}}} \qquad \text{C.2.12}$$

In the energy expression of B polarizing A $U_{\mathrm{pol}}^{\mathrm{A}}$, the excited states of A are being summed over while B is held in its ground state. In other words, the permanent field of B is polarizing A. A similar explanation holds for $U_{\mathrm{pol}}^{\mathrm{B}}$. In the dispersion energy between A and B $U_{\mathrm{disp}}^{\mathrm{AB}}$, both excited states of A and B are being summed over. This term corresponds to the induced moments of A and B spontaneously polarizing each other.

The above expressions can be expressed in terms of moment operators $\hat{M}^{(n),A}$ by substituting in $\hat{H}^1$ (C.2.3). In order to evaluate $U_{\text{pol}}^{\text{A}}$, it is first noted that

$$\begin{aligned}\langle 00|H^1|\alpha 0\rangle &= \sum_{n=0}^{\infty}\sum_{m=0}^{\infty}\langle 00|\hat{M}^{(n),A}\hat{M}^{(m),B}|\alpha 0\rangle \cdot \nabla^{(n),A}\nabla^{(m),B}\frac{1}{\left|\vec{R}^A-\vec{R}^B\right|} \\ &= \sum_{n=0}^{\infty}\sum_{m=0}^{\infty}\hat{M}_{0\alpha}^{(n),A}\Theta_0^{(m),B}\cdot\nabla^{(n),A}\nabla^{(m),B}\frac{1}{\left|\vec{R}^A-\vec{R}^B\right|} \\ &= \sum_{n=0}^{\infty}\hat{M}_{0\alpha}^{(n),A}\cdot\nabla^{(n),A}V^{B\to A}(R)\end{aligned} \qquad \text{C.2.13}$$

where $\Theta_0^{(m),B}$ is the permanent multipole moment of B and $V^{B\to A}(R)$ is the potential from B onto A (A.7.3):

$$V^{B\to A}(R) = \sum_{m=0}^{\infty}\Theta_0^{(m),B}\cdot\nabla^{(m),B}\frac{1}{\left|\vec{R}^A-\vec{R}^B\right|} \qquad \text{C.2.14}$$

$U_{\text{pol}}^{\text{A}}$ (C.2.10) then becomes

$$\begin{aligned}U_{\text{pol}}^{\text{A}} &= -\sum_{\alpha\neq 0}\sum_{n=0}^{\infty}\sum_{m=0}^{\infty}\frac{\hat{M}_{0\alpha}^{(n),A}\hat{M}_{\alpha 0}^{(m),A}}{E_{\alpha 0}^{\text{A}}}\cdot\nabla^{(n),A}V^{B\to A}(R)\nabla^{(m),A}V^{B\to A}(R) \\ &= -\frac{1}{2}\sum_{\alpha\neq 0}\sum_{n=0}^{\infty}\sum_{m=0}^{\infty}\frac{\hat{M}_{0\alpha}^{(n),A}\hat{M}_{\alpha 0}^{(m),A}+\hat{M}_{0\alpha}^{(m),A}\hat{M}_{\alpha 0}^{(n),A}}{E_{\alpha 0}^{\text{A}}}\cdot\nabla^{(n),A}V^{B\to A}(R)\nabla^{(m),A}V^{B\to A}(R) \\ &= -\frac{1}{2}\sum_{n=0}^{\infty}\sum_{m=0}^{\infty}\alpha^{(n)(m),A}\cdot\nabla^{(n),A}V^{B\to A}(R)\nabla^{(m),A}V^{B\to A}(R)\end{aligned} \qquad \text{C.2.15}$$

where $\alpha^{(n)(m),A}$ is the n^{th} - m^{th} pole polarizability tensor for molecule A (B.2.16). A similar result holds for $U_{\text{pol}}^{\text{B}}$. The evaluation of the dispersion energy $U_{\text{disp}}^{\text{AB}}$ in terms of moments is more involved and is discussed in the following section.

C.3 Dispersion

The dispersion energy given in C.2.12 will now be evaluated in terms of moment operators and polarizabilities. Before proceeding, the following intermediate result will be useful:

$$\begin{aligned}\left\langle 00\left|H^{1}\right|\alpha\beta\right\rangle &= \sum_{n=1}^{\infty}\sum_{m=1}^{\infty}\hat{M}_{0\alpha}^{(n),A}\hat{M}_{0\beta}^{(m),B}\cdot\nabla^{(n),A}\nabla^{(m),B}\frac{1}{R^{AB}} \\ &= \sum_{n=1}^{\infty}\sum_{m=1}^{\infty}\hat{M}_{0\alpha}^{(n),A}\hat{M}_{0\beta}^{(m),B}\cdot T^{(n)(m)}\end{aligned} \qquad \text{C.3.1}$$

where $T^{(n)(m)} \equiv \nabla^{(n),A}\nabla^{(m),B}\frac{1}{R^{AB}}$ for brevity. C.3.1 can be inserted into C.2.12 to yield:

$$U_{\text{disp}}^{\text{AB}} = -\sum_{\substack{n,m,\\p,q}}^{\infty}\sum_{\alpha\neq 0}\sum_{\beta\neq 0}\frac{\hat{M}_{0\alpha}^{(n),A}\hat{M}_{0\beta}^{(m),B}\hat{M}_{\alpha 0}^{(p),A}\hat{M}_{\beta 0}^{(q),B}}{E_{\alpha 0}^{\text{A}}+E_{\beta 0}^{\text{B}}}\cdot T^{(n)(m)}T^{(p)(q)} \qquad \text{C.3.2}$$

Since the denominator is a sum $E_{\alpha 0}^{\text{A}}+E_{\beta 0}^{\text{B}}$ and not a product $E_{\alpha 0}^{\text{A}}E_{\beta 0}^{\text{B}}$, the sum over α and β can not directly be expressed in terms of molecular polarizability tensors for molecules A and B. However the following identity, which can be proved by contour integration, is used to express the sum as a product:

$$\frac{1}{A+B} = \frac{2}{\pi}\int_{0}^{\infty}\frac{AB}{(A^{2}+\nu^{2})(B^{2}+\nu^{2})}d\nu \qquad \text{C.3.3}$$

Using this identity, C.3.2 becomes[10]:

$$U_{\text{disp}}^{\text{AB}} = -\frac{2}{\pi}\sum_{\substack{n,m,\\p,q}}^{\infty}\int_{0}^{\infty}d\nu\sum_{\alpha\neq 0}\frac{E_{\alpha 0}^{\text{A}}\hat{M}_{0\alpha}^{(n),A}\hat{M}_{\alpha 0}^{(p),A}}{\left(E_{\alpha 0}^{\text{A}}\right)^{2}+\nu^{2}}\sum_{\beta\neq 0}\frac{E_{\beta 0}^{\text{B}}\hat{M}_{0\beta}^{(m),B}\hat{M}_{\beta 0}^{(q),B}}{\left(E_{\beta 0}^{\text{B}}\right)^{2}+\nu^{2}}\cdot T^{(n)(m)}T^{(p)(q)} \qquad \text{C.3.4}$$

Recall the frequency depend molecular polarizability tensor given in B.3.12:

$$\alpha^{(n)(m)}(\omega) \equiv \sum_{\alpha}\frac{\omega_{\alpha 0}}{\hbar(\omega_{\alpha 0}^{2}-\omega^{2})}\left[M_{0\alpha}^{(n)}\hat{M}_{\alpha 0}^{(m)}+\hat{M}_{0\alpha}^{(m)}M_{\alpha 0}^{(n)}\right] \qquad \text{C.3.5}$$

where $\omega \equiv \frac{E}{\hbar}$. This is applied to the sum over α and β to yield:

$$U_{\text{disp}}^{\text{AB}} = -\frac{\hbar}{2\pi} \sum_{\substack{n,m,\\ p,q}}^{\infty} \int_0^{\infty} d\nu \alpha^{(n)(p),A}(i\nu) \alpha^{(m)(q),B}(i\nu) \cdot T^{(n)(m)} T^{(p)(q)} \qquad \text{C.3.6}$$

Now consider the simplest case of dipole-dipole dispersion ($n = m = p = q = 1$):

$$U_{\text{disp}}^{\text{AB}} = -\frac{\hbar}{2\pi} \int_0^{\infty} d\nu \alpha_{ij}^{A}(i\nu) \alpha_{kl}^{B}(i\nu) \nabla_{ik}^{(2),A} \frac{1}{R^{AB}} \nabla_{jl}^{(2),A} \frac{1}{R^{AB}} \qquad \text{C.3.7}$$

If the molecular polarizability tensor is isotropic as in the case for an atom, then $\alpha_{ij} = \alpha \delta_{ij}$. Using the result for the dipole-dipole interaction matrix for point multipoles (A.6.3) $\nabla_{ij}^{(2)} \frac{1}{R} = R_i R_j \frac{3}{R^5} - \delta_{ij} \frac{1}{R^3}$, C.3.7 becomes:

$$\begin{aligned} U_{\text{disp}}^{\text{AB}} &= -\frac{\hbar}{2\pi} \int_0^{\infty} d\nu \alpha^{A}(i\nu) \alpha^{B}(i\nu) \nabla_{ik}^{(2),A} \frac{1}{R^{AB}} \nabla_{ik}^{(2),A} \frac{1}{R^{AB}} \\ &= -\frac{\hbar}{2\pi} \int_0^{\infty} d\nu \alpha^{A}(i\nu) \alpha^{B}(i\nu) \left(R_i R_k \frac{3}{R^5} - \delta_{ik} \frac{1}{R^3} \right) \left(R_i R_k \frac{3}{R^5} - \delta_{ik} \frac{1}{R^3} \right) \\ &= -\frac{3\hbar}{\pi R^6} \int_0^{\infty} d\nu \alpha^{A}(i\nu) \alpha^{B}(i\nu) \\ &= -\frac{C_{AB}}{R^6} \end{aligned} \qquad \text{C.3.8}$$

where

$$C_{AB} \equiv \frac{3\hbar}{\pi} \int_0^{\infty} d\nu \alpha^{A}(i\nu) \alpha^{B}(i\nu) \qquad \text{C.3.9}$$

If Gaussian dipoles were used, $\nabla_{pq}^{(2)} \frac{1}{R}$ is replaced by

$\nabla_{pq}^{(2)} \frac{erf(\beta R)}{R} = R_p R_q \beta^5 B_2(x) - \delta_{pq} \beta^3 B_1(x)$, where $x \equiv \beta R$, $\beta \equiv \frac{\beta_A \beta_B}{\sqrt{\beta_A^2 + \beta_B^2}}$, and $B_1(x)$ and $B_2(x)$ are defined in 2.9.6. In this case, C.3.7 becomes:

$$
\begin{aligned}
U_{\text{disp}}^{\text{AB}} &= -\frac{C_{AB}}{6}\left(R_i R_k \beta^5 B_2(x) - \delta_{ik}\beta^3 B_1(x)\right)\left(R_i R_k \beta^5 B_2(x) - \delta_{ik}\beta^3 B_1(x)\right) \\
&= -\frac{C_{AB}}{6}\beta^6\left(x^4 B_2(x)^2 - 2x^2 B_1(x)B_2(x) + 3B_1(x)^2\right)
\end{aligned}
\qquad \text{C.3.10}
$$

C.3.10 is continuous and finite for all x, while C.3.8 diverges as R^{-6} for small x. However for large x, $B_1(x) \cong \frac{1}{x^3}$ and $B_2(x) \cong \frac{3}{x^5}$. In this case, the Gaussian dipoles behave as point dipoles and C.3.10 becomes:

$$
\begin{aligned}
U_{\text{disp}}^{\text{AB}} &\cong -\frac{C_{AB}}{6}\beta^6\left(\frac{9}{x^6} - \frac{6}{x^6} + \frac{3}{x^6}\right) \\
&= -\frac{C_{AB}}{R^6}
\end{aligned}
\qquad \text{C.3.11}
$$

Damping functions[11-13] have been applied to dispersion models in order to make the interaction finite for small R. The result for $U_{\text{disp}}^{\text{AB}}$ with Gaussian dipoles in C.3.10 can be used in place of a damping function.

If higher order multipole terms are included, the dispersion energy can be expressed as a series[14-16]

$$
U_{\text{disp}}^{\text{AB}} = -\frac{C_6}{R^6} - \frac{C_8}{R^8} - \frac{C_{10}}{R^{10}} .. \qquad \text{C.3.12}
$$

where C_6 corresponds to dipole-dipole dispersion, C_8 corresponds to dipole-quadrapole dispersion, and C_{10} corresponds to quadrapole-quadrapole and dipole-octapole dispersion.

A method is needed to calculate the dispersion coefficients[17 18] C_{AB} in C.3.9. One strategy is to calculate $\alpha^A(iv)$ and $\alpha^B(iv)$ for several values of v from C.3.5 using ab-initio methods and then perform the integral for C_{AB} numerically. Another way to calculate C_{AB} is to first approximate $\alpha^A(iv)$ as:

$$\alpha^A(i\nu) \cong \frac{\alpha^A(0)}{1+\left(\frac{\nu}{\eta^A}\right)^2} \qquad \text{C.3.13}$$

where η^A is an empirical parameter. Using this function for $\alpha^A(i\nu)$, the integral for C_{AA} in C.3.9 becomes:

$$\begin{aligned} C_{AA} &= \frac{3\hbar}{\pi}\int_0^\infty d\nu \alpha^A(i\nu)\alpha^A(i\nu) \\ &= \frac{3\hbar\eta^A}{4}\alpha^A(0)^2 \end{aligned} \qquad \text{C.3.14}$$

or

$$\eta^A = \frac{4C_{AA}}{3\hbar\alpha^A(0)^2} \qquad \text{C.3.15}$$

The integral for C_{AB} where A and B are different is found to be:

$$\begin{aligned} C_{AB} &= \frac{3\hbar}{\pi}\alpha^A(0)\alpha^B(0)\int_0^\infty d\nu \frac{1}{\left(1+\left(\frac{\nu}{\eta^A}\right)^2\right)\left(1+\left(\frac{\nu}{\eta^B}\right)^2\right)} \\ &= \frac{3\hbar}{\pi}\alpha^A(0)\alpha^B(0)\frac{\pi}{2}\frac{\eta^A\eta^B}{\eta^A+\eta^B} \\ &= \frac{2\alpha^A(0)\alpha^B(0)C_{AA}C_{BB}}{\alpha^B(0)^2C_{AA}+\alpha^A(0)^2C_{BB}} \end{aligned} \qquad \text{C.3.16}$$

This result is known as the Slater-Kirkwood[19] combination rule.

C.4 References

[1] A. Stone, *Intermolecular Forces*, (Oxford University Press, New York, 1996)

[2] A. J. Stone and R. J. A. Tough, Chem. Phys. Lett. **110** (**2**), 123 (1984)

[3] A. D. Buckingham, Adv. chem. Phys. **12**, 107 (1967)

[4] C. G. Gray and K. E. Gubbins, *Theory of Molecular Fluids Volume 1: Fundamentals*, (Oxford University Press, New York, 1984)

[5] G. C. Maitland, M. Rigby, E. B. Smith, and W. A. Wakeham, *Intermolecular Forces, Their Origin and Determination*, (Oxford University Press, New York, 1981)

[6] P. Claverie and R. Rein, Int. J. Quantum Chem. **2**, 537 (1969)

[7] K. Kitaura and K. Morokuma, Int. J. Quantum Chem. **10**, 325 (1976)

[8] P. S. Bagus, K. Hermann, and C. W. Bauschlicher, Jr., J. Chem. Phys. **80**, 4378 (1984)

[9] B. Jeziorski, R. Moszynski, and K. Szalewicz, Chem. Rev. **94**, 1887 (1994)

[10] H. B. G. Casimir and D. Polder, Phys. Rev. **73**, 360 (1948)

[11] Q. Wu and W. Yang, J. Chem. Phys. **116** (**2**), 515 (2002)

[12] R. Ahlrichs, R. Penco, and G. Scoles, Chem. Phys. **19**, 119 (1977)

[13] W. T. M. Mooij, F. B. van Duijneveldt, J. G. C. M. van Duijneveld-van de Rijdt, and B. P. van Eijck, J. Phys. Chem. A **103**, 9872 (1999)

[14] J. O. Hirschfelder and W. M. Meath, Adv. Chem. Phys. **12**, 1 (1976)

[15] H. Margenau and N. Kestner, *Theory of Intermolecular Forces*, (Pergamon, London, 1967)

[16] R. Eisenshitz and F. London, Z. Phys. **60**, 491 (1930)

[17] M. D. Peña, C. Pando, and J. A. R. Renuncio, J. Chem. Phys **72** (**9**), 1 (1980)

[18] H. L. Kramer and D. R. Herschbach, J. Chem. Phys. **53** (**7**), 2792 (1970)

[19] J. C. Slater and J. G. Kirkwood, Phys. Rev. **37**, 682 (1931)

Appendix D. Ewald Summation

D.1 Introduction

Long range electrostatic interactions decay slowly. For example, the interaction energy between two point charges falls as R^{-1}. In molecular dynamics simulations, pair-wise additive interactions are often truncated outside a specified non-bonded cut-off. Large cut-offs would be needed if electrostatic interactions were simply truncated at a certain distance. Special techniques such as the Ewald summation method[1-4] for periodic systems and the fast multipole method[5] for non-periodic systems were developed to speed up the convergence of long range electrostatic interactions.

In this appendix, the Ewald summation is method is derived for a periodic system of point charges and point dipoles. Since the system is periodic, part of the energy can be calculated in Fourier space. This part of the energy is called the reciprocal sum. The other part of the energy has a small periodic component and decays quickly in coordinate space. This part of the energy is called the direct sum. In addition, there is a self-energy correction and a second energy correction called the adjusted sum for pairs of particles which were not intended to include (e.g. 1-2 or 1-3 particle interactions). In the following section, the Ewald summation method is discussed in more detail.

In addition to the reciprocal, direct, self, and adjusted energy contributions to the Ewald energy, there is a dipole surface term which depends on the dipole moment of the unit cell. The energy of a unit cell interacting with other unit cells in a crystal is a conditionally convergent series. The dipole surface term depends on the order of summation in the series. For example, if the unit cell interactions were summed in the

order of an ever increasingly sized cube, the result would be different if the unit cell interactions were summed in a spherically. The dipole surface term will not be considered here. See references[2-4] for more details.

The Ewald method scales[6] as $N^{3/2}$ for large N, where N is the number of particles. A method to speed up the reciprocal Fourier sum by interpolating the complex exponentials on a grid of points has been developed. This method, called Particle Mesh Ewald[7], scales as $N \log N$ for large N, and has been employed extensively in Molecular Dynamcs simulations[8-12].

D.2 Ewald Summation

From the results in appendix A, the energy between particle i with charge q^i and dipole $\vec{\mu}^i$ and a particle j with charge q^j and dipole $\vec{\mu}^j$ is given by:

$$U_{ij} = \left(q^i + \vec{\mu}^i \cdot \nabla^i\right)\left(q^j - \vec{\mu}^j \cdot \nabla^i\right)\frac{1}{\left|\vec{r}^{\,ij}\right|} \qquad \text{D.2.1}$$

Consider a collection of particles (i = 1, 2.. N) in a box which defines the system. The interaction energy U_{box} for the N particles with charges q^i and dipoles $\vec{\mu}^i$ is a sum over all pairs.

$$U_{box} = \frac{1}{2}\sum_{i \neq j}\left(q^i + \vec{\mu}^i \cdot \nabla^i\right)\left(q^j - \vec{\mu}^j \cdot \nabla^i\right)\frac{1}{\left|\vec{r}^{\,ij}\right|} \qquad \text{D.2.2}$$

In periodic boundary conditions, images of this box are replicated in a lattice arrangement surrounding the box in 3D space. Suppose the sides of the box are given by the vectors $\vec{a}_r$ (r = 1, 2, 3). Each new box is generated using translation vectors

$\vec{n} = n_1\vec{a}_1 + n_2\vec{a}_2 + n_3\vec{a}_3$, where n_i are integers. The interaction energy of all the particles in the central box with all of the particles in the other boxes is given by

$$U = \frac{1}{2}\sum_i \sum_j \left(q^i + \vec{\mu}^i \cdot \nabla^i\right)\left(q^j - \vec{\mu}^j \cdot \nabla^i\right)\sum_{\vec{n}}{}^* \frac{1}{\left|\vec{r}^{\,ij} + \vec{n}\right|} \qquad \text{D.2.3}$$

The * indicates that if $\vec{n} = 0$, omit the $i = j$ term and any other terms in the 'masked list', e.g. do not count 1-2 or 1-3 Coulomb interactions between particles that are bonded to or adjacent of each other.

This series in D.2.3 converges slowly. A method to speed the convergence of this series is to first note:

$$\frac{1}{\left|\vec{r}^{\,ij} + \vec{n}\right|} = \frac{2}{\sqrt{\pi}}\int_0^\infty d\rho e^{-\rho^2\left|\vec{r}^{\,ij}+\vec{n}\right|^2} = \frac{2}{\sqrt{\pi}}\int_0^\beta d\rho e^{-\rho^2\left|\vec{r}^{\,ij}+\vec{n}\right|^2} + \frac{2}{\sqrt{\pi}}\int_\beta^\infty d\rho e^{-\rho^2\left|\vec{r}^{\,ij}+\vec{n}\right|^2} \qquad \text{D.2.4}$$

where β is defined as the Ewald parameter. The second term on the right side of D.2.4 can be written as:

$$\frac{2}{\sqrt{\pi}}\int_\beta^\infty d\rho e^{-\rho^2\left|\vec{r}^{\,ij}+\vec{n}'\right|^2} = \frac{erfc\left(\beta\left|\vec{r}^{\,ij} + \vec{n}\right|\right)}{\left|\vec{r}^{\,ij} + \vec{n}\right|} \qquad \text{D.2.5}$$

where $erfc(x) \equiv 1 - erf(x) = \frac{2}{\sqrt{\pi}}\int_x^\infty du \exp(-u^2)$ is the complementary error function

which decays rapidly for large $x > 1$. The sum over translation vectors in D.2.3 becomes:

$$\sum_{\vec{n}} \frac{1}{\left|\vec{r}^{\,ij} + \vec{n}\right|} = \sum_{\vec{n}} \frac{2}{\sqrt{\pi}}\int_0^\beta d\rho e^{-\rho^2\left|\vec{r}^{\,ij}+\vec{n}\right|^2} + \sum_{\vec{n}} \frac{erfc\left(\beta\left|\vec{r}^{\,ij} + \vec{n}\right|\right)}{\left|\vec{r}^{\,ij} + \vec{n}\right|} \qquad \text{D.2.6}$$

The second term in D.2.6. converges quickly. The first term converges slowly, but it can be written as a Fourier series.

$$\sum_{\vec{n}} \frac{2}{\sqrt{\pi}}\int_0^\beta d\rho e^{-\rho^2\left|\vec{r}^{\,ij}+\vec{n}\right|^2} = \sum_{\vec{m}} c_{\vec{m}} e^{2\pi i\vec{m}\cdot\vec{r}^{\,ij}} \qquad \text{D.2.7}$$

$\vec{m} = m_1\vec{a}_1^* + m_2\vec{a}_2^* + m_3\vec{a}_3^*$ and $\vec{a}_i^*$ are the reciprocal vectors: $\vec{a}_i \cdot \vec{a}_j^* = \delta_{ij}$.

$$c_{\vec{m}^*} = \frac{1}{V_{cell}} \int_{V_{cell}} d^3 r^{ij} e^{-2\pi i \vec{m}\cdot\vec{r}^{ij}} \sum_{\vec{n}} \frac{2}{\sqrt{\pi}} \int_0^{\beta} d\rho e^{-\rho^2 \left|\vec{r}^{ij}+\vec{n}\right|^2} \qquad \text{D.2.8}$$

Let $\vec{r} = \vec{r}^{ij} + \vec{n}$. The sum over $\vec{n}$ can be transformed to an integral over all space, since $e^{2\pi i \vec{m}\cdot\vec{n}} = 1$. For $\vec{m} \neq 0$

$$c_{\vec{m}^*} = \frac{1}{V_{cell}} \frac{2}{\sqrt{\pi}} \int_0^{\beta} d\rho \int_{\substack{all \\ space}} d^3 r e^{-\rho^2 r^2} e^{-2\pi i \vec{m}\cdot\vec{r}} = \frac{1}{V_{cell} \pi\, m^2} e^{-\frac{m^2\pi^2}{\beta^2}} \qquad \text{D.2.9}$$

D.2.7 becomes

$$\sum_{\vec{n}} \frac{2}{\sqrt{\pi}} \int_0^{\beta} d\rho e^{-\rho^2 \left|\vec{r}^{ij}+\vec{n}\right|^2} = \sum_{\vec{m}} \frac{1}{V_{cell} \pi\, m^2} e^{-\frac{m^2\pi^2}{\beta^2}} e^{2\pi i \vec{m}\cdot\vec{r}^{ij}} \qquad \text{D.2.10}$$

The $\vec{m} = 0$ term is omitted since $c_0 = \frac{\pi^{\frac{3}{2}}}{V_{cell}\beta^3}$ and

$$\frac{1}{2} \sum_i \sum_j \left(q_i + \vec{\mu}_i \cdot \nabla_i\right)\left(q_j - \vec{\mu}_j \cdot \nabla_i\right) \frac{\pi^{\frac{3}{2}}}{V_{cell}\rho^3} = 0$$

because of charge neutrality and c_0 is a constant. Substituting D.2.10 into D.2.6

$$\sum_{\vec{n}} \frac{1}{\left|\vec{r}^{ij}+\vec{n}\right|} = \sum_{\vec{m}^* \neq 0} \frac{1}{V_{cell} \pi\, m^2} e^{-\frac{m^2\pi^2}{\beta^2}} e^{2\pi i \vec{m}\cdot\vec{r}^{ij}} + \sum_{\vec{n}} \frac{erfc\left(\beta\left|\vec{r}^{ij}+\vec{n}\right|\right)}{\left|\vec{r}^{ij}+\vec{n}\right|} \qquad \text{D.2.11}$$

By subtracting off the terms that are self-interactions ($i = j$ if $\vec{n} = 0$) and the adjusted term from the direct sum, the sum over lattice vectors in D.2.4 becomes

$$\begin{aligned} \sum_{\vec{n}}{}^{*} \frac{1}{\left|\vec{r}^{ij}+\vec{n}\right|} = \sum_{\vec{m}\neq 0} \frac{1}{V_{cell} \pi\, m^2} e^{-\frac{m^2\pi^2}{\beta^2}} e^{2\pi i \vec{m}^*\cdot\vec{r}^{ij}} + \sum_{\vec{n}'}{}^{*} \frac{erfc\left(\beta\left|\vec{r}^{ij}+\vec{n}'\right|\right)}{\left|\vec{r}^{ij}+\vec{n}'\right|} + \\ + \delta_{(i,j)\in M} \frac{erfc\left(\beta r^{ij}\right)-1}{r^{ij}} + \lim_{\vec{r}^i \to \vec{r}^j} \frac{erfc\left(\beta r^{ij}\right)-1}{r^{ij}} \end{aligned} \qquad \text{D.2.12}$$

The total lattice energy in D.2.3 can be written as a reciprocal sum, a direct sum, self interaction.

$$U = U_{rec} + U_{dir} + U_{adj} + U_{self} \tag{D.2.13}$$

$$\begin{aligned}
U_{rec} &\equiv \frac{1}{2}\sum_i \sum_j \left(q^i + \vec{\mu}^i \cdot \nabla^i\right)\left(q^j - \vec{\mu}^j \cdot \nabla^i\right) \sum_{\vec{m}\neq 0} \frac{1}{V_{cell}\pi\, m^2} e^{-\frac{m^2\pi^2}{\beta^2}} e^{2\pi i \vec{m}\cdot\vec{r}^{ij}} \\
U_{dir} &\equiv \frac{1}{2}\sum_i \sum_j \left(q^i + \vec{\mu}^i \cdot \nabla^i\right)\left(q^j - \vec{\mu}^j \cdot \nabla^i\right) \sum_{\vec{n}}{}^{*} \frac{erfc\left(\beta\left|\vec{r}^{ij} + \vec{n}\right|\right)}{\left|\vec{r}^{ij} + \vec{n}\right|} \\
U_{adj} &\equiv \frac{1}{2}\sum_{(i,j)\in M} \left(q^i + \vec{\mu}^i \cdot \nabla^i\right)\left(q^j - \vec{\mu}^j \cdot \nabla^i\right) \frac{erfc\left(\beta r^{ij}\right) - 1}{r^{ij}} \\
U_{self} &\equiv \frac{1}{2}\sum_i \sum_j \left(q^i + \vec{\mu}^i \cdot \nabla^i\right)\left(q^j - \vec{\mu}^j \cdot \nabla^i\right) \lim_{\substack{\vec{r}^i \to \vec{r}^j \\ i \to j}} \frac{erfc\left(\beta r^{ij}\right) - 1}{r^{ij}}
\end{aligned} \tag{D.2.14}$$

Reciprocal Sum

The reciprocal sum for the Ewald energy in D.2.4 can be expressed as:

$$U_{rec} = \frac{1}{2\pi V_{cell}} \sum_{\vec{m}\neq 0} \frac{e^{-\frac{m^{*2}\pi^2}{\beta^2}}}{m^2} S(\vec{m}) S(-\vec{m}) \tag{D.2.15}$$

where the structure functions $S(\vec{m})$ are defined by

$$S(\vec{m}) \equiv \sum_j \left(q^j + 2\pi i \vec{m} \cdot \vec{\mu}^j \cdot\right) e^{2\pi i \vec{m}\cdot\vec{r}^j} \tag{D.2.16}$$

The gradient of D.2.16 with respect to $\vec{r}^i$ is $\frac{\partial S(\vec{m})}{\partial \vec{r}^i} = 2\pi i \vec{m}\left(q^i + 2\pi i \vec{m} \cdot \vec{\mu}^i\right) e^{2\pi i \vec{m}\cdot\vec{r}^i}$. This is used to evaluate the reciprocal force contribution on particle i $\vec{F}^i_{rec}$ as the negative gradient of D.2.15 with respect to $\vec{r}^i$ which is given by:

$$\vec{F}^i_{rec} = \frac{2i}{V_{cell}} \sum_{\vec{m}\neq 0} \frac{e^{-\frac{m^{*2}\pi^2}{\beta^2}}}{m^2} \vec{m}\left(S(\vec{m})\left(q^i - 2\pi i \vec{m} \cdot \vec{\mu}^i\right) e^{-2\pi i \vec{m}\cdot\vec{r}^i}\right) \tag{D.2.17}$$

The electrostatic potential[13] at particle *i* can be found by taking the variation of energy D.2.15 when q^i is a test charge $\varphi_{rec}(\vec{r}^{\,i}) \equiv \lim_{\delta q^i \to 0} \frac{\delta U_{rec}}{\delta q^i}$:

$$\varphi_{rec}(\vec{r}^{\,i}) = \frac{1}{\pi V_{cell}} \sum_{\vec{m} \neq 0} \frac{e^{-\frac{m^{*2}\pi^2}{\beta^2}}}{m^2} S(\vec{m}) e^{-2\pi i \vec{m} \cdot \vec{r}^{\,i}} \qquad \text{D.2.18}$$

Finally, the electric field can be found by taking the real part of the negative gradient of $\varphi_{rec}(\vec{r}^{\,i})$ with respect to $\vec{r}^{\,i}$

$$\vec{E}_{rec}(\vec{r}^{\,i}) = \frac{2i}{V_{cell}} \sum_{\vec{m} \neq 0} \frac{e^{-\frac{m^{*2}\pi^2}{\beta^2}}}{m^2} \vec{m} S(\vec{m}) e^{-2\pi i \vec{m} \cdot \vec{r}^{\,i}} \qquad \text{D.2.19}$$

Direct Sum

The direct sum is given in D.2.14 as:

$$U_{dir} = \frac{1}{2} \sum_j \sum_k \sum_{\vec{n}}{}^{*} \left(q^j q^k + \left(q^k \vec{\mu}^j - q^j \vec{\mu}^k \right) \cdot \nabla^j - \vec{\mu}^j \vec{\mu}^k \cdot \nabla^j \nabla^j \right) \frac{erfc\left(\beta \left| \vec{r}^{\,jk} + \vec{n} \right|\right)}{\left| \vec{r}^{\,jk} + \vec{n} \right|} \qquad \text{D.2.20}$$

The direct sum force on particle on particle i is found by taking the negative gradient of U_{dir} with respect to $\vec{r}^{\,i}$:

$$\vec{F}^i_{dir} = -\sum_j \sum_{\vec{n}}{}^{*} \left(q^i q^j \nabla^i + \left(q^j \vec{\mu}^i - q^i \vec{\mu}^j \right) \cdot \nabla^i \nabla^i - \vec{\mu}^i \vec{\mu}^j \cdot \nabla^i \nabla^i \nabla^i \right) \frac{erfc\left(\beta \left| \vec{r}^{\,ij} + \vec{n} \right|\right)}{\left| \vec{r}^{\,ij} + \vec{n} \right|} \qquad \text{D.2.21}$$

The direct sum electrostatic potential $\varphi_{dir}(\vec{r}^{\,i})$ is given by:

$$\varphi_{dir}(\vec{r}^{\,i}) = \sum_j \sum_{\vec{n}}{}^{*} \left(q^j - \vec{\mu}^j \cdot \nabla^j \right) \frac{erfc\left(\beta \left| \vec{r}^{\,ij} + \vec{n} \right|\right)}{\left| \vec{r}^{\,ij} + \vec{n} \right|} \qquad \text{D.2.22}$$

Finally, the direct sum electric field is the negative gradient of $\varphi_{dir}(\vec{r}^{\,i})$ with respect to $\vec{r}^{\,i}$:

$$\vec{E}_{dir}(\vec{r}^{\,i}) = -\sum_j \sum_{\vec{n}}{}^{*} \left(q^j \nabla^i + \vec{\mu}^j \cdot \nabla^i \nabla^i\right) \frac{erfc\left(\beta \left|\vec{r}^{\,ij} + \vec{n}\right|\right)}{\left|\vec{r}^{\,ij} + \vec{n}\right|} \qquad \text{D.2.23}$$

The gradient tensors $\nabla^{(n)} \frac{erfc(\beta r)}{r}$ can be evaluated using the same method that was used to evaluate $\nabla^{(n)} \frac{1}{R}$ in appendix A.6 and $\nabla^{(n)} \frac{erf(\beta R)}{R}$ in section 2.9. The result is given by:

$$\nabla^{(1)} \frac{erfc(\beta R)}{R} = -\vec{R}\beta^3 C_1(x) \qquad \text{D.2.24}$$

$$\nabla^{(2)} \frac{erfc(\beta R)}{R} = \hat{x}_p \hat{x}_q \left(R_p R_q \beta^5 C_2(x) - \delta_{pq} \beta^3 C_1(x)\right) \qquad \text{D.2.25}$$

$$\nabla^{(3)} \frac{erfc(\beta R)}{R} = \hat{x}_p \hat{x}_q \hat{x}_r \left((\delta_{pq} R_r + \delta_{pr} R_q + \delta_{rq} R_p)\beta^5 C_2(x) - R_p R_q R_r \beta^7 C_3(x)\right) \qquad \text{D.2.26}$$

where $x \equiv \beta R$, and the dimensionless $C_n(x)$ functions are defined by: $C_0(x) \equiv \frac{erf(x)}{x}$, $C_{n+1}(x) \equiv -\frac{1}{x}\frac{dC_n}{dx}$. The first four functions are given by:

$$\begin{aligned}
C_0(x) &= \frac{erfc(x)}{x} \\
C_1(x) &= \frac{erfc(x)}{x^3} + \frac{2}{\sqrt{\pi}} e^{-x^2} \frac{1}{x^2} \\
C_2(x) &= \frac{3erfc(x)}{x^5} + \frac{2}{\sqrt{\pi}} e^{-x^2} \left(\frac{3}{x^4} + \frac{2}{x^2}\right) \\
C_3(x) &= \frac{15erfc(x)}{x^7} + \frac{2}{\sqrt{\pi}} e^{-x^2} \left(\frac{15}{x^6} + \frac{10}{x^4} + \frac{4}{x^2}\right)
\end{aligned} \qquad \text{D.2.27}$$

Adjusted Sum

The adjusted sum energy is defined in D.2.14 as:

$$U_{adj} = -\frac{1}{2}\sum_{(i,j)\in M}\left(q^i + \vec{\mu}^i\cdot\nabla^i\right)\left(q^j - \vec{\mu}^j\cdot\nabla^i\right)\frac{erf\left(\beta r^{ij}\right)}{r^{ij}} \qquad \text{D.2.28}$$

where $erfc(x) = 1 - erf(x)$ was used. The procedure to evaluate the force, electrostatic potential, and electric field is the same as the one used to evaluate the same properties in the direct sum. The results will be listed below for completeness.

$$\vec{F}^i_{adj} = \sum_{(i,j)\in M}\left(q^i q^j\nabla^i + \left(q^j\vec{\mu}^i - q^i\vec{\mu}^j\right)\cdot\nabla^i\nabla^i - \vec{\mu}^i\vec{\mu}^j\cdot\nabla^i\nabla^i\nabla^i\right)\frac{erf\left(\beta r^{ij}\right)}{r^{ij}}$$

$$\varphi_{adj}(\vec{r}^{\,i}) = -\sum_{(i,j)\in M}\left(q^j - \vec{\mu}^j\cdot\nabla^j\right)\frac{erf\left(\beta r^{ij}\right)}{r^{ij}} \qquad \text{D.2.29}$$

$$\vec{E}_{adj}(\vec{r}^{\,i}) = \sum_{(i,j)\in M}\left(q^j\nabla^i + \vec{\mu}^j\cdot\nabla^i\nabla^i\right)\frac{erf\left(\beta r^{ij}\right)}{r^{ij}}$$

The gradient tensors $\nabla^{(n)}\,\frac{erf(\beta R)}{R}$ were evaluated in section 2.9.

Self Energy Correction

The self energy correction is defined in D.2.14 and given by:

$$U_{self} = -\frac{1}{2}\lim_{\substack{\vec{r}^i\to\vec{r}^j\\ i\to j}}\sum_i\sum_j\left(q^i q^j + \left(\vec{\mu}^i q^j - \vec{\mu}^j q^i\right)\cdot\nabla^i - \vec{\mu}^i\vec{\mu}^j\cdot\nabla^i\nabla^i\right)\frac{erf\left(\beta r^{ij}\right)}{r^{ij}} \qquad \text{D.2.30}$$

The force, electrostatic potential, and electric field are found in a way similar to that used in the direct sum and the adjusted sum:

$$\vec{F}^i_{self} = \lim_{\substack{\vec{r}^i \to \vec{r}^j \\ i \to j}} \sum_j \left(q^i q^j \nabla^i + \left(q^j \vec{\mu}^i - q^i \vec{\mu}^j \right) \cdot \nabla^i \nabla^i - \vec{\mu}^i \vec{\mu}^j \cdot \nabla^i \nabla^i \nabla^i \right) \frac{erf\left(\beta r^{ij}\right)}{r^{ij}}$$

$$\varphi_{self}(\vec{r}^i) = -\lim_{\substack{\vec{r}^i \to \vec{r}^j \\ i \to j}} \sum_j \left(q^j - \vec{\mu}^j \cdot \nabla^j \right) \frac{erf\left(\beta r^{ij}\right)}{r^{ij}} \qquad \text{D.2.31}$$

$$\vec{E}_{self}(\vec{r}^i) = \lim_{\substack{\vec{r}^i \to \vec{r}^j \\ i \to j}} \sum_j \left(q^j \nabla^i + \vec{\mu}^j \cdot \nabla^i \nabla^i \right) \frac{erf\left(\beta r^{ij}\right)}{r^{ij}}$$

The limits of the gradient tensors $\nabla^{(n)} \frac{erf(\beta R)}{R}$ as $R \to 0$ can be found from 2.9.2 – 2.9.4 and are given by:

$$\lim_{R \to 0} \nabla^{(0)} \frac{erf(\beta R)}{R} = \beta B_0(0) \qquad \text{D.2.32}$$

$$\lim_{R \to 0} \nabla^{(1)} \frac{erf(\beta R)}{R} = 0 \qquad \text{D.2.33}$$

$$\lim_{R \to 0} \nabla^{(2)} \frac{erf(\beta R)}{R} = -\hat{x}_p \hat{x}_q \delta_{pq} \beta^3 B_1(0) = \mathbf{I} \beta^3 B_1(0) \qquad \text{D.2.34}$$

$$\lim_{R \to 0} \nabla^{(3)} \frac{erf(\beta R)}{R} = 0 \qquad \text{D.2.35}$$

$B_0(0)$ and $B_1(0)$ can be found from their Taylor series given in 2.9.7 as $\frac{2}{\sqrt{\pi}}$ and $\frac{4}{3\sqrt{\pi}}$, respectively. Therefore, the self energy terms are:

$$\begin{aligned} U_{self} &= -\frac{\beta}{\sqrt{\pi}} \sum_i q^i q^i + \frac{2}{3} \vec{\mu}^i \cdot \vec{\mu}^i \beta^2 \\ \vec{F}^i_{self} &= 0 \\ \varphi_{self}(\vec{r}^i) &= -\frac{2}{\sqrt{\pi}} \beta q^i \\ \vec{E}_{self}(\vec{r}^i) &= \frac{4\beta^3}{3\sqrt{\pi}} \vec{\mu}^i \end{aligned} \qquad \text{D.2.36}$$

This concludes the derivation for the Ewald summation method for a periodic system of point charges and point dipoles. A typical value of the Ewald parameter β is

$0.3Å^{-1}$. For this value, the direct sum converges at a cutoff 8.0 Å, and the reciprocal sum converges after 4-5 reciprocal vectors.

D.3 References

[1] Ewald P. Ann. Phys. **64**, 253-287 (1921)

[2] S. W. Leeuw, J. W. Perram, E. R. Smith, Proc. R. Soc. Lond. A. **373**, 27-56 (1980)

[3] S. W. Leeuw, J. W. Perram, E. R. Smith, Proc. R. Soc. Lond. A. **373**, 57-66 (1980)

[4] S. W. Leeuw, J. W. Perram, E. R. Smith, Proc. R. Soc. Lond. A. **388**, 177-193 (1980)

[5] C. L. Berman and L. Greengard, J. Math. Phys. **35**, 6036 (1994)

[6] C. G. Lambert, T. A. Darden, and J. A. Board, J. Comput, Phys. **126**, 274 (1996)

[7] R. W. Hockney and J. W. Eastwood, *Computer Simulation Using Particles*, (McGraw-Hill, New York, 1981)

[8] T. A. Darden, D. York, and L. Pedersen, J. Chem. Phys. **9**8 (12) 10089 – 10092 (1993)

[9] U. Essmann, L. Perera, M. L. Berkowitz, T. Darden, H. Lee, and L. G. Pedersen, J. Chem. Phys. **103** (19) 8577 - 8593

[10] A. Toukmaji, C. Sagui, J. Board, and T. A. Darden, J. Chem. Phys. **113**, 10913-10927 (2000)

[11] C. Sagui and T. A. Darden, J. Chem. Phys. **114** (15) 6578 – 6591 (2001)

[12] C. Sagui, L. G. Pedersen, and T. A. Darden, J. Chem. Phys. **120** (1), 73 (2004)

[13] J. D. Jackson, *Classical Electrodynamics*, (Wiley, New York, 1999)